University of Alberta

Behaviour of concrete deep beams with high strength reinforcement

by

Juan de Dios Garay Moran ©

A thesis submitted to the Faculty of Graduate Studies and Research
in partial fulfillment of the requirements for the degree of

Master of Science
in
Structural Engineering

Department of Civil and Environmental Engineering

Edmonton, Alberta
Spring 2008

Library and
Archives Canada

Published Heritage
Branch

395 Wellington Street
Ottawa ON K1A 0N4
Canada

Bibliothèque et
Archives Canada

Direction du
Patrimoine de l'édition

395, rue Wellington
Ottawa ON K1A 0N4
Canada

Your file Votre référence
ISBN: 978-0-494-45812-9
Our file Notre référence
ISBN: 978-0-494-45812-9

NOTICE:
The author has granted a non-exclusive license allowing Library and Archives Canada to reproduce, publish, archive, preserve, conserve, communicate to the public by telecommunication or on the Internet, loan, distribute and sell theses worldwide, for commercial or non-commercial purposes, in microform, paper, electronic and/or any other formats.

The author retains copyright ownership and moral rights in this thesis. Neither the thesis nor substantial extracts from it may be printed or otherwise reproduced without the author's permission.

AVIS:
L'auteur a accordé une licence non exclusive permettant à la Bibliothèque et Archives Canada de reproduire, publier, archiver, sauvegarder, conserver, transmettre au public par télécommunication ou par l'Internet, prêter, distribuer et vendre des thèses partout dans le monde, à des fins commerciales ou autres, sur support microforme, papier, électronique et/ou autres formats.

L'auteur conserve la propriété du droit d'auteur et des droits moraux qui protège cette thèse. Ni la thèse ni des extraits substantiels de celle-ci ne doivent être imprimés ou autrement reproduits sans son autorisation.

In compliance with the Canadian Privacy Act some supporting forms may have been removed from this thesis.

While these forms may be included in the document page count, their removal does not represent any loss of content from the thesis.

Conformément à la loi canadienne sur la protection de la vie privée, quelques formulaires secondaires ont été enlevés de cette thèse.

Bien que ces formulaires aient inclus dans la pagination, il n'y aura aucun contenu manquant.

Canada

ABSTRACT

The Strut-and-Tie Method is a widely accepted design approach for reinforced concrete deep beams. However, there are differences between various design code implementations with respect to reinforcement tie influences on the capacity of adjacent concrete struts. Furthermore, each design code specifies different limits on the maximum permitted design stress for the ties. This study validates the Strut-and-Tie Modeling approach for deep beams incorporating high strength steel reinforcement.

Laboratory tests of ten large-scale deep beams were conducted, where primary test variables included the shear-span-to-depth ratio, longitudinal reinforcement ratio and strength, and presence of web reinforcement. The results showed that member capacity decreased as the shear-span-to-depth ratio increased, and as the longitudinal reinforcement ratio decreased. The inclusion of web reinforcement significantly increased the member strength and ductility. It was possible to design members to efficiently exploit the high strength reinforcing steel when applying Strut-and-Tie modeling techniques according to CSA A23.3-04, ACI 318-05 and Eurocode 2 provisions.

ACKNOWLEDGEMENT

As a foreign student it was a unique opportunity and a great experience to obtain my degree at such a prestigious institution as the University of Alberta. Without support of many individuals, this would not have been possible.

I would like to express my gratitude to my supervisor, Dr. Adam Lubell, for his guidance and support in the accomplishment of my thesis, and who never hesitated to provide help. I would also like to thank Dr. Gilbert Grondin for his guidance and encouragement during my studies.

The technical assistance of Richard Helfrich and Sean Watt is gratefully acknowledged. I would also like to thank Sylwester Zagaj for his valuable help during the tests.

The support of MMFX Technologies Corporation through the donation of the high strength reinforcing steel and the financial support of the University of Alberta and the Natural Sciences and Engineering Research Council of Canada (NSERC) are gratefully acknowledged.

Finally, my deep gratitude and eternal thanks to my parents Juan de Dios and Rebeca, my first teachers, who always supported and encouraged me throughout all of my life in my search of knowledge. I also would like to thank my girlfriend Roxana for her infinite inspiration.

TABLE OF CONTENT

1. INTRODUCTION 1

1.1 Context and Motivation 1

1.2 Research Significance 3

1.3 Scope and objectives 4

1.4 Thesis Organization 5

2. LITERATURE REVIEW 7

2.1 General 7

2.2 Concrete members with high strength reinforcing steel 8

2.3 Deep beams 10

2.4 Strut and Tie Method 12

2.4.1 Elements of a Strut and Tie Model 15

2.4.1.1 Struts or compression stress fields 16

2.4.1.2 Ties 16

2.4.1.3 Nodes 17

2.4.2 Modes of failure 18

2.4.3 Configurations for Strut and Tie Models 18

2.4.3.1 Direct Strut and Tie Model 19

2.4.3.2 Indirect Strut and Tie Model 20

2.4.3.3 Combined Strut and Tie Model 20

2.4.4 Selection of a Strut and Tie Model for practical design or analysis 21

2.5 Code provisions for Strut and Tie Method 22

2.5.1 CSA A23.3-04 22

2.5.2 ACI 318-05 25

2.5.3 Eurocode 2 EN 1992-1-1 29

2.5.4 Comparison of Code Provisions for Strut and Tie Method 32

2.6 ASTM A1035 reinforcing steel 33

2.6.1 Tensile properties 33

2.6.2 Compression strength 35

2.6.3 Shear strength 35

2.6.4 Bond strength 35

2.7 Summary 37

3. EXPERIMENTAL PROGRAM 39

3.1 General 39

3.2 Details of Test Specimens 39

3.2.1 Details of specimen MS1-1 42

3.2.2 Details of Specimen MS1-2 43

3.2.3 Details of Specimen MS1-3 44

3.2.4 Details of Specimen MS2-2 45

3.2.5 Details of Specimen MS2-3 46

3.2.6 Details of Specimen MS3-2 47

3.2.7 Details of Specimen NS1-4 48

3.2.8 Details of Specimen NS2-4 49

3.2.9 Details of Specimen MW1-2 50

3.2.10 Details of Specimen MW3-2 51

3.3 Fabrication of specimens 52

3.4 Material properties 53

3.4.1 Concrete 53

3.4.2 Reinforcing Steel 56

3.5 Test Set-Up 60

3.5.1Loading points 60

3.5.2 Supports 61

3.6 Instrumentation 62

3.6.1 Strain gauges 63

3.6.2 LVDTs and Demec Gages 66

3.6.3 Data acquisition system and Camera system 69

3.7 Test Procedure 69

4. EXPERIMENTAL RESULTS 70
4.1 Presentation of results 70
4.2 Specimen MS1-1 71
4.2.1 Load-deflection response of specimen MS1-1 72
4.2.2 Crack development of specimen MS1-1 73
4.2.3 Strains in reinforcement and average strains in concrete for specimen MS1-1 74
4.3 Specimen MS1-2 79
4.3.1 Load-deflection response of specimen MS1-2 80
4.3.2 Crack development of specimen MS1-2 80
4.3.3 Strains in reinforcement and average strains in concrete for specimen MS1-2 81
4.4 Specimen MS1-3 85
4.4.1 Load-deflection response of specimen MS1-3 86
4.4.2 Crack development for specimen MS1-3 86
4.4.3 Strains in reinforcement and average strains in concrete of specimen MS1-3 87
4.5 Specimen MS2-2 90
4.5.1 Load-deflection response of specimen MS2-2 91
4.5.2 Crack development of specimen MS2-2 91
4.5.3 Strains in reinforcement and average strains in concrete for specimen MS2-2 92
4.6 Specimen MS2-3 96
4.6.1 Load-deflection response for specimen MS2-3 97
4.6.2 Crack patterns for specimen MS2-3 97
4.6.3 Strains in reinforcement and average strains in concrete for specimen MS2-3 98
4.7 Specimen MS3-2 101
4.7.1 Load-deflection response for specimen MS3-2 102
4.7.2 Crack development for specimen MS3-2 102

4.7.3 Strains in reinforcement and average strains in concrete for specimen MS3-2 103
4.8 Specimen MW1-2 106
4.8.1 Load-deflection response for specimen MW1-2 107
4.8.2 Crack development for specimen MW1-2 107
4.8.3 Strains in reinforcement and average strains in concrete for specimen MW1-2 108
4.9 Specimen MW3-2 111
4.9.1 Load-deflection response for specimen MW3-2 112
4.9.2 Crack patterns for specimen MW3-2 112
4.9.3 Strains in reinforcement and average strains in concrete for specimen MW3-2 113
4.10 Specimen NS1-4 116
4.10.1 Load-deflection response for specimen NS1-4 116
4.10.2 Crack development for specimen NS1-4 117
4.10.3 Strains in reinforcement and average strains in concrete for specimen NS1-4 118
4.11 Specimen NS2-4 121
4.11.1 Load-deflection response for specimen NS2-4 121
4.11.2 Crack development for specimen NS2-4 122
4.11.3 Strains in reinforcement and average strains in concrete for specimen NS2-4 123

5. ANALYSIS AND COMPARISON OF EXPERIMENTAL RESULTS 127
5.1 Specimens with vertical web reinforcement 127
5.1.1 Influence of shear span to depth ratio 127
129
5.1.1.1 Specimens with different a/d and constant ρ of 1.13 % 129
5.1.1.2 Specimens with different a/d and constant ρ of 2.29% 135
5.1.2 Influence of main reinforcement ratio 139
5.1.2.1 Specimens with a/d of 1.2 and different ρ 140

5.1.2.2 Specimens with a/d of 1.8 and different ρ 145
5.2 Specimens without web reinforcement 149
5.3 Strength contribution of web reinforcement 153
5.3.1 Specimens MS1-2 and MW1-2 154
5.3.2 Specimens MS3-2 and MW3-2 158
5.4 Summary 162

6. VALIDATION OF DESIGN CODE ANALYTICAL MODELS 164
6.1 General 164
6.2 Sectional Method 166
6.3 Direct Strut and Tie Model (STM-D) 168
6.4 Combined strut and tie Model (STM-C) 172
6.5 Individual Analysis and discussion of specimens 175
6.5.1 Specimens with web reinforcement 175
6.5.1.1 Beam with ρ=0.52% and a/d=1.19 175
6.5.1.2 Beams with ρ=1.13% and different shear span 176
6.5.1.2.1 Specimen MS1-2 178
6.5.1.2.2 Specimen MS2-2 179
6.5.1.2.3 Specimen MS3-2 180
6.5.1.3 Beams with ρ=2.29% and different shear span to depth ratio 181
6.5.1.3.1 Specimen MS1-3 182
6.5.1.3.2 Specimen MS2-3 183
6.5.1.4 Specimen with same a/d and different ρ 185
6.5.1.5 Beams reinforced with normal strength steel 187
6.5.1.5.1 Specimen NS1-4 187
6.5.1.5.2 Specimen NS2-4 188
6.5.2 Beams without web reinforcement 189
6.5.2.1 Specimen MW1-2 190
6.5.2.2 Specimen MW3-2 191
6.6 Summary 191

7. **SUMMARY AND CONCLUSIONS** 193
- 7.1 Experimental Program 193
- 7.2 Analytical Methods 195
- 7.3 Use of ASTM A1035 Reinforcement in Deep Beams 198

8. **RECOMMENDATIONS FOR FUTURE RESEARCH** 199

REFERENCES 201

APPENDIX A 204
- A.1 Specimen MS1-1 205
- A.2 Specimen MS1-2 212
- A.3 Specimen MS1-3 219
- A.4 Specimen MS2-2 226
- A.5 Specimen MS2-3 233
- A.6 Specimen MS3-2 241
- A.7 Specimen MW1-2 250
- A.8 Specimen MW3-2 257
- A.9 Specimen NS1-4 264
- A.10 Specimen NS2-4 271

APPENDIX B 279
- B.1 SECTIONAL METHOD 280
  - B.1.1 Sectional Flexure Analysis 280
    - B.1.1.1 Reinforcement properties 281
  - B.1.2 Sectional Shear Analysis 282

LIST OF TABLES

Table 2-1 Development length of the bars in tension for ACI 318-05 27

Table 3-1 Test specimens details 40

Table 3-2 Nominal concrete specifications 53

Table 3-3 Compression test results and age of samples at the day of the beam test 55

Table 3-4 ASTM A1035 reinforcing steel properties 56

Table 3-5 Grade 400R reinforcing steel properties 56

Table 3-6 Distances measured from midspan to the locations where deflections were measured 68

Table 4-1 Material properties, failure loads and modes of failure 71

Table 4-2 Load and $\%P_{max}$ at different crack stages of specimen MS1-1 73

Table 4-3 Loads and $\%P_{max}$ for yielding of reinforcement for specimen MS1-1 75

Table 4-4 Load and $\%P_{max}$ at different crack stages of specimen MS1-2 81

Table 4-5 Loads and $\%P_{max}$ for yielding of reinforcement for specimen MS1-2 82

Table 4-6 Load and $\%P_{max}$ at different crack stages of specimen MS1-3 87

Table 4-7 Loads and $\%P_{max}$ for yielding of reinforcement for specimen MS1-3 88

Table 4-8 Load and $\%P_{max}$ at different crack stages of specimen MS2-2 92

Table 4-9 Loads and $\%P_{max}$ for yielding of reinforcement for specimen MS2-2 93

Table 4-10 Load and $\%P_{max}$ at different crack stages of specimen MS2-3 98

Table 4-11 Loads and $\%P_{max}$ for yielding of reinforcement for specimen MS2-3 99

Table 4-12 Load and $\%P_{max}$ at different crack stages of specimen MS3-2 103

Table 4-13 Loads and $\%P_{max}$ for yielding of reinforcement for specimen MS3-2 104

Table 4-14 Load and $\%P_{max}$ at different crack stages for specimen MW1-2 108

Table 4-15 Load and $\%P_{max}$ at different crack stages of specimen MW3-2 113

Table 4-16 Load and $\%P_{max}$ at different crack stages 117

Table 4-17 Loads and $\%P_{max}$ for yielding of reinforcement 118

Table 4-18 Load and $\%P_{max}$ at different crack stages 122

Table 4-19 Loads and $\%P_{max}$ for yielding of reinforcement 123

Table 5-1 Comparison of specimens MS1-2, MS2-2 and MS3-2 129

Table 5-2 Deflections and P_{max} for specimens MS1-2, MS2-2 and MS3-2 132

Table 5-3 Loads at first flexural and strut cracks and percentage of P_{max} for specimens MS1-2, MS2-2 and MS3-2 134

Table 5-4 Comparison of specimens MS1-3 and MS2-3 135

Table 5-5 Deflections and P_{max} for specimens MS1-3 and MS2-3 137

Table 5-6 Loads at first flexural and strut cracks and percentage of P_{max} for specimens MS1-2 and MS2-3 138

Table 5-7 Comparison of specimens MS1-1, MS1-2 and MS1-3 140

Table 5-8 Deflections and P_{max} for specimens MS1-1, MS1-2 and MS1-3 142

Table 5-9 Load at first flexural and strut cracks and percentage of P_{max} at the occurrence of the cracks 144

Table 5-10 Comparison of specimens MS2-2 and MS2-3 145

Table 5-11 Deflections and P_{max} for specimens MS2-2 and MS2-3 146

Table 5-12 Load at first flexural and strut cracks and percentage of P_{max} at the occurrence of the cracks for specimens MS2-2 and MS2-3 148

Table 5-13 Comparison of specimens MW1-2 and MW3-2 149

Table 5-14 Deflections and P_{max} for specimens MW1-2 and MW3-2 151

Table 5-15 Loads at first flexural and strut cracks and percentage of maximum load for specimens MW1-2 and MW3-2 152

Table 5-16 Comparison of specimens MS1-2 and MW1-2 154

Table 5-17 Deflections and P_{max} for specimens MS1-2 and MW1-2 155

Table 5-18 Load at first flexural and strut cracks and percentage of P_{max} at the occurrence of the cracks for specimens MS1-2 and MW1-2 158

Table 5-19 Comparison of specimens MS3-2 and MW3-2 158

Table 5-20 Deflections and P_{max} for specimens MS3-2 and MW3-2 160

Table 5-21 Load at first flexural and strut cracks and percentage of P_{max} at the occurrence of the cracks 162

Table 6-1 Failure load at test and predicted loads using Sectional Shear Analysis 167

Table 6-2 Failure load at test and predicted loads using Sectional Flexural Analysis 167

Table 6-3 Maximum applied load versus predicted load (P_{max}/P_p) using STM-D 171

Table 6-4 First measured failure load versus predicted load (P_f/P_c) using STM-D 171

Table 6-5 Maximum applied load at test versus predicted load (P_{max}/P_p) using STM-C 174

Table 6-6 First measured failure load versus predicted load (P_f/P_c) for STM-C 175

Table A-1 Loads and deflections at important events during the test of specimen MS1-1 205

Table A-2 Flexural and diagonal crack widths at different loading stages of specimen MS1-1 205

Table A-3 Location of strain gauges for specimen MS1-1 207

Table A-4 Strains monitored by demec gages rosettes for specimen MS1-1 211

Table A-5 Deflections and important observations at different load stages for specimen MS1-2 212

Table A-6 Flexural and diagonal crack widths at different loading stages of specimen MS1-2 212

Table A-7 Location of strain gauges for specimen MS1-2 214

Table A-8 Concrete strains at the top of the specimen at last two manual readings 218

Table A-9 Loads and deflections at important events during the test of specimen MS1-3 219

Table A-10 Flexural and diagonal crack widths at different loading stages of specimen MS1-3 221

Table A-11 Location of strain gauges for specimen MS1-3 221

Table A-12 Strains monitored by demec gages rosettes for specimen MS1-3 225

Table A-13 Loads and deflections at important events during the test of specimen MS1-1 MS2-2 226

Table A-14 Crack width at different stages of loading for specimen MS2-2 226

Table A-15 Location of strain gauges for specimen MS2-2 228
Table A-16 Concrete strains at the top of the specimen at last two manual readings 232
Table A-17 Deflections and important observations at different load stages for specimen MS2-3 233
Table A-18 Crack width at different stages of loading for specimen MS2-3 233
Table A-19 Location of strain gauges for specimen MS2-3 235
Table A-20 Strains monitored by demec gages rosettes for specimen MS2-3 238
Table A-21 Loads and deflections at important events during the test of specimen MS3-2 241
Table A-22 Flexural and diagonal crack widths at different loading stages of specimen MS3-2 241
Table A-23 Location of strain gauges for specimen MS3-2 244
Table A-24 Strains monitored by demec gages rosettes for specimen MS3-2 247
Table A-25 Loads and deflections at important events during the test of specimen MW1-2 250
Table A-26 Flexural and diagonal crack widths at different loading stages of specimen MW1-2 250
Table A-27 Location of strain gauges for specimen MW1-2 252
Table A-28 Strains monitored by demec gages rosettes for specimen MS1-1 254
Table A-29 Deflections and important observations at different load stages for specimen MW3-2 257
Table A-30 Flexural and diagonal crack widths at different loading stages of specimen MW3-2 257
Table A-31 Location of strain gauges for specimen MW3-2 259
Table A-32 Strains monitored by demec gages rosettes for specimen MW3-2 261
Table A-33 MS1 Loads and deflections at important events during the test of specimen NS1-4 264
Table A-34 Location of strain gauges for specimen NS1-4 266
Table A-35 Strains monitored by demec gages rosettes for specimen NS1-4 268

Table A-36 Loads and deflections at important events during the test of specimen NS2-4 271

Table A-37 and diagonal crack widths at different loading stages of specimen NS2-4 271

Table A-38 Location of strain gauges for specimen NS2-4 273

Table A-39 Strains monitored by demec gages rosettes for specimen NS2-4 278

LIST OF FIGURES

Figure 2-1	Comparison between Strut and Tie Method and Sectional Method [from Collins and Mitchell, 1991].	12
Figure 2-2	Basic compression stress fields or struts	16
Figure 2-3	Classification of nodes (a) CCC node, (b) CCT node, (c) CTT node and (d) TTT node	17
Figure 2-4	Nodal zones (a) hydrostatic and (b) extended nodal zone	18
Figure 2-5	(a) Direct strut and tie model, (b) indirect strut and tie model and (c) combined strut and tie model	19
Figure 2-6	Direct Strut and Tie Model	20
Figure 2-7	(a) Strut without transverse tension stress, (b) Strut with transverse tension stress	29
Figure 2-8	Stress-strain curves for ASTM A1035 and 400R grade reinforcing steel bars [from El-Hacha and Rizkalla, 2002]	34
Figure 3-1	Symbolic dimensions of specimens	41
Figure 3-2	Beam MS1-1: (a) Cross section (b) Elevation.	42
Figure 3-3	Beam MS1-2: (a) Cross section (b) Elevation.	43
Figure 3 4	Beam MS1-3: (a) Cross section (b) Elevation	44
Figure 3 5	Beam MS2-2: (a) Cross section (b) Elevation	45
Figure 3 6	Beam MS2-3: (a) Cross section (b) Elevation	46
Figure 3-7	Beam MS3-2: (a) Cross section (b) Elevation	47
Figure 3-8	Beam NS1-4: (a) Cross section (b) Elevation	48
Figure 3-9	Beam NS2-4: (a) Cross section (b) Elevation	49
Figure 3-10	Beam MW1-2: (a) Cross section (b) Elevation	50
Figure 3-11	Beam MW3-2: (a) Cross section (b) Elevation	51
Figure 3-12	Formwork transversal section details	52
Figure 3-13	Vibration of the concrete during casting	53
Figure 3-14	Compression test of concrete cylinder	54
Figure 3-15	Flexural test to obtain the modulus of rupture	55

Figure 3-16 Stress-strain response of ASTM A1035 reinforcement (a) #3 Bars (b) #4 bars (c) #6 bars and (d) #7 bars 57

Figure 3-17 Stress-strain response for Grade 400R reinforcement (a) 10M bar and (b) 20M bar 57

Figure 3-18 Comparison between predicted stress-strain response and measured stress-strain response for (a) ASTM A1035 bars #4 and (b) ASTM A1035 bars #6. 59

Figure 3-19 General set up 60

Figure 3-20 Loading point details 61

Figure 3-21 Supports details 62

Figure 3-22 Strain gauge locations for beam MS1-1 64

Figure 3-23 Strain gauge locations of beam MS1-2 64

Figure 3-24 Strain gauge locations of beam MS1-3 64

Figure 3-25 Strain gauge locations of beam MS2-2 64

Figure 3-26 Strain gauge locations of beam MS2-3 65

Figure 3-27 Strain gauge locations of beam MS3-2 65

Figure 3-28 Strain gauge locations of beam NS1-4 65

Figure 3-29 Strain gauge locations of beam NS2-4 65

Figure 3-30 Strain gauge locations of beam MW1-2 66

Figure 3-31 Strain gauge locations of beam MW1-3 66

Figure 3-32 LVDT rosettes 67

Figure 3-33 LVDT locations 68

Figure 3-34 Demec gauge locations 68

Figure 4-1 Specimen MS1-1 after failure 72

Figure 4-2 Deflection at midspan and 450 mm from midspan for specimen MS1-1 73

Figure 4-3 Crack development of specimen MS1-1 at 72% of P_{max} 74

Figure 4-4 Strain distribution along the bar located in the lowest layer of main tension reinforcement of specimen MS1-1 75

Figure 4-5 Comparison of results using demec gages and LVDTs. (a) Average strains in diagonal D1 direction , (b) average strains in diagonal D2 direction and (c) average strain in vertical direction 77
Figure 4-6 (a) Principal tension strain, (b) principal compression strain and (c) angle of principal strains of specimen MS1-1 78
Figure 4-7 Strain in top strut between loading points of specimen MS1-1 79
Figure 4-8 Specimen MS1-2 after failure 79
Figure 4-9 Deflection at midspan and 450 mm from midspan of specimen MS1-2 80
Figure 4-10 Crack development at 74.7% of P_{max} for specimen MS1-2 81
Figure 4-11 Strain distribution along the bar located in the lowest layer of main tension reinforcement of specimen MS1-2 82
Figure 4-12 (a) Principal tension strain, (b) Principal compression strain and (c) angle of principal strains of specimen MS1-2 84
Figure 4-13 Strain in top strut of specimen MS1-2 85
Figure 4-14 Specimen MS1-3 after failure 85
Figure 4-15 Deflection at midspan and 450 mm from midspan of specimen - MS1-3 86
Figure 4-16 Crack development at 72.8% of P_{max} of specimen MS1-3 87
Figure 4-17 Strain distribution along the bar located in the lowest layer of main tension reinforcement of specimen MS1-3 88
Figure 4-18 (a) Principal tension strain, (b) Principal compression strain and (c) angle of principal strains of specimen MS1-3 89
Figure 4-19 Strains in the compression zone between the loading points of specimen MS1-3 90
Figure 4-20 Specimen MS2-2 after failure 90
Figure 4-21 Deflection at midspan and 675 mm from midspan of specimen MS2-2 91
Figure 4-22 Crack development at 69.8% of P_{max} 92
Figure 4-23 Strain distribution along the bar located in the lowest layer of main tension reinforcement of specimen MS2-2 93

Figure 4-24 (a) Principal tension strain, (b) Principal compression strain and (c) angle of principal strains of specimen MS2-2 95
Figure 4-25 Demec gauges reading and strain gauge readings in the compression zone located between loading points of specimen MS2-2 96
Figure 4-26 Specimen MS2-3 after failure 96
Figure 4-27 Deflection at midspan and 675 mm from midspan for specimen MS2-3 97
Figure 4-28 Crack development at 73% of P_{max} for specimen MS2-3 98
Figure 4-29 Strain distribution along the bar located in the lowest layer of main tension reinforcement of specimen MS2-3 99
Figure 4-30 (a) Principal tension strain, (b) Principal compression strain and (c) angle of principal strains of specimen MS2-3 100
Figure 4-31 Strain at compression zone between the loading points of specimen MS2-3 101
Figure 4-32 Specimen MS3-2 after failure 101
Figure 4-33 Deflection at midspan and 725 mm from midspan of specimen MS3-2 102
Figure 4-34 Crack development at 69.3% of P_{max} for specimen MS3-2 103
Figure 4-35 Strain distribution along the bar located in the lowest layer of main tension reinforcement of specimen MS3-2 104
Figure 4-36 (a) Principal tension strain, (b) Principal compression strain and (c) angle of principal strains of specimen MS3-2 105
Figure 4-37 Strain in top strut of specimen MS3-2 106
Figure 4-38 Specimen MW1-2 after failure 106
Figure 4-39 Deflection at midspan and 450 mm from midspan of specimen MW1-2 107
Figure 4-40 Crack development and crack width of MW1-2 at 76.5% of P_{max} 108
Figure 4-41 Strain distribution along the bar located in the lowest layer of main tension reinforcement of specimen MW1-2 109
Figure 4-42 (a) Principal tension strain, (b) Principal compression strain and (c) angle of principal strains of specimen MW1-2 110

Figure 4-43	Strains in top strut using demec gages and strain gages for specimen MW1-2	111
Figure 4-44	Specimen MW3-2 after failure	111
Figure 4-45	Deflection at midspan and 725 mm from midspan of specimen MW3-2	112
Figure 4-46	Crack development of specimen MW3-2 at 73% of P_{max}	113
Figure 4-47	Strain distribution along the bar located in the lowest layer of main tension reinforcement of specimen MW3-2	114
Figure 4-48	(a) Principal tension strain and (b) Principal compression strain developed in the diagonal struts of specimen MW3-2.	115
Figure 4-49	Strains in top strut using demec gages and strain gages for specimen MW3-2	115
Figure 4-50	Specimen NS1-4 after failure	116
Figure 4-51	Deflection at midspan and 450 mm from midspan of specimen NS1-4	117
Figure 4-52	Crack development at 70.2% of P_{max} for specimen NS1-4	118
Figure 4-53	Strain distribution along the bar located in the lowest layer of main tension reinforcement of specimen NS1-4	119
Figure 4-54	(a) Principal tension strain, (b) Principal compression strain and (c) angle of principal strains of specimen NS1-4	120
Figure 4-55	Specimen NS2-4 after failure	121
Figure 4-56	Deflection at midspan and 675 mm from midspan of specimen NS2-4	122
Figure 4-57	Crack development at 74.2 % of P_{max} for specimen NS2-4	123
Figure 4-58	Strain distribution along the bar located in the lowest layer of main tension reinforcement of specimen NS2-4	124
Figure 4-59	(a) Principal tension strain, (b) Principal compression strain and (c) angle of principal strains of specimen NS2-4	125
Figure 4-60	Strain in top strut of specimen NS2-4	126
Figure 5-1	Total load to *a/d* relationship for specimens with web reinforcement	129

Figure 5-2 (a) Load-deflection response and (b) moment-deflection response for specimens MS1-2, MS2-2 and MS3-2 131
Figure 5-3 Load-strain response for specimens MS1-2, MS2-2 and MS3-2 132
Figure 5-4 Strain distribution along the lowest reinforcement bar for specimens (a) MS1-2, (b) MS2-2 and (c) MS3-2 at different loading stages 133
Figure 5-5 Crack development of (a) MS1-2 at 1800 kN, (b) MS2-2 at 1200 kN and (c) MS3-2 at 960 kN 134
Figure 5-6 (a) Load-deflection and (b) moment-deflection response for specimens MS1-3 and MS2-3 136
Figure 5-7 Load-strain response for the first (lowest) layer of specimens MS1-3 and MS2-3 137
Figure 5-8 Strain distribution along the lowest bar of main tension reinforcement for specimens (a) MS1-3 and (b) MS2-3 138
Figure 5-9 Crack development at 73% of P_{max} for (a) Specimen MS1-3 (b) Specimen MS2-3 139
Figure 5-10 Load-ρ relationship for specimens with *a/d*=1.2 and 1.8 140
Figure 5-11 Load-deflection response for specimens MS1-2, MS2-2 and MS3-2 142
Figure 5-12 Load-strain response for the first layer of the main tension reinforcement for specimens MS1-1, MS1-2 and MS1-3 143
Figure 5-13 Strain distribution along the bottom reinforcing bar at approximately 90 % of P_{max} 143
Figure 5-14 Crack development of (a) MS1-1 at 900 kN , (b) MS1-2 at 1600 kN and (c) MS1-3 at 2000 kN 144
Figure 5-15 Load-deflection response for specimens MS2-2 and MS2-3 146
Figure 5-16 Load-strain response for the first layer of the main tension reinforcement 147
Figure 5-17 Strain distribution along the bottom bar at approximately 90 % of P_{max} 147
Figure 5-18 Crack development of (a) MS2-2 at 1200 kN and (b) MS2-3 at 1800 kN 148

Figure 5-19 (a) Load-deflection response and (b) moment-deflection response for specimens MW1-2 and MW3-2 150
Figure 5-20 Load-strain response for MW1-2 and MW3-2 151
Figure 5-21 Strain distribution along the bottom bar for (a) MW1-2 and (b) MW3-2 at different loading stages 152
Figure 5-22 (a) Crack development of MW1-2 at 1200 kN (72.5%of P_{max}) and (b) Crack development of MW3-2 at 300 kN (73%of P_{max}) 153
Figure 5-23 Influence of web reinforcement on member strength 154
Figure 5-24 Load-deflection response for specimens MS1-2 and MW1-2 155
Figure 5-25 Load-strain response for the first layer of the main tension reinforcement 156
Figure 5-26 Strain distribution along the bottom reinforcing bars for specimens MS1-2 and MW1-2 157
Figure 5-27 Crack development of MS1-2 at (a) 1400 kN and (b) 2000 kN 157
Figure 5-28 Crack development and crack width of MW1-2 at 1400 kN 158
Figure 5-29 Load-deflection response for specimens MS3-2 and MW3-2 159
Figure 5-30 Load-strain response for the first layer of the main tension reinforcement 160
Figure 5-31 Strain distribution along the bottom bar at approximately 90 % of P_{max} for specimens MS3-2 and MW3-2 and at 350 kN for specimen MS3-2. 161
Figure 5-32 Crack development of specimen MS3-2 at (a) 400 kN and (b) 960 kN 161
Figure 5-33 Crack development of specimen MW3-2 at 300 kN 162
Figure 6-1 Direct Strut and Tie Model 168
Figure 6-2 Combined Strut and Tie Method 172
Figure 6-3 P_{max}/P_p for three different a/d and ρ=1.13% using (a) STM-D and (b) STM-C 177
Figure 6-4 P_{max}/P_p for two different a/d and ρ=2.29% using (a) STM-D and (b) STM-C 182

Figure 6-5 P_{max}/P_p for three different ρ and a/d=1.2 using (a) STM-D and (b) STM-C 186
Figure 6-6 P_{max}/P_p for three different ρ and a/d=1.8 using (a) STM-D and (b) STM-C 187
Figure A-1 Load-time response of specimen MS1-1 205
Figure A-2 Crack patterns at different loading stages of specimen MS1-1 206
Figure A-3 Strain gages locations of specimen MS1-1 207
Figure A-4 Strains at a bar located in the lowest layer of main tension reinforcement of specimen MS1-1 207
Figure A-5 Strains at midspan of the three layers of main tension reinforcement in specimen MS1-1 208
Figure A-6 Strains of stirrups located in the shear spans of specimen MS1-1 208
Figure A-7 Strains on the horizontal web reinforcement of specimen MS1-1 208
Figure A-8 Strains at the interior and exterior edges of the supports 209
Figure A-9 Strain at the interior edge of one support for the three layers of tension reinforcement of specimen MS1-1 209
Figure A-10 Average Strains in the (a) diagonal strain D1, (b) diagonal strain D2 and (c) vertical strain of specimen MS1-1 210
Figure A-11 Maximum shear strain in diagonal struts of specimen MS1-1 211
Figure A-12 Load-time response of specimen MS1-2 212
Figure A-13 Crack patterns at different loading stages from 400 kN to 1600 kN of specimen MS1-2 213
Figure A-14 Crack patterns at 1800 kN and 2000 kN for specimen MS1-2 214
Figure A-15 Strain gages locations of specimen MS1-2 214
Figure A-16 Strains at a bar located in the lowest layer of main tension reinforcement of specimen MS1-2 215
Figure A-17 Strains at midspan of the three layers of main tension reinforcement in specimen MS1-2 215
Figure A-18 Strains of stirrups located in the shear spans of specimen MS1-2 215
Figure A-19 Strains on the horizontal web reinforcement of specimen MS1-2 216

Figure A-20 Strains at the interior and exterior edges of the supports of specimen MS1-2 216
Figure A-21 Strain at the interior edge of one support for the three layers of tension reinforcement of specimen MS1-2 216
Figure A-22 Average Strains in the (a) diagonal strain D1, (b) diagonal strain D2 and (c) vertical strain of specimen MS1-2 217
Figure A-23 Maximum shear strain in diagonal struts of specimen MS1-2 218
Figure A-24 Load-time response of specimen MS1-3 219
Figure A-25 Crack patterns at 400 kN and 800 kN of specimen MS1-3 219
Figure A-26 Crack patterns at different loading stages from 800 kN to 2000 kN of specimen MS1-3 220
Figure A-27 Strain gages locations of specimen MS1-3 221
Figure A-28 Strains at a bar located in the lowest layer of main tension reinforcement of specimen MS1-3 222
Figure A-29 Strains at midspan of the three layers of main tension reinforcement in specimen MS1-3 222
Figure A-30 Strains of stirrups located in the shear spans of specimen MS1-3 222
Figure A-31 Strains on the horizontal web reinforcement of specimen MS1-3 223
Figure A-32 Strains at the interior and exterior edges of the supports of specimen MS1-3 223
Figure A-33 Strain at the interior edge of one support for the three layers of tension reinforcement of specimen MS1-3 223
Figure A-34 Average Strains in the (a) diagonal strain D1, (b) diagonal strain D2 and (c) vertical strain of specimen MS1-3 224
Figure A-35 Maximum shear strain in diagonal struts of specimen MS1-3 225
Figure A-36 Load-time response for specimen MS2-2 226
Figure A-37 Crack patterns at different loading stages of specimen MS2-2 227
Figure A-38 Strain gages locations of specimen MS2-2 228
Figure A-39 Strains at a bar located in the lowest layer of main tension reinforcement of specimen MS2-2 228

Figure A-40 Strains at midspan of the three layers of main tension reinforcement in specimen MS2-2 229

Figure A-41 Strains of stirrups located in the shear spans of specimen MS2-2 229

Figure A-42 Strains on the horizontal web reinforcement of specimen MS2-2 229

Figure A-43 Strains at the interior and exterior edges of the supports of specimen MS2-2 230

Figure A-44 Strain at the interior edge of one support for the three layers of tension reinforcement of specimen MS2-2 230

Figure A-45 Average Strains in the (a) diagonal strain D1, (b) horizontal strain and (c) vertical strain of specimen MS2-2 231

Figure A-46 Maximum shear strain in diagonal struts of specimen MS2-2 232

Figure A-47 Load-time response of specimen MS2-3 233

Figure A-48 Crack patterns at different loading stages of specimen MS2-3 234

Figure A-49 Strain gages locations of specimen MS2-3 235

Figure A-50 Strains at a bar located in the lowest layer of main tension reinforcement of specimen MS2-3 236

Figure A-51 Strains at midspan of the three layers of main tension reinforcement in specimen MS2-3 236

Figure A-52 Strains on the horizontal web reinforcement of specimen MS2-3 236

Figure A-53 Strains of stirrups located in the shear spans of specimen MS2-3 237

Figure A-54 Strains at the interior and exterior edges of the supports of specimen MS2-3 237

Figure A-55 Strain at the interior edge of one support for the three layers of tension reinforcement of specimen MS2-3 238

Figure A-56 Average Strains in the (a) diagonal strain D1, (b) horizontal strain and (c) vertical strain of specimen MS2-3 239

Figure A-57 Maximum shear strain in diagonal struts of specimen MS2-3 240

Figure A-58 Load-time response of specimen MS3-2 241

Figure A-59 Crack patterns at 200 kN, 400 kN and 600 kN of loading at test of specimen MS3-2 242

Figure A-60 Crack patterns at 800 kN and 960 kN of loading at test of specimen MS3-2 243

Figure A-61 Strain gages locations of specimen MS3-2 244

Figure A-62 Strains at a bar located in the lowest layer of main tension reinforcement of specimen MS3-2 245

Figure A-63 Strains at midspan of the three layers of main tension reinforcement in specimen MS3-2 245

Figure A-64 Strains on the horizontal web reinforcement of specimen MS3-2 245

Figure A-65 Strains of stirrups located in the shear spans of specimen MS3-2 246

Figure A-66 Strains at the interior and exterior edges of the supports of specimen MS3-2 246

Figure A-67 Strain at the interior edge of one support for the three layers of tension reinforcement of specimen MS3-2 247

Figure A-68 Average Strains in the (a) diagonal strain D1, (b) diagonal strain D2 and (c) vertical strain of specimen MS3-2 248

Figure A-69 Maximum shear strain in diagonal struts of specimen MS3-2 249

Figure A-70 Load-time response of specimen MS1-1 250

Figure A-71 Crack patterns at different loading stages from 200 kN to 1200 kN of specimen MW1-2 251

Figure A-72 Crack patterns at 1400 kN of specimen MW1-2 252

Figure A-73 Strain gages locations of specimen MW1-2 252

Figure A-74 Strains at a bar located in the lowest layer of main tension reinforcement of specimen MW1-2 253

Figure A-75 Strains at midspan of the three layers of main tension reinforcement in specimen MW1-2 253

Figure A-76 Strains at the interior and exterior edges of the supports of specimen MW1-2 253

Figure A-77 Strain at the interior edge of one support for the three layers of tension reinforcement of specimen MW1-2 254

Figure A-78 Average Strains in the (a) diagonal strain D1, (b) diagonal strain D2 and (c) horizontal strain of specimen MW1-2 255

Figure A-79 Maximum shear strain in diagonal struts of specimen MW1-2 256

Figure A-80 Load-time response of specimen MW3-2 257

Figure A-81 Crack patterns at different loading stages of specimen MW3-2 258

Figure A-82 Strain gages locations of specimen MW3-2 259

Figure A-83 Strains at a bar located in the lowest layer of main tension reinforcement of specimen MW3-2 260

Figure A-84 Strains at midspan of the three layers of main tension reinforcement in specimen MW3-2 260

Figure A-85 at the interior and exterior edges of the supports of specimen MW3-2 261

Figure A-86 Strain at the interior edge of one support for the three layers of tension reinforcement of specimen MW3-2 261

Figure A-87 Average Strains in the (a) diagonal strain D1, (b) diagonal strain D2 and (c) horizontal strain of specimen MW3-2 262

Figure A-88 Maximum shear strain in diagonal struts of specimen MW3-2 263

Figure A-89 Load-time response of specimen NS1-4 264

Figure A-90 Crack patterns at 150 kN and 260 kN of specimen NS1-4 264

Figure A-91 Crack patterns at different loading stages from 350 kN to 1350 kN of specimen NS1-4 265

Figure A-92 Strain gages locations of specimen NS1-4 266

Figure A-93 Strains at a bar located in the lowest layer of main tension reinforcement of specimen NS1-4 266

Figure A-94 Strains at midspan of the three layers of main tension reinforcement in specimen NS1-4 267

Figure A-95 Strains of stirrups located in the shear spans of specimen NS1-4 267

Figure A-96 Strains on the horizontal web reinforcement of specimen NS1-4 267

Figure A-97 Strains at the interior and exterior edges of the supports of specimen NS1-4 268

Figure A-98 Strain at the interior edge of one support for the three layers of tension reinforcement of specimen NS1-4 268

Figure A-99 Average Strains in the (a) diagonal strain D1, (b) diagonal strain D2 and (c) vertical strain of specimen NS1-4 269

Figure A-100 Maximum shear strain in diagonal struts of specimen NS1-4 270
Figure A-101 Load-time response of specimen NS2-4 271
Figure A-102 Crack patterns at different loading stages of specimen NS2-4 272
Figure A-103 Strain gages locations of specimen NS2-4 273
Figure A-104 Strains at a bar located in the lowest layer of main tension reinforcement of specimen NS2-4 274
Figure A-105 Strains at midspan of the three layers of main tension reinforcement in specimen NS2-4 274
Figure A-106 Strains of stirrups located in the shear spans of specimen NS2-4 275
Figure A-107 Strains on the horizontal web reinforcement of specimen NS2-4 275
Figure A-108 Strains at the interior and exterior edges of the supports of specimen NS2-4 276
Figure A-109 Strain at the interior edge of one support for the three layers of tension reinforcement of specimen NS2-4 276
Figure A-110 Average Strains in the (a) diagonal strain D1, (b) horizontal strain and (c) vertical strain of specimen NS2-4 277
Figure A-111 Maximum shear strain 278
Figure B-1 Sectional Flexure Analysis 280
Figure B-2 Location of Sections for shear analysis 282

LIST OF SYMBOLS

a = shear span measured from center of support to center of loading point
a = angle between shear reinforcement and the longitudinal axis
A_{nz} = smaller area between the area of the face of the nodal zone perpendicular to the load acting in that face and the area of a section through the nodal zone perpendicular to the resultant force on the section.
A_{si} = total area of surface reinforcement at spacing s_i in the $i-th$ layer for reinforcement crossing a strut at an angle α_i to the axis of the strut.
A_{sw} = area of shear reinforcement within length s
A_{tr} = total cross sectional area of reinforcement that is within spacing s and crosses the potential plane of bond splitting through the reinforcement being developed.
A_v = sum of the cross sectional areas of the stirrup legs
b = width of beam
b_w = width of the member web
C = forces in compression strut
C_b = thickness of clear bottom concrete cover
C_{si} = half clear spacing between splice bars
C_{so} = thickness of clear side concrete cover
c'_{min} = minimum of concrete covers surrounding bar or half clear spacing between bars, minimum of C_{si} and (C_b or C_{so})
d = effective depth of beam
d_b = nominal diameter of steel bar
D1 = strain perpendicular to diagonal strut axis
D2 = strain in the direction of diagonal strut axis
E_c = modulus of elasticity
f_{ce} = effective compressive stress of the concrete
f_{cen} = effective compressive strength of the concrete in the nodal zone.

f_{ck} = characteristic compressive strength

f_{ctd} = design value of concrete tensile strength

f'_c = specified compressive strength of the concrete

f_u = maximum strength of steel

f_r = modulus of rupture of concrete

f_y = yield strength of steel (Effective yield strength according to the 0.2% offset method for ASTM A1035 reinforcing steel)

f_{yk} = yield stress

f_{yt} = the specified yield strength of the transverse reinforcing steel in ksi or psi (consistent units must be used)

h = height of beam

k_1 = bar location factor

k_2 = coating factor

k_3 = concrete density factor

k_4 = bar size factor

K_{tr} = transverse reinforcement index

l_d = development length of reinforcement

l = span

n = number of bars or wires being spliced or developed along the plane of splitting.

n = number of bars or wires being spliced or developed along the potential plane of bond splitting

P_{max} = maximum load reached at test

P_p = lowest predicted capacity of all modes considered

P_{pv} = predicted total capacity using the Sectional Shear Method

P_{pm} = predicted total capacity using Sectional flexure analysis

Pt = measured load corresponding to the first failure mode reached during the test

Pt = predicted load for the first failure mode reached during the test

s = maximum center to center spacing of transverse reinforcement within l_d

s = spacing of the stirrups
T = tension force in main reinforcement
Z = effective lever arm at section
α = reinforcement location factor.
α_{ct} = is a coefficient taking account of long term effects on the tensile strength and of unfavorable effects, resulting from the way the load is applied
α_1 = ratio of average stress in rectangular compression block to the specified concrete strength
β = coating factor.
β_n = strength reduction factor for nodes
β_s = strength reduction factor for struts
β_1 = ratio of depth of rectangular compression block to depth to the neutral axis
γ_{xy} = shear strain
γ_c = partial safety factor
γ_s = partial factor for steel
ε_1 = principal tensile strain
ε_2 = principal compressive strain
ε_s = tensile strain in the tie inclined at θ_s to the compressive strut
ε_u = strain corresponding to the maximum strength of reinforcing steel

εx = horizontal average strain of concrete
εy = vertical average strain in concrete
ε_y = yield strain of steel (Effective yield strain according to the 0.2% offset method for ASTM A1035 reinforcing steel)
η_1 = coefficient related to the quality of the bond condition and the position of the bar
η_2 = is related to the bar diameter
θ_s = smallest angle between the compressive strut and the adjoining tensile ties

ρ = reinforcement ratio

σ_{sd} = design stress at the inner edge of the node region

5

ϕ = bar diameter

ϕ_c = resistance factor for concrete

ϕ_s = resistance factor for reinforcement

λ = lightweight aggregate concrete factor

μ = deflection ductility

ν = strength reduction factor for concrete cracked in shear

Δ = deflection

1. INTRODUCTION

1.1 Context and Motivation

For decades, methods of design and analysis for concrete members reinforced with normal strength steel have been developed. Recently, reinforcing steel (ASTM A1035) with strength higher than conventional steel has become commercially available. The introduction of high strength reinforcing steel can be useful to reduce the quantity of reinforcement required, thereby lessening reinforcement congestion and improving constructability. Furthermore, the improved corrosion resistance of ASTM A1035 reinforcement makes it well suited for application in foundations, bridges, buildings or offshore structures.

The mechanical properties of the high strength reinforcing steel are different from traditional reinforcing steel, including the lack of a defined yield point and corresponding yield plateau. The effective yield strength of ASTM A1035 reinforcement, using the 0.2% offset method, is approximately twice that of traditional Grade 400R steel reinforcement having a nominal yield strength of about 400 MPa. These differences might affect the structural performance of reinforced concrete members, making it necessary to validate existing design methods for the case of members with high strength reinforcement.

For satisfactory behavior of reinforced concrete structures, all structural members must be designed to ensure adequate performance at the serviceability limit state and at the ultimate limit state. This project studied the behavior of reinforced concrete members that can be classified as Non-slender or Deep Beams. In order to select an adequate method of design for this type of beam, it is necessary to differentiate between slender and non-slender beams.

Beams subjected to concentrated loading can be classified as slender or non-slender according to their shear span to depth ratio (a/d). A slender beam is generally regarded as a beam with $a/d > 2.5$ and a non-slender beam is a beam with $a/d < 2.5$. The method of design for each type of beam varies due to the development, under loading, of different strain distributions within the member. Slender beams develop a linear distribution of axial strains over the member depth and can be designed by traditional sectional methods. On the other hand, non-slender beams can not be accurately designed using sectional methods due to a non-linearity in the strain distribution. The Strut and Tie Method (STM) is a lower bound solution approach for capacity that is recognized as an important tool for the design of non-slender beams, since it considers the member capacity as a function of *a/d* [e.g., Schlaich et al., 1987 and Marti, 1985].

The current design provisions for non-slender beams incorporated into several codes of practice are based on extensive research focused on members with "normal" strength steel reinforcement. These provisions allow the design of concrete members using maximum *design* yield strengths (f_y) up to certain limits, which vary slightly between the codes. CSA A23.3-04 allows design using Strut-and-Tie methods with reinforcement yield strength f_y up to of 500 MPa. ACI 318-05 sets a limit for f_y of 550 MPa for longitudinal reinforcement and 410 MPa for shear reinforcement, where shear reinforcement is assumed to represent the reinforcement perpendicular to the member longitudinal axis. Eurocode 2 allows the use of f_y up to 500 MPa. In order to utilize reinforcing steel yield strengths higher than the limits established by the codes in design or analysis of structural members, it is necessary to validate whether the current codified design provisions remain valid for higher values of f_y. This systematic validation is needed before routine design is permitted which fully utilizes the additional reinforcing steel strength towards achieving stronger and more cost-effective structures. In this report, "normal" reinforcing steel strength refers to reinforcement that is in general conformance with the existing code limits. "High strength reinforcement" refers to strengths exceeding these limits.

For non-slender or deep beams reinforced with normal strength reinforcing steel, with the minimum required shear reinforcement and without excessive main tensile reinforcement, yielding of the main tension reinforcement frequently occurs prior to the shear failure load [e.g., Rogowsky et al, 1986; Oh and Shin, 2001; Aguilar et al., 2002]. Using high strength reinforcing steel as main tension reinforcement could help to develop higher beam capacity prior to yielding of the main tension steel. For comparison, the effective yield strain of the high strength ASTM A1035 steel, according to the 0.2% offset method, is in the range of 0.006, or about 2.5 to 3 times the yield strain of traditional normal strength reinforcement. For deep beams reinforced with normal strength reinforcing steel, it is necessary to have large reinforcement ratios in order to achieve high shear strength prior to yielding of the main tension reinforcement or diagonal strut failure. If high strength longitudinal reinforcement is provided, a lower reinforcement ratio may be possible.

Recently, research has been carried out to study the behavior of concrete members reinforced with an innovative high strength reinforcing steel designated as ASTM A1035 [Malhas, 2002 and Vijay et al., 2002]. ASTM A1035 is characterized by an effective yield strength of at least 830 MPa. This earlier research focused on validating current design methods for flexure-critical slender beams. These researchers concluded that current code methods can be used for the design of slender beams incorporating ASTM A1035 reinforcement. However, limited previous research has examined the performance of non-slender beams where the traditional sectional model assumption of 'plane sections remain plane' does not apply. Now, the current design provisions need to be validated and the behavior studied, for non-slender beams reinforced with high strength steel.

1.2 Research Significance

Due to the importance of concrete strength on the ultimate capacity of non-slender beams, which are members usually acting under high shear-compression stresses, many research projects have focused on the behavior of non-slender beams constructed with high strength concrete [e.g., Quintero et al., 2006; Oh and Shin, 2001; Foster and Gilbert, 1998]. Even though steel reinforcement also plays a very important role in the ultimate strength of the system [Wastein and Mathey, 1958; Tan and Lu, 1999; Oh and Shin, 2001], no previous research has systematically focused on the influence of using higher strength steel reinforcement in non-slender concrete beams.

This project studied the behavior of non-slender reinforced concrete beams constructed with high strength steel reinforcement. The effective yield strength of the reinforcement utilized in this study was approximately 860 MPa, conforming to ASTM A1035. The project also verified the viability of the Strut and Tie Model design technique for predicting failure loads when using high strength steel as reinforcement. The influence on deep beam behavior at ultimate and service conditions was considered for parameters which included: strain in the longitudinal reinforcement, angle of diagonal struts, and the presence or omission of distributed vertical reinforcement within the shear span. Note that each design code gives different importance to the influence of these parameters on the overall strength of the beams. Thus, the accuracy of beam capacity predictions according to CSA A23.3-04, ACI 318-05 and Eurocode 2 provisions was also examined in this project.

1.3 Scope and objectives

The main objectives of this research project were to study the behavior of non-slender beams reinforced with high strength steel and to verify the adequacy of three codes (CSA A23.3, ACI 318-05 and Eurocode 2) in the prediction of failure loads using their current design methods for this type of beam.

For non-slender beams, each code suggests the use of alternative design methods. One of these methods is the Strut and Tie Method (STM), which has been shown to give good predictions of the capacity of non-slender beams reinforced with normal strength steel [Quintero et al., 2006; Matamoros and Hong, 2003; Matamoros et al., 2002; Tan and Lu, 1999; Foster and Gilbert, 1998; Rogowsky and McGregor, 1986]. This project validated the viability of this method in the design of non slender beams reinforced with high strength steel.

To achieve the objectives, an experimental program included testing to failure of ten deep beams under four-point bending. Eight beams were reinforced with high strength reinforcing steel (approximate effective f_y=860 MPa and f_u=1100 MPa) and two control beams utilized normal strength reinforcing steel (f_y=401 MPa and f_u=800 MPa). The concrete strength in the specimens varied from 23 to 48 MPa. Specimens tested were designed considering variation of longitudinal reinforcement ratio, shear span to depth ratio, and presence/omission of vertical web reinforcement. These specimen configurations allowed evaluation of the influence of these parameters on the behavior of these specimens. The specimens were designed to satisfy the general requirements of the three codes for minimum reinforcement ratio, minimum distributed web reinforcement, concrete cover, spacing between bars and reinforcement development lengths. It is important to mention that for most previous research done on deep beams, the beam-end anchorage techniques for the longitudinal steel utilized 90° hooks or mechanical anchorage devices. This project provided straight development lengths to study the behavior of the reinforcement beyond the supports and to verify the adequacy of straight development length as an anchorage technique for non-slender beams.

To compare the accuracy of the capacity predictions from the CSA A23.3-04, ACI 318-05 and Eurocode 2 provisions, the specimens were analyzed using two different Strut and Tie models: the Direct Strut and Tie Model and the Combined Strut and Tie Model. Predicted load capacities and failure modes predicted were compared against results obtained from the test.

1.4 Thesis Organization

This thesis comprises eight chapters describing a research project focused on the behavior and analysis of concrete deep beams reinforced with high strength steel.

Chapter 2 contains a literature review on previous research and application for reinforced concrete members with high strength reinforcing steel. A discussion of the provisions given by three codes (CSA A23.3-04, ACI 318-05 and Eurocode 2) for the design of non-slender beams using the Strut and Tie Method is included. Also, a literature review is provided on the material properties of the high strength steel used in this project.

Chapter 3 presents a description of the experimental program carried out in this project, which includes detailing, fabrication, instrumentation and test set up of the specimens. The measured properties of the materials used in this project are also provided in this chapter.

The experimental results are presented in Chapter 4. Data obtained during each test is presented using tables, graphs and figures. This information includes load deflection response, crack development, strains along the main longitudinal reinforcement, strains in the web reinforcement, principal strains and angle of principal strains developed in the diagonal struts for each of the specimens.

A comparison between the results of specimens is shown in Chapter 5. This presentation separates the beams into two groups: beams with web reinforcement and beams without web reinforcement. For each group, the influence of reinforcement ratio and shear span to depth ratio on the capacity of the specimens was studied. The influence of web reinforcement on the overall behavior of deep beams was also studied through a comparison of the two groups.

Code predictions are compared to the test results in Chapter 6, to verify the viability of the design of deep beams reinforced with high strength steel using current codes provisions.

Conclusions from this project and recommendations for future research are presented in Chapters 7 and 8 respectively.

2. LITERATURE REVIEW

In this chapter, a literature review is presented of previous research on the behaviour of reinforced concrete members incorporating high strength steel reinforcement. Also, a plasticity truss-model technique suitable for the design of deep beams is described. This technique, called Strut and Tie Modeling, was adopted by codes of practice for the design of non-slender reinforced concrete members such as deep beams. Design provisions for three codes (CSA A23.3-04, ACI 318-05 and Eurocode 2) considered in this project are discussed. Finally, material properties of the high strength reinforcing steel used in this project are also presented.

2.1 General

The use of high strength steel reinforcement (ASTM A1035) in concrete structures is gaining popularity due to its higher effective yield strength, improved corrosion resistance in comparison with normal strength reinforcing steel and better behaviour under low temperatures [Darwin et al, 2002 and El-Hacha, 2002]. Normal strength reinforcing steel becomes brittle around -17° to -28° C, while ASTM A1035 reinforcing steel maintains excellent mechanical behavior at temperatures below -128° C [MMFX Technologies Corporation, 2008].

The mechanical properties of high strength reinforcing steel can be useful to reduce the quantity of reinforcement required, thereby lessening reinforcement congestion and improving constructability. The improved corrosion resistance [Darwin et al, 2002] makes ASTM A1035 ideal for use as reinforcement in foundations, bridges, buildings, offshore structures, etc.

ASTM A1035 high strength steel has been used as reinforcement for concrete bridge decks and foundation walls for two primary reasons: the viability of concrete member design using the highest yield strength allowed by current design codes [Seliem et al, 2008] and the improved corrosion resistance compared to traditional Grade 400R reinforcement. However, the use of the full strength of the high strength reinforcing steel bars is not allowed in practical designs because of limitations on permitted design stress in current design code provisions. These provisions, some of which are semi-empirical, are based on research completed on reinforced concrete members containing normal strength reinforcement. The stress-strain response of ASTM A1035 and conventional reinforcing steel are similar for values only up to the yielding point of conventional steel. After that point, the strain-stress responses of both types of reinforcing steel are different. The main differences include the non linear stress-strain response for ASTM A1035 steel after an applied stress of approximately 650 MPa, and the lack of a defined yield point and corresponding yield plateau for ASTM A1035. Yielding strains in ASTM A1035 using the 0.2% offset method are about three times the yielding strains of conventional reinforcing steel.

2.2 Concrete members with high strength reinforcing steel

Research on the performance of concrete members reinforced with high strength reinforcing steel has been mainly focused on the flexural behavior of slender beams.

Malhas (2002) tested 22 slender beams (*a/d* ~ 3.3) under four point bending. All specimens had cross-section 305 mm wide x 457 mm high. Two types of reinforcing steel were used: high strength ASTM A1035 reinforcing steel and normal strength reinforcing steel. Specimens were longitudinally and vertically reinforced either with ASTM A1035 or normal strength steel. These beams were designed using f'_c of 40 MPa and 60 MPa. The reinforcement ratios were between 0.21% and 1.0%. Malhas observed that all specimens exhibited ductile behavior prior to flexural failure. Malhas concluded that ultimate strengths of the beams were accurately predicted using the ACI 318 code theories and that detailing of development length and serviceability deflections appeared adequate using this code. Malhas also observed that after flexural cracking, the stiffness of the beams reinforced with high strength steel reinforcement was significantly reduced compared with the beams reinforced with normal strength steel. Other than the reduction in flexural stiffness, Malhas concluded that the behavior of slender beams using high strength steel were comparable with those beams reinforced with normal strength steel. Therefore, he stated that the direct replacement of regular steel with high strength steel was reasonable for slender beams.

Vijay et al (2002) carried out a project to study the bending behavior of slender beams reinforced with high strength ASTM A1035 steel. The results obtained during the tests were compared with the predictions using ACI 318 code provisions. Four beams were tested under four-point bending with *a/d* of approximately 3.5. Cross section dimensions of 305 mm wide x 457 mm high were similar for all the specimens. Concrete strength varied from 55 MPa to 77 MPa and reinforcement ratios used were between 0.40% and 0.80%. The researchers concluded that theories used in ACI 318 can also be used to predict the flexural capacity of slender beams with high strength reinforcement. Recent work by Yotakhong (2003) supported these conclusions.

Ansley et al (2002) compared the behavior of slender beams reinforced with high strength ASTM A1035 reinforcing steel and similar slender beams reinforced with normal strength reinforcing steel. All specimens had cross-section 305 mm wide x 457 mm high. Two types of reinforcing steel were used, high strength ASTM A1035 reinforcing steel and normal strength reinforcing steel. To compare the flexural behavior of slender beams reinforced with different types of steel (ASTM A1035 and conventional Grade 60), two beams with the same dimensions and different types of reinforcement were tested under four-point bending with *a/d* of 4.0. They also compared the contribution to shear strength of stirrups made with ASTM A1035 and conventional Grade 60 reinforcing steel. For this purpose, two shear-critical beams, one with ASTM A1035 steel stirrups and another with normal strength steel stirrups, were tested under three-point bending with *a/d* of 1.4. For the flexure-critical tests, the authors found that the behavior of the beams up to the yield point of the normal reinforcing steel was similar, regardless of the reinforcement strength. After that point, the load-deflection curve for the beam reinforced with high strength steel maintained the same path. However, for the beam with normal steel, the deflection rates increased, governed by yielding of the main tension reinforcement. At failure, the beam reinforced with high strength steel resisted 76% more applied load and it had 40% more ductility, considered by Ansley as the area under the load-deflection response, than the beam reinforced with normal strength steel. For the beams designed to fail by shear, it was concluded that the high strength steel stirrups played a minor part in the shear capacity of the section, with an increase in capacity of only 9%. However, only one specimen with high strength steel stirrups was tested and additional tests are required to generalize the contribution to shear strength of stirrups made with high strength steel.

The bond behavior of ASTM A1035 steel has also been studied. Modifications of design equations in ACI 318-05 code for development length have been proposed. Section 2.6.4 describes some important conclusions made in bond behavior research and the equations proposed for development length and splice length of ASTM A1035 reinforcing steel.

Limited previous research has examined the performance of non-slender beams where the traditional sectional model assumption of 'plane sections remain plane' does not apply. Due to the importance of this type of member in some concrete structures, it is necessary to investigate their behavior. This project studied the behavior of deep beams reinforced with high strength steel under four-point bending. Practical examples of deep beams with similar type of loadings are transfer girders or bridge pier caps.

The behavior of non slender beams or deep beams cannot be accurately predicted using the traditional sectional methods of design because the Bernoulli bending theory does not apply. Since the axial strain distribution is not linear over the member height in deep beams, alternative design methods are necessary. The most common design method for deep beams is the Strut and Tie Method described in Section 2.4.

2.3 Deep beams

Non-slender beams, or deep beams, are frequently found in reinforced concrete structures. Examples of this type of beam include transfer girders, bridge piers and foundation walls where large concentrated loads are located close to the supports and where the shear-span-to-depth ratio (*a/d*) is less than 2.5. These structural members need special attention in their design due to the development of non-linear strain gradients under loading.

Deep beams are structural members loaded in a way that a significant part of the load transfer to the supports is through direct compression struts or arch action. Generally, a beam is classified as a deep beam according to the overall span to overall depth ratio (*L/h*) or the shear span to depth ratio (*a/d*). Each of the design codes used in this project establishes different limits for these ratios to classify a beam as a deep beam. CSA A23.3-04 considers deep beams as flexural members with $L/h<2$. For ACI 318-05 and Eurocode 2, deep beam design methods apply for $L/h<4$ or for beam regions with $a/d<2$.

Traditional sectional design methods for slender beams, where Bernoulli theory applies, do not accurately predict the behavior of deep beams. It has long been recognized that the strength of beams increases for smaller shear-span-to-depth ratios (*a/d)* [Kani et al., 1979; Varghese and Krishnamoorthy, 1966; Watstein and Mathey, 1958] and that the sectional approaches do not accurately predict the shear capacity of members with $a/d<2.5$ [Collins and Mitchell, 1991; Rogowsky and MacGregor, 1986]. Since the 1960's, there has been strong interest in developing simple but accurate techniques to design and analyze non-slender members, including deep beams. It was necessary then, to find a technique that considered the gain in capacity of the beams for smaller *a/d* ratios. The Strut and Tie Method (STM) gave the designers a very important tool to predict the capacity of deep beams as it considers the capacity as a function of *a/d.* This method analyzes concrete members with a plastic truss analogy that transfers the forces from the loading point to the supports using concrete struts and reinforcement ties [Schlaich et al., 1987; Marti, 1985].

Other parameters that influence the capacity of non-slender beams are the concrete strength and reinforcement ratio [e.g., Selvam and Thomas, 1987; Oh and Shin, 2001].

A comparison between the traditional methods (sectional methods) and the STMs to predict the capacity of beams with different *a/d* ratios was done by Collins and Mitchell (1991), using results from beams tested by Kani [Kani et al., 1979]. This comparison is illustrated in Figure 2-1.

Many design codes (e.g., ACI 318, CSA A23.3, Eurocode 2, ASSHTO LRFD, etc.) have adopted the Strut and Tie Method (STM) as a permitted technique to predict the ultimate capacity of concrete members with non-linear strain distributions. It is a consistent method of design for disturbed regions. Within the limits that each code establishes for the usage of this design method, the STM has been shown to give accurate prediction of the behavior of deep beams [e.g. Collins and Mitchell, 1991; Tan and Lu, 1999; Aguilar et al., 2002; Quintero et al., 2006].

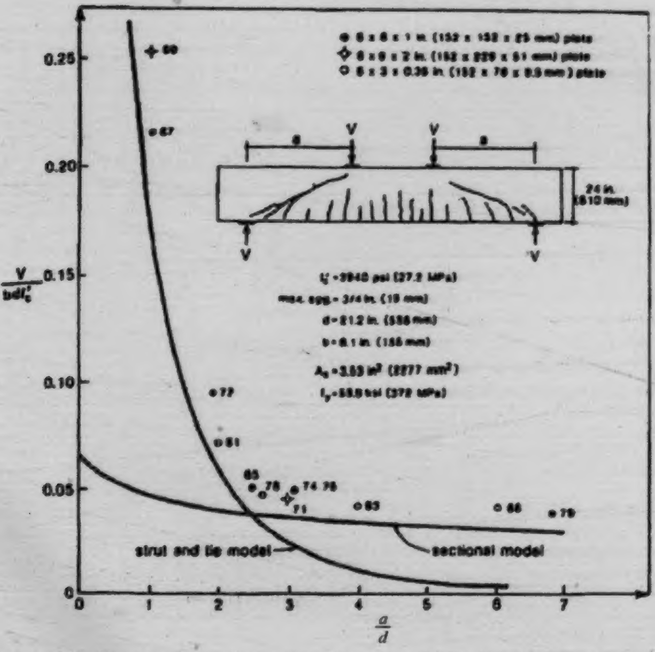

Figure 2-1 Comparison between Strut and Tie Method and Sectional Method [from Collins and Mitchell, 1991]

Other methods for the design of deep beams have been proposed [Zsutty, 1968; Bazant and Kim, 1984; Nielsen, 1998]. The most recent method of design proposed was the Unified Shear Strength Model [Choi et al, 2007], which considers that the overall shear strength of a beam is given by the combined failure mechanism of tensile cracking and crushing of the top compression zone. These methods can be used for design of slender and/or non-slender beams with and without web reinforcement. However, none of these methods have been adopted by current design codes, and are not considered further in this study.

2.4 Strut and Tie Method

Design of concrete members where Bernoulli bending theory applies can be accurately predicted using the traditional sectional methods of design. However, for concrete members with disturbed regions, where the assumption of 'plane sections remain plane' does not apply, the Strut and Tie Method (STM) is probably the most practical and accurate hand calculation technique for design. The STM analyzes concrete members with a plastic truss analogy to internally transfer the applied forces from the loading points to the supports using concrete struts acting in compression and steel reinforcing ties acting in tension [e.g., Schlaich et al., 1987; Marti, 1985]. The struts and ties are interconnected at nodes. The forces in the elements must always satisfy statical equilibrium with the applied loads. Various stress limits are defined for the struts, ties and nodes.

STM are recommended to be used in the design of members with regions with non-linear strain distributions due to geometrical discontinuities, like dapped-end beams, corbels, pile caps or corners of a frame. They are also appropriate at locations of statical discontinuities like deep beams, regions of members near to supports or at concentrated loads (Schlaich et al, 1987).

STM is a lower bound solution approach for capacity, which implies that the actual failure load will be equal to or greater than the calculated failure load. This can be possible if the system has enough ductility to redistribute the force flow within the member when necessary. This redistribution allows the entire system to reach a higher load capacity than the force flow model assumed in the analysis.

Schlaich et al (1987), Marti (1985), Rogowsky and MacGregor (1986) and others have described how the STM can be developed by following an assumed flow path of forces in a region of a structural member. Adoption of STM techniques into design codes has occurred over the last few decades. CSA A23.3-84 was the first North American design code to adopt the STM as a standard design technique of concrete members with disturbed regions, with provisions based on the Compression Field Theory (Collins, 1978). More recently, ACI 318-02 incorporated the STM in its Appendix A. Considerable research has been completed to study the viability of the STM for the design of deep beams using STM provisions given in the codes. Representative research done to study the viability of STM as a design technique for deep beams is described below.

Collins and Mitchell (1991) studied the accuracy of the provisions in the CSA A23.3-84 to predict the behavior of deep beams loaded under four-point bending. Members in the study had web reinforcement and represented different *a/d* ratios. Collins and Mitchell (1991) found that CSA A23.3-84 STM provisions provided accurate predictions of the capacity of deep beams up to *a/d* of about 2.5. Beyond that limit, the predictions were very conservative and it was recommended to use the sectional shear design methods. Figure 2-1 shows the prediction of slender and deep beams using the Strut and Tie Method and the Sectional Method for shear.

Tan and Lu (1999) analyzed twelve deep beams loaded in four point bending using STM techniques. All specimens had the same reinforcement ratio of 2.6% with three different *a/d* ratios: 0.56, 0.84 and 1.13. The concrete strength varied from 41 MPa to 54 MPa. Three of the twelve beams were built without web reinforcement. The design code provisions used to predict the load capacity of the specimens were from CSA A23.3-94, in which the Strut and Tie Method provisions were similar to the current CSA A23.3-04 design code. The researchers concluded that the STM provisions provided uniform safety margins of capacity for deep beams with web reinforcement, since the quality of predictions did not deteriorate with the change in *a/d*. The average test/predicted capacity of specimens with web reinforcement was 1.10. For beams without web reinforcement, the predictions became more conservative for larger *a/d* ratios. The average test/predicted capacity of specimens without web reinforcement was 1.27.

Aguilar et al (2002) studied the accuracy of the Strut and Tie Method given in Appendix A of the ACI 318-02 code in the prediction of four deep beams loaded in four-point bending. Appendix A of ACI 318-02 is similar to the current ACI 318-05 code provisions. The specimens tested had the same reinforcement ratio of 1.2% and same *a/d* of 1.13. Three beams had more than the minimum web reinforcement and one specimen had no horizontal web reinforcement and less than the minimum vertical web reinforcement in the shear span zone specified in Appendix A of ACI 318-02 Code. The capacity of all specimens, despite different failure modes, was within 6% of each other. The researchers found that by using the STM for the analysis, good predictions were obtained with an average test/predicted capacity ratio of 1.26.

Quintero et al (2006) studied the adequacy of the strut strength factors described in the Appendix A of ACI 318-05 to be used with STM. Twelve beams with the same reinforcement ratio and concrete strengths from 22 MPa to 50MPa were tested. Different *a/d* ratios from 0.66 to 1.15 and different web reinforcement ratios were also considered. They concluded that the strut strength factors given in the ACI 318-05 code for normal strength concrete bottle shaped struts crossed by either minimum transverse reinforcement or no reinforcement are adequate.

For non-slender beams with normal strength concrete, normal strength reinforcement and minimum web reinforcement ratios, the reduction factors for strut strength established in the ACI 318-05 and CSA A23.3-04 codes for the STM technique have been shown to give safe predictions of capacity [e.g. Collins and Mitchell, 1991; Tan and Lu, 1999; Aguilar et al., 2002; Quintero et al., 2006]. However, it is important to consider the adequacy of those reductions factors in the design of deep beams reinforced with high strength steel reinforcement using Strut and Tie Method. Strain conditions of the reinforcement and differences in dowel action are the principal parameters that differentiate the behavior of the strut between beams reinforced with normal steel and those reinforced with high strength steel. In ACI 318-05, the strut strength reduction factors account for parameters that affect the strut strength including concrete strength, transversal reinforcement arrangements (when applicable), strain conditions of reinforcement, dowel action and uncertainties in the truss model [Quintero et al, 2006 and Aguilar et al, 2002]. However, these reduction factors have an empirical origin based on research completed for concrete members reinforced with normal strength steel. In CSA A23.3-04, the strut strength reduction factor takes into consideration the strain conditions of reinforcement crossing the struts, but they omit direct consideration of the effect of dowel action.

2.4.1 Elements of a Strut and Tie Model

A Strut and Tie Model is a truss-model representation of a reinforced concrete member (or region) consisting of concrete struts acting in compression and steel reinforcing ties acting in tension. The struts and ties are interconnected at nodes. The forces in the elements must always satisfy statical equilibrium with the applied loads. The overall principles of the Strut and Tie Model technique or Strut and Tie Method, described in Section 2.4, are the same for the three sets of code provisions used in this project (CSA A23.3-04, ACI 318-05 and Eurocode 2). However, differences exist in the strength reduction factors that each code method assigns for the elements of the Strut and Tie Model. Section 2.5 describes the provisions for STM given by CSA A23.3-04, ACI 318-05 and Eurocode 2.

2.4.1.1 Struts or compression stress fields

The struts or compression stress fields can be prismatic, bottle shaped or fan shaped [Schlaich, 1987]. In the prismatic strut, the stress field remains parallel along the axis of the strut and it has a uniform cross section over the strut length. In the fan shaped stress field, the width of the stress field at each end will vary. No transverse stresses are developed in a fan shaped stress field, since the flow of stresses is along the radial direction of the fan. In bottle shaped stress fields, the width of the strut at its mid-length location can be larger than the stress field width at the ends. Thus, transverse stresses can occur. Figure 2-2 illustrates the different types of compression stress fields.

In design, the dimensions of the struts should ensure that the stresses in the strut are smaller than the maximum effective compressive strength of the concrete.

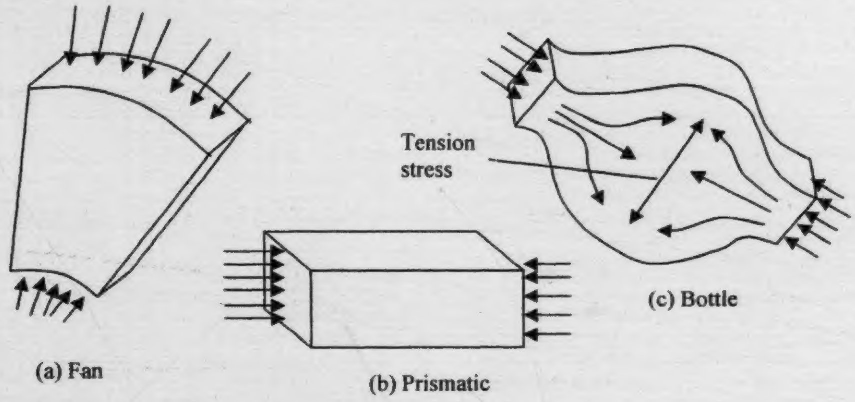

Figure 2-2 Basic compression stress fields or struts

2.4.1.2 Ties

The ties in a Strut and Tie model are composed of the reinforcing steel and the portion of concrete bonded to the steel that works in tension. However, in practical design, the concrete surrounding the reinforcing steel is ignored when determining the tensile resistance of the tie.

2.4.1.3 Nodes

Nodes are the points where the forces are transferred between the struts and ties or where struts and ties intersect. The classification of the nodes is given according to the forces that they connect, developing four different states of stress in the nodal zone, as CCC, CCT, CTT and TTT nodes [Schlaich, 1987].

A node that connects only compressive forces is called **CCC** node. **CCT** is a node under the action of one tension force and two (or more) compression forces. A **CTT** node connects one compression force and two (or more) tension forces. Finally, the node under tension forces only is called **TTT** node. Figure 2-3 illustrates the different types of nodes.

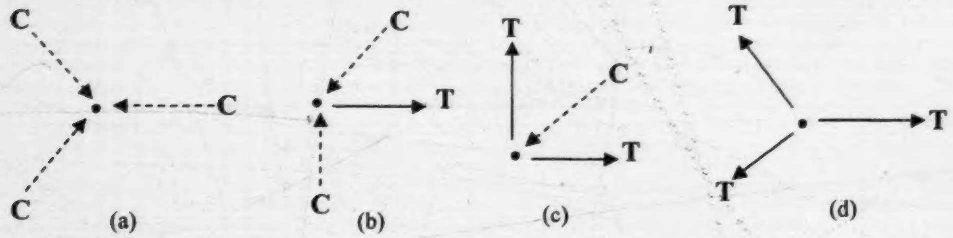

Figure 2-3 Classification of nodes (a) CCC node, (b) CCT node, (c) CTT node and (d) TTT node

The regions around the nodes are called **nodal zones.** These regions can be classified as hydrostatic nodal zones or non-hydrostatic nodal zones. In a hydrostatic nodal zone, the stresses on all the loaded faces of the node are equal and the axis of the struts and/or ties are perpendicular to the loaded faces. For a non-hydrostatic nodal zone, the stress taken on a surface perpendicular to the strut axis must be determined. An extended nodal zone can be used for the analysis of the stresses in the region, including determination of reinforcement anchorage requirements. The ACI 318-05 Code defines a nodal zone as “a portion of a member bounded by the intersection of the effective strut width w_s and the effective tie width w_t.”[ACI Committee 318, 2005]. Examples of hydrostatic and extended nodal zones formed at the supports of deep beams are illustrated in Figure 2-4.

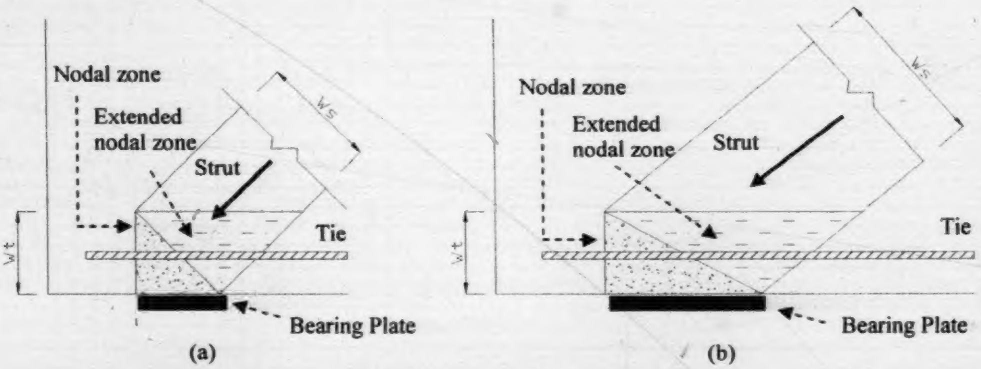

Figure 2-4 Nodal zones (a) hydrostatic and (b) extended nodal zone

2.4.2 Modes of failure

The STM is a method for evaluating the ultimate limit state of a member. Therefore, during the analysis or design of concrete elements, different modes of failure can be assumed. The predicted ultimate capacity of a concrete member designed by STMs will be governed by crushing of the struts, yielding of the tension ties, failure of the nodes by reaching stresses larger than the allowable nodal stresses, or by anchorage failure of the reinforcement.

2.4.3 Configurations for Strut and Tie Models

For a given planar deep beam with concentrated loads, different admissible configurations of Strut and Tie Models can be developed. These configurations, shown in Figure 2-5 and described in the following sections, are classified herein as the Direct Strut and Tie Model (STM-D), the Indirect Strut and Tie Model (STM-I) and the Combined Strut and Tie Model (STM-C).

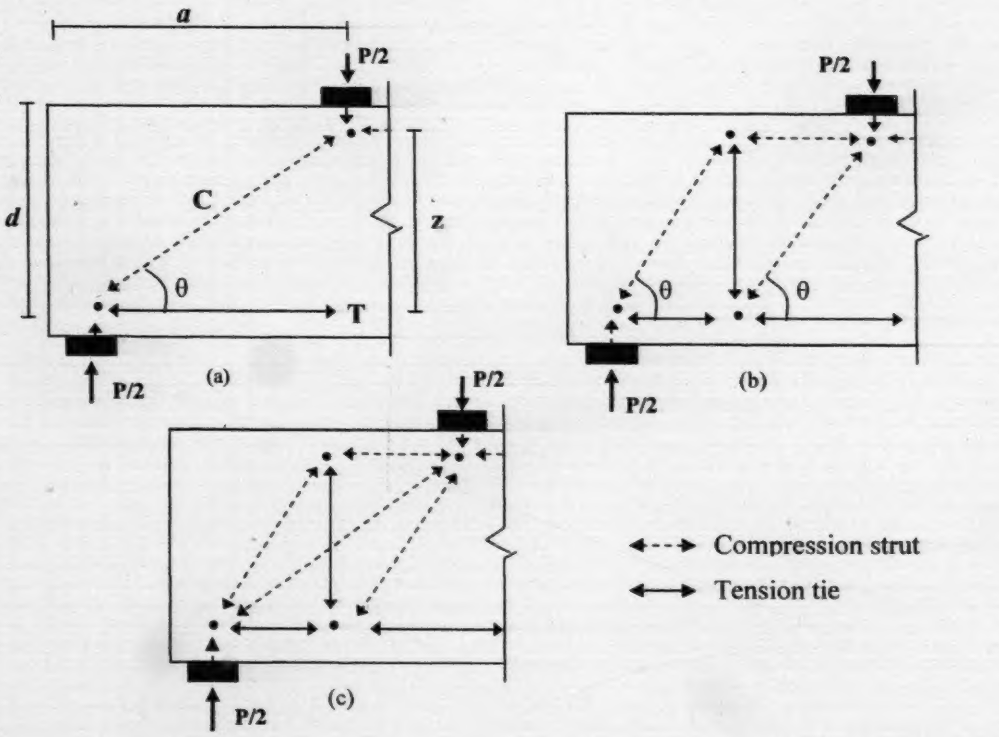

Figure 2-5 (a) Direct strut and tie model, (b) indirect strut and tie model and (c) combined strut and tie model

2.4.3.1 Direct Strut and Tie Model

In the design of simply supported deep beams subject to two concentrated loads, several ways to present the stress flows can be done. The simplest configuration to represent the flow of the forces using a Strut and Tie Model consists of three compression struts and a tension tie (see Figures 2-5a and 2-6). One horizontal compression strut is located between the loading points and the other two struts are diagonally-oriented from the loading points to the supports. The tension tie goes from support to support. The location of the tension tie is at the centroid of the line of action of the reinforcement. For this project, this model is called Direct Strut and Tie Model (STM-D). All assumptions considered in capacity predictions according to the STM-D model are presented in Chapter 6.

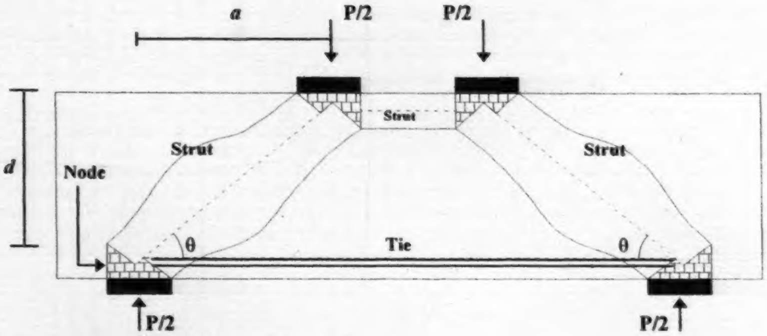

Figure 2-6 Direct Strut and Tie Model

2.4.3.2 Indirect Strut and Tie Model

In this model, the forces are transmitted from the loading point to the support through a series of parallel diagonal compression struts and associated ties. Two assumptions must be satisfied. No strut is developed directly from the loading point to the support and the vertical ties must have enough capacity to return the vertical component of the strut forces to the top of the member. The form of this model could include multiple panels within the truss configuration. Analysis in this project utilized two-panel truss models. This model is called Indirect Strut and Tie Model (STM-I) (see Figure 2-5b).

2.4.3.3 Combined Strut and Tie Model

In this Strut and Tie Model, the primary shear strength comes from a truss developed from the contribution of the vertical web reinforcement, similar to STM-I. After yielding of the vertical web reinforcement, additional load is also taken by the direct diagonal strut going from the loading points to the supports. For this project, this model is called Combined Strut and Tie Model (STM-C), See Figure 2-5c. Since this model reflects the combination of two simpler models, special attention is required in the areas of overlapping stresses, to avoid stress concentration in the nodes beyond the stress limits.

Only the ACI 318-05 code directly mentions in Commentary RA.2.3, how to analyze the nodal zones when they are subject to more than three forces. ACI 318-05 suggests resolving some of the forces to end up with three intersecting forces. This criterion was used to analyze the deep beams in this project using the Combined Strut and Tie Model for the three design codes (ACI 318-05, CSA A23.3-04 and Eurocode 2).

2.4.4 Selection of a Strut and Tie Model for practical design or analysis

The traditional Strut and Tie Model selected by researchers to study the accuracy of codes provisions in the prediction of failure loads for deep beams is the Direct Strut and Tie Model [e.g., Quintero et al., 2006; Aguilar et al., 2002; Tan and Lu, 1999]. This model has been selected because it is the simplest configuration to describe the flow of forces in deep beams. However, other models have been proposed to give improved prediction ability, with the model selection usually based on *a/d* ratios.

Foster and Gilbert (1998) proposed the selection of different strut and tie models for design based on the shear span to internal lever arm ratios (*a/z*), where "*z*" is the flexural lever arm that would typically be 0.85*d* to 0.9*d*. They suggested the use of the Direct Strut and Tie Model for $a/z<1$, the Combined Strut and Tie Model for $1< a/z <\sqrt{3}$ and the Two Panel Truss Model (i.e. STM-I) for $a/z>\sqrt{3}$. Figure 2-5 shows the three different strut and tie models mentioned by Foster and Gilbert (1998).

Brown et al (2006) studied the contribution of the transverse reinforcement towards the capacity of deep beams. The authors analyzed test results for 494 specimens contained in an assembled database with *a/d* between 0.2 and 9.7. For the analysis, the researchers used the Strut and Tie Method. They compared the accuracy in predictions of the three Strut and Tie Models mentioned in Section 2.4.3. The observations indicated that for $a/d<0.7$ the Direct Strut and Tie Model is the most appropriate to use since only the direct strut from the loading point to the support forms and contributes to the capacity of the beam. For $0.7< a/d <1.7$, the contribution of the vertical reinforcement became more important but the Direct Strut Mechanism was still the dominant contributor to the beam capacity. Finally, for $a/d > 1.7$ the two panel strut and tie model started to dominate due to a larger contribution of the web reinforcement, not only in crack control but also for carrying the vertical loads.

2.5 Code provisions for Strut and Tie Method

The design of concrete structures using the Strut and Tie Method is allowed by the three design codes (CSA A23.3-04, ACI 318-05 and Eurocode 2) examined in this study. Each design code method is used to predict the behavior of the deep beams tested in this project. Provisions for design of nodes, struts, ties, web reinforcement and development lengths are discussed for each code.

2.5.1 CSA A23.3-04

CSA A23.3-04 states that a flexural member with clear span to overall depth ratio less than 2 must be designated as a deep flexural member and in its design, a non-linear distribution of strains should be taken into account. According to the provisions in this code, the Strut and Tie Method is an appropriate method to design deep flexural members.

The Saint Venant's Principle states that the difference between the stresses caused by statically equivalent load systems is insignificant at distances greater that the largest dimension of the area over which the loads are acting. Based in this principle, CSA A23.3-04 also suggests the STM for design of disturbed regions. Thus, according to this statement, a beam with a shear span to overall depth ratio less than two can be designed using STM. All the beams tested in this project fit into this criterion.

According to CSA A23.3-04 code provisions, the **strength of the strut** is limited by the effective compressive stress of the concrete f_{ce} which is calculated with Equation (2.1). f_{ce} is based on the Modified Compression Field Theory relationships [Vecchio and Collins, 1986].

$$f_{ce} = \frac{f'_c}{0.8 + 170\varepsilon_1} \leq 0.85 f'_c \tag{2.1}$$

where ε_1 is calculated with Equation (2.2)

$$\varepsilon_1 = \varepsilon_s + (\varepsilon_s + 0.002)\cot^2\theta_s \qquad (2.2)$$

θ_s = smallest angle between the compressive strut and the adjoining tensile ties

ε_s = tensile strain in the tie inclined at θ_s to the compressive strut

The expression for ε_1 assumes that the principal compressive strain ε_2 in the direction of the strut is equal to -0.002 mm/mm, which corresponds to the strain at peak compressive stress of the concrete. ε_1 is also affected by the strains in the reinforcement. Note that the use of ASTM A 1035 reinforcing steel may develop higher values of ε_s than similar beams using normal strength steel with the same axial force capacity. Hence, the strength of the diagonal struts designed by CSA A23.3-04 is sensitive to the selected reinforcement type.

In Equation (2.2), larger values for θ_s will result in smaller values of ε_1 and higher values of f_{ce}. Even though no limitations for θ_s are mentioned in CSA A23.3-04, the practical range of θ_s is from 25° to 65° [Rogowsky and MacGregor, 1986].

In CSA A23.3-04, the effective compressive strength of the concrete struts should be multiplied by a resistance factor (ϕ_c) equal to 0.65. In this research project, this resistance factor was not considered.

In **nodal zones**, CSA A23.3-04 has established the following stress limits for concrete:

$0.85\phi_c f'_c$ in node regions bounded by compressive struts and bearing areas (CCC node)

$0.75\phi_c f'_c$ in node regions anchoring a tension tie in only one direction (CCT node)

$0.65\phi_c f'_c$ in node regions anchoring more than one tension tie (CTT or TTT node)

The strength in the **tension tie** according to CSA A23.3-04 is limited by the yield capacity of the tie. Thus, the maximum stress should be taken as $\phi_s f_y$, where $\phi_s = 0.85$.

The **anchorage of the tension tie** reinforcement must be able to resist the calculated tension stresses at the inner edge of the extended nodal region. The anchorage or development length (l_d) of the reinforcement can be designed using the general development length equation (Equation (2.3)) and/or using the simplified development length equation (Equation (2.5)).

The *general development length* in CSA A23.3-04 is given by Equation (2.3)

$$l_d = 1.15\frac{k_1k_2k_3k_4}{(d_{cs}+K_{tr})}\frac{f_y}{\sqrt{f'_c}}A_b, \qquad (d_{cs}+K_{tr}) \le 2.5d_b \tag{2.3}$$

where

k_1= bar location factor: 1.3 for horizontal reinforcement placed in such a way that more than 300 mm of fresh concrete is cast in the member below the development length or splice; 1.0 for other cases.

k_2= coating factor: 1.5 for epoxy coated reinforcement with clear cover less than $3d_b$, or with clear spacing between bars being developed less than; 1.2 for all other epoxy-coated reinforcement; 1.0 for uncoated reinforcement.

k_3= concrete density factor: 1.3 for structural low density concrete; 1.2 for structural semi-low-density concrete; 1.0 for normal-density concrete.

k_4 =bar size factor: 0.8 for 20M and smaller bars and deformed wires; 1.0 for 25M and larger bars.

The product k_1k_2 needs not to be taken greater than 1.7.

K_{tr}= factor that represents the contribution of transverse reinforcement across potential planes of splitting, given by:

$$K_{tr} = \frac{A_{tr}f_{yt}}{10.5sn} \tag{2.4}$$

A_{tr} =total cross sectional area of reinforcement that is within spacing s and crosses the potential plane of bond splitting through the reinforcement being developed.

s = maximum center to center spacing of transverse reinforcement within l_d.

n = number of bars or wires being spliced or developed along the potential plane of bond splitting.

CSA A23.3-04 also includes simplified development length equations to calculate the development. These equations can be used when clear cover and clear spacing of the bars or wire being developed are at least d_b and $1.4d_b$, respectively.

Equation (2.5) can be used for members containing minimum ties or minimum stirrups within l_d. Also, it can be used for slabs, walls, shells, or folded plates having clear spacing of not less than $2d_b$ between bars being developed.

$$0.45k_1k_2k_3k_4\frac{f_y}{\sqrt{f'_c}}d_b \tag{2.5}$$

Equation (2.6) is used for any other cases.

$$0.6k_1k_2k_3k_4\frac{f_y}{\sqrt{f'_c}}d_b \tag{2.6}$$

The **minimum web reinforcement** established by CSA A23.3 for deep flexural members is 0.2% of the gross concrete area in horizontal and vertical direction. An orthogonal grid of reinforcement should be located near to each face of the deep beam and the spacing of this reinforcement should not exceed 300 mm in each direction.

2.5.2 ACI 318-05

The definition of a deep beam in ACI 318-05 is different from the definition given by the CSA A23.3-04 code. In ACI 318-05, the definition is based in the Saint Venant's principle. ACI 318-05 defines a Deep Beam as "a member loaded on one face and supported on the opposite face so that compression struts can develop between the loads and the supports, and have either: (a) clear spans, l_n, equal to or less than four times the overall member depth; or (b) regions with concentrated loads within twice the member depth from the face of the support"[ACI Committee 318, 2005]. ACI 318-05 suggests the use of STM to design these types of concrete members.

The STM provisions are included in Appendix A of ACI 318-05. Their use for the design of deep beams is limited to members with an angle between the diagonal compression strut and the tension tie not less than 25°.

CSA A23.3-04 uses different resistance factors for the design of the Strut and Tie Model elements (ϕ_c=0.65, ϕ_s=0.85). However, in ACI 318-05, a general STM resistance factor (ϕ_{STM}) of 0.75 can be used for all the elements. The strut, node and tie calculations described below are used to arrive at a nominal capacity, which is reduced according to the factor ϕ_{STM}.

The compressive **strength of a strut** without longitudinal reinforcement should be taken as the smaller value of effective compressive strength of the concrete in the strut or the effective compressive strength of the concrete in the adjacent nodal zone.

According to ACI 318-05, the strength of a strut depends on the geometry of the strut, and the presence or omission of distributed reinforcement crossing the strut. The effective compressive strength of the concrete in a strut is calculated with Equation (2.7).

$$f_{ce} = 0.85\beta_s f'_c \tag{2.7}$$

where

β_s=1.0 for struts with uniform cross section area over its length, 0.75 for bottle-shaped struts with distributed reinforcement crossing and 0.60 for bottle-shaped struts without distributed reinforcement crossing. 0.40 is used for struts in tension members or the tension flanges of members.

The compression strength of **nodal zones** is calculated with Equation (2.8).

$$F_{nn} = f_{cen} A_{nz} \tag{2.8}$$

where:

A_{nz}= smaller of (1) area between the area of the face of the nodal zone perpendicular to the load acting on that face, and (2) the area of a section through the nodal zone perpendicular to the resultant force on the section.

f_{cen}= effective compressive strength of the concrete in the nodal zone. It is calculated with equation (2.9).

$$f_{cen} = 0.85\beta_n f'_c \tag{2.9}$$

Where

β_n=1.0 for nodal zones bounded by struts or bearing areas or both (CCC nodes), 0.80 for nodal zones anchoring one tie (CCT nodes) and 0.60 for nodal zones anchoring more than one tie (CTT node).

The strength in non-prestressed **tension ties** in ACI 318-05 is taken as $f_{ut} = f_y$, with a f_y limit of 550 MPa for longitudinal reinforcement and 410 MPa for shear reinforcement.

The **anchorage or development length** (l_d) of the tension tie reinforcement required to resist the tension stress at the inner edge of the node region can be calculated using the appropriate equation from Table 2-1 or Equation (2.10). Note that these equations are provided in U.S. Customary units of ksi and inches.

Table 2-1 Development length of the bars in tension for ACI 318-05

	No. 6 and smaller bars and deformed wires	N0. 7 and larger bars
Clear spacing of bars or wires being developed or spliced not less than d_b, clear cover not less than d_b, and stirrups or ties throughout l_d not less than the code minimum or clear spacing of bars or wires being developed or spliced not less than $2d_b$ and clear cover not less than d_b	$\left(\frac{f_y\psi_t\psi_e\lambda}{25\sqrt{f'_c}}\right)d_b$	$\left(\frac{f_y\psi_t\psi_e\lambda}{20\sqrt{f'_c}}\right)d_b$
Other cases	$\left(\frac{3f_y\psi_t\psi_e\lambda}{50\sqrt{f'_c}}\right)d_b$	$\left(\frac{3f_y\psi_t\psi_e\lambda}{40\sqrt{f'_c}}\right)d_b$

$$l_d = \left(\frac{3}{40}\frac{f_y}{\sqrt{f'_c}}\frac{\psi_t\psi_e\psi_s\lambda}{\left(\frac{c_b+k_{tr}}{d_b}\right)}\right)d_b, \left(\frac{c_b+k_{tr}}{d_b}\right) \le 2.5 \tag{2.10}$$

where

$$k_{tr} = \frac{A_{tr}f_{yt}}{1500sn} \tag{2.11}$$

s = maximum center to center spacing of transverse reinforcement within l_d

n = number of bars or wires being spliced or developed along the plane of splitting.

ψ_t=1.3 where horizontal reinforcement is placed such that more than 12 in. of fresh concrete is cast below the development length or splice; 1.0 for other situations.

ψ_e=1.5 for epoxy-coated bars or wires with cover less than $3d_b$ or clear spacing less than $6d_b$; 1.2 for all the epoxy-coated bars or wires; and 1.0 for uncoated reinforcement.

The product $\psi_t\psi_e$ should not be greater than 1.7

ψ_s=0.8 for No. 6 and smaller bars and deformed wires; 1.0 for No. 7 and larger bars.

λ=1.3 for lightweight concrete. λ can be calculated as $\frac{6.7\sqrt{f'_c}}{f_{ct}} \leq 1.0$ when f_{ct} is specified. For normal weight concrete λ should be taken as 1.0.

The **web reinforcement** requirements in ACI 318-05 establishes that to use the reduction factors β_s for struts with reinforcement (i.e. β_s=1.0 or β_s=0.75), the axis of the struts should be crossed by reinforcement that helps to resist the compression and tension forces developed in the strut. The layers of reinforcement crossing the struts should satisfy Equation (2.12). If the reinforcement does not satisfy these minimum reinforcement requirements, β_s should be taken as 0.60.

$$\sum \frac{A_{si}}{b_s S} \sin \alpha_i \geq 0.003 \qquad \textbf{(2.12)}$$

A_{si} = total area of surface reinforcement at spacing S in the $i-th$ layer for reinforcement crossing a strut at an angle α_i to the axis of the strut.

2.5.3 Eurocode 2 (EN 1992-1-1)

Section 6 of Eurocode 2 (EN 1992-1-1) mentions that the discontinuity regions of beams and other members where Bernoulli theory does not apply can be designed using Strut and Tie Models. This means that the conceptual definition of a deep beam is similar to the concept given by ACI 318-05. It also mentions that STMs can be used for members where a linear distribution within the cross section is assumed.

The design **strength of a concrete strut** in EN 1992-1-1 is calculated using Equation (2.13) or Equation (2.14) in SI units.

Equation (2.13) is used for the design strength of struts without transverse tension stress. Equation (2.14) is used for the design strength of concrete struts in cracked compression zones with transverse tension stress. Figure 2-7 shows struts with and without transverse tension stress

In design of deep beams, no limits in the angle between the diagonal compression strut and the tension tie are mentioned in Eurocode 2..

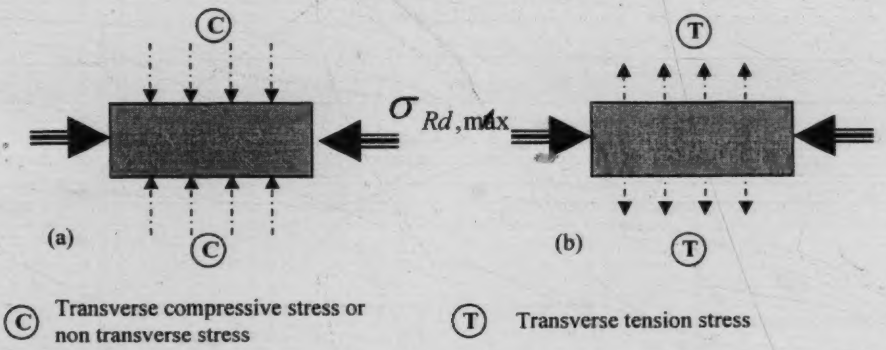
Ⓒ
$\sigma_{Rd,max}$
Ⓣ
(a)
Ⓒ
(b)
Ⓣ
Ⓒ Transverse compressive stress or non transverse stress
Ⓣ Transverse tension stress

Figure 2-7 (a) Strut without transverse tension stress, (b) Strut with transverse tension stress

$$\sigma_{Rd,\max} = f_{cd} \tag{2.13}$$

$$\sigma_{Rd,\max} = 0.6\nu f_{cd} \tag{2.14}$$

Where

$$\nu = 1 - \frac{f_{ck}}{250}$$

f_{ck} = Characteristic compressive strength (f'_c)

$$f_{cd} = \frac{\alpha_{ct} f_{ck}}{\gamma_c}$$

α_{ct} = is a coefficient taking account of long term effects on the tensile strength and of unfavorable effects, resulting from the way the load is applied. The recommended value is 1.0.

γ_c = partial safety factor. 1.5 for persistent and transient and 1.2 for accidental loads.

The design strength of the **Nodal Zones** in EN 1992-1-1 is determined by:

$\sigma_{Rd,\max} = k_1 v f_{cd}$ for node regions where no ties are present (CCC node)

$\sigma_{Rd,\max} = k_2 v f_{cd}$ for node regions with anchored ties in one direction (CCT node)

$\sigma_{Rd,\max} = k_3 v f_{cd}$ for node regions with anchored ties provided in more than one direction (CTT node)

According to EN 1992-1-1, the recommended values for the k factors are: k_1 = 1.0, k_2 = 0.85, and k_3 = 0.75

The design **strength of tension ties** is based on:

$$f_{yd} = \frac{f_{yk}}{\gamma_s}$$

γ_s = partial factor for steel. 1.15 for persistent and transient loads and 1.0 for accidental loads.

f_{yk} = yield stress

The **anchorage of the tension tie** reinforcement should be able to resist the calculated tension stresses at the inner edge of the node region. The anchorage or development length (l_d) is calculated with Equation (2. 15) , in SI units.

$$l_{bd} = \left(\frac{\phi}{4}\right)\left(\frac{\sigma_{sd}}{f_{bd}}\right) \tag{2. 15}$$

Where:

ϕ = bar diameter

σ_{sd} = design stress at the inner edge of the node region

$f_{bd} = 2.25\eta_1\eta_2 f_{ctd}$

η_1 = coefficient related to the quality of the bond condition and the position of the bar during concreting. 1.0 when good conditions are obtained; 0.7 for all other cases and for bars in structural elements built with slip-forms, unless it can be shown that good bond conditions exist.

η_2 = is related to the bar diameter: 1.0 for $\phi \leq 32mm$ and $\frac{(132-\phi)}{100}$ for $\phi > 32mm$

f_{ctd} = design value of concrete tensile strength

$f_{ctd} = \frac{\alpha_{ct} f_{ctk,0.05}}{\gamma_c}$

α_{ct} =1.0. Coefficient taking account of long term effects on the tensile strength and of unfavorable effects, resulting from the way the load is applied.

The ratio of **minimum web reinforcement** must be calculated with Equation (2.16).

$$\rho_w = \frac{A_{sw}}{sb_w \sin\alpha} > \frac{\left(0.08\sqrt{f_{ck}}\right)}{f_{yk}} \tag{2.16}$$

where:

A_{sw} = area of shear reinforcement within length s

s = spacing of shear reinforcement measured along the longitudinal axis of the member

b_w = is the width of the member web

α = angle between shear reinforcement and the longitudinal axis

2.5.4 Comparison of Code Provisions for Strut and Tie Method

The behaviour of deep beams depends of several parameters including *a/d* ratio, main reinforcement ratio, influence of web reinforcement and the concrete strength. Each design code considers the influence of these parameters in a different manner. The major differences are briefly described.

The CSA A23.3-04 STM provisions directly consider a decrease in strut strength as the angle between the struts and ties decreases. Furthermore, CSA A23.3-04 STM provisions directly consider a decrease in strut capacity due to increased strains in the reinforcement that crosses the strut. ACI 318-05 does not directly consider the angle of the strut with respect to the tie, nor the strain in the reinforcement, in the calculation of strut strength. Instead, the same empirical strut capacity factors apply to all struts, and the smallest strut-to-tie angle is limited to values larger than 25°. Note that the empirical reduction factors used in ACI 318-05 may also account for other parameters that affect the shear resistance of deep beams like the dowel action of the longitudinal reinforcement and the effect of web reinforcement [Quintero et al., 2006 and Aguilar et al., 2002]. Eurocode 2, as ACI 318-05, does not directly consider the angle of the strut with respect to the tie, nor the strain in the reinforcement, in the calculation of strut strength, but the strut efficiency factors are smaller than those in ACI 318-05. Eurocode 2 and CSA A23.3-04 do not consider the case of struts without web reinforcement, hence the design of deep beams without web reinforcement is not permitted. On the other hand, ACI 318-05 Code allows the design of deep beams without web reinforcement.

The efficiency factors used for CSA A23.3-04, ACI 318-05 and Eurocode 2 to calculate the strength of reinforced struts are based on minimum web reinforcement quantities, which vary slightly between the codes. However, for the most common STM used in the design of deep beams (i.e., STM-D), additional strength obtained from the use of higher web reinforcement ratios would not be considered.

Every code uses different resistance factors; CSA A23.3-04 and Eurocode 2 assign different resistance factors to concrete struts and to steel ties, while ACI 318-05 uses a common resistance factor for all concrete struts and steel tie elements. In this project, all the resistance factors used in the analysis of the specimens were taken as 1.0.

2.6 ASTM A1035 reinforcing steel

ASTM A1035 reinforcing steel is a material that exhibits different mechanical properties than conventional Grade 400R steel reinforcement. ASTM A13035 is stronger, more ductile, tougher and is significantly more corrosion resistant than conventional steel [El-Hacha and Rizkalla, 2002 and Darwin et al, 2002]. This reinforcing steel was formerly called MMFX2 reinforcing steel, prior to an ASTM standardization process. Some differences in the mechanical properties of MMFX2 and steel conforming to the ASTM A1035 standard may exist, but they are considered minor in the context of this project and would be accounted for through the use of coupon test results for the properties.

2.6.1 Tensile properties

El-Hacha and Rizkalla (2002) completed tension coupon tests for three bar sizes (U.S. #4, #6 and #8) of ASTM A1035 reinforcing steel. Test results showed that the modulus of elasticity for ASTM A1035 steel is the same as that of Grade 400R reinforcing steel, at approximately 200 000 MPa. As ASTM A1035 does not have a defined yield point and corresponding yield plateau, the yield strength needs to be determined using the 0.2% offset, 0.5% strain and 0.7% strain methods. The overall average effective yield strength for the bars tested by El-Hacha and Rizkalla using the 0.2% offset, 0.5% strain and 0.7% strain methods were 818 MPa, 750 MPa and 851 MPa respectively. The strain at the 0.2% offset yield strength was 0.0062 mm/mm. The ultimate tensile strength was 1190 MPa with a strain at ultimate stress of 0.05 mm/mm. At failure, the strain was approximately 0.12 mm/mm.

Figure 2-8 illustrates the difference in the strain-stress response of MMFX2 similar to ASTM A 1035 and Grade 400R reinforcing steels.

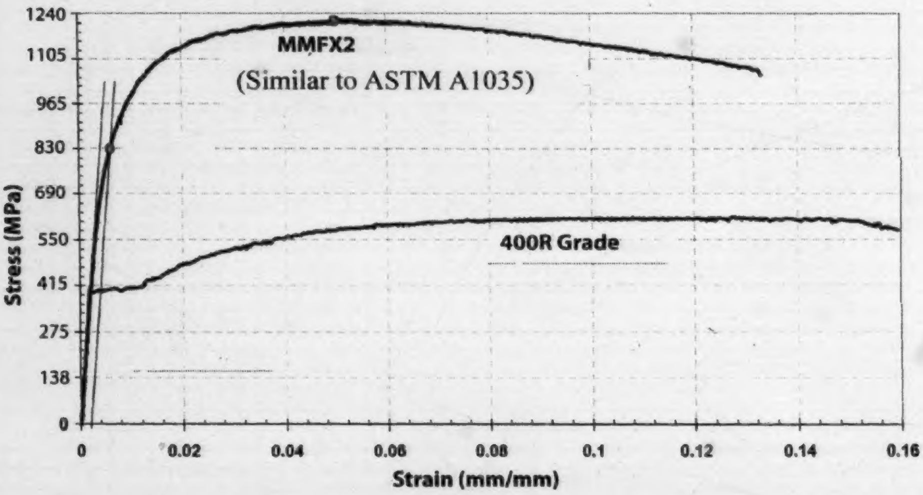

Figure 2-8 Stress-strain curves for ASTM A1035 and 400R grade reinforcing steel bars [After El-Hacha and Rizkalla, 2002]

To predict the strain-stress behavior of ASTM A1035 reinforcing bars, Vijay et al (2002) proposed Equations (2.17) and (2.18).

$$\sigma = 1131.084\left[1-e^{-182.058\varepsilon}\right] \text{ for U.S. \#4 bar size} \tag{2.17}$$

$$\sigma = 1192.662\left[1-e^{-168\varepsilon}\right] \text{ for U.S. \#8 bar size} \tag{2.18}$$

where:

$\sigma =$ tensile stress in the bar in MPa

$\varepsilon =$ % strain

However, Vijay et al (2002) indicated that more research was required to establish a general equation for the prediction of the strain-stress response of the ASTM A1035 bars.

Yotakhong (2003) proposed Equation (2. 19) to predict the strain-stress response of ASTM A1035 bars #6.

$$\sigma = 1220.238\left[1-e^{-185\varepsilon}\right] \text{ for bars \#6} \tag{2. 19}$$

where

σ = tensile stress in the bar in MPa

ε = % strain

2.6.2 Compression strength

The modulus of elasticity in compression for the #4, #6 and #8 ASTM A1035 reinforcing bars tested by El-Hacha and Rizkalla (2002) was 200 000 MPa. The average yield strength using the 0.2% offset, 0.5% strain and 0.7% strain method was 815 MPa, 750 MPa and 852 MPa respectively. The average yield strain (0.2% offset) measured was 0.007. The Poisson's ratio was 0.26.

2.6.3 Shear strength

The results of the #4, #6 and #8 ASTM A1035 rebars tested by El Hacha and Rizkalla (2002) showed that the average shear strength was 762 MPa. The average shear modulus of rigidity was 79 235 MPa.

2.6.4 Bond strength

El-Hacha and Rizkalla, 2002, tested three specially designed reinforced concrete specimens of T-section configuration to evaluate the bond strength and development length of ASTM A1035 reinforcing steel bars. Three bar sizes (# 4, #6, and #8) were used and different embedment length of about 8d$_b$, 18d$_b$, 38d$_b$, 58d$_b$, 78d$_b$ and 98d$_b$ were provided. Tension was applied to the bars using a hydraulic jack. According to test results [El-Hacha and Rizkalla, 2002], the ACI 318-99 Code predicted conservative development lengths by a factor of two using Equations (2. 20) and (2. 21).

$$l_d = \left(\frac{\alpha\beta\lambda f_y}{25\sqrt{f'_c}} \right) d_b \text{ for bars #6 and smaller} \tag{2. 20}$$

$$l_d = \left(\frac{\alpha\beta\lambda f_y}{20\sqrt{f'_c}} \right) d_b \text{ for bars greater than #6} \tag{2. 21}$$

where

α = reinforcement location factor. 1.3 for horizontal reinforcement so placed than more than 12 in. of fresh concrete is cast in the member below the development length.

β=Coating factor. 1.0 when uncoated reinforcement is used.

λ=lightweight aggregate concrete factor. 1.0 when normal weight concrete is used.

Recently, El-Hacha et al (2006) studied the required bond length of ASTM A1035 bars for beam-end specimens. A total of four beam-end specimens reinforced with ASTM A1035 and with nominal dimension of 356 mm wide, 508 mm high, and 2032 mm long were tested. Tension was applied to the bars using a hydraulic jack. Test results indicated that the prediction given by ACI 318-02 provisions were conservative using the confinement limitation of concrete and transverse reinforcement surrounding the bonded length imposed by the code. They also studied tension splice length requirements for ASTM A 1035 reinforcing bars and found that for stress levels in reinforcement more than 550 MPa, the splice length calculated using ACI 318-02 code provisions becomes unconservative. The authors proposed a modified splice length equation (in SI units):

$$l_d = \left(\frac{\dfrac{f_y}{\sqrt{f'_c}} - 51}{\dfrac{4}{9}\left(\dfrac{c'_{min} + 0.5d_b + k_{tr}}{d_b} \right)} \right) d_b \qquad \textbf{(22)}$$

Where

$k_{tr} = \dfrac{A_{tr} f_{yt}}{556sn}$

c'_{min} =minimum of concrete covers surrounding bar or half clear spacing between bars, minimum of C_{si} and (C_b or C_{so})

C_{si}=half clear spacing between splice bars

C_b=thickness of clear bottom concrete cover

C_{so}=thickness of clear side concrete cover

d_b= nominal diameter of steel bar

2.7 Summary

The mechanical properties of ASTM A1035 high strength reinforcing steel bring additional benefits to reinforced concrete members, including a reduction of the required quantity of reinforcement required and improved corrosion resistance. The mechanical properties of ASTM A1035 high strength reinforcing steel are different from traditional reinforcing steel, including the lack of a defined yield point and corresponding yield plateau. The effective yield strength of ASTM A1035 reinforcement, using the 0.2% offset method, is approximately 830 MPa.

Previous research focused on reinforced concrete members using high strength steel reinforcement showed that direct replacement of normal steel with high strength steel was reasonable for slender beams designed with current code theories [Malhas, 2002]. These design codes theories gave accurate predictions even for design yield strength higher than the limits established by the codes [Malhas, 2002; Vijay, 2002; Yotakhong, 2003]. However, limited previous research has examined the performance of non-slender beams reinforced with high strength steel, where the traditional sectional model assumption of 'plane sections remain plane' does not apply.

Design provisions for non-slender beams incorporated into several codes of practice are based on extensive research focused on members with "normal" strength steel reinforcement. These provisions use a plasticity-base truss analogy, called the Strut and Tie Method. For deep beams reinforced with normal strength steel and minimum web reinforcement, Member capacity is in good agreement with the analytical results using the Strut and Tie Method provisions. Due to the importance of concrete strength in the ultimate capacity of non-slender beams, which are members usually acting under high shear-compression stresses, many research projects have focused on the behavior of non-slender beams constructed with high strength concrete [e.g., Quintero et al, 2006; Oh and Shin, 2001; Foster and Gilbert, 1998]. Even though steel reinforcement also plays a very important role in the ultimate strength of the system [Wastein and Mathey, 1958; Tan et al, 1999; Oh and Shin, 2001], no previous research has systematically focused on the significance of using higher strength steel reinforcement in non-slender concrete beams. The lower reinforcement ratio and corresponding higher reinforcement strains are primary parameters that differentiate the response of deep beams with high strength reinforcement from comparable members with normal strength reinforcement.

Design provisions for the Strut and Tie Method were discussed for three codes, CSA A23.3-04, ACI 318-05 and Eurocode 2. In ACI 318-05 and Eurocode 2, the strut strength reduction factors have an empirical origin based in research done with concrete member reinforced with normal strength steel. In CSA A23.3-04, the strut strength reduction factor considers the strain conditions in the reinforcement crossing the struts but they omit direct consideration of the effect of dowel action.

3. EXPERIMENTAL PROGRAM

3.1 General

An experimental program was conducted to study the behavior of deep beams under four-point bending containing high strength longitudinal reinforcing steel (ASTM A1035). Specimens were constructed at full scale, according to the general requirements of CSA A23.3-04, ACI 318-05 and Eurocode 2 design provisions.

Different parameters were examined for their influence on specimen behaviour. These parameters were the shear span to depth ratio (*a/d*), the longitudinal main reinforcement ratio (ρ), and the presence or omission of vertical web reinforcement. The strength of main longitudinal reinforcement was studied through comparison against specimens with Grade 400R normal strength reinforcement.

A total of ten specimens were constructed. Six beams were reinforced longitudinally with high strength steel and contained normal strength vertical web reinforcement. Two specimens were longitudinally and vertically reinforced with normal strength steel reinforcement. Finally, two specimens were built with only main longitudinal high strength steel and no web reinforcement. Concrete with compressive strength ranging from 23 MPa to 48 MPa was used in the specimens.

Details of the geometry and reinforcement configurations, the materials properties and the test set up for each specimen are explained in this chapter.

3.2 Details of Test Specimens

All ten beams were made at full scale and designed according to the general requirements of the three design codes: CSA A23.3-04, ACI 318-05 and Eurocode 2 (EN1992-1-1). Specimen design took into consideration main tension steel ratios, minimum web reinforcement requirements, necessary reinforcement development lengths, typical concrete covers and spacing between bars.

ASTM A1035 reinforcing steel bars (sizes: #3, #4, #6 and #7) and Grade 400R reinforcing steel bars (sizes: 10M and 20M) were used as the main tension reinforcement and as the horizontal web reinforcement. Six beams were longitudinally reinforced using high strength ASTM A1035 reinforcing steel bars and Grade 400R reinforcing steel bars for vertical web reinforcement. Two beams were reinforced using only longitudinal ASTM A1035 reinforcing steel without vertical web reinforcement. Two beams were reinforced using only Grade 400R reinforcing steel in the main tension and web reinforcement.

For all the beams, constant cross-section dimensions of b=300 mm and h=607 mm were provided. However, different span lengths were utilized to obtain shear span to depth ratios (a/d) of 1.2, 1.8 and 2.4. The percentage of longitudinal main reinforcement, calculated as A_s/bd, varied from 0.52% to 2.29%. For all specimens, the centerline to centerline distance between the loading points was 500 mm. Bearing plates at the loading points and at the supports were 200 mm length x 300 mm width x 50 mm height. Concrete cover provided to the stirrups was 25 mm.

Specimen dimensions, material properties and reinforcement details of the specimens are summarized in Table 3-1. Corresponding symbolic dimensions are shown in Figure 3-1. Additional details on specific geometry for each specimen are reported in Sections 3.2.1 to 3.2.10.

Table 3-1 Test specimens details

Beam	b (mm)	d (mm)	L (mm)	a (mm)	a/d	Main tension reinforcement	ρ (%)	vertical web reinforcement Grade 400R	f'_c (MPa)	f_y* (MPa)	ε_y**
MS1-1	300	501	1700	600	1.19	6-#4ASTM A1035	0.52	10M@200mm	46	838	0.0063
MS1-2	300	503	1700	600	1.19	6-#6 ASTM A1035	1.13	10M@200mm	44	870	0.0063
MS1-3	300	506	1700	600	1.18	9-#7 ASTM A1035	2.29	10M@200mm	44	880	0.0065
MS2-2	300	503	2300	900	1.79	6-#6 ASTM A1035	1.13	10M@200mm	47	870	0.0063
MS2-3	300	506	2300	900	1.78	9-#7 ASTM A1035	2.29	10M@200mm	43	880	0.0065
MS3-2	300	503	2900	1200	2.38	6-#6 ASTM A1035	1.13	10M@150mm	48	870	0.0063
NS1-4	300	507	1700	600	1.18	9-20MGrade 400R	1.77	10M@200mm	23	401	0.0020
NS2-4	300	507	2300	900	1.80	9-20MGrade 400R	1.77	10M@200mm	25	401	0.0020
MW1-2	300	503	1700	600	1.19	6-#6 ASTM A1035	1.13	N/A	39	870	0.0063
MW3-2	300	503	2900	1200	2.38	6-#6 ASTM A1035	1.13	N/A	43	870	0.0063

*Effective yield stress (0.2% offset method) for ASTM A1035 reinforcing steel and yield stress for Grade 400R reinforcing steel

** Strain corresponding to effective yield stress value

For all the specimens with vertical web reinforcement, stirrups from 10M reinforcing bars (Grade 400R) were used. The distribution of the stirrups was in general conformance with the design requirements for deep beams according to CSA A23.3-04, ACI 318-05 and Eurocode 2. The spacing of stirrups was selected to be 200 mm along the whole length in all of the beams with web reinforcement, except for beam MS3-2 where the spacing was 150 mm.

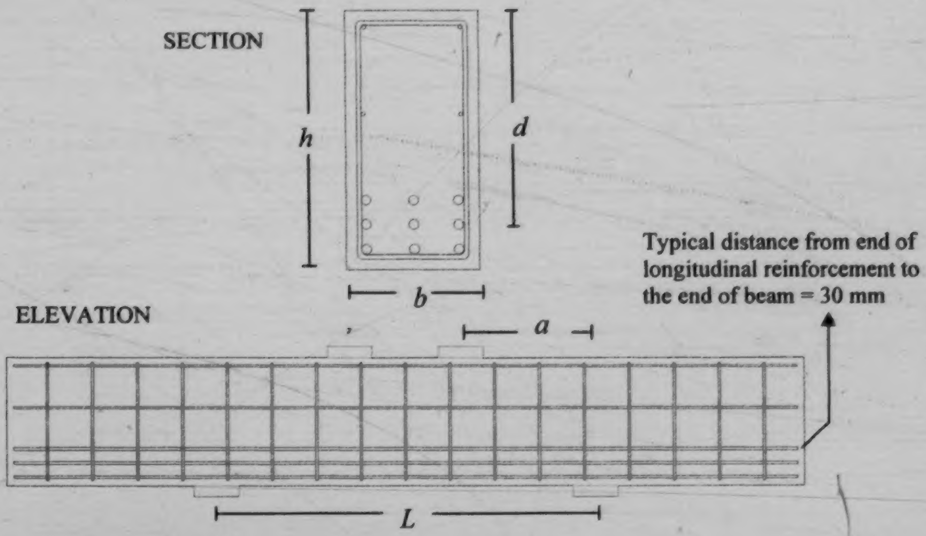

Typical distance from end of longitudinal reinforcement to the end of beam = 30 mm

Figure 3-1 Symbolic dimensions of specimens

The development length at the beam end used to anchor the main longitudinal reinforcement was similar for all specimens. The provided development length of approximately 1000 mm was selected from the largest development length required at the time of predicted failure of the specimens.

The nomenclature used in this project is, described for one specimen, as follows:

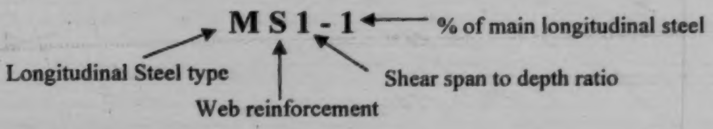

Longitudinal Steel type: **M** for High strength ASTM A1035 reinforcing steel and **N** for Grade 400R reinforcing steel.

Web reinforcement: **S** for specimens with vertical web reinforcement and **W** for specimens without vertical web reinforcement.

Shear span to depth ratio (a/d): 1 for *a/d* of 1.19; **2** for *a/d* of 1.78 and **3** for *a/d* of 2.38.

Percent of longitudinal main reinforcement: **1** for 0.52%; **2** for 1.13%, **3** for 2.29% and **4** for 1.77%.

3.2.1 Details of specimen MS1-1

Beam MS1-1 had a rectangular cross section of 300 x 607 mm. The longitudinal main tensile reinforcement consisted of 6-#4 ASTM A1035 bars with an effective yield strength f_y of 838 MPa (according to the 0.2% offset method) that was distributed in three layers spaced at 65 mm. This arrangement of main longitudinal steel gave a reinforcement ratio ρ of 0.52%. Vertical web reinforcement consisted of 10M Grade 400R bars with f_y of 405 MPa and average longitudinal spacing of 200 mm. Longitudinal web reinforcement consisted of 2-#4 ASTM A1035 bars at the top and 2-#3 ASTM A1035 bars near mid-height. The beam span was 1700 mm and the shear span, *a*, was 600 mm, giving a shear span to depth ratio of 1.19.

Dimensions and reinforcement details of beam MS1-1 are shown in Figure 3-2. All dimensions shown in this figure are in mm.

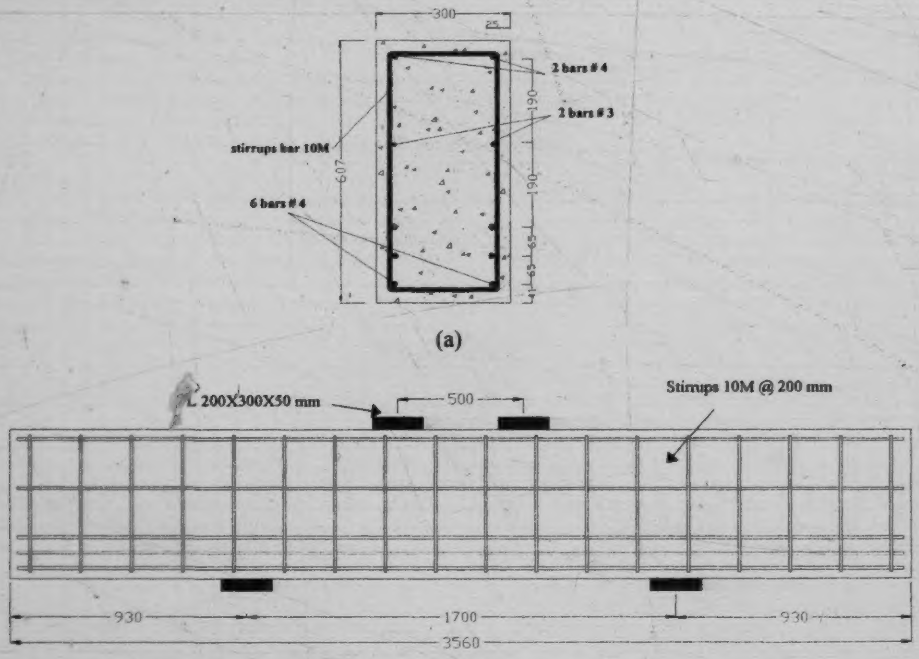

(a)

(b)

Figure 3-2 Beam MS1-1: (a) Cross section (b) Elevation.

3.2.2 Details of Specimen MS1-2

Beam MS1-2 had a rectangular cross section of 300 x 607 mm. The longitudinal main tensile reinforcement consisted of 6-#6 ASTM A1035 bars with an effective yield strength f_y of 870 MPa (according to the 0.2% offset method) that was distributed in three layers spaced at 60 mm. This arrangement of main longitudinal steel gave a reinforcement ratio ρ of 1.13%. Vertical web reinforcement consisted of 10M Grade 400R bars with f_y of 405 MPa and average longitudinal spacing of 200 mm. Longitudinal web reinforcement consisted of 2-#4 ASTM A1035 bars at the top and 2-#4 ASTM A1035 bars near mid-height. The beam span was 1700 mm and the shear span, *a*, was 600 mm, giving a shear span to depth ratio of 1.19.

Reinforcement details of beam MS1-2 are shown in Figure 3-3. The dimensions shown in this figure are in mm.

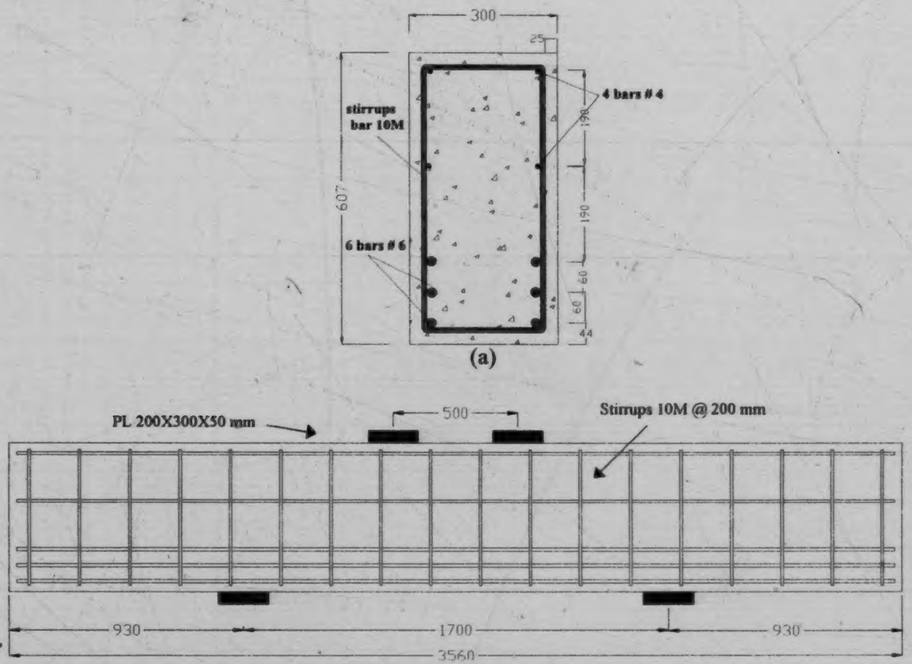

(a)

(b)

Figure 3-3 Beam MS1-2: (a) Cross section (b) Elevation.

3.2.3 Details of Specimen MS1-3

Beam MS1-3 had a rectangular cross section of 300 x 607 mm. The longitudinal main tensile reinforcement consisted of 9-#7 bars with an effective yield strength f_y of 870 MPa (according to the 0.2% offset method) that was distributed in three layers spaced at 55 mm. This arrangement of main longitudinal steel gave a reinforcement ratio ρ of 2.29 %. Vertical web reinforcement consisted of 10M Grade 400R bars with f_y of 405 MPa and average longitudinal spacing of 200 mm. Longitudinal web reinforcement consisted of 2-#4 ASTM A1035 bars at the top and 2-#3 ASTM A1035 bars near mid-height. The beam span was 1700 mm and the shear span, *a*, was 600 mm, giving a shear span to depth ratio of 1.19.

Dimensions and reinforcement details of beam MS1-3 are shown in Figure 3-4. It is noted that the stirrups location starts at the midspan, unlike the spacing used in MS1-1 and MS1-2. This stirrup arrangement was also used for beam NS1-4, which is similar to MS1-3 except for the reinforcement strength. Thus the stirrup arrangement selected assisted in making comparisons in the behavior of these beams.

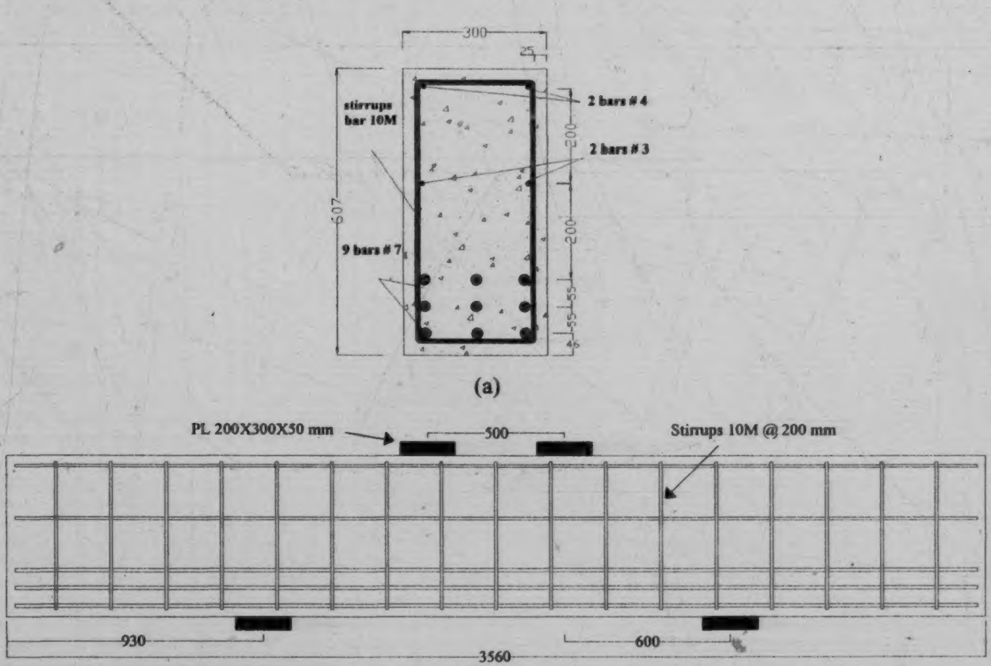

(a)

(b)

Figure 3-4 Beam MS1-3: (a) Cross section (b) Elevation

3.2.4 Details of Specimen MS2-2

Beam MS2-2 had a rectangular cross section of 300 x 607 mm. The longitudinal main tensile reinforcement consisted of 6-#6 bars with an effective yield strength f_y of 870 MPa (according to the 0.2% offset method) that was distributed in three layers spaced at 60 mm. This arrangement of main longitudinal steel gave a reinforcement ratio ρ of 1.13%. Vertical web reinforcement consisted of 10M Grade 400R bars with f_y of 405 MPa and average longitudinal spacing of 200mm. Longitudinal web reinforcement consisted of 2-#4 ASTM A1035 bars at the top and 2-#4 ASTM A1035 bars near mid-height. The beam span was 2300 mm and the shear span, *a*, was 900 mm, giving shear span to depth ratio of 1.79.

Dimension and reinforcement details of beam MS2-2 are shown in Figure 3-5. All dimensions shown in this figure are in mm.

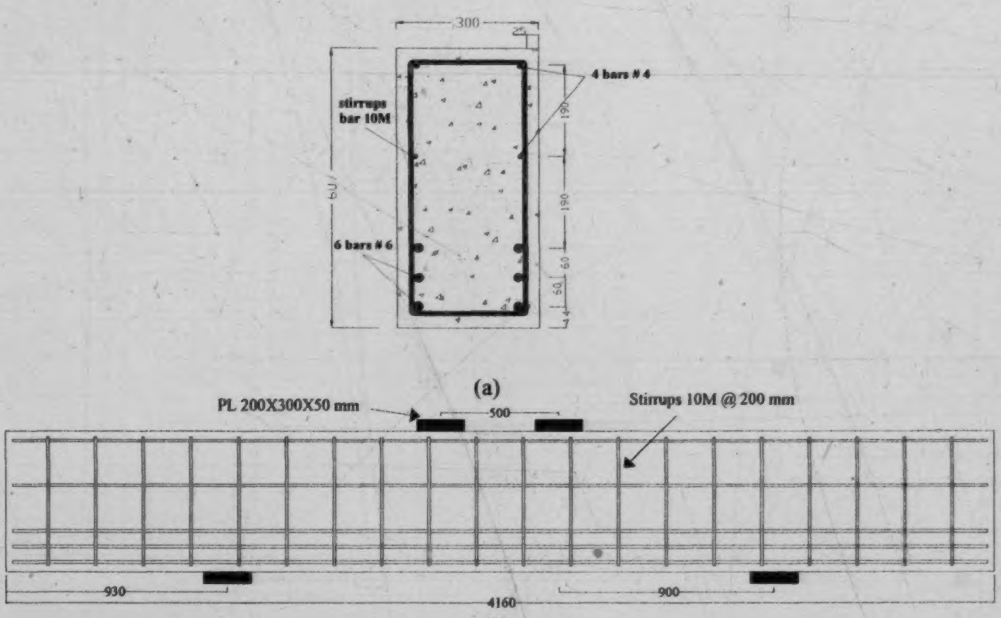

(a)

(b)

Figure 3-5 Beam MS2-2: (a) Cross section (b) Elevation

3.2.5 Details of Specimen MS2-3

Beam MS2-3 had a rectangular cross section of 300 x 607 mm. The longitudinal main tensile reinforcement consisted of 9-#7 ASTM A1035 bars with an effective yield strength f_y of 870 MPa (according to the 0.2% offset method) that was distributed in three layers spaced at 55 mm. This arrangement of main longitudinal steel gave a reinforcement ratio ρ of 2.29 %. Vertical web reinforcement consisted of 10M Grade 400R bars with f_y of 405 MPa and average longitudinal spacing of 200 mm. Longitudinal web reinforcement consisted of 2-#4 ASTM A1035 bars at the top and 2-#4 ASTM A1035 bars near mid-height. The beam span was 2300 mm and the shear span, *a*, was 900 mm, giving a shear span to depth ratio of 1.78.

Dimension and reinforcement details of beam MS2-3 are shown in Figure 3-6. All dimensions shown in this figure are in mm.

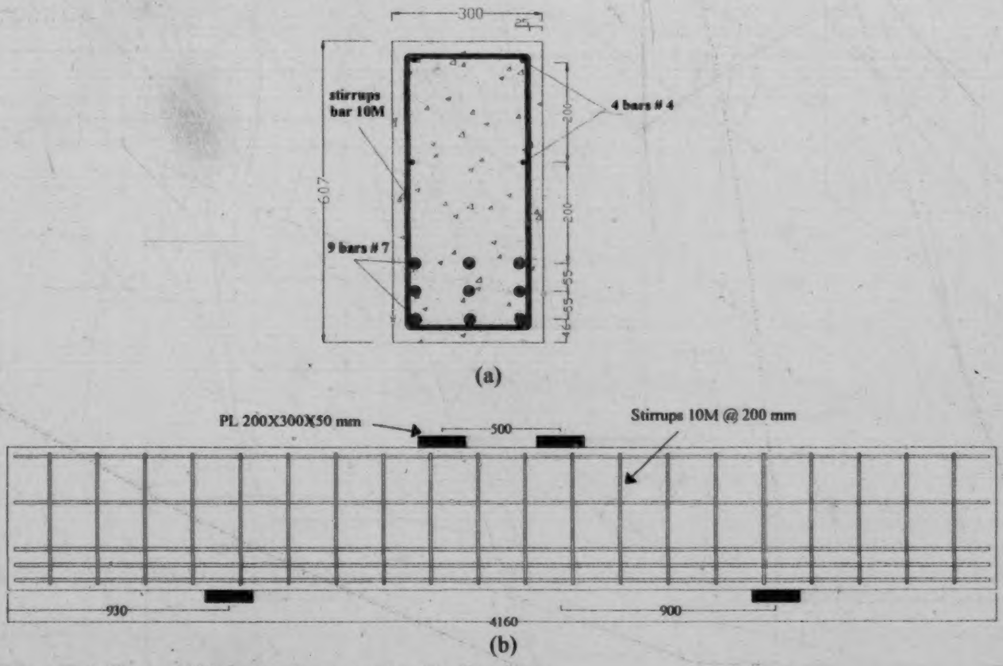

(a)

(b)

Figure 3-6 Beam MS2-3: (a) Cross section (b) Elevation

3.2.6 Details of Specimen MS3-2

Beam MS3-2 had a rectangular cross section of 300 x 607 mm. The longitudinal main tensile reinforcement consisted of 6-#6 ASTM A1035 bars with an effective yield strength f_y of 870 MPa (according to the 0.2% offset method) that was distributed in three layers spaced at 60 mm. This arrangement of main longitudinal steel gave a reinforcement ratio ρ of 1.13%. Vertical web reinforcement consisted of 10M Grade 400R bars with f_y of 405 MPa and average longitudinal spacing of 150 mm. Longitudinal web reinforcement consisted of 2-#4 ASTM A1035 bars at the top and 2-#4 ASTM A1035 bars near mid-height. The beam span was 2900 mm and the shear span, *a*, was 1200 mm. For this specimen, the shear span to depth ratio was 2.38.

Dimension and reinforcement details of beam MS3-2 are shown in Figure 3-7. All dimensions shown in the figure are in mm.

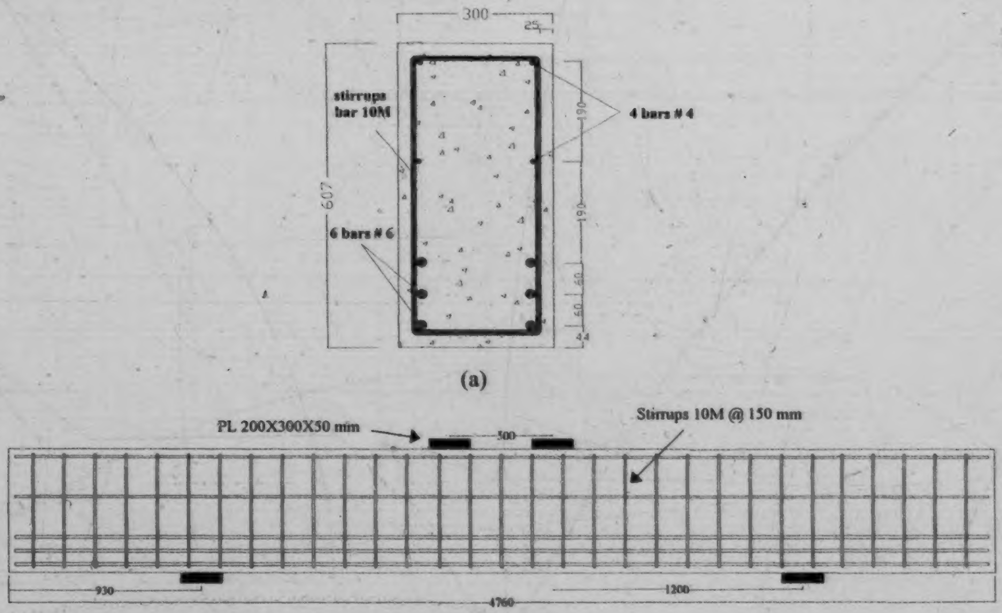

(a)

(b)

Figure 3-7 Beam MS3-2: (a) Cross section (b) Elevation

3.2.7 Details of Specimen NS1-4

Beam NS1-4 had a rectangular cross section of 300 x 607 mm. The longitudinal main tensile reinforcement consisted of 9–20M Grade 400R bars with a yield strength f_y of 394 MPa that was distributed in three layers spaced at 55 mm. This arrangement of main longitudinal steel gave a reinforcement ratio ρ of 1.77 %. Vertical web reinforcement consisted of 10M Grade 400R bars with f_y of 405 MPa and average longitudinal spacing of 200 mm. Longitudinal web reinforcement consisted of 2-10M Grade 400R bars at the top and 2-10M Grade 400R bars near mid-height. The beam span was 1700 mm and the shear span, *a,* was 600 mm, giving a shear span to depth ratio of 1.18.

Dimension and reinforcement details of beam NS1-4 are shown in Figure 3-8. All dimensions shown in the figure are in mm.

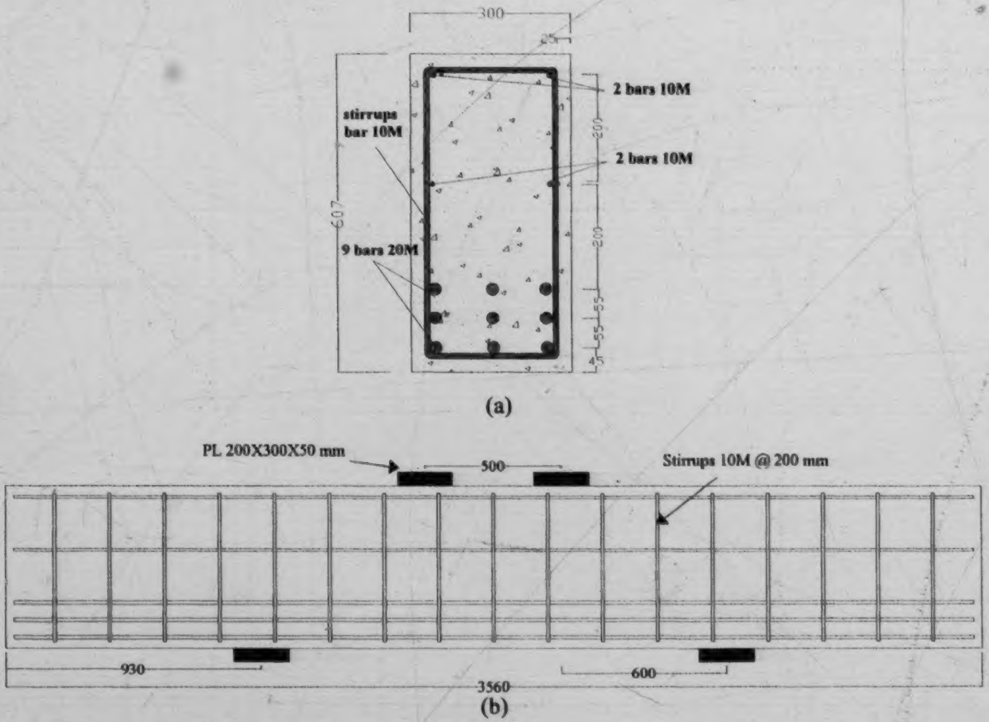

Figure 3-8 Beam NS1-4: (a) Cross section (b) Elevation

3.2.8 Details of Specimen NS2-4

Beam NS2-4 had a rectangular cross section of 300 x 607 mm. The longitudinal main tensile reinforcement consisted of 9–20M Grade 400R bars with a yield strength f_y of 394 MPa that was distributed in three layers spaced at 55 mm. This arrangement of main longitudinal steel gave a reinforcement ratio ρ of 1.77%. Vertical web reinforcement consisted of 10M Grade 400R bars with f_y of 405 MPa and average longitudinal spacing of 200 mm. Longitudinal web reinforcement consists of 2-10M Grade 400R bars at the top and 2-10M Grade 400R bars near mid-height. The beam span was 2300 mm and the shear span, a, was 900 mm, giving a shear span to depth ratio of 1.80.

Dimension and reinforcement details of beam NS1-4 are shown in Figure 3-9. All dimensions shown in this figure are in mm.

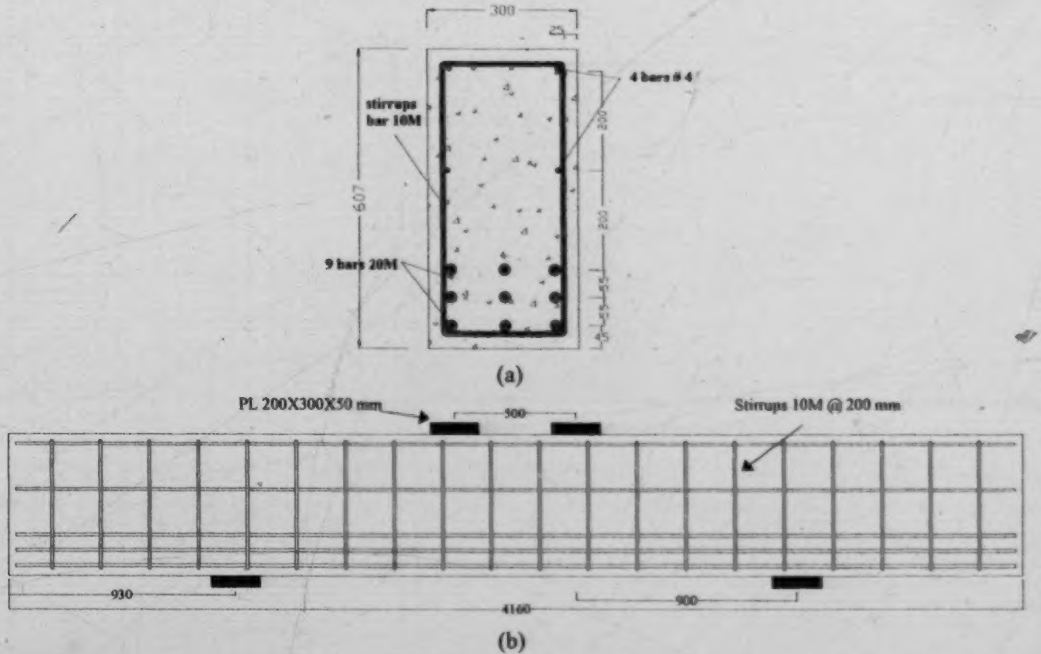

(a)

(b)

Figure 3-9 Beam NS2-4: (a) Cross section (b) Elevation

3.2.9 Details of Specimen MW1-2

Beam MW1-2 had a rectangular cross section of 300 x 607 mm. The longitudinal main tensile reinforcement consisted of 6–#6 ASTM A1035 bars with an effective yield strength f_y of 870 MPa (according to the 0.2% offset method) that was distributed in three layers spaced at 60 mm. This arrangement of main longitudinal steel gave a reinforcement ratio ρ of 1.13%. No vertical web reinforcement was provided within the beam span. Three 10M stirrups at 200 mm spacing were provided at beam ends beyond the supports. 2-#4 ASTM A1035 bars were placed at the top of the beam to hold the stirrups at the end of the beam and to maintain the same longitudinal reinforcement configuration with respect to the beams with vertical web reinforcement. The beam span was 1700 mm and the shear span, *a,* was 600 mm, giving a shear span to depth ratio of 1.19.

Dimension and reinforcement details of beam MW1-2 are shown in Figure 3-10. All dimensions in this figure are in mm.

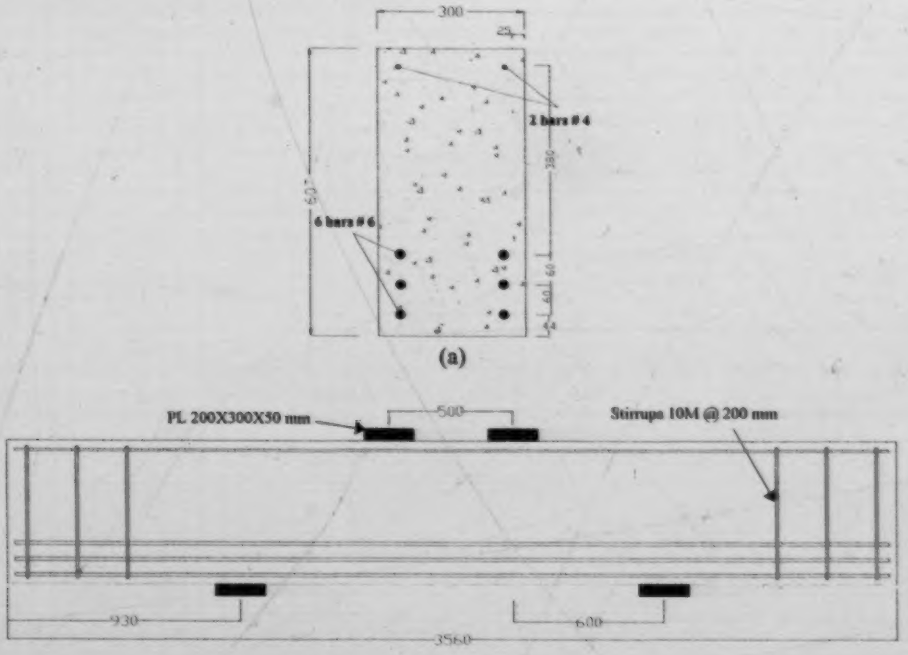

(a)

(b)

Figure 3-10 Beam MW1-2: (a) Cross section (b) Elevation

3.2.10 Details of Specimen MW3-2

Beam MW3-2 had a rectangular cross section of 300 x 600 mm. The longitudinal main tensile reinforcement consisted of 6–#6 ASTM A1035 bars with a yield strength f_y of 870 MPa (according to the 0.2% offset method) that was distributed in three layers and spaced at 60 mm. This arrangement of main longitudinal steel gives a reinforcement ratio ρ of 1.13%. No vertical web reinforcement was provided within the beam span. Three 10M stirrups at 200 mm spacing were provided at beam ends beyond the supports. 2-#4 ASTM A1035 bars were placed at the top of the beam to hold the stirrups at the end of the beam and to maintain the same longitudinal reinforcement configuration with respect to the beams with vertical web reinforcement. The beam span was 2900 mm and the shear span, *a*, was 1200 mm, giving a shear span to depth ratio of 238.

Dimensions and reinforcement details are shown in Figure 3-11. All dimensions in the figure are in mm.

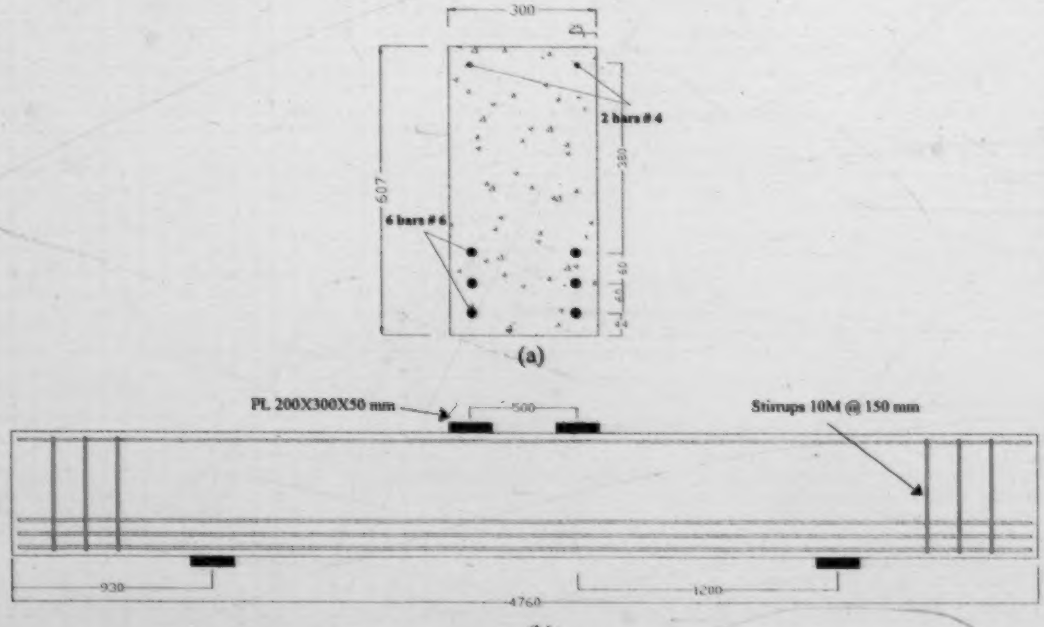

(a)

(b)

Figure 3-11 Beam MW3-2: (a) Cross section (b) Elevation

3.3 Fabrication of specimens

All specimens were built in the I. F. Morrison Structural Engineering Laboratory at the University of Alberta. Formwork to simultaneously cast two specimens was constructed. The formwork was leveled and all dimensions were checked prior to each casting. Details of a transverse section through the formwork are shown in Figure 3-12.

The process of construction of each specimen started with the instrumentation of the reinforcing bars (See Section 3.6.1). Once all strain gauges were installed, the reinforcing steel cages were assembled and the steel cages were carefully placed in the formwork. Concrete was cast and vibrated. Figure 3-13 shows the vibration of the concrete during the casting process.

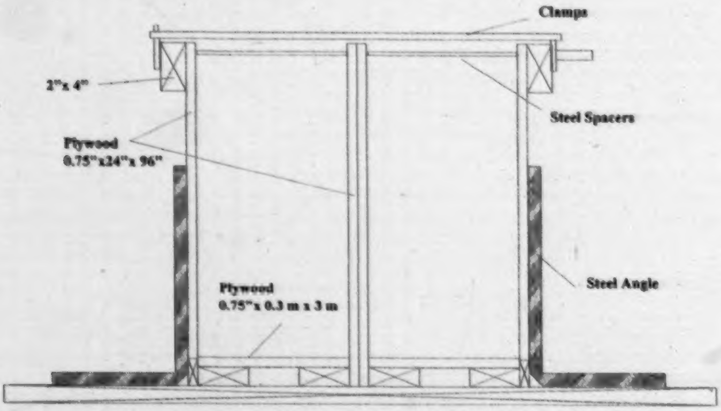

Figure 3-12 Formwork transversal section details

Five castings were programmed to build a total of ten reinforced concrete deep beam specimens. The specimens were moist cured under plastic for two weeks, removed from the formwork and stored in the ambient laboratory environment until testing. Cylinder and prism samples were also cast at the same time as the beams and were cured under the same conditions. The age of the specimens and cylinder samples at day of test is shown in Table 3-3.

Figure 3-13 Vibration of the concrete during casting

3.4 Material properties

3.4.1 Concrete

Initial design of the specimens was completed on the basis of normal strength concrete with a nominal compressive strength of 30 MPa. All concrete was supplied by a local ready-mix concrete company. The concrete specifications ordered are shown in Table 3-2. Five batches of concrete were ordered to cast two beams at a time. Table 3-3 shows the batch number and corresponding specimen designations.

Table 3-2 Nominal concrete specifications

f'_c	30 MPa
Aggregate size	20 mm
Air content	1-4%
Slump	80 mm

Cylinders samples were made using molds 150 mm diameter by 300 mm height and were prepared by a certified technician at the day of casting. Cylinders were cured under the same conditions as the beam specimens and tested in a Tinius Olson universal testing machine on the same day as the corresponding beam test. Figure 3-14 shows a concrete cylinder during the compression test.

The compressive strength obtained from the concrete supplier varied from 39 to 48 MPa for beams reinforced with high strength steel. Concrete strength of 23 and 25 MPa was obtained for specimens NS1-4 and NS2-4, reinforced with normal strength steel. See Table 3-3. The measured concrete strength values were used in the analysis of all the specimens.

Figure 3-14 Compression test of concrete cylinder

At the day of the casting for some of the beams, small prisms were also made using molds 150 x150 x 450 mm. The prisms were used to determine the modulus of rupture f_r under four point loading over a span at 300 mm (see Table 3-3). All the test prisms were cured under the same conditions as the corresponding beam specimens. Figure 3-15 shows the flexural test to obtain the modulus of rupture.

The tensile strength f_t was obtained from the splitting test of 150 mm diameter and 300 height cylinders (see Table 3-3).

Figure 3-15 Flexural test to obtain the modulus of rupture

Compressive and tensile concrete strength, modulus of rupture and age of the samples at the day of the beam test are shown in Table 3-3. The strength values given are the average values of three samples tested at the day of test.

Table 3-3 Compression test results and age of samples at the day of the beam test

Beam	Batch #	f'_c (MPa)	f_t (MPa)	f_r (MPa)	Age (days)
MS1-1	III	46	2.55	4.48	54
MS1-2	III	44	-	-	63
MS1-3	II	44	-	-	36
MS2-2	IV	47	2.95	5.17	67
MS2-3	II	43	-	-	95
MS3-2	IV	48	-	-	75
NS1-4	I	23	-	3.88	43
NS2-4	I	25	-	-	106
MW1-2	V	39	2.88	4.68	24
MW3-2	V	43	-	-	30

3.4.2 Reinforcing Steel

The reinforcing steel used in this project consisted of two different types of steel: Grade 400R reinforcing steel and ASTM A1035 reinforcing steel. 10M and 20M (Canadian standard sizes) Grade 400R reinforcing steel bars and #3, #4, #6 and #7 (American standard sizes) ASTM A1035 reinforcing steel bars were used.

The average yield strength f_y and modulus of elasticity E_s were obtained from the stress-strain curve of two tension coupon tests for each bar size. All bars of the same size were from the same heat of steel. The tension coupon samples were 500 mm long and were tested in a MTS 1000 machine under displacement control and tested until failure. To measure the strain in the samples, a 50 mm gauge length extensometer was utilized. The extensometers used were not able to measure the load-elongation response of the coupon tests to maximum strain and were removed prior to failure. The Grade 400R reinforcement showed well defined yield plateaus. For ASTM A1035 coupon tests, the 0.2% offset method was used to determine an effective f_y magnitude. E_s was obtained from the slope of the linear part of the stress-strain curve of reinforcing steel. The stress-strain response of ASTM A1035 reinforcing steel remained linear up to approximately 650 MPa.

Table 3-4 and Table 3-5 show the average properties obtained from the tension coupon tests of ASTM A1035 and Grade 400R reinforcing steel bars respectively.

Table 3-4 ASTM A1035 reinforcing steel properties

Bar #	Area (mm^2)	f_y * (MPa)	ε_y**	f_u (MPa)	ε_u	E_s (MPa)
3	71	855	0.0063	1067	0.047	197250
4	129	838	0.0063	1017	0.051	195150
6	284	870	0.0063	1040	0.039	203300
7	387	880	0.0065	1070	0.037	199450

* Effective yield stress using 0.2% offset method

**Strain corresponding to the effective yield stress

Table 3-5 Grade 400R reinforcing steel properties

Bar	Area (mm^2)	f_y* (MPa)	ε_y **	f_u (MPa)	ε_u	E_s (MPa)
10M	100	408	0.0021	660	0.083	204850
20M	300	401	0.0020	540	0.116	197850

* Yield stress

**Yield strain

Figure 3-16 shows the stress-strain curve of two specimens for each bar size (#3, #4, #6 and #7) of ASTM A1035 steel. Figure 3-17 shows the stress-strain curve of bars 10M and 20M (Grade 400R) used in this project.

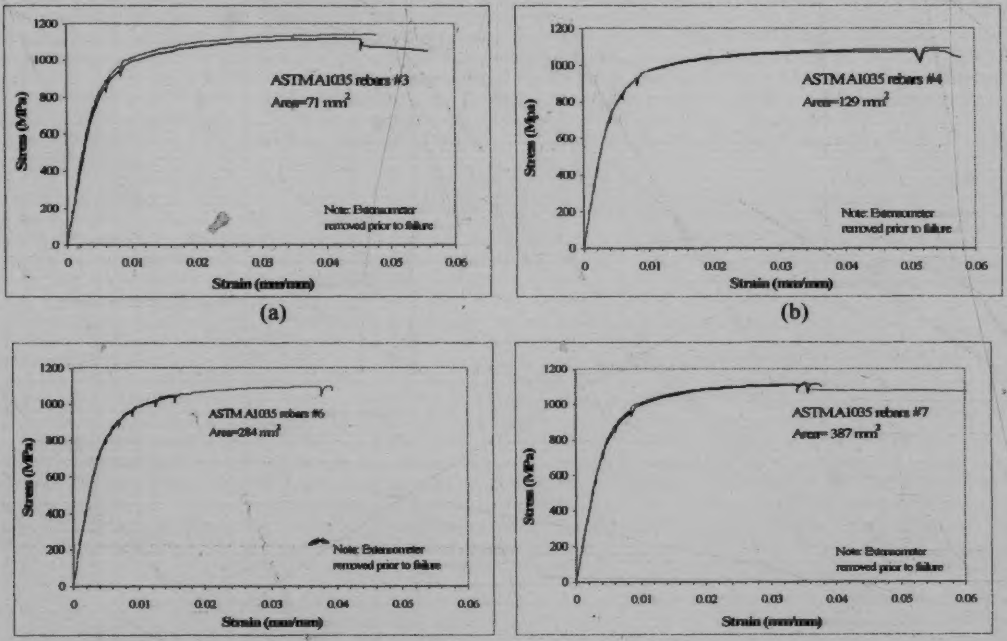

(a)

(b)

(c)

(d)

Figure 3-16 Stress-strain response of ASTM A1035 reinforcement (a) #3 Bars (b) #4 bars (c) #6 bars and (d) #7 bars

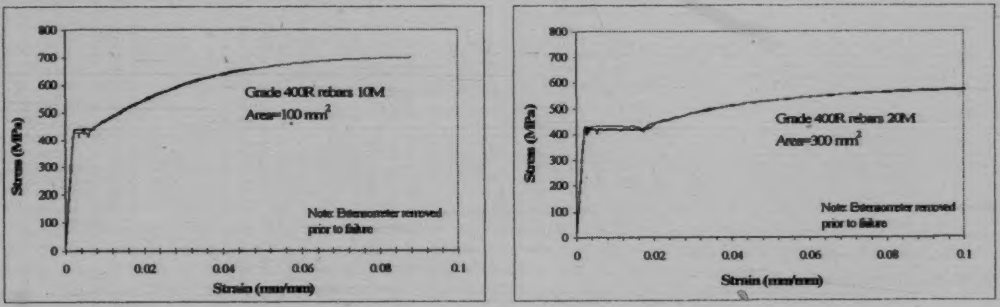

(a)

(b)

Figure 3-17 Stress-strain response for Grade 400R reinforcement (a) 10M bar and (b) 20M bar

Vijay et al (2002) and Yotakhong (2003) proposed equations to predict the stress-strain response of #4 and #6 ASTM A1035 bars, respectively (see Section 2.6.1). The comparison between these equations and the stress-strain response obtained from the tension coupon tests carried out in this research project are shown in Figure 3-18. The curves obtained from the equations did not accurately predict the behaviour measured during the coupon tests. The initial stress-strain response up to 350 MPa and 400 MPa was accurately predicted using Vijay and Yotakhong's equations, respectively. After those points, predictions did not follow the real curve (Figure 3-18). The predicted strain at the effective yield stress f_y (0.2% offset method) of 838 MPa for bar #4 was 0.0074, while the strain measured at f_y (0.2% offset method) was 0.0063. The predicted strain at the effective yield stress f_y (0.2% offset method) of 870 MPa for bar #6 was 0.0068, while the strain measured at f_y (0.2% offset method) was 0.0063.

During the analysis of the specimens in this study, polynomial equations for the stress-strain response were developed from the tension coupon test results using an Excel spreadsheet. Equations 3-1 to 3-3 were used to model the stress-strain response of the ASTM A1035 reinforcing steel.

For ASTM A1035 bar #4

$$\varepsilon_s = 2.438739\text{x}10^{-14}\,\sigma^4 - 2.8275066\text{x}10^{-11}\,\sigma^3 + 1.0710662\text{x}10^{-8}\,\sigma^2 + 3.7244197\text{x}10^{-6}\,\sigma + 1.2946302\text{x}10^{-5} \tag{3-1}$$

For ASTM A1035 bar #6

$$\varepsilon_s = 2.22469457\text{x}10^{-19}\sigma^6 - 6.05365314\text{x}10^{-16}\,\sigma^5 + 6.37542137\text{x}10^{-13}\,\sigma^4 - 3.13120671\text{x}10^{-10}\,\sigma^3 + 7.0514228\text{x}10^{-8}\,\sigma^2 - 1.14746053\text{x}10^{-6}\,\sigma + 7.99239995\text{x}10^{-5} \tag{3-2}$$

For ASTM A1035 bar #7

$$\varepsilon_s = -3.7454288137\text{x}10^{-20}\sigma^6 + 1.3243332487\text{x}10^{-16}\sigma^5 - 1.5178347317\text{x}10^{-13}\sigma^4 + 7.8272117499\ \text{x}10^{-11}\sigma^3 - 1.8218824418\ \text{x}10^{-8}\sigma^2 + 6.7707955845\ \text{x}10^{-6}\sigma - 3.2008484593\ \text{x}10^{-5} \tag{3-3}$$

where

ε_s= strain in the reinforcing steel bar (mm/mm)

σ= stress in the reinforcing steel bar (MPa)

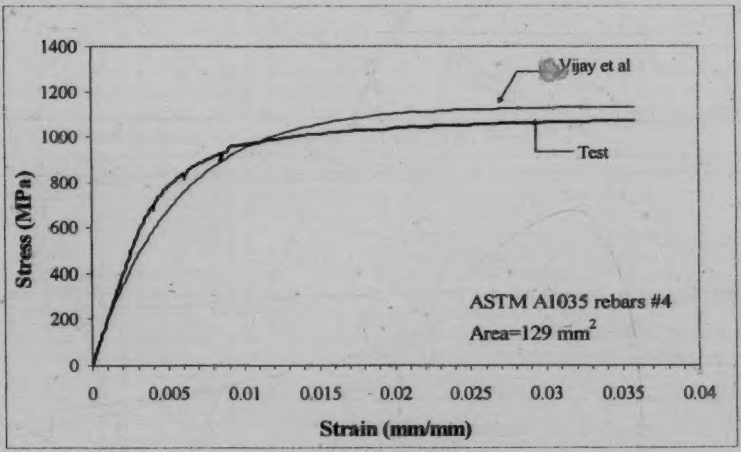

(a)

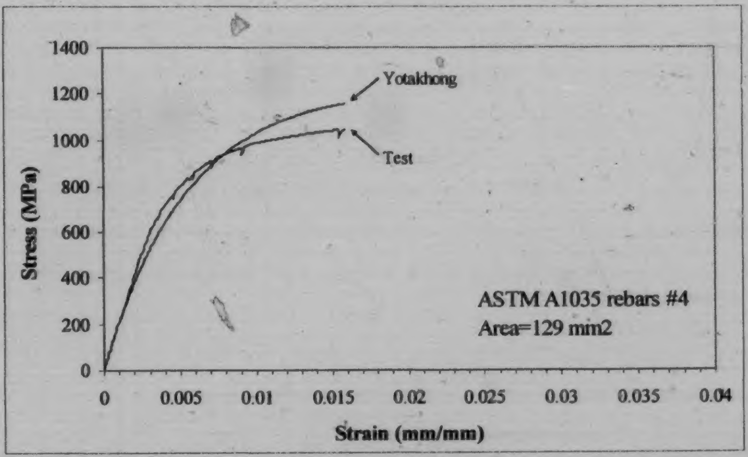

(b)

Figure 3-18 Comparison between predicted stress-strain response and measured stress-strain response for (a) ASTM A1035 bars #4 and (b) ASTM A1035 bars #6.

3.5 Test Set-Up

All specimens were simply supported and loaded at two points. Figure 3-19 shows the typical beam set up prior to test.

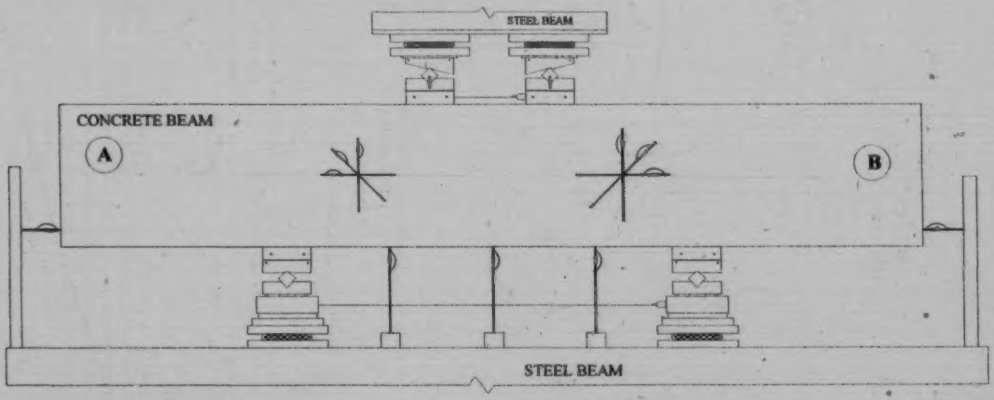

Figure 3-19 General set up

3.5.1 Loading points

A stiff steel spreader beam was used to distribute the load from the crosshead of the MTS 6000 universal testing machine to the two loading points. Steel plates 300 mm length, 200 mm width and 50 mm thick were used as bearing plates at the load points. The spacing between centers of the loading plates was 500 mm. A thin layer of high strength plaster capping was used to smooth out the uneven concrete surface below the bearing plates. Resting on the bearing plates were knife edge supports. Over the knife edges were 40 mm diameter roller assemblies placed between 50 mm thick plates. This arrangement allowed free rotation and elongation of the beam. One of the roller assemblies at the loading points was fixed to provide translation stability during the loading process.

The relative longitudinal movement of the loading points during the test was measured using a cable transducer affixed to the interior faces of the loading point system. Figure 3-20 shows the details of the configuration at loading points.

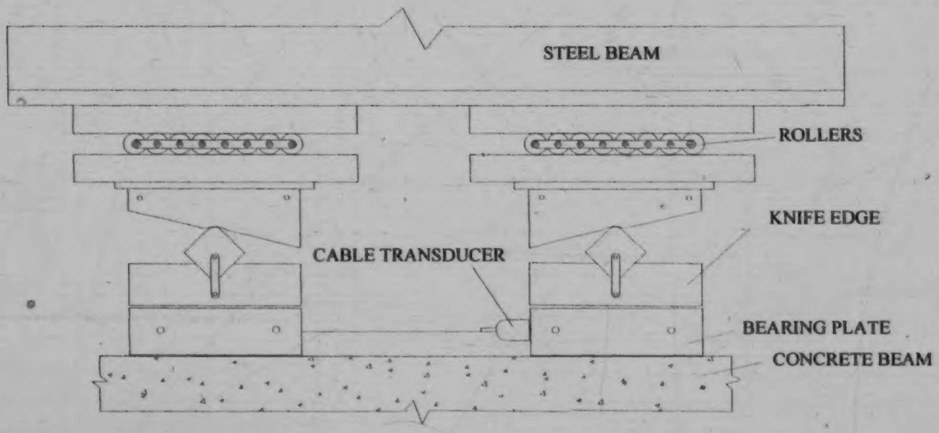

Figure 3-20 Loading point details

3.5.2 Supports

Plates similar to the loading bearing plates described in Section 3.5.1 were used as support bearing plates at the ends of the span. These plates rested on knife edge supports, with each knife edge supported on a load cell. The load cells were mounted on 40 mm roller assemblies placed between two 50 mm thick steel plates. This support arrangement allowed free elongation and in plane rotation of the beam.

The support rollers were supported on a strongly reinforced steel beam. The steel beam was supported on the laboratory strong floor.

High strength capping material (plaster) was used between the bearing plates and the specimen, to smooth out the uneven concrete surface. A cable transducer was placed on the interior faces of the supports to measure their displacement during the test.

Details of the support arrangement are illustrated in Figure 3-21.

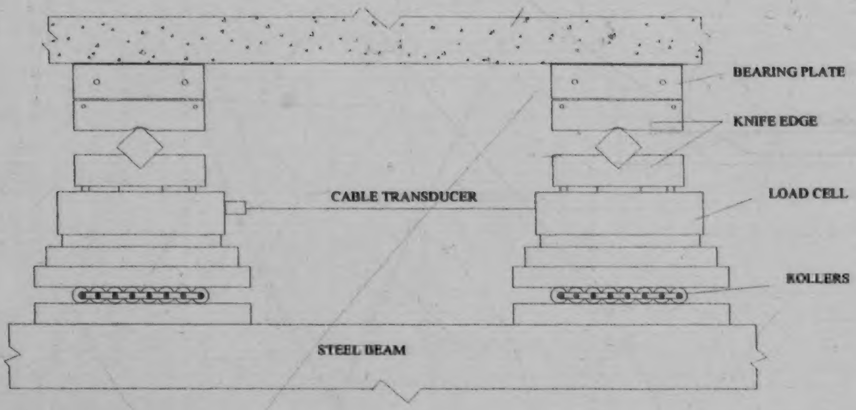

Figure 3-21 Supports details

3.6 Instrumentation

To analyze the behavior of the beams, instrumentation was used in important zones of the specimens, Strains in the reinforcement, average strains in the concrete at the diagonal struts locations, member deflections and the crack development were important parameters measured during the experimental program. For this purpose, strain gauges, linear variable displacement transformers (LVDTs), demec gauges and crack width comparator gauges were used.

Electrical resistance strain gauges were used to measure the strain of the reinforcement in locations of interest. To monitor the strain distribution of the main longitudinal reinforcement, strain gauges were placed at various locations along the three layers of reinforcement. The behaviour of the web reinforcement was also monitored using strain gauges affixed to the stirrups and to the longitudinal web reinforcement located in the shear span zone. Strain readings in the web reinforcement helped to determine the contribution of this reinforcement within the load capacity of the beam.

Deformation rosettes constructed with multiple LVDTs were placed at the specimen mid-height on the diagonal line between the centre of the loading plate and the centre of the support plate. This location corresponded to the centerline of the direct compression strut between the loading point and the adjacent support. This arrangement allowed calculation of the principal strains and corresponding angle of inclination along the diagonal strut.

Demec gauges in a rosette configuration were placed at similar locations to the LVDTs, but on the opposite face of the beam. The purpose of the demec gauges was to compare the results with the data obtained from the LVDTs.

At the compression strut location between the two loading points, demec gages were also placed on the side face of the specimen to allow measurement of the axial compressive strain at the different stages of loading.

3.6.1 Strain gauges

The strain gauges used in this project were regular 120 Ω gauges. All the strain gauges were placed on the reinforcing bars prior to building the steel cages. The quantity of strain gauges for each beam specimen varied from 22 to 39.

The surface of the reinforcing bars was prepared using a grinder and sand paper to achieve a smooth area, always considering to not reduce the cross section of the bar. Each strain gauge was attached to the bar surface using an appropriate adhesive (Cyano-Acrylate base strain gauge cement). After the adhesive cured, a waterproof coating and layer of silicon sealant were placed over the gauges to prevent damage during the casting and curing of the concrete.

Strain gauges were placed along the longitudinal reinforcement to measure the distribution of strains along the clear span, to measure variation of strain between the interior and exterior edges of the supports, to measure the strain variation at the same location (interior edge of the support) for the three different reinforcement layers and to measure the strain in the vertical and horizontal web reinforcement located in the shear span.

From Figure 3-22 to Figure 3-27, the strain gauge locations for the specimens longitudinally reinforced with high strength steel and normal strength steel stirrups are illustrated. Distances from the midspan to the location of the strain gages located on the longitudinal reinforcement are shown in Appendix A. Strain gauges on the stirrups are located at mid-height.

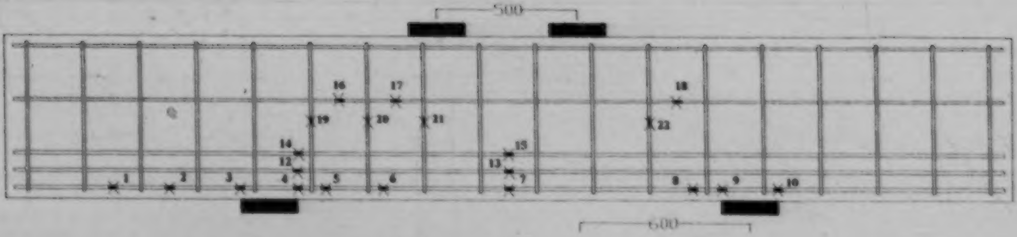

Figure 3-22 Strain gauge locations for beam MS1-1

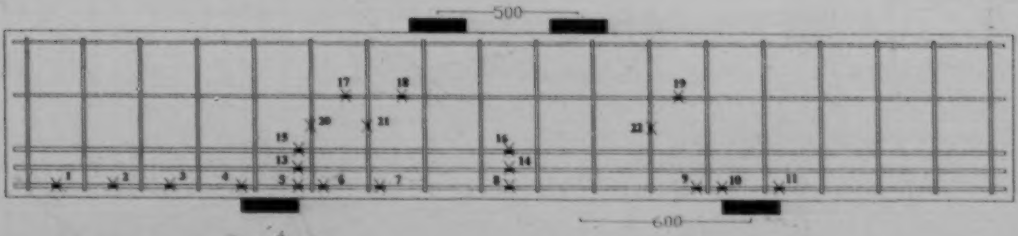

Figure 3-23 Strain gauge locations of beam MS1-2

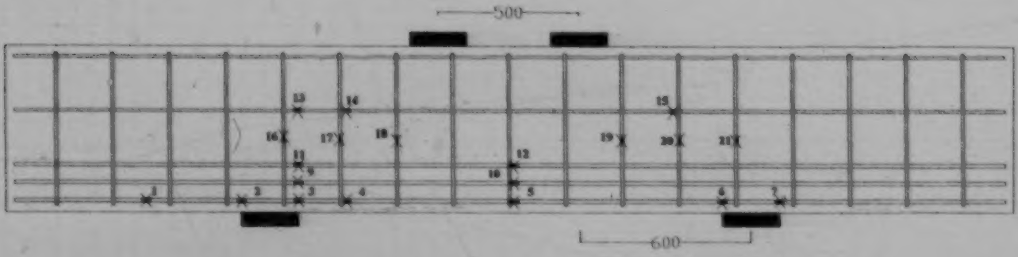

Figure 3-24 Strain gauge locations of beam MS1-3

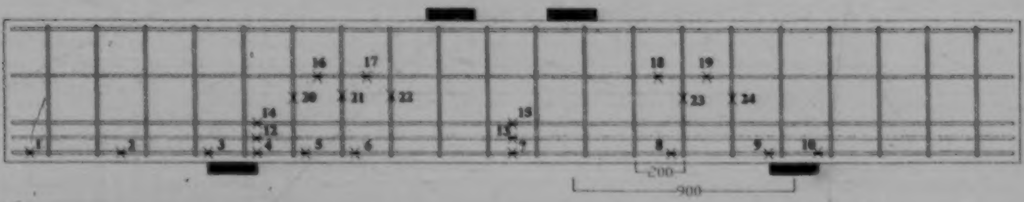

Figure 3-25 Strain gauge locations of beam MS2-2

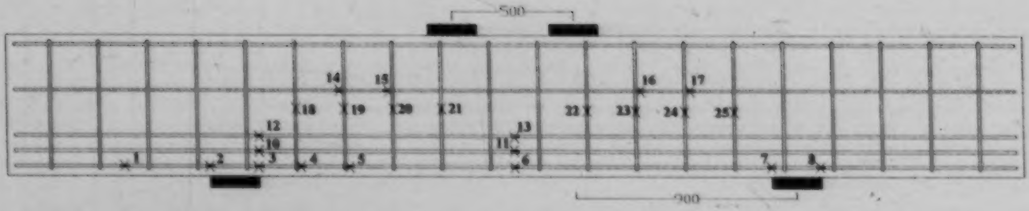

Figure 3-26 Strain gauge locations of beam MS2-3

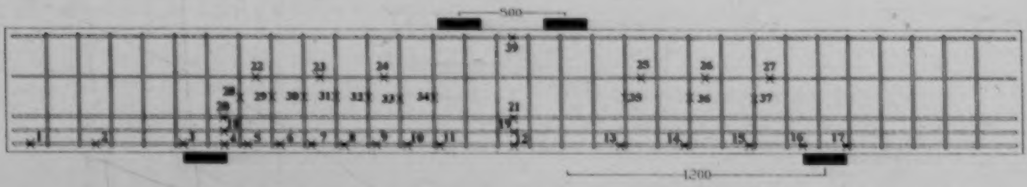

Figure 3-27 Strain gauge locations of beam MS3-2

Figure 3-28 and Figure 3-29 show the strain gauge locations for the specimens reinforced with normal strength steel.

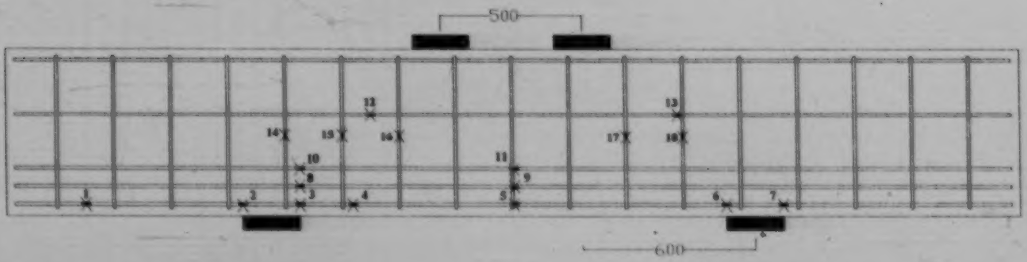

Figure 3-28 Strain gauge locations of beam NS1-4

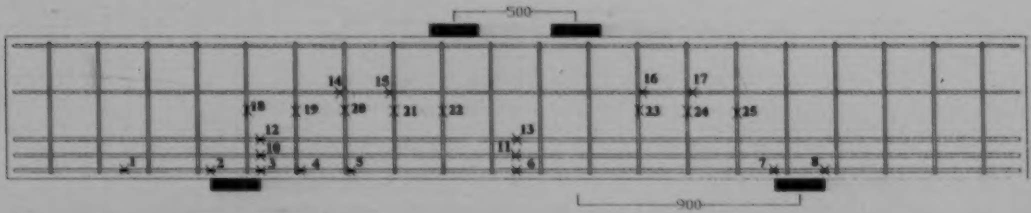

Figure 3-29 Strain gauge locations of beam NS2-4

Figure 3-30 and Figure 3-31 show the strain gauge locations for the beams with high strength reinforcing steel and no web reinforcement.

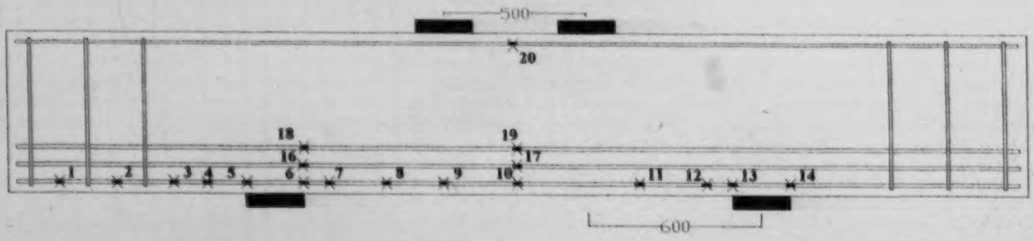

Figure 3-30 Strain gauge locations of beam MW1-2

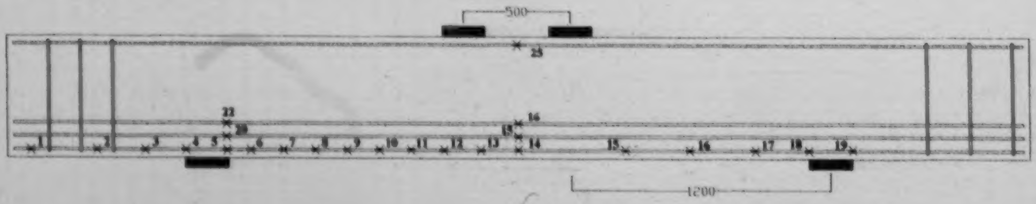

Figure 3-31 Strain gauge locations of beam MW1-3

3.6.2 LVDTs and Demec Gages

A total of eleven linear variable displacement transformers (LVDTs) were placed on each specimen. A LVDT rosette (see Figure 3-32) was built on the diagonal compression struts on each beam. Two LVDT rosettes with different diameters, 380 mm and 280 mm, were used (see Figure 3-33). The variation in diameters resulted from the available LVDT sizes in the laboratory. These rosettes helped to monitor the average strain in three directions for the diagonal struts. To verify the accuracy of the readings from these LVDTs, demec gauge rosettes were installed on the opposite face of the beams. The results showed that similar readings were obtained in most cases, with the main advantage of the LVDTs being the availability of continuous readings throughout the tests, allowing important events during the test to be monitored.

To place the LVDTs on the concrete beam face, 20 mm deep holes were carefully made using a hammer drill. 3/8 inch diameter threaded rods were installed into the holes with epoxy. The LVDTs were affixed to the threaded rods. Figure 3-32 shows one LVDT rosette arrangement. The direction of the LVDTs within the arrangement varied for different beams, but 3 directions separated by 45 degrees were used in all cases.

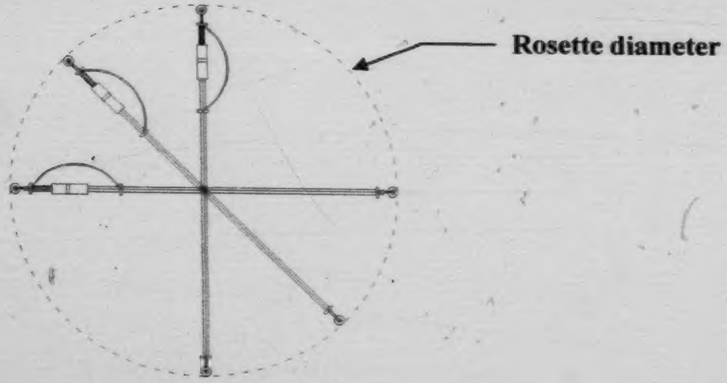

Figure 3-32 LVDT rosettes

Five more LVDTs were placed on the beams to measure global specimen deformation. Three of the LVDTs were placed to measure the vertical deflection along the beams. The other two of LVDTs were placed at each end of the specimen to measure axial deformations of the specimens. Details of LVDT locations on the specimens are shown in Figure 3-33.

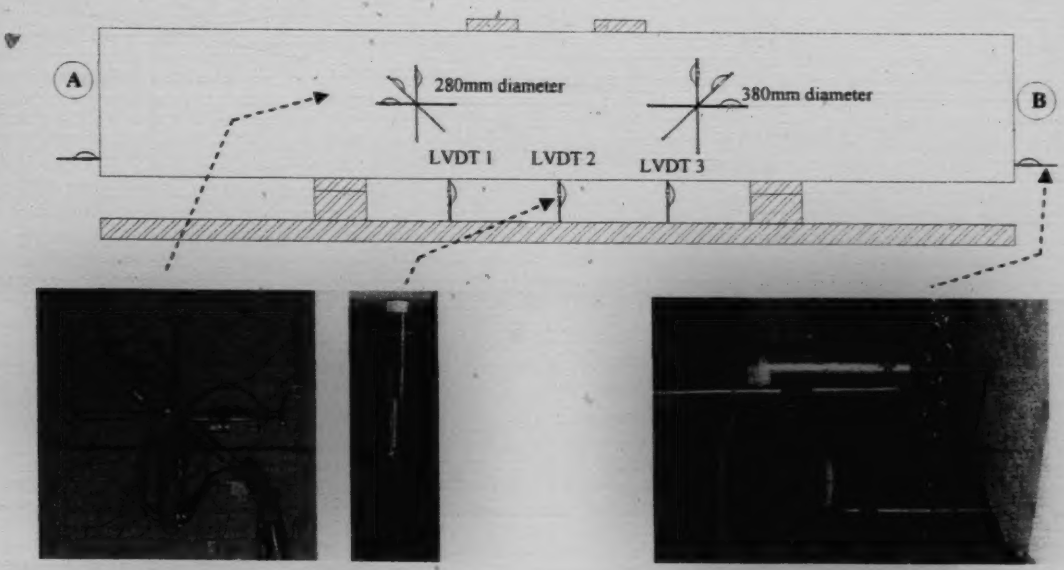

Figure 3-33 LVDT locations

For the LVDTs that measured the vertical deflection of the beam at three points, the distance to the midspan changed for each beam. Table 3-6 shows the distances from the midspan to the LVDT locations on the bottom of the beams.

Table 3-6 Distances measured from midspan to the locations where deflections were measured

Test Specimen	LVDT 1 (mm)	LVDT 2(mm)	LVDT 3(mm)
MS1-1	425	0	425
MS1-2	425	0	425
MS1-3	425	0	425
MS2-2	675	0	675
MS2-3	675	0	675
MS3-2	725	0	725
NS1-4	425	0	425
NS2-4	675	0	675
MW1-2	425	0	425
MW3-2	725	0	725

The locations of demec gauges placed on the opposite face of the specimens are shown in Figure 3-34.

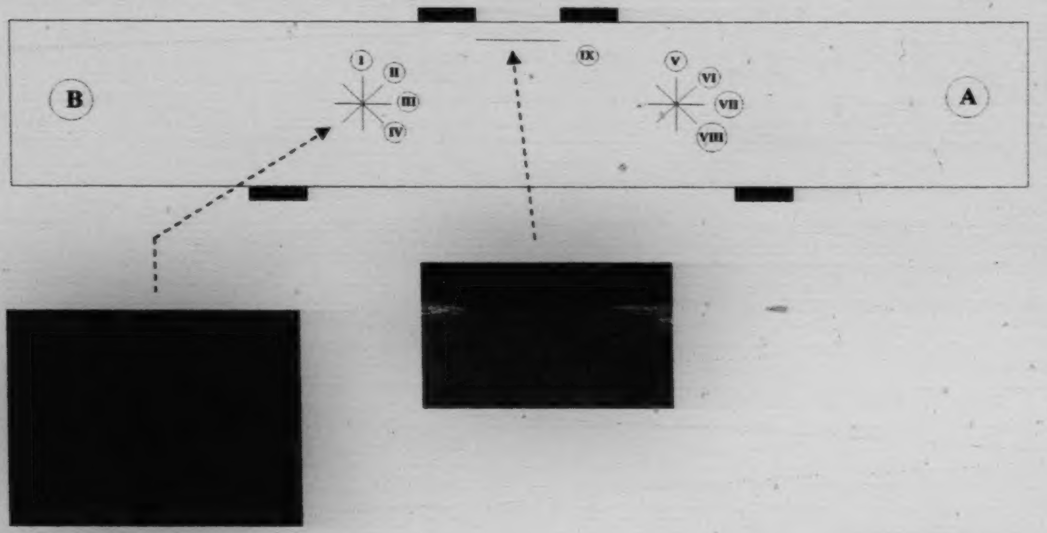

Figure 3-34 Demec gauge locations

3.6.3 Data acquisition system and Camera system

A data acquisition system was used to store all instrumentation readings during each test. Up to 57 channels were monitored. All strain gauge readings were zeroed prior to the start of the test. The sample rates for measurements were every 10 kN of applied load for stages of loadings up to approximately 70 % of the predicted failure load. Once 70 % of the predicted failure load was reached, data was acquired every 2 seconds.

A video camera was used to record each test, especially during the test failure.

3.7 Test Procedure

Tests were carried out using a MTS 6000 universal testing machine.

To easily locate the beam cracks on the pictures taken during the test, a 100 mm grid was drawn on each face of the beam. Shrinkage cracks were marked prior to the test in order to avoid confusion with the flexural and shear cracks during the test. An initial photograph was taken for each beam.

Once the set up was ready, one of the rollers on the top of the beam was fixed to avoid problems of instability of the system during loading stages.

The load was applied through the two loading points using a series of load stages. The interval of manual readings varied for each beam and they are described in Chapter 4. In general, manual readings were taken each 200 kN at early stages and every 100 kN towards the end of each test. At each interval, the loading was held while demec gauge readings were taken. All cracks were marked with a black marker and the crack widths were measured using a crack comparator gauge. The crack width measurements were recorded on the specimen using stickers and a photograph was taken once all the cracks were measured. After all photographs were taken, the loading process resumed until the next required load stage was reached and the same procedure was followed.

4. EXPERIMENTAL RESULTS

4.1 Presentation of results

The results obtained from the laboratory test for each of the specimens described in Chapter 3 are presented in this chapter.

Load-deflection response, crack patterns, crack widths and reinforcement strains at different locations were monitored for each specimen during the tests. Each specimen was studied based on the information obtained from manual readings, photographs and the data acquisition systems. Also, average strains developed on the concrete surface and monitored by LVDTs or demec gauges are presented in this chapter. These average concrete strains were measured in the direct diagonal struts located between the loading points and the supports and along the horizontal strut between the loading points.

Graphs presented in this chapter show information about load-deflection response, strain distribution along the main tension reinforcement, principal strains, angles of principal strains and strain at the compression zone between loading points. The load-strain responses for the rest of strain gauges and LVDTs in each test are provided in Appendix A.

The loads for important events during each test are indicated in this chapter. These loads, taken as the total loads monitored by the load cells at both supports, include the loads corresponding to first flexural cracking, formation of the first diagonal strut cracks in each shear span, first yielding of stirrups when applicable, first yielding of the three different layers of longitudinal main reinforcement when applicable and at the stages of manual demec gauge readings. For all the tests, similar load cell readings were obtained at both supports, indicating that the specimens were symmetrically loaded.

For each specimen, the loads corresponding to serviceability deflection limits according to CSA A23.3-04 and ACI 318-05 are identified. The deflection limits identified in the CSA A23.3-04 and ACI 318-05 design codes are *l/180* for flat roofs not supporting or attached to non-structural elements likely to be damaged by large deflections and *l/360* for floors not supporting or attached to non-structural elements likely to be damaged by large deflections.

Crack development during each test was examined. Only the crack patterns at approximately 70% of P_{max} are shown in this chapter. Crack patterns at this percentage of P_{max} were selected for comparison because load stages at approximately 70% of P_{max} were taken for all the specimens. Furthermore, this load level would be similar to the typical service load level, if the corresponding design model could accurately predict the maximum member capacity. Complete histories of crack development for every load stage are provided in Appendix A. The serviceability crack width limits set by CSA A23.3-04 and ACI 318-05 are 0.33 mm and 0.4 mm, depending on the exposure class against environmental influences. Eurocode 2 establishes similar crack width limits, corresponding to 0.3 mm for exposed structures and 0.4 for non-exposed structures. The loads corresponding to crack widths reaching approximately 0.33 mm and 0.4 mm (by interpolation) are identified in this chapter.

Table 4-1 summarizes key results for the specimens. Additional details for individual specimens are provided in Sections 4.2 to 4.11.

Table 4-1 Material properties, failure loads and modes of failure of all specimens

Specimen	a/d	ρ (%)	f'_c (MPa)	f_y* (MPa)	ε_y	Load at first crack (kN)		Mode of failure	P_{max} (kN)	$\Delta@P_{max}$** at midspan (mm)
						Flexural	Strut			
MS1-1	1.19	0.52	46	838	0.0063	200	354	Flexure	1252	13.66
MS1-2	1.19	1.13	44	870	0.0063	271	410	Flexure	2142	14.90
MS1-3	1.18	2.29	44	880	0.0065	389	640	Splitting strut	2747	7.86
MS2-2	1.79	1.13	47	870	0.0063	192	376	Flexure	1432	24.62
MS2-3	1.78	2.29	43	880	0.0065	293	560	Flexure-Splitting strut	2055	12.50
MS3-2	2.38	1.13	48	870	0.0063	130	258	Flexure	1154	35.06
MW1-2	1.19	1.13	39	870	0.0063	257	393	Splitting strut	1568	7.50
MW3-2	2.38	1.13	43	870	0.0063	99	247	Splitting strut	411	9.08
NS1-4	1.18	1.77	23	401	0.0020	102	351	Flexure-Splitting strut	1567	7.50
NS2-4	1.80	1.77	25	401	0.0020	192	153	Flexure	1078	13.28

*Effective yield stress (0.2% offset method) for ASTM A1035 reinforcing steel and yield stress for Grade 400R reinforcing steel

** Deflection at the maximum load reached during the test

4.2 Specimen MS1-1

Specimen MS1-1 was the specimen with the lowest ρ of 0.52%. It had an a/d ratio of 1.2. The failure mode observed was flexural failure. Yielding of the three layers of main tension reinforcement and web reinforcement was observed prior to failure. After reaching its maximum load (P_{max}) at 1252 kN, the capacity of the specimen started decreasing until failure of main tension reinforcement occurred. Figure 4-1 shows specimen MS1-1 after failure.

Figure 4-1 Specimen MS1-1 after failure

Shrinkage cracks were marked prior to the start of loading. Once the test started, the loading process was by displacement control. The load was held at different intervals to take demec gauge readings, to mark crack patterns and measure the crack widths, and to photograph the specimen. There were eleven load stages, as shown in Section A.1 of Appendix A.

4.2.1 Load-deflection response of specimen MS1-1

The deflection at midspan corresponding to P_{max} was 13.66 mm. The first serviceability deflection limit (*l/360)* of 4.72 mm was reached at a total applied load of 804 kN, or 64.2 % of P_{max}. The second serviceability limit (*l/180)* of 9.44 mm was reached at a load of 1128 kN, or 90.1% of P_{max}. Figure 4-2 illustrates the deflection at midspan and at locations 450 mm from midspan for specimen MS1-1.

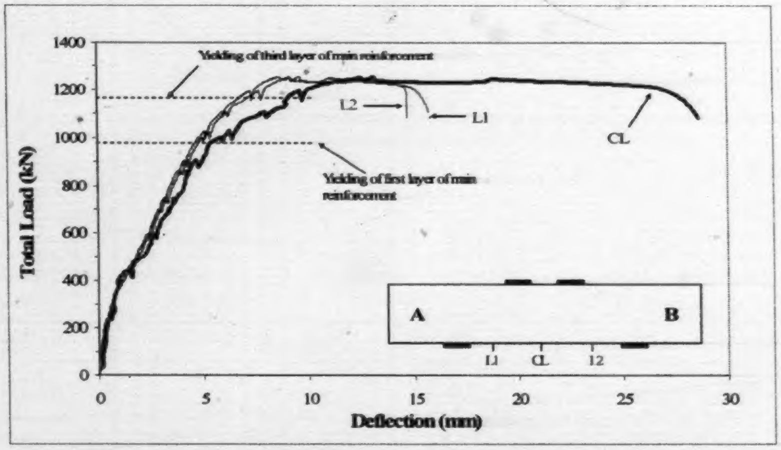

Figure 4-2 Deflection at midspan and 450 mm from midspan for specimen MS1-1

4.2.2 Crack development of specimen MS1-1

Flexural and diagonal strut cracks were developed in specimen MS1-1. The widest diagonal strut crack developed at each shear span went from the interior edge of the support to the center of the load bearing plate. Some other small diagonal strut cracks were also observed.

The flexural and flexural-diagonal strut cracks were developed at the location of the stirrups. The main shear crack started approximately at mid height of the specimen propagating toward the interior edge of the support and to the middle of the compression zone (node) at the loading point. Table 4-2 shows the load and percentage of maximum load for the first flexural crack, first diagonal strut cracks at both sides and approximate load when serviceability limit cracks width for specimen MS1-1 were reached.

Table 4-2 Load and %P_{max} at different crack stages of specimen MS1-1

Cracks	Load *(kN)*	% P_{max}
First Flexural crack (FC)	200	16.0
First Diagonal strut A (DSA)	365	29.2
First Diagonal Strut B (DSB)	354	28.3
Serviceability limit 0.33 mm at FC	377	30.1
Serviceability limit 0.4 mm at FC	407	32.5
Serviceability limit 0.33 mm at DSA	498	39.8
Serviceability limit 0.33 mm at DSB	547	43.7
Serviceability limit 0.4 mm at DSA	600	47.9
Serviceability limit 0.4 mm at DSB	600	47.9

The load corresponding to the first flexural crack was obtained where the slope changed on the load-deflection plot (Figure 4-2). The value was also compared against the load-strain response from the strain gauges located on the longitudinal reinforcement at midspan. The approximate loads corresponding to the serviceability limits for crack width were obtained from linear interpolation of crack width measurements between load stages.

Figure 4-3 illustrates the crack patterns and crack widths at a load of 900 kN (72% of P_{max}) for specimen MS1-1. The widest crack at 72% of P_{max} was the diagonal strut crack at shear span A, with a measured width of 1.0 mm.

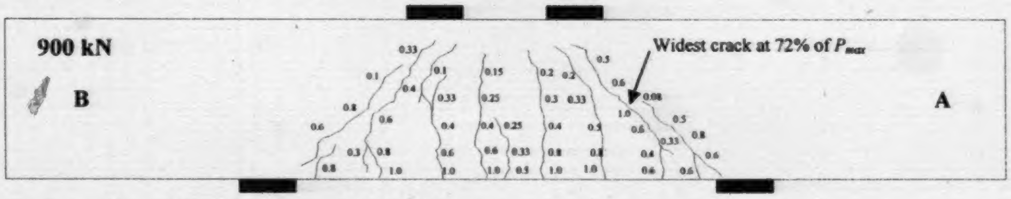

Figure 4-3 Crack development of specimen MS1-1 at 72% of P_{max}

4.2.3 Strains in reinforcement and average strains in concrete for specimen MS1-1

The measured strain in each of the three layers of main longitudinal reinforcement and in the web reinforcement all reached the effective yield strength, shown in Table 3-1, prior to the maximum applied load P_{max}. (see Table 4-3). After strains in the three layer of the longitudinal reinforcement exceeded the effective yield strain according to the 0.2% offset method, crushing of the concrete in the compression zone between the loading points was observed. Loading continued under displacement control and necking of the main tension reinforcement was observed in the crack opening. The test ended after the tension reinforcement suddenly failed by rupture at this location. No cracking suggesting a bond or anchorage failure was observed at the ends of the specimen.

Table 4-3 Loads and %P_{max} for yielding of reinforcement for specimen MS1-1

Yielding of reinforcement	Load (*kN*)	% P_{max}
1st layer of main reinforcement	990	79.1
2nd layer of main reinforcement	no data	
3rd layer of main reinforcement	1174	93.8
Vertical web reinforcement at end A	995	79.5
Vertical web reinforcement at end B	887	70.8
Horizontal web reinforcement at end A	1225	97.8
Horizontal web reinforcement at end B	no data	

The variation in strain along one bar in the lowest layer of main longitudinal reinforcement for different loading stages is shown in Figure 4-4. The figure illustrates that the development length for the longitudinal reinforcement beyond the support was adequate, since no strains were detected in the bar beyond 300 mm from the exterior edge of the bearing plate. The strain distribution for the bar along the specimen span was relatively uniform. Strains at the exterior edges of the supports were small compared to the strains developed in the clear span due to anchorage of the reinforcement forces from the action of diagonal compression struts formed between the loading points to the supports.

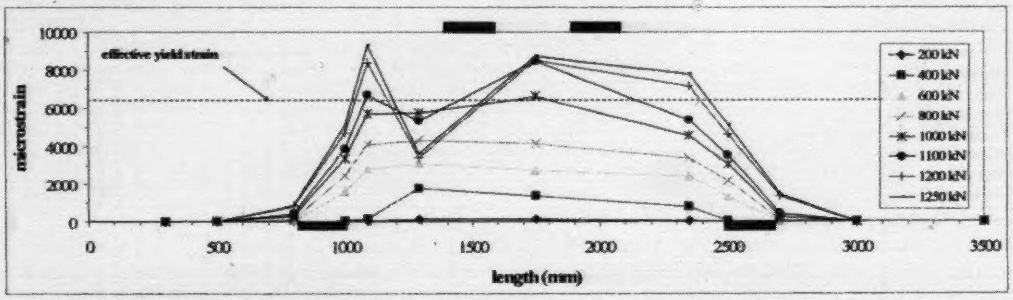

Figure 4-4 Strain distribution along the bar located in the lowest layer of main tension reinforcement of specimen MS1-1

Demec gauges and LVDTs were used to determine the average concrete strains for different directions within a rosette configuration on the path of the direct diagonal struts. Set up of these LVDTs and demec gauges was shown in Figure 3-33 and Figure 3-34. In general, demec gauge readings and LVDT readings were similar for all specimens. Figure 4-5 compares LVDT data with the demec gauge manual readings for side A of specimen MS1-1 in the vertical, diagonal compression and diagonal tension directions. It can be observed that both methods of measurements gave similar results. However, the LVDT gauges provided continuous readings, allowing for easier monitoring of strains corresponding to important events in the loading process. Furthermore, a disadvantage of demec gauge rosettes compared to the LVDT rosettes is the smaller diameter: 200 mm for demec rosettes and 380 or 280 mm for LVDT rosettes. Taking into account that the strains measured by the gauges are average strains, the smaller diameter demec rosettes may not measure a representative area of cracked and uncracked concrete, thus giving poorer quality calculations for the average strains.

Figure 4-6 shows the principal tension and compression strains developed in the diagonal strut and the angle corresponding to the principal compressive strains relative to the horizontal axis. The results are more meaningful in later loading stages where the average strains relative to the instrumentation sensitivity are larger.

The strain for the top strut located between loading points was monitored for this specimen using manual readings from demec gages located 70 mm from the top fiber of the specimen up to a load of 1200 kN. These manual readings are plotted in Figure 4-7.

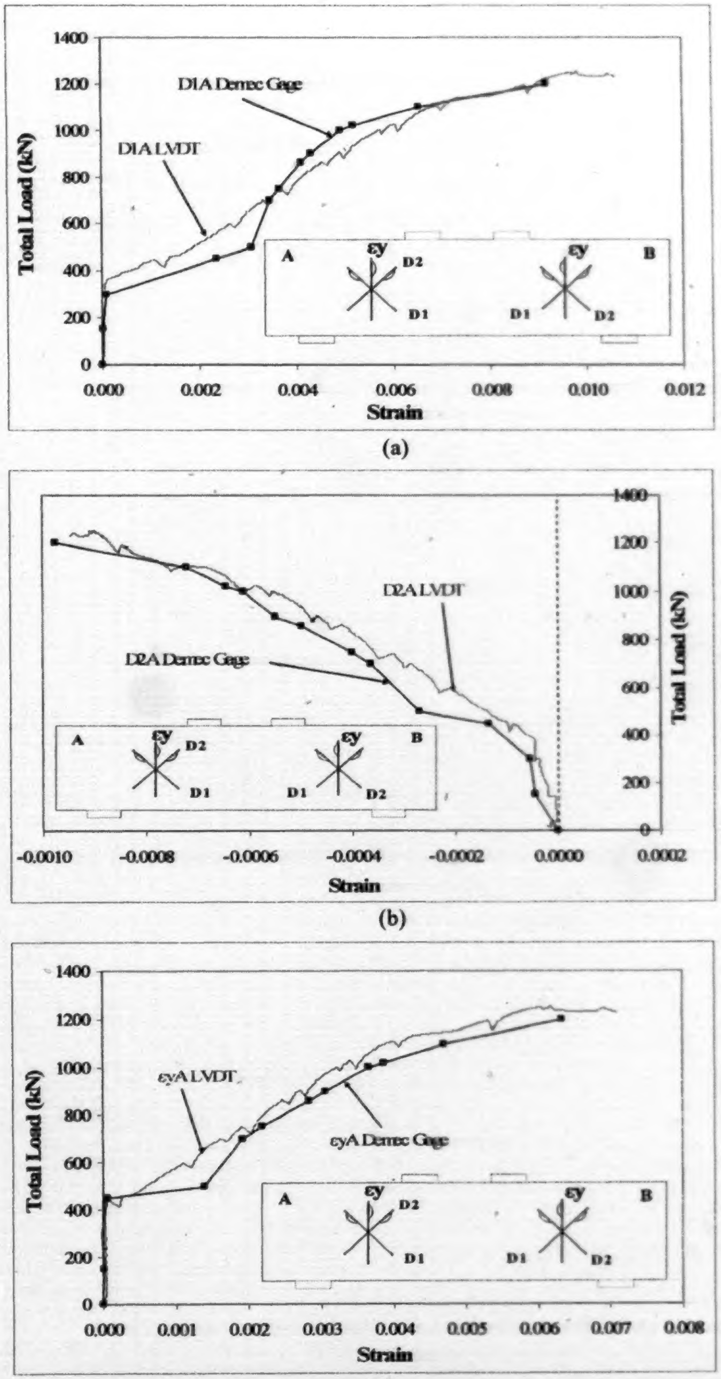

(c)

Figure 4-5 Comparison of results using demec gages and LVDTs. (a) Average strains in diagonal D1 direction , (b) average strains in diagonal D2 direction and (c) average strain in vertical direction

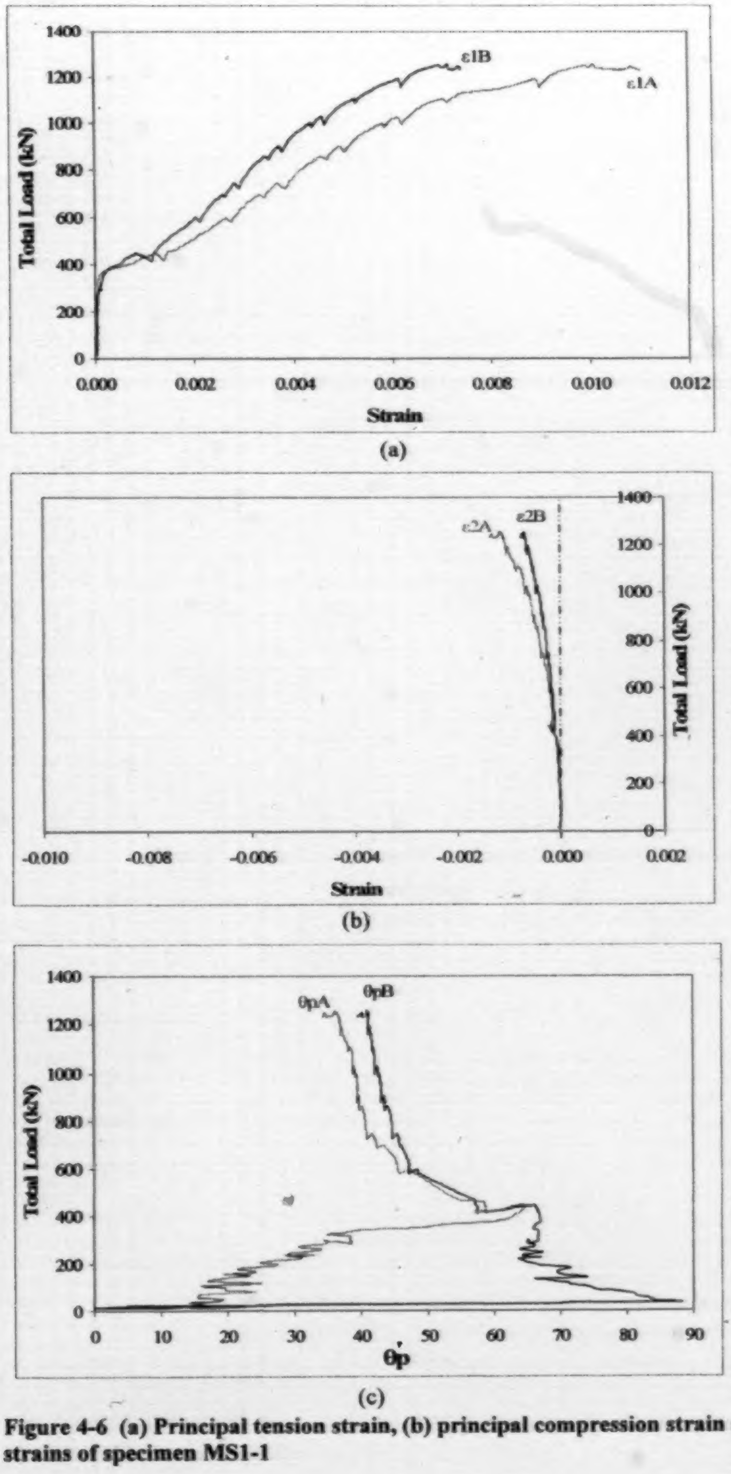

(a)

(b)

(c)

Figure 4-6 (a) Principal tension strain, (b) principal compression strain and (c) angle of principal strains of specimen MS1-1

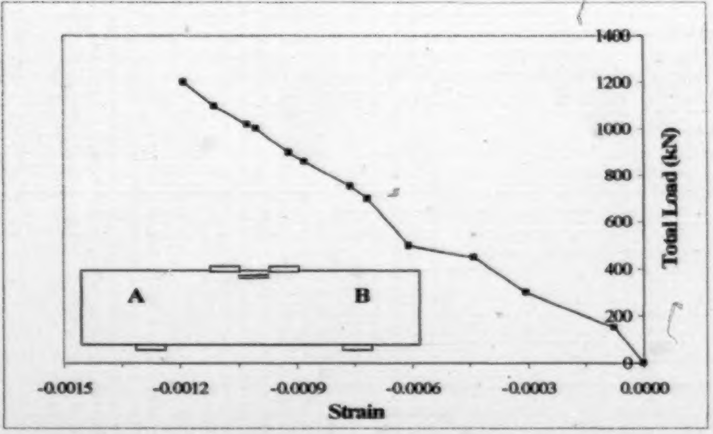

Figure 4-7 Strain in top strut between loading points of specimen MS1-1

4.3 Specimen MS1-2

Specimen MS1-2 had the same dimensions as specimen MS1-1 but a higher reinforcement ratio ρ of 1.13%. The effective yielding strain was reached in the lowest two layers of main tension reinforcement and crushing of the compression zone between the loading points were observed prior to P_{max} of 2142 kN. After P_{max}, the load started to drop for increased deflection, until diagonal strut failure occurred. The vertical web reinforcement of specimen MS1-2 yielded prior to P_{max}. Figure 4-8 shows specimen MS1-2 after failure.

Figure 4-8 Specimen MS1-2 after failure

As was done for specimen MS1-1, marking of shrinkage cracks was carried out prior to the loading process. There were a total of eleven load stages where all necessary readings were taken, as shown in Section A.2 of Appendix A.

4.3.1 Load-deflection response of specimen MS1-2

Figure 4-9 illustrates the deflection at midspan and at locations 450 mm from midspan for specimen MS1-2. The deflection at midspan when the specimen reached P_{max} was 14.90 mm. The first serviceability deflection limit *(l/360)* of 4.72 mm was reached at a total applied load of 1278 kN, or 59.7 % of P_{max}. The second serviceability limit *(l/180)* of 9.44 mm was reached at a load of 1978 kN, or 92.3% of P_{max}.

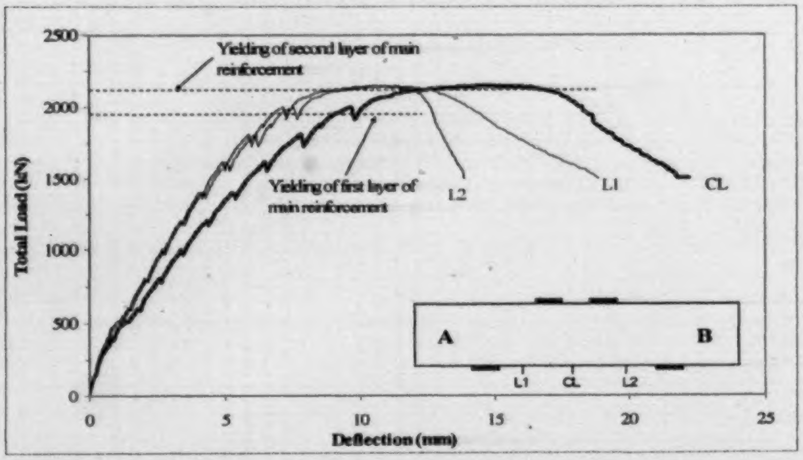

Figure 4-9 Deflection at midspan and 450 mm from midspan of specimen MS1-2

4.3.2 Crack development of specimen MS1-2

Both flexural and diagonal strut cracks developed in specimen MS1-2. Flexural cracks developed in the constant moment region. The flexural and flexural-diagonal strut cracks developed at the locations of the stirrups. A main diagonal strut crack developed at each shear span, going from the interior edge of the support plate to the center of the loading plate. These strut cracks initially formed at approximately mid-height of the specimen. A smaller crack was also observed at the diagonal strut at side B, on the exterior side of the main strut crack.

Table 4-4 shows the load and percentage of maximum load corresponding to the first flexural crack, first diagonal strut cracks at each shear span and at the approximate load corresponding to the serviceability limits for crack widths for specimen MS1-2. The procedure used to obtain the loads for these crack conditions is explained in Section 4.2.2.

Table 4-4 Load and %P_{max} at different crack stages of specimen MS1-2

Cracks	Load (kN)	% P_{max}
First Flexural crack (FC)	271	12.7
First Diagonal strut A (DSA)	410	19.1
First Diagonal Strut B (DSB)	456	21.3
Serviceability limit 0.33 mm at FC	860	40.1
Serviceability limit 0.4 mm at FC	1000	46.7
Serviceability limit 0.33 mm at DSA	800	37.3
Serviceability limit 0.33 mm at DSB	820	38.3
Serviceability limit 0.4 mm at DSA	822	38.4
Serviceability limit 0.4 mm at DSB	866	40.4

Figure 4-10 illustrates the crack patterns and crack widths at a load of 1600 kN (74.7% of P_{max}) for specimen MS1-2. The widest crack at 74.7% of P_{max} was the diagonal strut crack at shear span A, with a measured width of 1.25 mm.

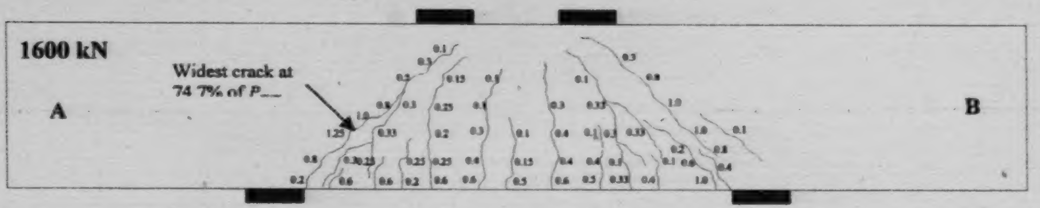

Figure 4-10 Crack development at 74.7% of P_{max} for specimen MS1-2

4.3.3 Strains in reinforcement and average strains in concrete for specimen MS1-2

For specimen MS1-2, longitudinal reinforcement strains corresponding to the effective yield strain (see Table 3-1) were reached for the two lowest layers of main tension reinforcement prior to the applied load P_{max}. Yielding of vertical web reinforcement (strains exceeding ε_y=0.002) was observed before P_{max} (See Table 4-5).

Crushing of the concrete in the compression zone between the loading points started at a total load of approximately 1950 kN or 91 % of P_{max}.

Table 4-5 Loads and %P_{max} for yielding of reinforcement for specimen MS1-2

Yielding of reinforcement	Load (kN)	% P_{max}
1st layer of main reinforcement	1938	90.5
2nd layer of main reinforcement	2124	99.2
3rd layer of main reinforcement	Not yielded	
Vertical web reinforcement at end A	1001	46.7
Vertical web reinforcement at end B	874	40.8
Horizontal web reinforcement at end A	Not yielded	
Horizontal web reinforcement at end A	Not yielded	

The strain distribution along one bar located at the lowest layer of main longitudinal reinforcement for different loading stages is shown in Figure 4-11. The figure illustrates that no strains on the bar were detected beyond 300 mm from the exterior edge of the bearing plate, indicating that the anchorage of the reinforcement was satisfactory. The strains along the bar in the zone between the loading points were generally of similar magnitude during the initial portion of the test. However, strain gauges located at the support edges or close to the supports showed different patterns for later loading stages. At higher loads, strains close to the supports were larger than strains at midspan due to the formation of wide cracks near the supports. This strain distribution is consistent with the Direct Strut Mechanism. Strains at the exterior edges of the supports were small compared to the strains developed in the clear span due to anchorage of the reinforcement forces from the action of diagonal compression struts formed between the loading points to the supports.

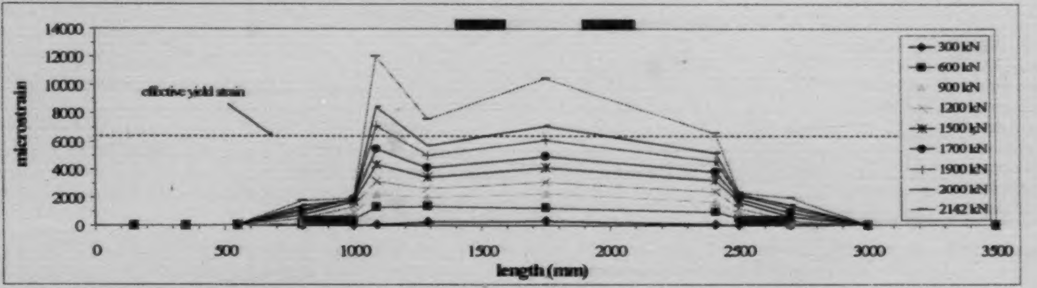

Figure 4-11 Strain distribution along the bar located in the lowest layer of main tension reinforcement of specimen MS1-2

Figure 4-12 shows the principal tension strains, principal compression strains and angle corresponding to the principal compressive strains relative to the horizontal axis. The results are more meaningful in later loading stages where the average strains relative to the instrumentation sensitivity are larger.

Horizontal strains for the top strut located between the loading points was monitored for this specimen using manual readings from demec gauges located 70 mm from the top fiber of the specimen up to a load of 2000 kN. These manual readings are plotted in Figure 4-13.

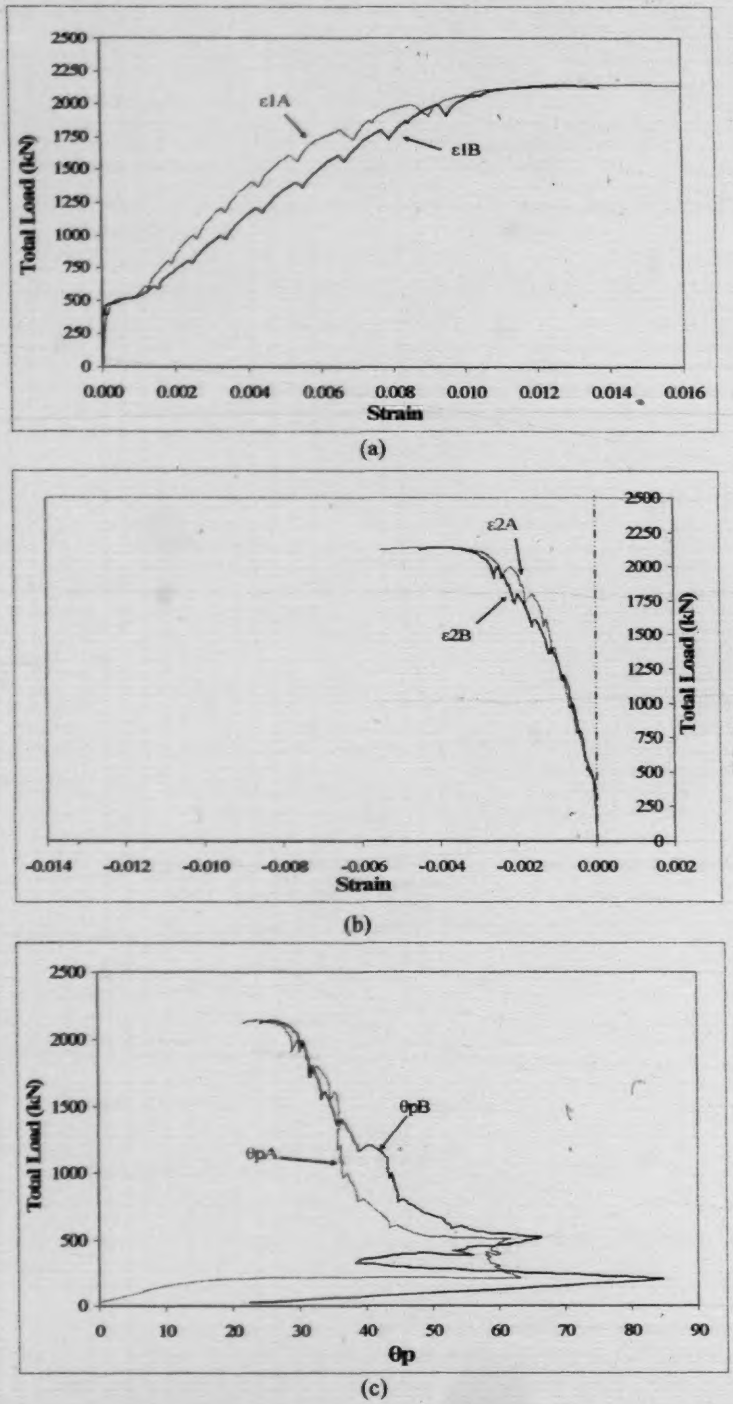

Figure 4-12 (a) Principal tension strain, (b) Principal compression strain and (c) angle of principal strains of specimen MS1-2

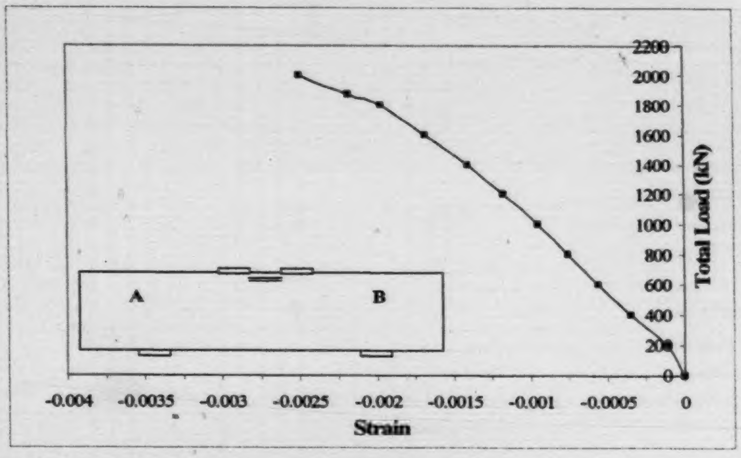

Figure 4-13 Strain in top strut of specimen MS1-2

4.4 Specimen MS1-3

Specimen MS1-3 had a shear span to depth ratio, *a/d*, of 1.18 and longitudinal reinforcement ratio, *ρ*, of 2.29%. A brittle diagonal strut failure was observed at a total load of 2747 kN. No cracks at the compression zone between the loading points or yielding in the main longitudinal reinforcement was detected. Yielding in vertical web reinforcement was monitored before reaching the failure load.

Figure 4-14 shows specimen MS1-3 after failure.

Figure 4-14 Specimen MS1-3 after failure

During the test, ten load stages were selected to take photographs and to take manual readings. These load stages are shown in Section A.3 of Appendix A.

4.4.1 Load-deflection response of specimen MS1-3

The deflection at midspan corresponding to P_{max} was 7.31 mm. The first serviceability deflection limit (*l/360)* of 4.72 mm was reached at a total applied load of 2166 kN, 78.8 % of P_{max}. The second serviceability limit (*l/180)* was not reached for this specimen prior to P_{max}. Figure 4-2 illustrates the load-deflection relationship at midspan and at locations 450 mm from midspan for specimen MS1-3. The slope of the load-deflection response stayed relatively constant during the entire load history. Note that for this specimen, the deflection readings at midspan (CL in Figure 4-15) were taken with a cable transducer, unlike the LVDTs used for the locations 450 mm from mid-span. The use of the cable transducer, which was less accurate than LVDTs, resulted in the deflection curve being less smooth compared with the curves from the LVDTsreadings (L1 and L2).

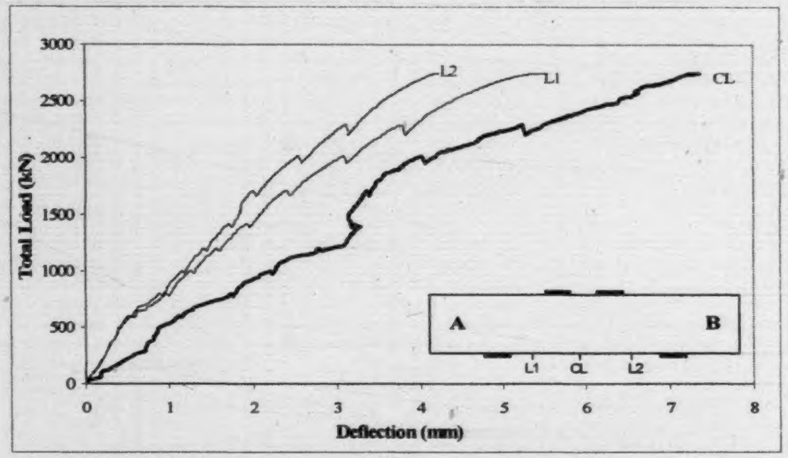

Figure 4-15 Deflection at midspan and 450 mm from midspan of specimen MS1-3

4.4.2 Crack development for specimen MS1-3

Both flexural and diagonal strut cracks developed in specimen MS1-3. The flexural crack widths remained relatively constant after the loading on the specimen reached 50% of P_{max} but the diagonal strut crack widths continued to increase for further loading stages. Diagonal strut cracks initially formed at mid-depth of the specimen and then propagated towards the inside edge of the support and towards the loading plate. All diagonal strut cracks were approximately parallel to each other.

Table 4-6 shows the load and percentage of maximum load corresponding to the first flexural crack, first diagonal strut cracks at both sides and the approximate load when serviceability limit for cracks widths of specimen MS1-3 were reached. The procedure used to obtain the loads for these crack conditions was explained in Section 4.2.2.

Table 4-6 Load and %P_{max} at different crack stages of specimen MS1-3

Cracks	Load (kN)	% P_{max}
First Flexural crack (FC)	389	14.2
First Diagonal strut A (DSA)	688	25.0
First Diagonal Strut B (DSB)	640	23.3
Serviceability limit 0.33 mm at FC	1490	54.2
Serviceability limit 0.4 mm at FC	1700	61.9
Serviceability limit 0.33 mm at DSA	1200	43.7
Serviceability limit 0.33 mm at DSB	1230	44.8
Serviceability limit 0.4 mm at DSA	1400	51.0
Serviceability limit 0.4 mm at DSB	1300	47.3

Figure 4-16 shows the crack patterns and crack widths at a load of 2000 kN (72.8% of P_{max}) for specimen MS1-3. The widest crack measured at 72.8% of P_{max} was the diagonal strut crack at shear span A, with a measured width of 1.25 mm.

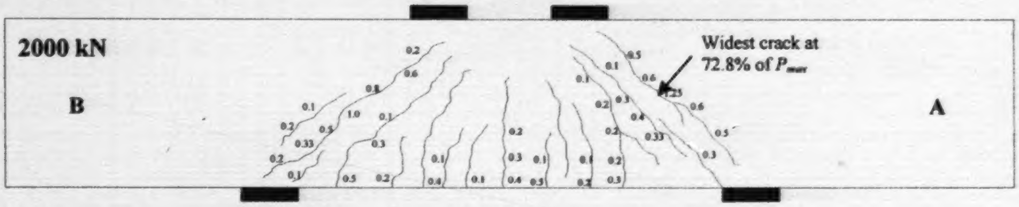

Figure 4-16 Crack development at 72.8% of P_{max} of specimen MS1-3

4.4.3 Strains in reinforcement and average strains in concrete of specimen MS1-3

No yielding was detected in the main tension reinforcement prior to the loading of P_{max}. At P_{max}, the maximum strain readings in the main tension reinforcement were 0.0035, 0.0031 and 0.0027 for first, second and third layers, respectively. Table 4-7 shows the loads and the percentage of P_{max} corresponding to yielding of vertical web reinforcement. Note that the yield strain of vertical web reinforcement was 0.002.

Table 4-7 Loads and $\%P_{max}$ for yielding of reinforcement for specimen MS1-3

Yielding of reinforcement	Load (kN)	$\% P_{max}$
1st layer of main reinforcement	Not yielded	
2nd layer of main reinforcement	Not yielded	
3rd layer of main reinforcement	Not yielded	
Vertical web reinforcement at end A	1391	50.6
Vertical web reinforcement at end B	1707	62.1
Horizontal web reinforcement at end A	Not yielded	
Horizontal web reinforcement at end A	Not yielded	

The variation in strain along one bar in the lowest layer of the main longitudinal reinforcement for different loading stages is shown in Figure 4-17. The figure illustrates that the anchorage length for the longitudinal reinforcement provided beyond the support was adequate, since no strains were detected in the bar beyond 300 mm from the exterior edge of the bearing plate. The strain distribution of the bar along the span of the specimen was relatively uniform. At the supports, the effect of the diagonal strut in anchoring the longitudinal reinforcement was observed through the strain reduction beyond the interior edges of the supports. No strain was detected in SG1, located close to the end of the bar, indicating that an adequate development length was used.

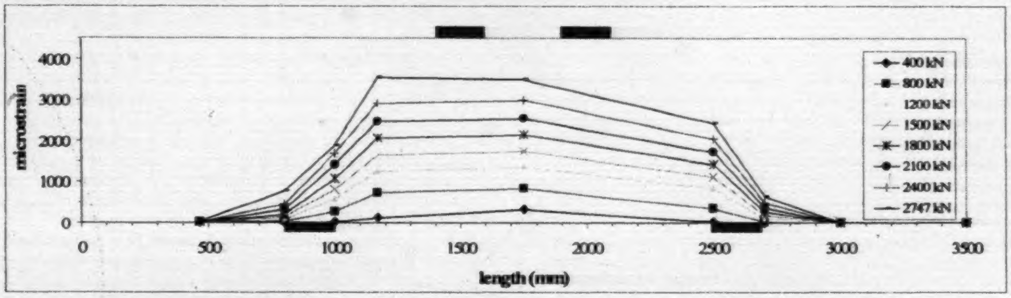

Figure 4-17 Strain distribution along the bar located in the lowest layer of main tension reinforcement of specimen MS1-3

Figure 4-18 shows the principal tension strains, principal compression strains and angle corresponding to the principal compressive strains relative to the horizontal axis. The results are more meaningful in later loading stages where the average strains relative to the instrumentation sensitivity are larger.

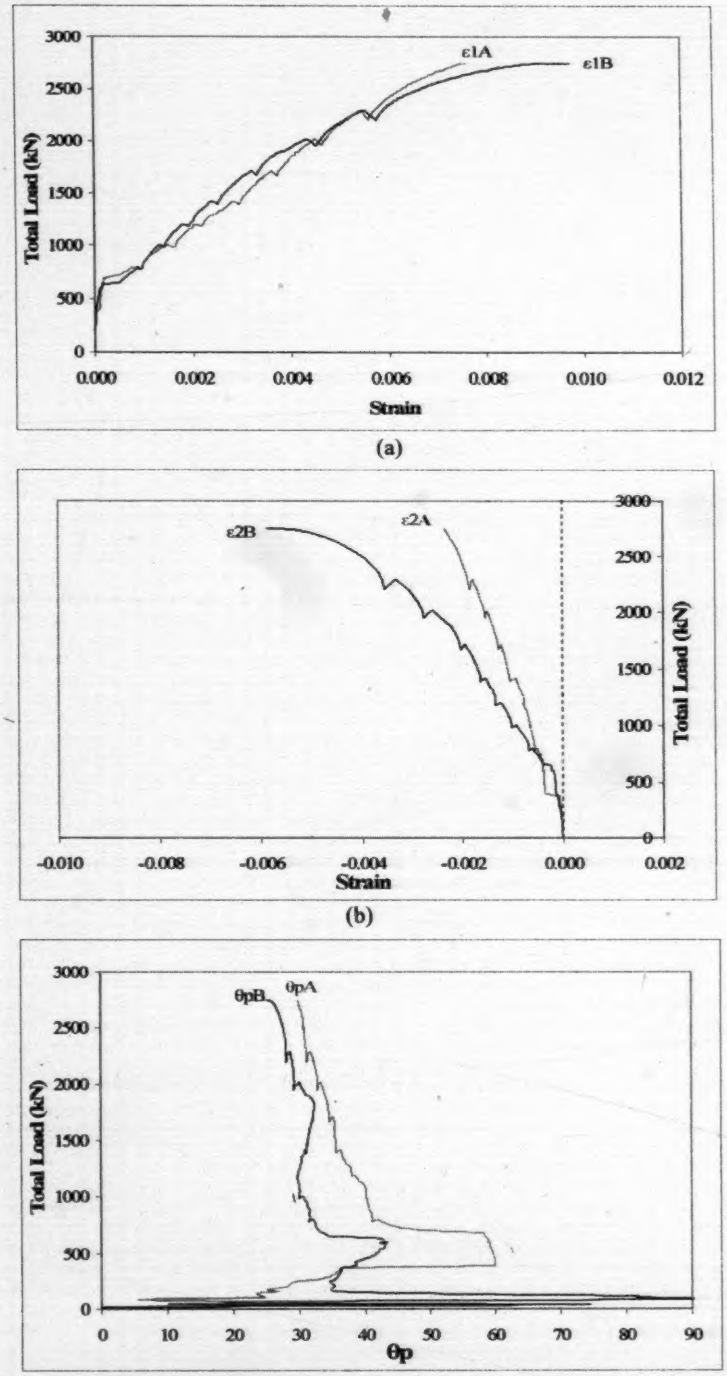

(a)

(b)

(c)

Figure 4-18 (a) Principal tension strain, (b) Principal compression strain and (c) angle of principal strains of specimen MS1-3

Horizontal strains for the top strut located between the loading points were monitored with manual readings from demec gauges located 70 mm from the top fiber of the specimen up to a load of 2300 kN. These manual readings are plotted in Figure 4-19.

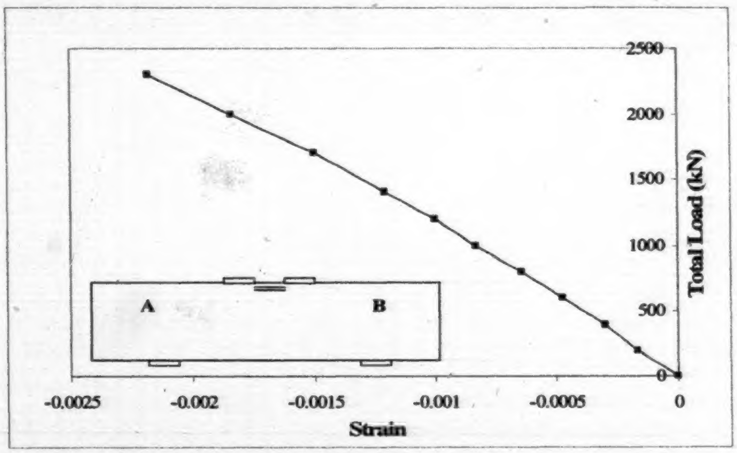

Figure 4-19 Strains in the compression zone between the loading points of specimen MS1-3

4.5 Specimen MS2-2

Specimen MS2-2 had a shear span to depth ratio of 1.79 and longitudinal reinforcement ratio ρ of 1.13%. The failure mode was by flexure (see Figure 4-20). Prior to P_{max} of 1432 kN in specimen MS2-2, strains exceeding the effective yield strain for the main tension reinforcement were detected, followed by crushing of the compression zone between the loading points.

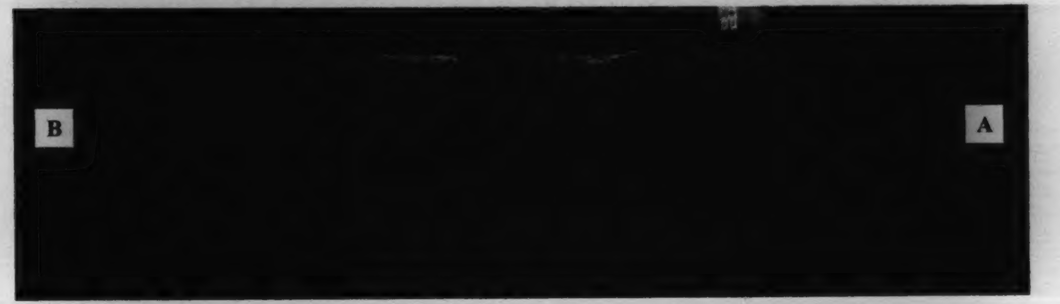

Figure 4-20 Specimen MS2-2 after failure

Shrinkage cracks were marked prior to the start of the loading process. There were a total of seven load stages where all necessary readings were taken, as shown in Section A.4 of Appendix A.

4.5.1 Load-deflection response of specimen MS2-2

Figure 4-23 illustrates the deflection at midspan and at locations 675 mm from midspan for specimen MS2-2. The deflection at midspan when the loading on the specimen reached P_{max} was 24.62 mm. The load at which specimen MS2-2 reached the first serviceability limit for deflection (*l/360)* was at a total applied load of 796 kN (55.6 % of P_{max}) with a deflection of 6.39 mm. The second serviceability limit for deflection (*l/180)* was reached at a load of 1236 kN (86.3 % of P_{max}) with a deflection of 12.78 mm.

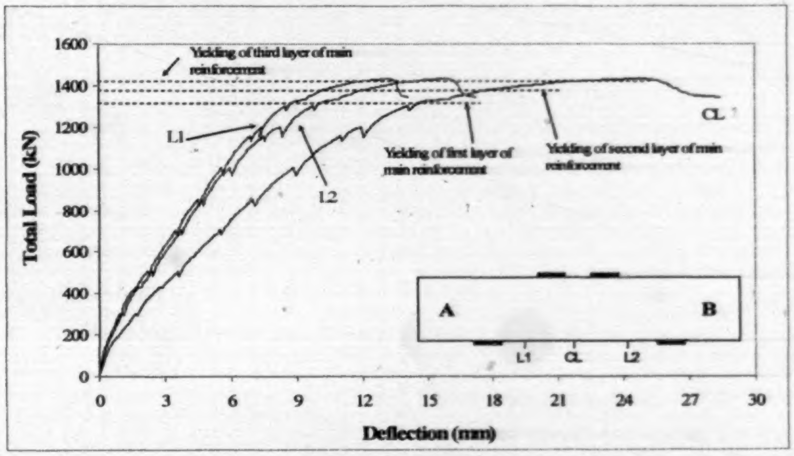

Figure 4-21 Deflection at midspan and 675 mm from midspan of specimen MS2-2

4.5.2 Crack development of specimen MS2-2

Both flexural and diagonal strut cracks developed in specimen MS2-2. The width of the flexural cracks and width of diagonal strut cracks both increased during the entire loading process. The entire length of the strut cracks were approximately parallel to each other and to the diagonal strut axis.

Table 4-8 shows the load and percentage of maximum load corresponding to the first flexural crack, first diagonal strut cracks at both sides and the serviceability limits for crack widths for specimen MS2-2.

Table 4-8 Load and $\%P_{max}$ at different crack stages of specimen MS2-2

Cracks	Load (kN)	$\% P_{max}$
First Flexural crack (FC)	192	13.4
First Diagonal strut A (DSA)	376	26.3
First Diagonal Strut B (DSB)	387	27.0
Serviceability limit 0.33 mm at FC	500	34.9
Serviceability limit 0.4 mm at FC	586	40.9
Serviceability limit 0.33 mm at DSA	565	39.5
Serviceability limit 0.33 mm at DSB	586	40.9
Serviceability limit 0.4 mm at DSA	600	41.9
Serviceability limit 0.4 mm at DSB	633	44.2

Figure 4-22 shows the crack development and crack widths up to 1000 kN (69.8% of P_{max}) for specimen MS2-2. The widest cracks measured at 69.8% of P_{max} were the flexural cracks at mid-span and the diagonal strut crack at both shear spans, all with widths of 1.0 mm.

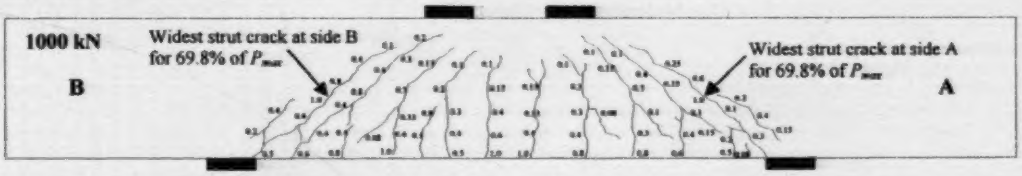
1000 kN
B
Widest strut crack at side B for 69.8% of P_{max}
Widest strut crack at side A for 69.8% of P_{max}
A

Figure 4-22 Crack development at 69.8% of P_{max}

4.5.3 Strains in reinforcement and average strains in concrete for specimen MS2-2

For specimen MS2-2, strains in the three layers of main tension reinforcement reached the effective yielding strain prior to the loading of P_{max}. At P_{max} the strains at midspan on the first, second and third layer of reinforcement were 0.0104, 0.0086 and 0.0065 respectively. Table 4-9 shows the loads and the percentage of P_{max} corresponding to yielding of the three layers of main tension reinforcement and yielding of web reinforcement for both sides of specimen MS2-2.

Table 4-9 Loads and $\%P_{max}$ for yielding of reinforcement for specimen MS2-2

Yielding of reinforcement	Load *(kN)*	$\% P_{max}$
1st layer of main reinforcement	1332	93.0
2nd layer of main reinforcement	1381	96.4
3rd layer of main reinforcement	1429	99.8
Vertical web reinforcement at end A	626	43.7
Vertical web reinforcement at end B	804	56.1
Horizontal web reinforcement at end A	Not yielded	
Horizontal web reinforcement at end B	Not yielded	

The strain distribution along one of the bars located at the lowest layer of main tension reinforcement is illustrated in Figure 4-23. The figure illustrates that the anchorage length for the longitudinal reinforcement beyond the support was adequate, since no strains were detected in the bar beyond 350 mm from the exterior edge of the bearing plate. For the initial part of the test, the strains in the reinforcement bar were relatively constant along the clear span. Due to the development of a crack close to support B, the strains at this location for loads close to P_{max} were larger than the strains monitored at midspan. Strains in the exterior edges of the supports were small compared with the strains developed in the clear span due anchorage of the reinforcement from the action of the diagonal compression strut formed between the loading points to the support.

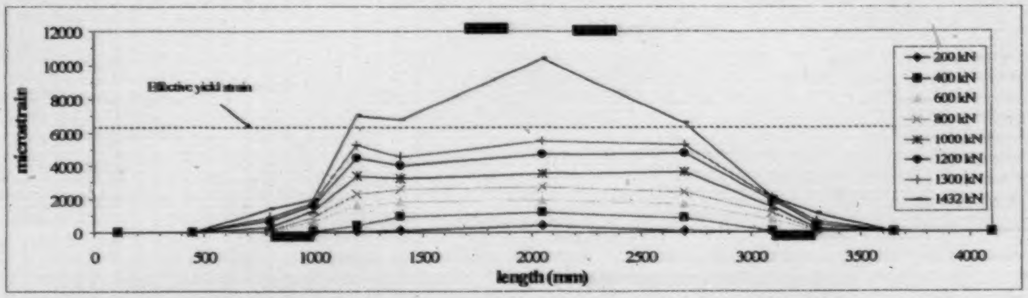

Figure 4-23 Strain distribution along the bar located in the lowest layer of main tension reinforcement of specimen MS2-2

Figure 4-24 shows the principal tension strains, principal compression strains and angle corresponding to the principal compressive strains relative to the horizontal axis for side B of specimen. The results are more meaningful in later loading stages where the average strains relative to the instrumentation sensitivity are larger. Principal strains and angle of principal strains could not be calculated at side A because the LVDTs rosette was damaged during the test and no readings were available.

Figure 4-25 shows the curves of the horizontal strains versus load taken using demec gages 70 mm from top fiber of the specimen and using strain gages located on the longitudinal reinforcement in the compression zone.

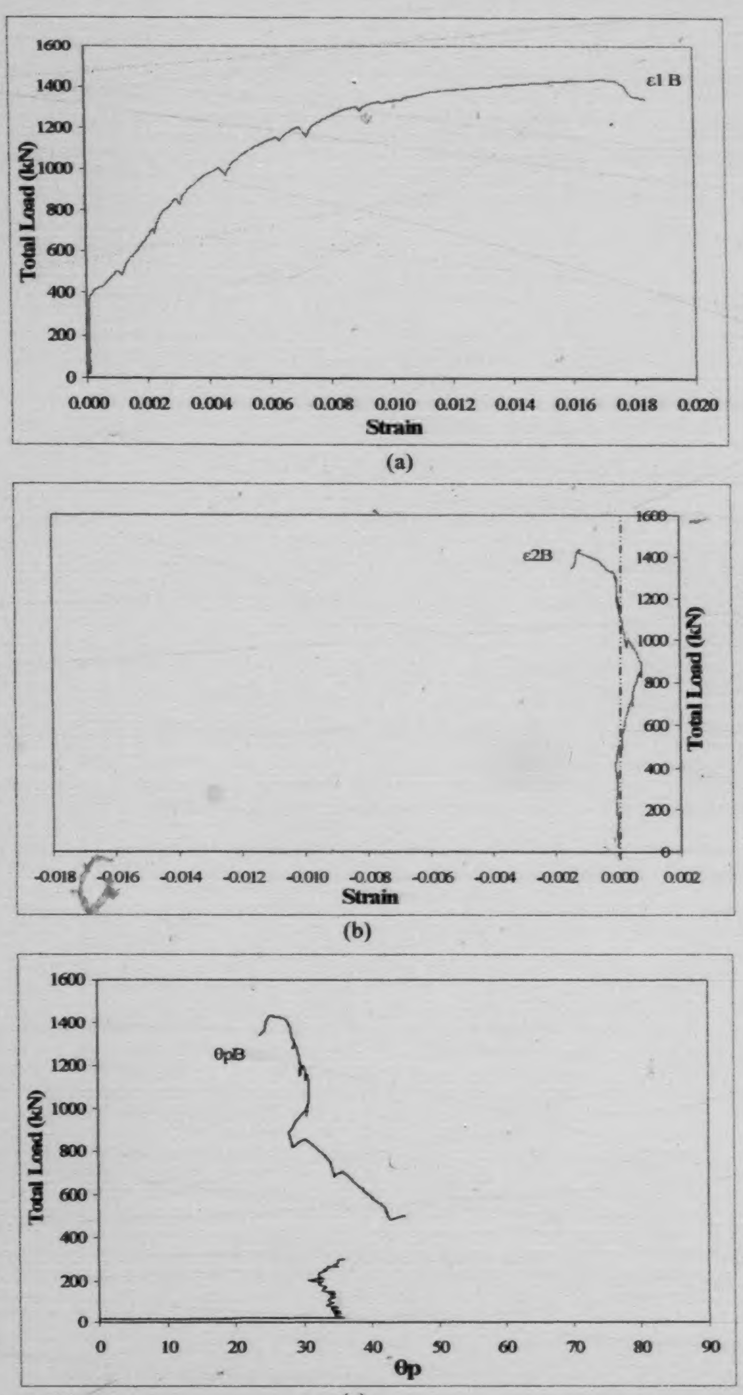

(a)

(b)

(c)

Figure 4-24 (a) Principal tension strain, (b) Principal compression strain and (c) angle of principal strains of specimen MS2-2

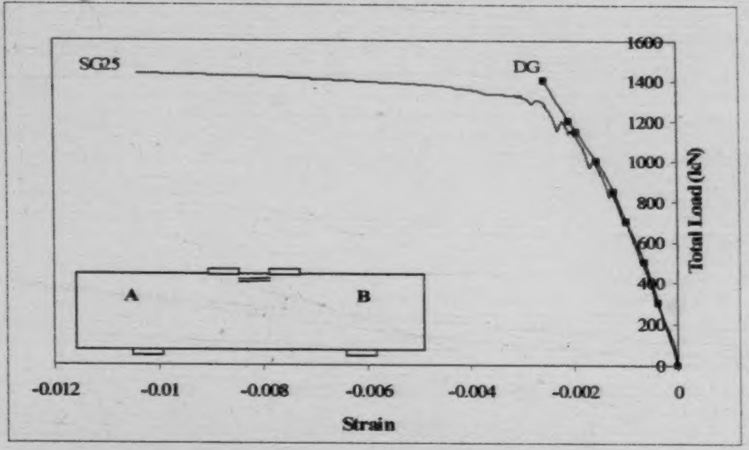

Figure 4-25 Demec gauges reading and strain gauge readings in the compression zone located between loading points of specimen MS2-2

4.6 Specimen MS2-3

Specimen MS2-3 had a shear span to depth ratio *a/d* of 1.78 and a longitudinal reinforcement ratio ρ of 2.29%. Brittle specimen failure caused by failure of the diagonal strut was observed. Prior to brittle failure, weakening of the capacity of the specimen was observed due to cracking of the compression zone between the loading points. The maximum load reached was 2055 kN. Yielding of the main longitudinal and horizontal web reinforcement was not observed. Vertical web reinforcement yielded prior to the failure load. Figure 4-26 shows specimen MS2-3 after failure.

Figure 4-26 Specimen MS2-3 after failure

Marking of shrinkage cracks was carried out prior to the loading process. There were a total of thirteen load stages where all necessary readings were taken, as shown in Section A.5 of Appendix A.

4.6.1 Load-deflection response for specimen MS2-3

Figure 4-27 illustrates the deflection at midspan and at locations 675 mm from midspan for specimen MS2-3. The deflection at midspan when the loading on the specimen reached P_{max} was 12.5 mm. The load at which specimen MS2-3 reached the first serviceability limit for deflection (*l/360)* was 1261 kN (61.4 % of P_{max}) with a deflection of 6.39 mm. The second serviceability limit for deflection (*l/180)* was reached at a load of 2003 kN (97.5 % of P_{max}) with a deflection of 12.78 mm.

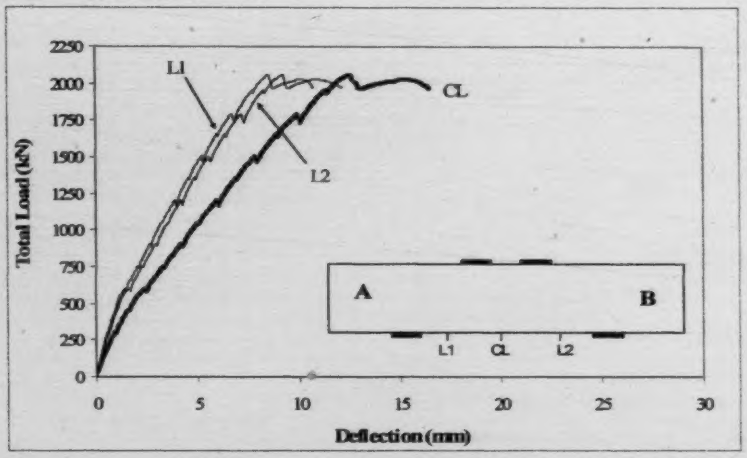

Figure 4-27 Deflection at midspan and 675 mm from midspan for specimen MS2-3

4.6.2 Crack patterns for specimen MS2-3

Both flexural and diagonal strut cracks developed in specimen MS3-2. Flexural cracks developed in the constant moment region. The flexural and flexural-diagonal strut cracks developed at the locations of the stirrups. Diagonal strut cracks parallel to each other were developed at each shear span. These strut cracks initially formed at approximately mid-height of the specimen.

5

Table 4-10 shows the load and percentage of maximum load corresponding to the first flexural crack, first diagonal strut cracks at each shear span and at the approximate load corresponding to the serviceability limits for crack widths for specimen MS2-3. The procedure used to obtain the loads for these crack conditions was explained in Section 4.2.2.

Table 4-10 Load and %P_{max} at different crack stages of specimen MS2-3

Cracks	Load *(kN)*	% P_{max}
First Flexural crack (FC)	293	14.3
First Diagonal strut A (DSA)	560	27.3
First Diagonal Strut B (DSB)	580	28.2
Serviceability limit 0.33 mm at FC	900	43.8
Serviceability limit 0.4 mm at FC	1023	49.8
Serviceability limit 0.33 mm at DSA	830	40.4
Serviceability limit 0.33 mm at DSB	900	43.8
Serviceability limit 0.4 mm at DSA	830	40.4
Serviceability limit 0.4 mm at DSB	900	43.8

Figure 4-28 illustrates the crack patterns and crack widths at a load of 1500 kN (73% of P_{max}) for specimen MS2-3. The widest cracks measured at 73% of P_{max} were the flexural cracks at mid-span and the diagonal strut crack at both shear spans, all with widths of 0.8 mm.

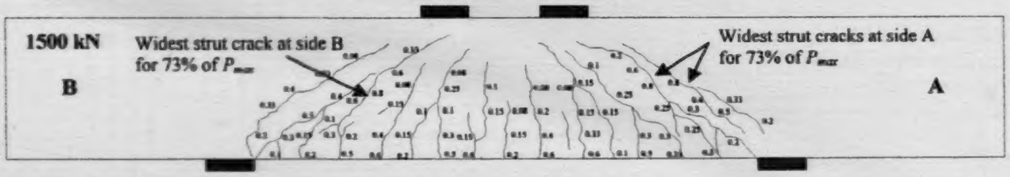
1500 kN
Widest strut crack at side B for 73% of P_{max}
B
Widest strut cracks at side A for 73% of P_{max}
A

Figure 4-28 Crack development at 73% of P_{max} for specimen MS2-3

4.6.3 Strains in reinforcement and average strains in concrete for specimen MS2-3

As also observed for specimen MS1-3, longitudinal reinforcement strains corresponding to the effective yield strain (see Table 4-11) were not reached prior to the applied load P_{max}. At P_{max}, strain gauges located at midspan on the three layers of the main tension reinforcement showed readings of 0.0042, 0.0033 and 0.0029 mm/mm for the first, second and third layer respectively.

Table 4-11 Loads and %P_{max} for yielding of reinforcement for specimen MS2-3

Yielding of reinforcement	Load *(kN)*	% P_{max}
1st layer of main reinforcement	Not yielded	
2nd layer of main reinforcement	Not yielded	
3rd layer of main reinforcement	Not yielded	
Vertical web reinforcement at A	833	40.5
Vertical web reinforcement at B	969	47.2
Horizontal web reinforcement at A	Not yielded	
Horizontal web reinforcement at A	Not yielded	

The strain distribution along one of the bars located at the lowest layer of main tension reinforcement is illustrated in Figure 4-29. The figure illustrates that the anchorage length for the longitudinal reinforcement beyond the support was adequate, since no strains were detected in the bar beyond 450 mm from the exterior edge of the bearing plate. The increment of strain rates for stages of loading close to P_{max} observed in previous specimens near to supports was not observed in specimen MS2-3. The strain distribution along the bar varies, with a decrease in strain occurring between the midspan and the supports. Strains at the exterior edges of the supports were small compared with the strains developed in the clear span due anchorage of the reinforcement from the action of the diagonal compression strut formed between the loading points to the support.

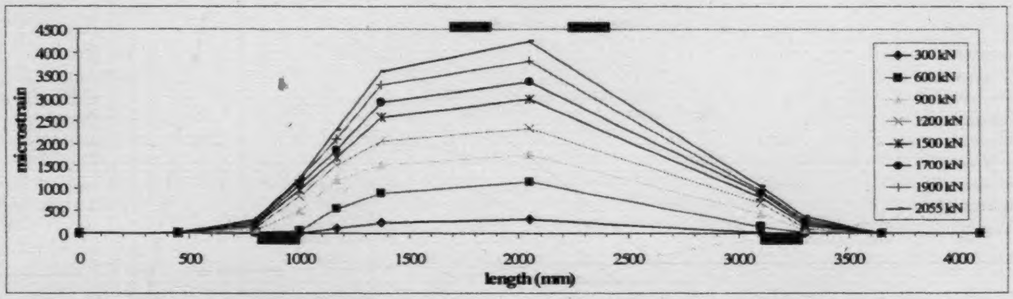

Figure 4-29 Strain distribution along the bar located in the lowest layer of main tension reinforcement of specimen MS2-3

Figure 4-30 shows the principal tension strains, principal compression strains and angle corresponding to the principal compressive strains relative to the horizontal axis. The results are more meaningful in later loading stages where the average strains relative to the instrumentation sensitivity are larger.

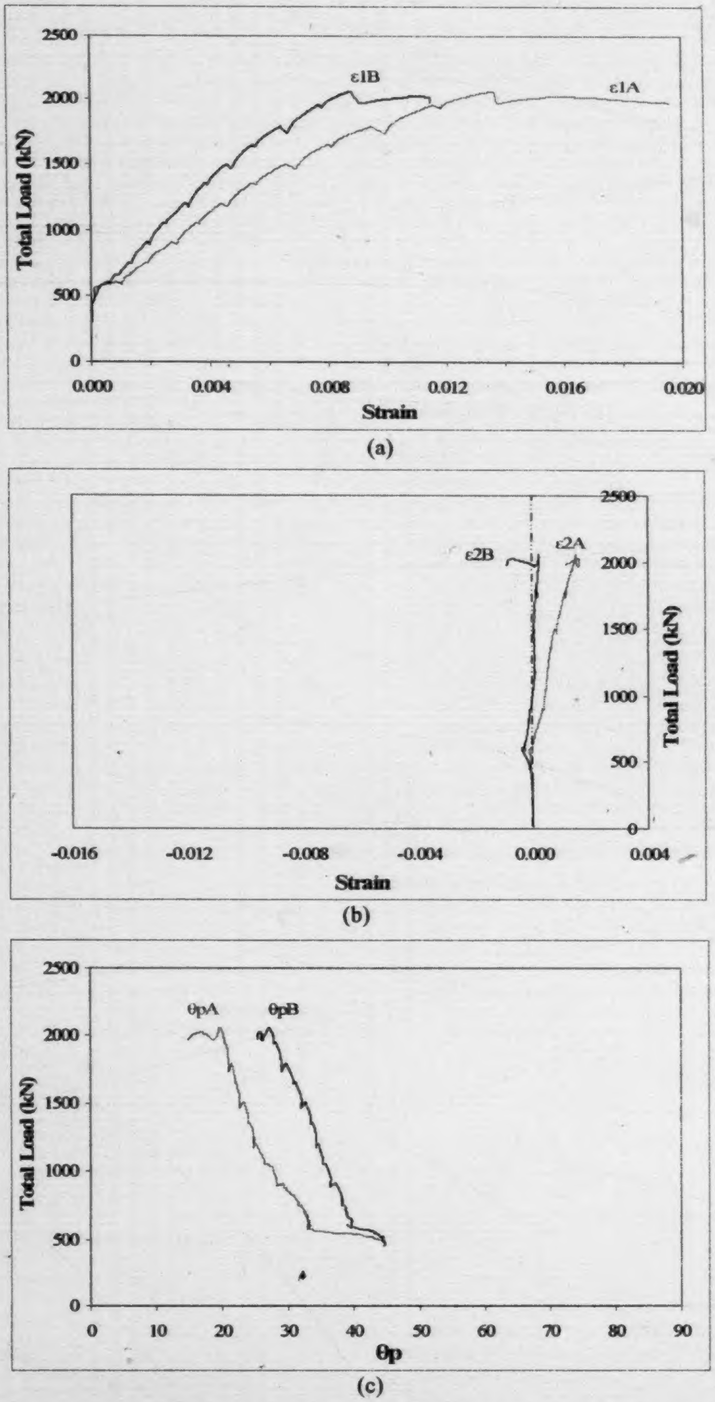

Figure 4-30 (a) Principal tension strain, (b) Principal compression strain and (c) angle of principal strains of specimen MS2-3

Horizontal strains for the top strut located between the loading points was monitored for this specimen using manual readings from demec gauges located 70 mm from the top fiber of the specimen up to a load of 1800 kN. These manual readings are plotted in Figure 4-31

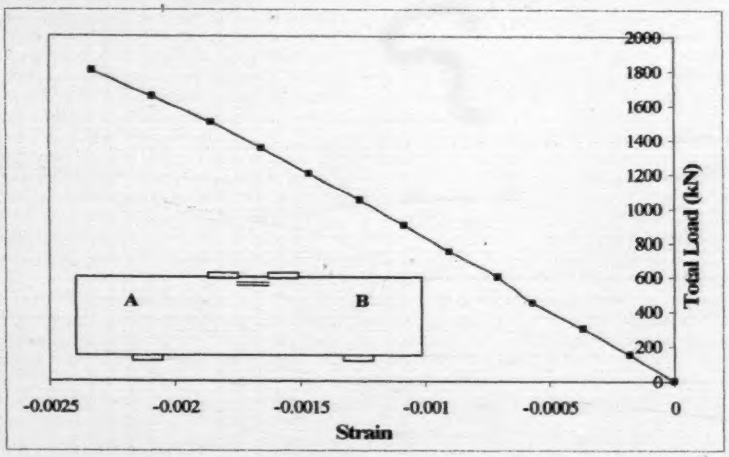

Figure 4-31 Strain at compression zone between the loading points of specimen MS2-3

4.7 Specimen MS3-2

Specimen MS3-2 had a shear span to depth ratio, *a/d,* of 2.38 and a reinforcement ratio, ρ, of 1.13%. The effective yielding strain was reached in the three layers of main tension reinforcement and crushing of the compression zone between the loading points were observed prior to P_{max} of 1154 kN. The vertical web reinforcement of specimen MS3-2 yielded prior to P_{max}. MS3-2 had the lowest capacity of the specimens with ASTM A1035 longitudinal main reinforcement and Grade 400R web reinforcement. Figure 4-32 shows specimen MS3-2 after failure.

Figure 4-32 Specimen MS3-2 after failure

Marking of shrinkage cracks was carried out prior to the loading process. The load was held at five different intervals (See Section A.6 of Appendix A) to take manual demec gages reading, to mark and measure the width of new and existing cracks and to take photographs of the specimen.

4.7.1 Load-deflection response for specimen MS3-2

Figure 4-33 illustrates the deflection at midspan and at locations 725 mm from midspan for specimen MS3-2. The deflection at midspan when the specimen reached P_{max} was 35.06 mm. The total applied load at the first serviceability limit (*l/360)* was 564 kN (48.8% of P_{max}) with a deflection of 8.06 mm. The second serviceability limit (*l/180)* was reached at a load of 896 kN (77.6% of P_{max}) with a deflection of 16.11 mm.

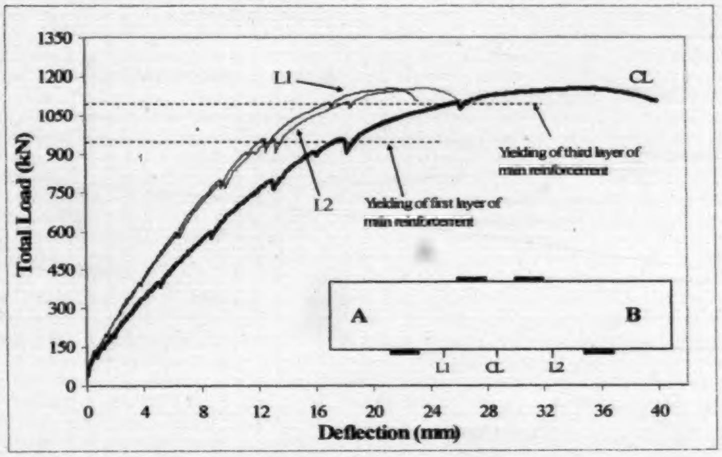

Figure 4-33 Deflection at midspan and 725 mm from midspan of specimen MS3-2

4.7.2 Crack development for specimen MS3-2

Both flexural and diagonal strut cracks were developed in specimen MS3-2. For this specimen, the widths of the cracks located in the constant moment region were larger than any other cracks located along the span. Crack patterns and crack widths of the specimen at different stages of loading are shown in section A.6 of Appendix A.

Table 4-12 shows the load and percentage of maximum load corresponding to the first flexural crack, first diagonal strut cracks at each shear span and at the approximate load corresponding to the serviceability limits for crack widths for specimen MS3-2. The procedure used to obtain the loads for these crack conditions was explained in Section 4.2.2.

Table 4-12 Load and %P_{max} at different crack stages of specimen MS3-2

Cracks	Load (kN)	% P_{max}
First Flexural crack (FC)	130	11.3
First Diagonal strut A (DSA)	258	22.4
First Diagonal Strut B (DSB)	298	25.8
Serviceability limit 0.33 mm at FC	464	40.2
Serviceability limit 0.4 mm at FC	520	45.1
Serviceability limit 0.33 mm at DSA	544	47.1
Serviceability limit 0.33 mm at DSB	553	47.9
Serviceability limit 0.4 mm at DSA	600	52.0
Serviceability limit 0.4 mm at DSB	600	52.0

Figure 4-34 illustrates the crack patterns and crack widths at a load of 800 kN (69.3% of P_{max}) for specimen MS3-2. The widest cracks at 69.3% of P_{max} were the flexure cracks at midspan, with a measured width of 0.8 mm.

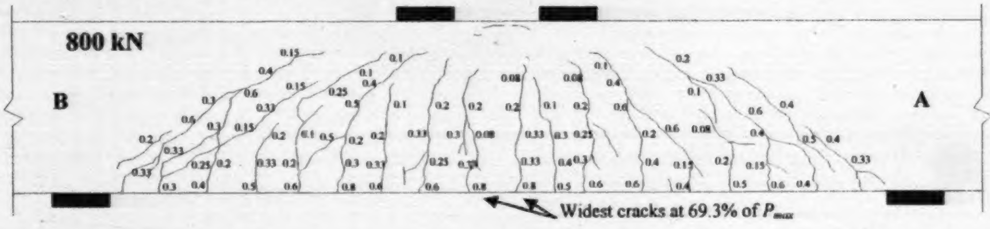

Figure 4-34 Crack development at 69.3% of P_{max} for specimen MS3-2

4.7.3 Strains in reinforcement and average strains in concrete for specimen MS3-2

For specimen MS3-2, longitudinal reinforcement strains corresponding to the effective yielding strain (see Table 3.1) were reached for the three layers of main tension reinforcement prior to the applied load P_{max}. Yielding of vertical web reinforcement (strains exceeding ε_y=0.002) was observed before P_{max} (see Table 4-3). Crushing of the concrete in the compression zone between the loading points started at a total load of approximately 885 kN or 76.7 % of P_{max}.

Table 4-13 Loads and %Pmax for yielding of reinforcement for specimen MS3-2

Yielding of reinforcement	Load *(kN)*	*% P_{max}*
1st layer of main reinforcement	976	84.6
2nd layer of main reinforcement	No data	
3rd layer of main reinforcement	1087	94.2
Vertical web reinforcement at end A	740	64.1
Vertical web reinforcement at end B	653	56.6
Horizontal web reinforcement at end A	No yielded	
Horizontal web reinforcement at end A	No yielded	

The strain distribution along the bars located at the lowest layer of main tension reinforcement for different loading stages is shown in Figure 4-35. The figure illustrates a gradual decrease in strains along the shear span for all stages of loading. This figure also shows that strains on the bar were no longer detected beyond 400 mm from the exterior edge of the bearing plate, indicating that the anchorage of the reinforcement was satisfactory.

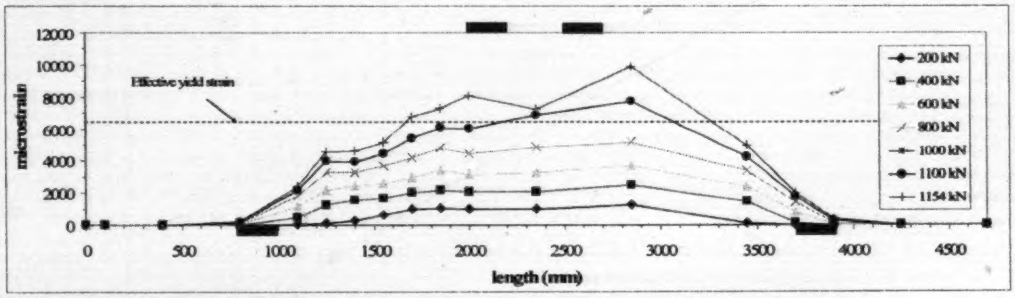

Figure 4-35 Strain distribution along the bar located in the lowest layer of main tension reinforcement of specimen MS3-2

Figure 4-36 shows the principal tension strains, principal compression strains and angle corresponding to the principal compressive strains relative to the horizontal axis for specimen MS3-2. The results are more meaningful in later loading stages where the average strains relative to the instrumentation sensitivity are larger.

Figure 4-37 shows the curves of the horizontal strains versus load taken using demec gages 70 mm from top fiber of the specimen and using strain gages located on the longitudinal reinforcement in the compression zone.

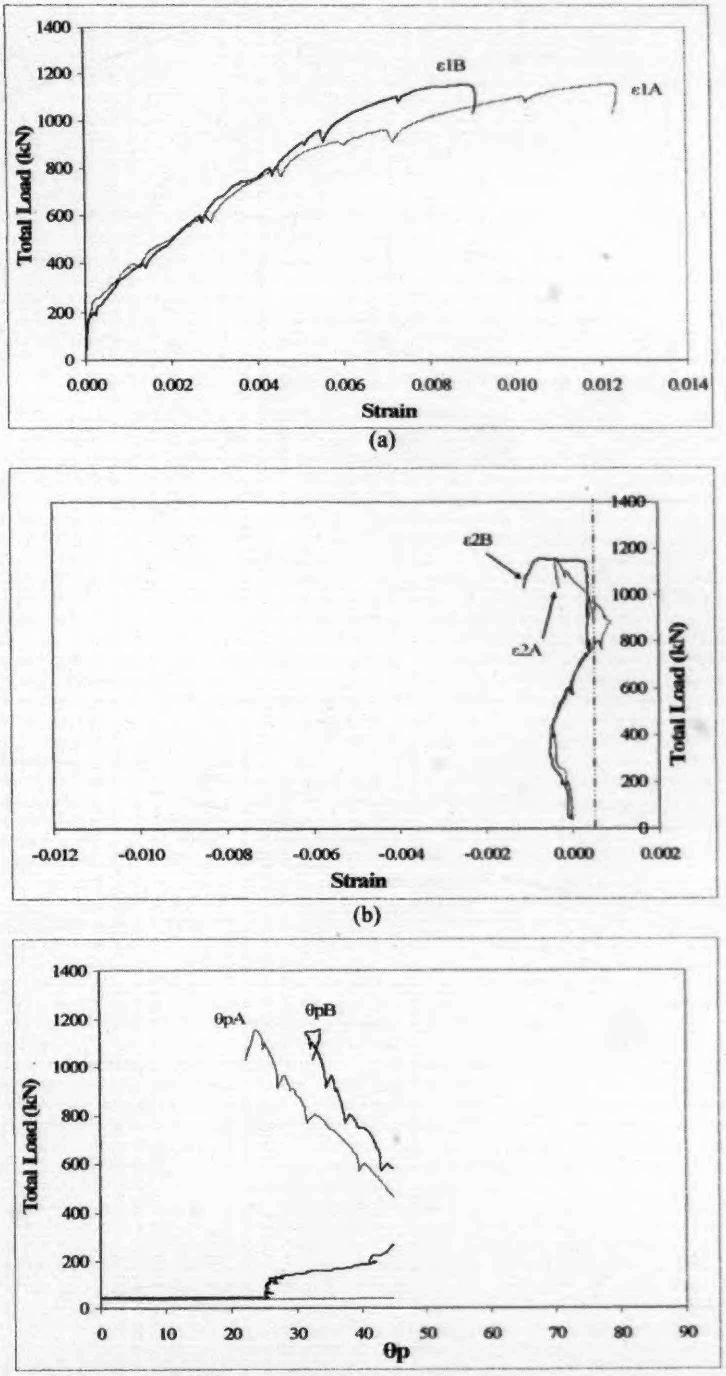

(a)

(b)

(c)

Figure 4-36 (a) Principal tension strain, (b) Principal compression strain and (c) angle of principal strains of specimen MS3-2

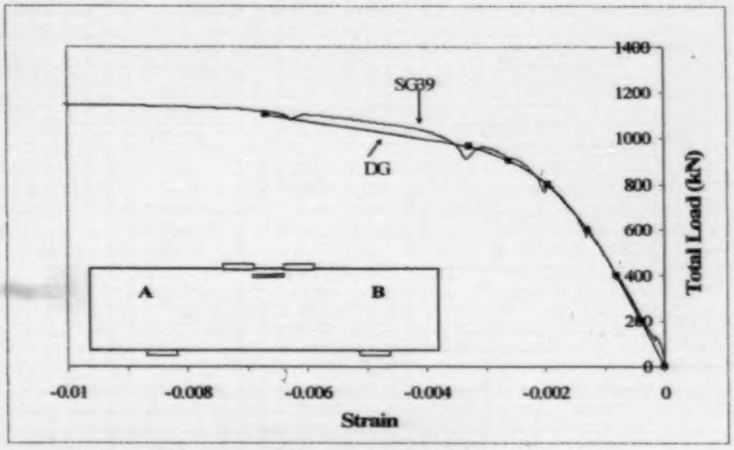

Figure 4-37 Strain in top strut of specimen MS3-2

4.8 Specimen MW1-2

Specimen MW1-2 had a reinforcement ratio, *ρ*, of 1.13% and a shear span to depth ratio, *a/d*, of 1.2. No web reinforcement was provided for this specimen. The failure mode was diagonal strut failure at a total applied load of 1568 kN. No yielding of the main tension reinforcement or crushing of the top strut between the loading points was observed prior to failure. Figure 4-38 shows specimen MW1-2 after failure.

Figure 4-38 Specimen MW1-2 after failure

The load was held at seven loading stages to take manual demec gauges readings, to mark and measures the widths of new and existing cracks and to take photographs of the specimen. These intervals are shown in Section A.7 of Appendix A.

4.8.1 Load-deflection response for specimen MW1-2

Figure 4-39 illustrates the load-deflection relationship at midspan and at 450 mm from midspan for specimen MW1-2. The deflection at midspan when the specimen reached P_{max} was 7.50 mm. The total load at which specimen MW1-2 reached the first serviceability limit (*l/360)* was at a applied load of 1250 kN (79.8% of P_{max}) with a deflection of 4.72 mm. The second serviceability limit (*l/180)* was never reached.

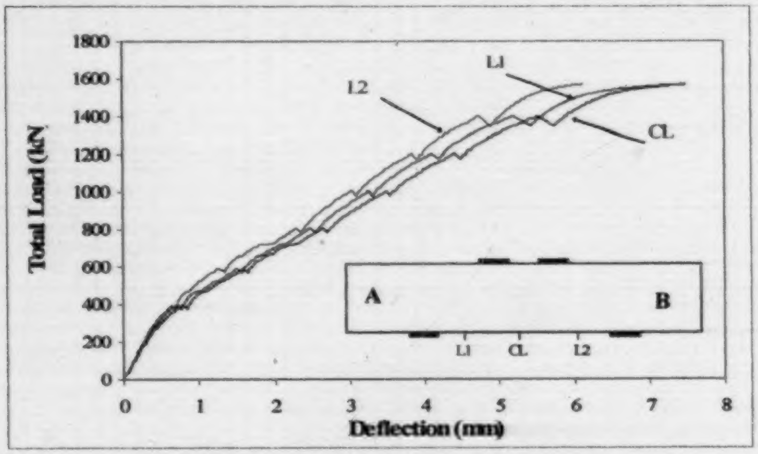

Figure 4-39 Deflection at midspan and 450 mm from midspan of specimen MW1-2

4.8.2 Crack development for specimen MW1-2

Both flexural and diagonal strut cracks were developed in specimen MW1-2. Flexural cracks were developed approximately every 200 mm along the span. One main diagonal strut crack was developed at each side. These cracks were developed from the interior edge of the supports to the interior edge of the loading points.

Table 4-14 shows the load and percentage of maximum load for the first flexural crack, first diagonal strut cracks at each shear span and at the approximate load corresponding to the serviceability limits for crack widths for specimen MW1-2. The procedure used to obtain the loads for these crack conditions was explained in Section 4.2.2

Table 4-14 Load and $\%P_{max}$ at different crack stages for specimen MW1-2

Cracks	Load (kN)	$\% P_{max}$
First Flexural crack (FC)	257	16.4
First Diagonal strut A (DSA)	393	25.1
First Diagonal Strut B (DSB)	450	28.7
Serviceability limit 0.33 mm at FC	630	40.2
Serviceability limit 0.4 mm at FC	700	44.6
Serviceability limit 0.33 mm at DSA	556	35.5
Serviceability limit 0.33 mm at DSB	702	44.8
Serviceability limit 0.4 mm at DSA	600	38.3
Serviceability limit 0.4 mm at DSB	742	47.3

The crack development and crack widths at 1200 kN (76.5% of P_{max}) for specimen MW1-2 is shown in Figure 4-40. The rest of crack development figures for each load interval are shown in Appendix A. The widest crack at 76.5% of P_{max} was the diagonal strut crack at shear span A, with a measured width of 1.25 mm.

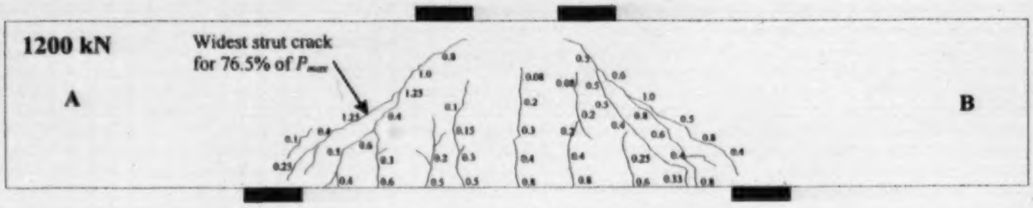

Figure 4-40 Crack development and crack width of MW1-2 at 76.5% of P_{max}

4.8.3 Strains in reinforcement and average strains in concrete for specimen MW1-2

No yielding of the main tension reinforcement was observed for specimen MW1-2. At the maximum applied load, the strains in the first and second layer of main tension reinforcement were 0.0047, 0.0036. The strain gauge located in the third layer failed and no readings were obtained.

The strain distribution along the bars located at the lowest layer of main tension reinforcement is shown in Figure 4-41. The strains at the midspan were the largest developed along the bar during the loading process, however, strains close to the support and at the location of the strut cracks are, for some stages of loading, as large as the strains developed at midspan. The influence of the diagonal strut developed between the loading points and supports is shown in this figure, where the difference between the strain developed at the edges of the supports is important. The development length given to specimen MW1-2 was adequate, as strains on the bar were no longer detected beyond 450 mm from the exterior edge of the bearing plate.

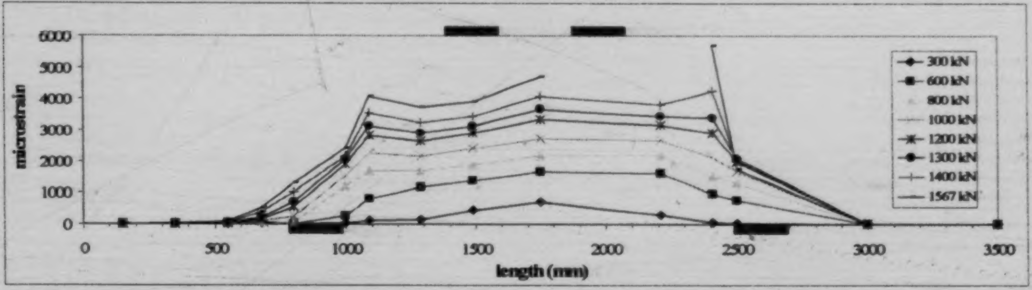

Figure 4-41 Strain distribution along the bar located in the lowest layer of main tension reinforcement of specimen MW1-2

Figure 4-42 shows the principal tension strains, principal compression strains and angle corresponding to the principal compressive strains relative to the horizontal axis. The results are more meaningful in later loading stages where the average strains relative to the instrumentation sensitivity are larger.

The horizontal strains at the compression zone between the loading points were monitored using demec gauges readings 70 mm from the top fiber of the specimen and using strain gauges located on the longitudinal reinforcement in the compression zone. Figure 4-43 shows the curves for strain-load relationship.

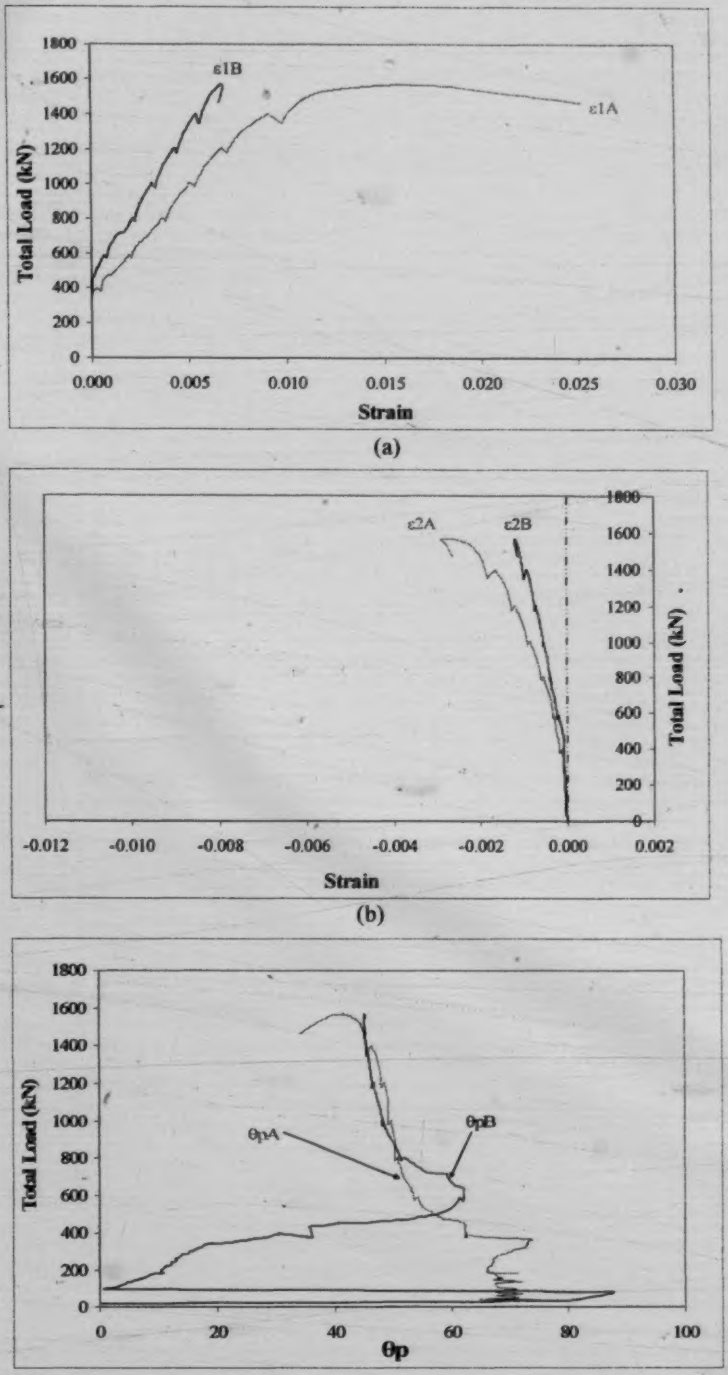

(a)

(b)

(c)

Figure 4-42 (a) Principal tension strain, (b) Principal compression strain and (c) angle of principal strains of specimen MW1-2

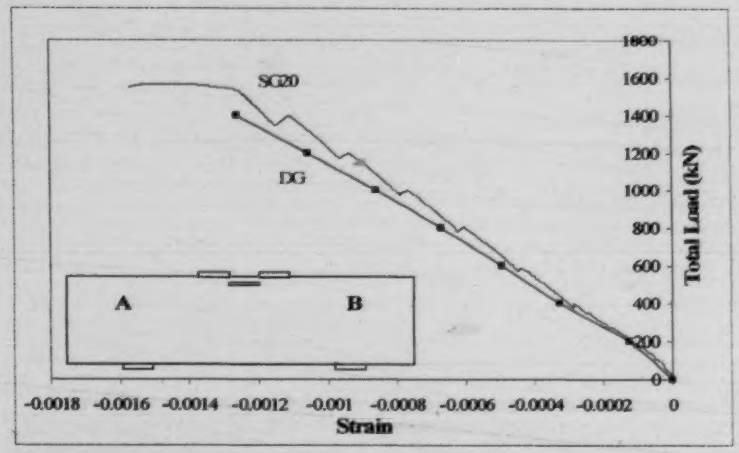

Figure 4-43 Strains in top strut using demec gages and strain gages for specimen MW1-2

4.9 Specimen MW3-2

Specimen MW3-2 had a reinforcement ratio, ρ, of 1.13% and a shear span to depth ratio, *a/d*, of 2.38. No web reinforcement was provided. The failure mode was splitting of the diagonal strut at side B at a load of 411 kN. No yielding in the main tension reinforcement or crushing of the top strut between loading points was observed prior to failure. Figure 4-44 shows specimen MW3-2 after failure.

Figure 4-44 Specimen MW3-2 after failure

Shrinkage cracks were marked prior to the start of loading. Once the test started, the loading process was by displacement control. The load was held at different intervals to take demec gauge readings, to mark crack patterns and measure the crack widths, and to photograph the specimen. There were a total of four load stages, as shown in Section A.8 of Appendix A.

4.9.1 Load-deflection response for specimen MW3-2

To measure the deflection of specimen MW3-2, three locations at the bottom of the specimen were selected to take measurements: midspan and 725 mm from midspan. The deflection at midspan when the specimen reached P_{max} was 9.09 mm. The load at which specimen MW3-2 reached the first serviceability limit (*l/360)* was at a applied load of 389 kN with a deflection of 8.06 mm and the second serviceability limit (*l/180)* was never reached. The first limit reached was at 94.6 % of the maximum load. Figure 4-45 illustrates the deflection at midspan and at 725 mm from midspan for specimen MW3-2.

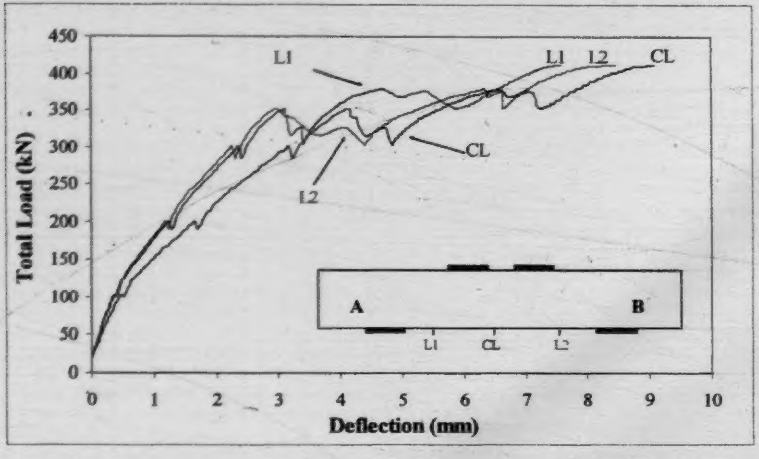

Figure 4-45 Deflection at midspan and 725 mm from midspan of specimen MW3-2

4.9.2 Crack patterns for specimen MW3-2

Both flexural and diagonal strut cracks were developed in specimen MW3-2. One main diagonal strut crack was developed on side B. No diagonal strut cracks were detected in side A. The main diagonal strut crack went from the interior edge of the support toward the compression zone between the loading plates following a curve trajectory.

Table 4-15 shows the load and percentage of maximum load for the first flexural crack. The approximate load corresponding to the serviceability limits for crack widths for specimen MW3-2 was not calculated because these limits were not reached prior to the last manual reading of the crack widths and no data was recorded.

Table 4-15 Load and $\%P_{max}$ at different crack stages of specimen MW3-2

Cracks	Load (kN)	$\% P_{max}$
First Flexural crack (FC)	99	24.1
First Diagonal strut A (DSA)	247	60.1
First Diagonal Strut B (DSB)	283	68.9

Figure 4-46 shows the crack development and crack widths of specimen MW3-2 up to a load of 300 kN, which represent 73% of P_{max}. Crack pattern drawings for other load intervals are shown in section A.8 of Appendix A. The widest crack at 73% of P_{max} was the diagonal strut crack at shear span B, with a measured width of 1.5 mm.

At a load of 350 kN, a suddenly drop in applied load to 300 kN was observed. After that, the specimen capacity recovered and the maximum load of 411 kN was reached.

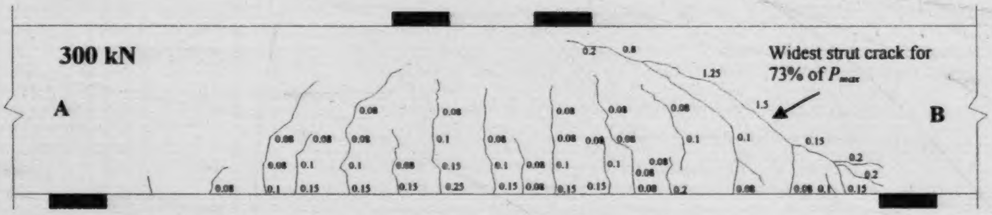

Figure 4-46 Crack development of specimen MW3-2 at 73% of P_{max}

4.9.3 Strains in reinforcement and average strains in concrete for specimen MW3-2

No yielding of the main tension reinforcement was observed for specimen MW3-2. At the maximum applied load, the strains in the three layers of main tension reinforcement were 0.0019, 0.0016 and 0.0012.

The variation in strain along the bars located at the lowest layer of main tension reinforcement is shown in Figure 4-47. The strains at the midspan were the largest developed along the bar during the loading process. However, strains close to crack locations, for some stages of loading, were larger at locations other that midspan.

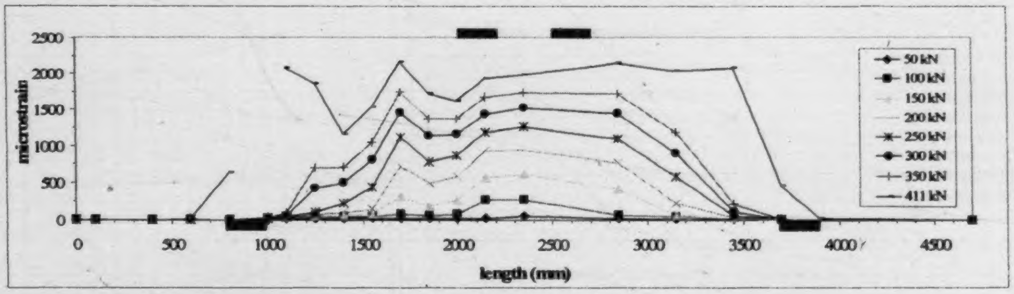

Figure 4-47 Strain distribution along the bar located in the lowest layer of main tension reinforcement of specimen MW3-2

Figure 4-48 shows the principal tension strains and principal compression strains developed in the shear spans of specimen MW3-2. Angle of principal compression strain are not shown because the data obtained from the LVDTs rosettes for very small strains did not provide accurate measurements suitable for calculation of the angle of principal strain.

The horizontal strains at the compression zone between the loading points were monitored using demec gauge readings 70 mm from the top fiber of the specimen and using strain gauges located in the longitudinal reinforcement in the compression zone. Figure 4-49 shows the load-strain curves.

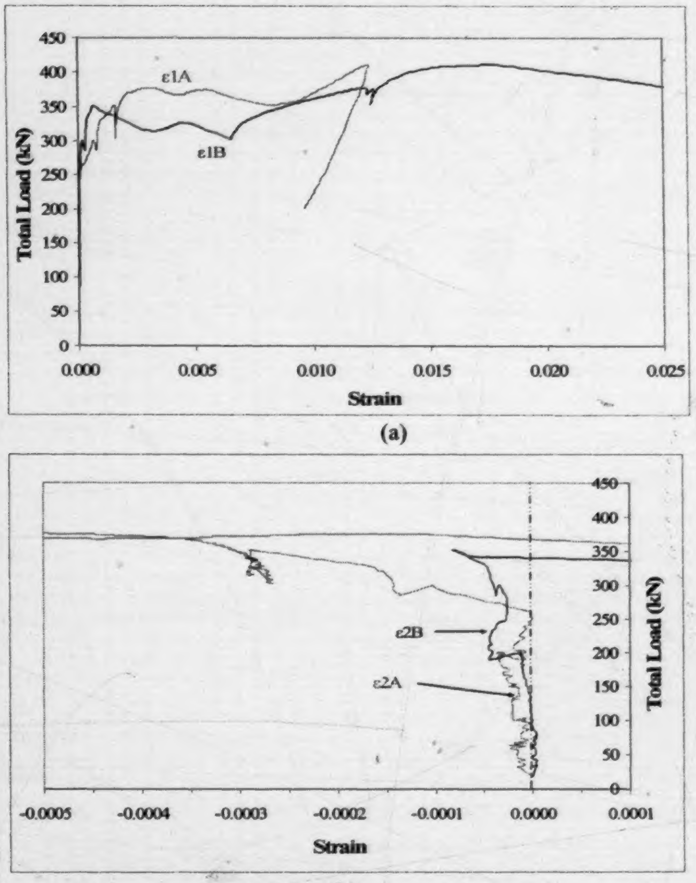

(a)

(b)

Figure 4-48 (a) Principal tension strain and (b) Principal compression strain developed in the diagonal struts of specimen MW3-2.

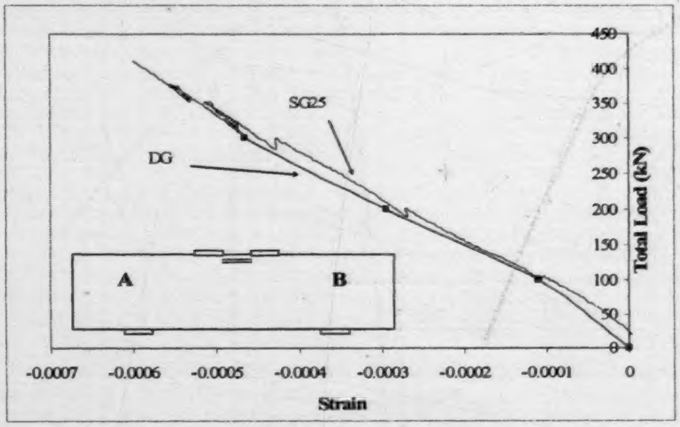

Figure 4-49 Strains in top strut using demec gages and strain gages for specimen MW3-2

4.10 Specimen NS1-4

Specimen NS1-4 was reinforced with normal strength (Grade 400R) steel. It had a shear span to depth ratio, *a/d*, of 1.18 and reinforcement ratio of 1.77%. The maximum load recorded for the specimen was 1567 kN. Cracking of the compression zone and yielding of the main tension reinforcement occurred prior to P_{max}. After P_{max} the specimen continued to be loaded until a brittle diagonal strut failure occurred. Stirrups yielded before P_{max}. Figure 4-50 illustrates specimen NS1-4 after failure.

Figure 4-50 Specimen NS1-4 after failure

4.10.1 Load-deflection response for specimen NS1-4

The deflection at midspan for P_{max} was 7.50 mm. The applied load at which specimen NS1-4 reached the first serviceability limit *(l/360)* was at 1412 kN (90.1% of P_{max}) with a deflection of 4.72 mm. The second serviceability limit *(l/180)* was not reached for this specimen.

Figure 4-17 illustrates the load deflection relationship at midspan and at 450 mm from midspan for specimen NS1-4. To measure deflections along the specimen span, LVDTs at 425 mm from midspan and a cable transducer at midspan were used. For the specimens in this study, deflections at midspan were always larger than the deflection at a certain distance from midspan. The accuracy of the cable compared to the LVDT and the relatively small total deflection of the specimen at failure may have resulted in the smaller variation in deflection readings for this specimen.

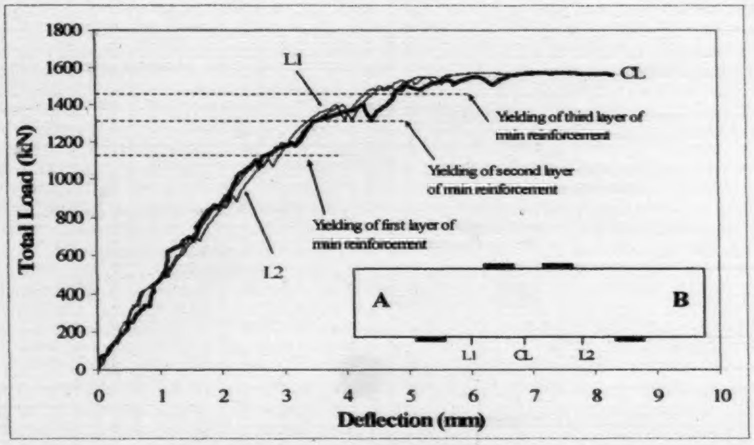

Figure 4-51 Deflection at midspan and 450 mm from midspan of specimen NS1-4

4.10.2 Crack development for specimen NS1-4

No crack widths were measured for this specimen and only crack length development was recorded. There were seven loading stages (see Section A.9 of Appendix A) where the loading process was held to compare all crack measurements.

Table 4-16 shows the load and percentage of maximum load for the first flexural crack and first diagonal strut cracks at both sides of specimen NS1-4.

Table 4-16 Load and %P_{max} at different crack stages

Cracks	Load (kN)	% P_{max}
First Flexural crack (FC)	102	6.5
First Diagonal strut A (DSA)	351	22.4
First Diagonal Strut B (DSB)	438	28.0

Figure 4-52 illustrates the crack patterns at a load of 1100 kN (70.2% P_{max}) of specimen NS1-4. Crack patterns for other load intervals are shown in Appendix A. No crack widths were recorded for this specimen.

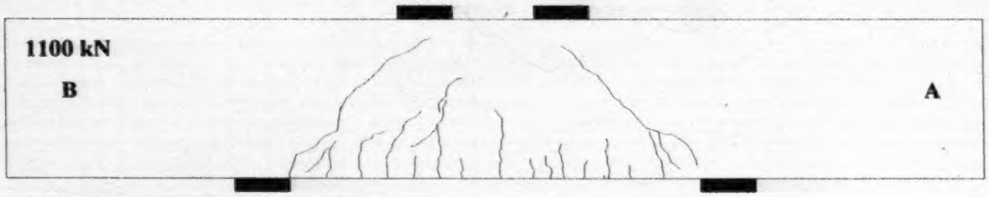

Figure 4-52 Crack development at 70.2% of P_{max} for specimen NS1-4

4.10.3 Strains in reinforcement and average strains in concrete for specimen NS1-4

For specimen NS1-4, all the layers of the main tension reinforcement yielded prior to P_{max}. The strain readings at P_{max} were 0.0055, 0.0047 and 0.0034 for the first, second and third layers respectively. Vertical web reinforcement yielded prior to P_{max}.

Table 4-17 shows the loads and the percentage of P_{max} at yielding of the three layers of main tension reinforcement, yielding of web reinforcement for both sides of specimen NS1-4.

Table 4-17 Loads and $\%P_{max}$ for yielding of reinforcement

Yielding of reinforcement	Load (kN)	$\% P_{max}$
1st layer of main reinforcement	1166	74.4
2nd layer of main reinforcement	1323	84.4
3rd layer of main reinforcement	1463	93.4
Vertical web reinforcement at A	1366	87.2
Vertical web reinforcement at B	1473	94.0
Horizontal web reinforcement at A	Not yielded	
Horizontal web reinforcement at B	Not yielded	

Strain distribution along one of the bars located at the lowest layer of main tension reinforcement for different loading stages is shown in Figure 4-53. The figure illustrates that no strains on the bar were detected beyond 350 mm from the exterior edge of the bearing plate, indicating that the anchorage of the reinforcement was satisfactory. The strains along the bar in the zone between the supports were generally of similar magnitude during the loading stages prior to yielding of the main tension reinforcement, when the strains at midspan increased at a larger rate than strains at locations closer to the supports. This strain distribution is consistent with the Direct Strut Mechanism. Strains at the exterior edges of the supports were small compared to the strains developed in the clear span due to anchorage of the reinforcement forces from the action of diagonal compression struts formed between the loading points to the supports.

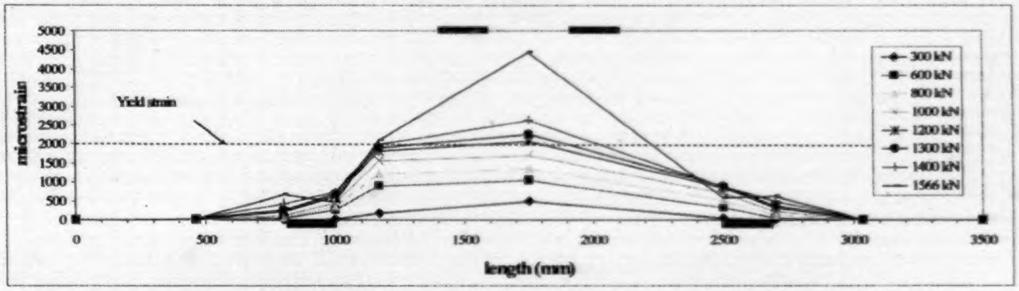

Figure 4-53 Strain distribution along the bar located in the lowest layer of main tension reinforcement of specimen NS1-4

Figure 4-54 shows the principal tension strains, principal compression strains and angle corresponding to the principal compressive strains relative to the horizontal axis. The results are more meaningful in later loading stages where the average strains relative to the instrumentation sensitivity are larger.

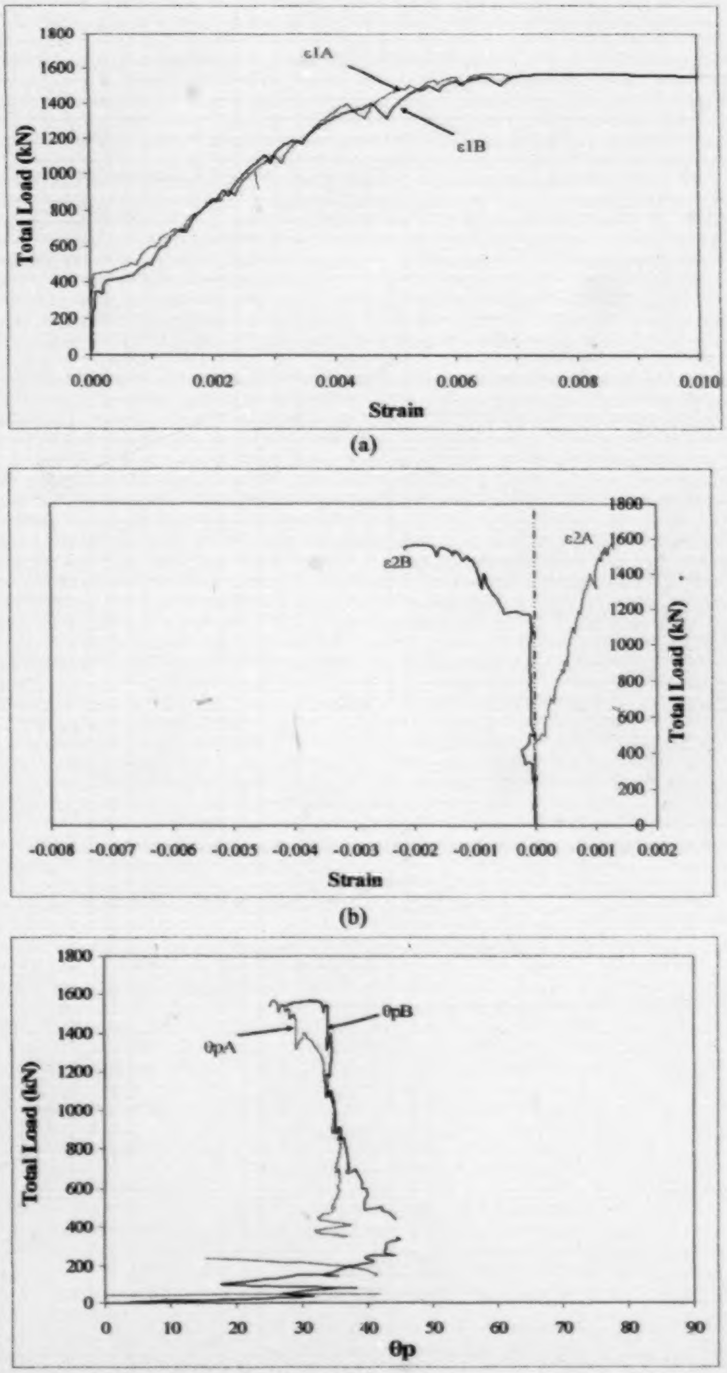

(a)

(b)

(c)

Figure 4-54 (a) Principal tension strain, (b) Principal compression strain and (c) angle of principal strains of specimen NS1-4

4.11 Specimen NS2-4

Specimen NS2-4 was reinforced with normal strength (Grade 400R) steel. It had a shear span to depth ratio, *a/d*, of 1.8 and reinforcement ratio of 1.77%. The failure mode was flexural failure. The maximum load reached by specimen NS2-4 was 1078 kN. Crushing of the compression zone and yielding of the main tension reinforcement occurred prior to P_{max}. Figure 4-55 shows specimen NS2-4 after failure.

Figure 4-55 Specimen NS2-4 after failure

Shrinkage cracks were marked prior to the start of loading. Once the test started, the loading process was by displacement control. The load was held at different intervals to take demec gauge readings, to mark crack patterns and measure the crack widths, and to photograph the specimen. There were eight load stages, as shown in Section A.10 of Appendix A.

4.11.1 Load-deflection response for specimen NS2-4

The deflection at midspan when the specimen reached P_{max} was 13.28 mm. The first serviceability deflection limit (*l/360)* of 4.72 mm was reached at a load of 829 kN (77.8% P_{max}). The second serviceability deflection limit (*l/180*) of 9.44 mm was reached at a load of 1065 kN (98.8 % of P_{max}). Figure 4-56 illustrates the load deflection relationship at midspan and at 675 mm from midspan for specimen NS2-4.

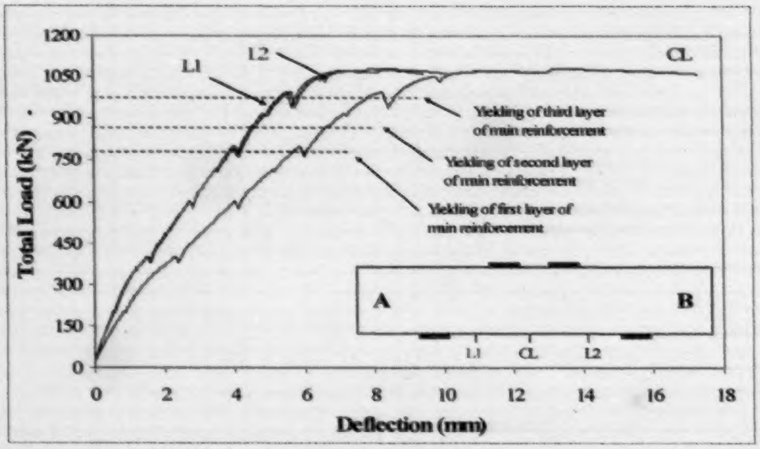

Figure 4-56 Deflection at midspan and 675 mm from midspan of specimen NS2-4

4.11.2 Crack development for specimen NS2-4

Both flexural and diagonal strut cracks developed in specimen NS2-4. The width of the flexural cracks and width of diagonal strut cracks both increased during the entire loading process. The entire lengths of the strut cracks were approximately parallel to each other and to the diagonal strut axis.

Table 4-18 shows the load and percentage of maximum load for the first flexural crack and first diagonal strut cracks at both sides of specimen NS2-4.

Table 4-18 Load and %P_{max} at different crack stages

Cracks	Load *(kN)*	% P_{max}
First Flexural crack (FC)	192	17.8
First Diagonal strut A (DSA)	314	29.1
First Diagonal strut B (DSB)	342	31.7
Serviceability limit 0.33 mm at FC	800	74.2
Serviceability limit 0.4 mm at FC	882	81.8
Serviceability limit 0.33 mm at DSA	544	50.5
Serviceability limit 0.33 mm at DSB	620	57.5
Serviceability limit 0.4 mm at DSA	600	55.7
Serviceability limit 0.4 mm at DSB	667	61.9

Figure 4-57 illustrates the crack development and crack widths developed up to the load of 800 kN (74.2% P_{max}) for specimen NS2-4. The crack patterns for each stage of loading are illustrated in Appendix A. The widest crack at 74.2% of P_{max} was the diagonal strut crack at shear span A, with a measured width of 0.8 mm.

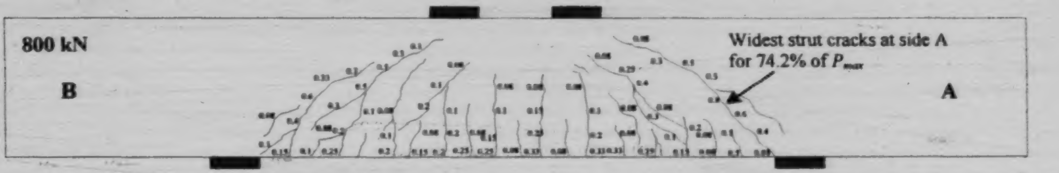

Figure 4-57 Crack development at 74.2 % of P_{max} for specimen NS2-4

4.11.3 Strains in reinforcement and average strains in concrete for specimen NS2-4

Yielding of the three layers of main tension reinforcement was observed prior to P_{max}. At maximum load, the strain gauges located at the three layers of the main tension reinforcement showed strains of 0.0074, 0.0051 and 0.0031 mm/mm for the first, second and third layer respectively.

Table 4-19 shows the loads and the percentage of P_{max} at yielding of the three layers of main tension reinforcement and yielding of web reinforcement for both sides of specimen NS2-4.

Table 4-19 Loads and %P_{max} for yielding of reinforcement

Yielding of reinforcement	Load (kN)	% P_{max}
1st layer of main reinforcement	774	71.8
2nd layer of main reinforcement	892	82.7
3rd layer of main reinforcement	964	89.4
Vertical web reinforcement at end A	No data	
Vertical web reinforcement at end B	805	74.7
Horizontal web reinforcement at end A	Not yielded	
Horizontal web reinforcement at end A	Not yielded	

The strain distribution along one bar in the lowest layer of main tension reinforcement is shown in Figure 4-58. The figure illustrates a decrease in bar strain near the supports compared to mid-span. This behavior was not observed for the specimens with shorter span, where strains distributions along the bottom bar between the supports was more uniform. The figure illustrates that no strains on the bar were detected beyond 400 mm from the exterior edge of the bearing plate, indicating that the anchorage of the reinforcement was satisfactory.

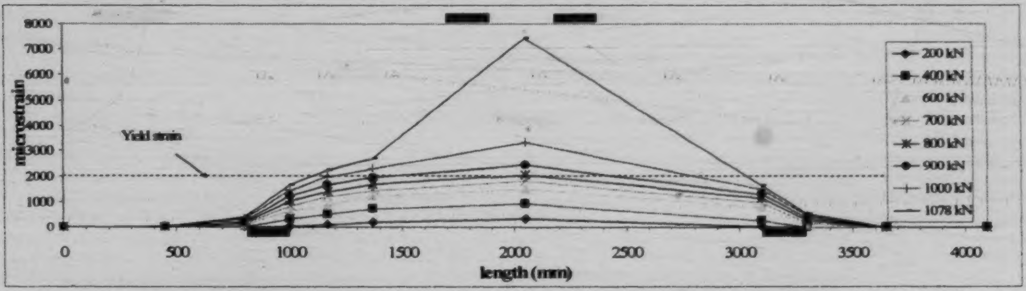

Figure 4-58 Strain distribution along the bar located in the lowest layer of main tension reinforcement of specimen NS2-4

Figure 4-59 shows the principal tension strains, principal compression strains and angle corresponding to the principal compressive strains relative to the horizontal axis. The results are more meaningful in later loading stages where the average strains relative to the instrumentation sensitivity are larger.

Horizontal strains in the top strut located between the loading points was monitored for this specimen using manual readings from demec gauges located 70 mm from the top fiber of the specimen up to a load of 2000 kN. These manual readings are plotted in Figure 4-60.

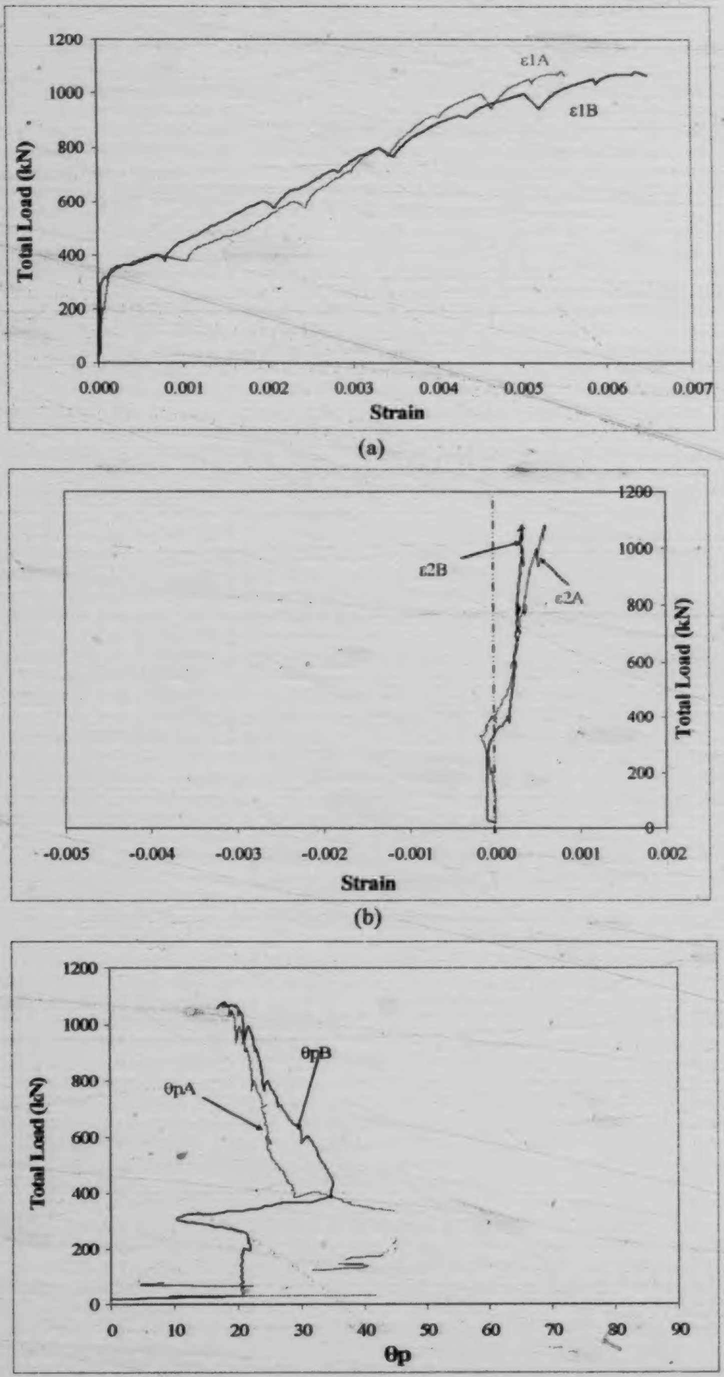

(a)

(b)

(c)

Figure 4-59 (a) Principal tension strain, (b) Principal compression strain and (c) angle of principal strains of specimen NS2-4

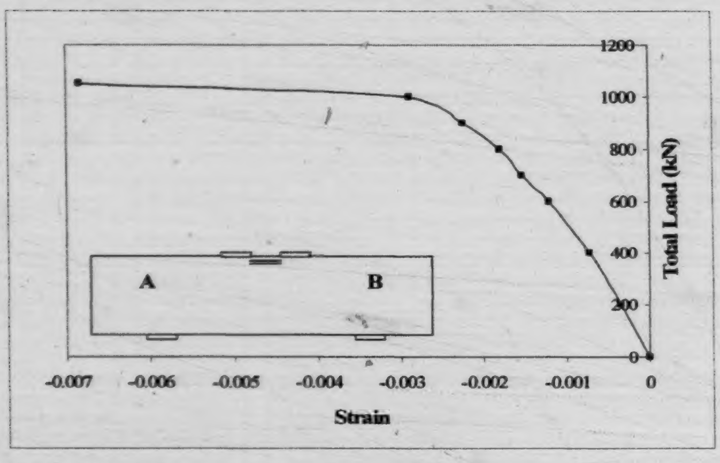

Figure 4-60 Strain in top strut of specimen NS2-4

5. ANALYSIS AND COMPARISON OF EXPERIMENTAL RESULTS

This chapter compares the experimental results of sets of beams grouped by similar characteristics, but with a single parameter that varies for each beam within the set. In this project, design and selection of the specimens considered the primary parameters of shear span to depth ratio, type of reinforcing steel, longitudinal reinforcement ratio and the presence or omission of web reinforcement. The influence of these parameters on the behaviour of the beams is analyzed and the results are compared for each set.

For analysis in this chapter, specimens were classified as specimens that contained vertical web reinforcement (i.e. stirrups) and specimens without vertical web reinforcement. The influence of the design parameters of a/d, ρ and type of steel reinforcement on the behaviour of the specimens were established for each classification. The two groups were also compared, to determine the influence of vertical web reinforcement on the capacity of deep beams reinforced with high strength reinforcement.

5.1 Specimens with vertical web reinforcement

5.1.1 Influence of shear span to depth ratio

In this section, two sets of specimens with similar reinforcement ratios and web reinforcement configurations, but different shear span to depth ratios, are analyzed. The first set includes specimens MS1-2, MS2-2 and MS3-2. The second set contains specimens MS1-3 and MS2-3. Specimens in the first and second sets have constant ρ of 1.13% and 2.29%, respectively. These two sets are analyzed separately because they have different ρ and because different failure modes were observed.

Specimens from the first set, with lower reinforcement ratio, failed by flexure with measured strains in main longitudinal reinforcement greater than the effective yield strain ε_y, followed by crushing of the top horizontal strut between the loading plates. Specimens from the second set, with higher reinforcement ratio, failed by splitting of the diagonal strut between the load and support plates (Specimen MS1-3) or by crushing of the top strut between the loading plates (Specimen MS2-3). The measured strains in the main longitudinal reinforcement were smaller than the effective yield strength for both specimens. For specimen MS2-3, sudden failure of the diagonal strut was observed after some crushing of the top strut between loading plates.

In the first set of beams, after reaching P_{max}, specimen MS1-2 behaved differently than specimens MS2-2 and MS3-2. For specimens MS2-2 and MS3-2, no splitting of the diagonal struts was observed prior to the end of the loading process. On the other hand, the loading process for specimen MS1-2 finished when sudden splitting of the diagonal strut occurred. This final failure of specimen MS1-2 came from a crack that went from the interior edge of the support to the compression zone between the loading plates. In the second set, prior to the diagonal strut failure of specimen MS2-3, a reduction in the measured load for increasing deflection started to occur when crushing of the compression zone between loading plates was observed. The splitting of the diagonal strut in specimen MS2-3 was different than specimen MS1-2 from the first set, as it came from a crack that went from the interior edge of the support plate to the exterior edge of the loading plate, independent of the cracks on the top strut between the loading plates.

The relationship between maximum load and the *a/d* ratio for beams with web reinforcement and having ρ of 1.13 % and 2.29% are plotted in Figure 5-1. The maximum load capacity of deep beams reinforced with ASTM A1035 reinforcing steel increased for smaller *a/d* ratios. This relationship has been observed previously for deep beams with normal strength reinforcement [Rogowsky et al, 1986; Oh and Shin, 2001].

Comparison of member performance within each set is provided in Sections 5.1.1.1 and 5.1.1.2.

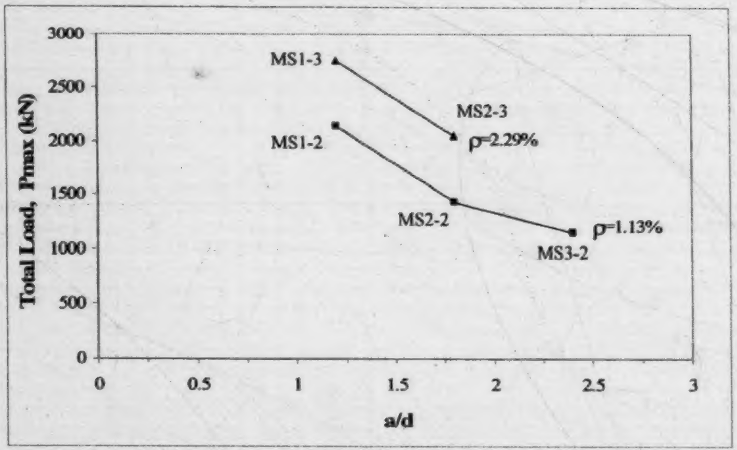

Figure 5-1 Total load to *a/d* relationship for specimens with web reinforcement

5.1.1.1 Specimens with different *a/d* and constant ρ of 1.13 %

The specimens considered in this set are specimens MS1-2, MS2-2 and MS3-2.

Table 5-1 summarizes important data for these specimens, including ρ, *a/d*, vertical web reinforcement arrangement, failure mode, maximum load reached during the test, deflection at maximum load and the secant stiffness of the beams at 60% of P_{max}.

Table 5-1 Comparison of specimens MS1-2, MS2-2 and MS3-2

Specimen	ρ (%)	*a/d*	vertical web reinforcement	f'_c (MPa)	Mode of failure	P_{max} (kN)	Deflection at midspan for P_{max} (mm)	Stiffness at 60% of P_{max} (kN/mm)
MS1-2	1.13	1.19	10M@200mm	44	Flexure	2142	14.9	235
MS2-2	1.13	1.79	10M@200mm	47	Flexure	1432	24.6	103
MS3-2	1.13	2.38	10M@150mm	48	Flexure	1154	35.1	57

Comparing MS1-2 and MS2-2, an increase in *a/d* of 50% resulted in a decrease in the capacity by 33 %. For beam MS3-2, where *a/d* was twice that of MS1-2, the capacity was reduced to 54% of the capacity of MS1-2. Figure 5-1 shows the variation in capacity for the three different *a/d* ratios in this set of beams.

The failure mode of all three beams in this comparison set was flexure. Even though the capacity for each beam was different, similar maximum mid-span moments of approximately 1300 kN-m were achieved for each beam. For this reason, with the failure mode governed by moment and not by shear, it is difficult to determine the exact influence of *a/d* on the shear capacity of the beam using the information from this set. Nevertheless, the failure loads provide a lower-bound estimate of the shear strength of the configuration, whereby an influence from *a/d* is evident.

Crushing of the compression zone between the loading plates and strains exceeding the effective yield strain of the main tension reinforcement were observed for all the specimens in this set prior to P_{max}. However, the behavior before P_{max} was different for all the specimens. For the specimens with larger *a/d* ratios, larger deflections occurred for the same magnitude of applied load.

The load-deflection response for the three specimens in the set is described in Figure 5-2a. The moment-deflection response shown in Figure 5-2b was plotted to normalize the effect of different clear span magnitudes amongst the beams in the set. The figure shows that for smaller *a/d* ratios, the stiffness of the beams increased and smaller deflections at failure were measured. This behaviour was due to the larger contribution of the direct compression strut that developed between the loading plates and the supports for smaller *a/d* ratios, and the larger influence of the vertical web reinforcement for larger *a/d* ratios.

To compare the stiffnesses of the beams, the secant slope of the load-deflection response to 60% of P_{max} was evaluated. A secant was drawn between the load-deflection condition corresponding to first flexural cracking and the point on the curve corresponding to 60% of P_{max}. A reduction of 56% in stiffness for MS2-2 with respect to MS1-2 and a reduction of 45% in stiffness for MS3-3 with respect to MS2-2 were obtained, demonstrating the reduction in stiffness as the *a/d* ratio increases.

In this study, the deflection ductility (μ) of each specimen was evaluated as the ratio of the deflection at P_{max} divided by the deflection corresponding to "yielding" of the entire system. "Yielding" was taken as the condition when the measured strains of the lowest layer of main tension reinforcement reached the effective yield strain according to the 0.2% offset method (see Table 3.1) or approximated as the load causing crushing of the top compression zone between loading plates, whichever occurred first. The values of

μ obtained were 1.65 for beam MS1-2, 1.80 for MS2-2 and 2.31 for MS3-2. According to these calculations, the deflection ductility (μ) increased for larger *a/d* ratios.

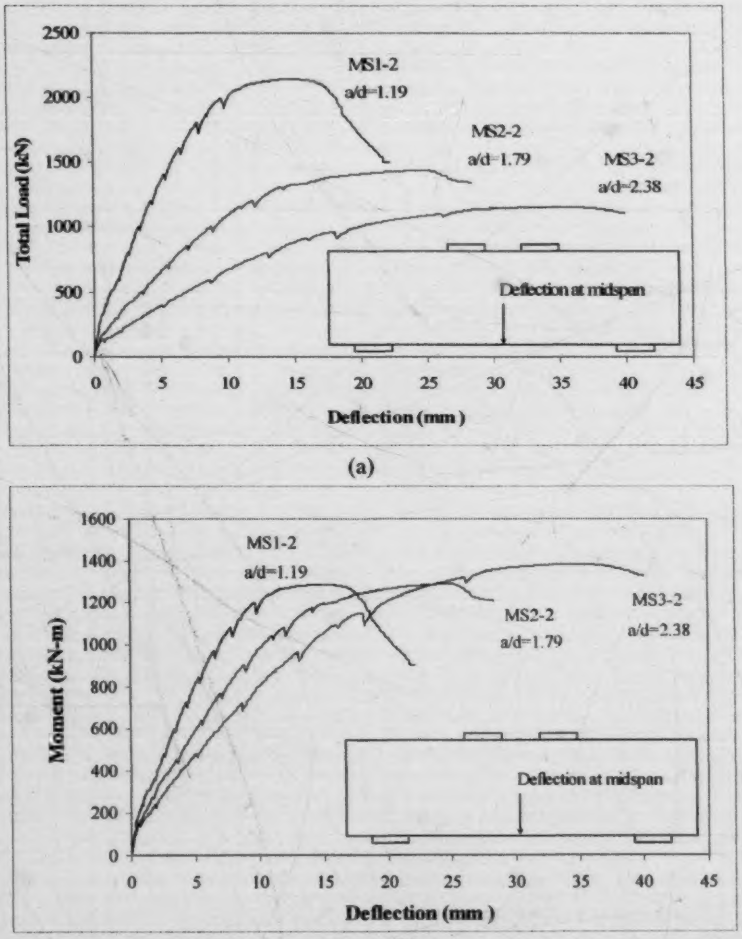

(a)

(b)

Figure 5-2 (a) Load-deflection response and (b) moment-deflection response for specimens MS1-2, MS2-2 and MS3-2

The applied loading corresponding to the common serviceability deflection criteria of *l/360* and *l/180* were analyzed. The deflection limit of *l/360* was reached at approximately one half of P_{max} and the second limit of *l/180* was reached close to P_{max} for all the specimens in the set. The deflection limits of *l/*360 and *l/180* were reached at larger percentages of P_{max} for smaller *a/d* ratios (see Table 5-2). In specimen MS1-2, the serviceability limits were reached at a higher stage of loading than the other two specimens, corresponding to 60 % of P_{max} and 92 % of P_{max} for the *l/360* and *l/180* serviceability limits, respectively. Details of the deflections at maximum loads and at serviceability limits are shown in Table 5-2.

Table 5-2 Deflections and P_{max} for specimens MS1-2, MS2-2 and MS3-2

Specimen	*a/d*	P_{max} *(kN)*	Δ @ P_{max} * at midspan *(mm)*	load at deflection *(kN)*		% P_{max}	
				l/180	*l/360*	*l/180*	*l/360*
MS1-2	1.19	2142	14.90	1978	1278	92.3	59.7
MS2-2	1.79	1432	24.62	1236	796	86.3	55.6
MS3-2	2.38	1154	35.06	896	564	77.6	48.9

*Deflection at the maximum load reached by the specimen

The strain in the lowest layer of the main tension reinforcement for all the specimens in this group was approximately 0.010 mm/mm at P_{max}. A strain of 0.010 mm/mm, corresponds to a stress of 985 MPa for the ASTM A1035 reinforcement. Figure 5-3 illustrates the load-strain response of the lowest layer of the main tension reinforcement at mid-span.

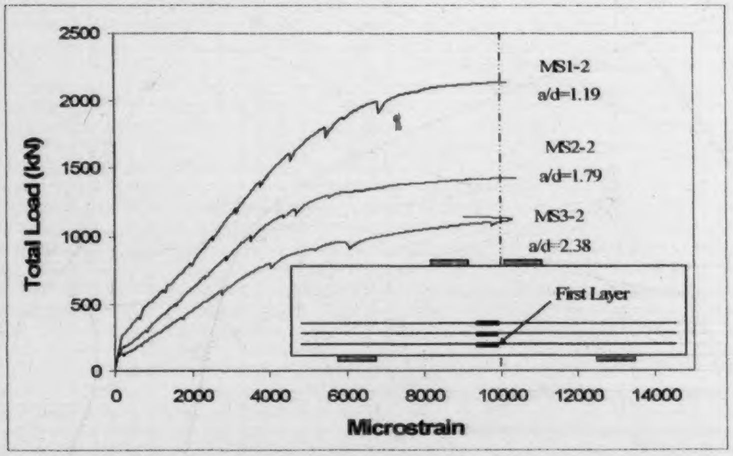

Figure 5-3 Load-strain response for specimens MS1-2, MS2-2 and MS3-2

Figure 5-4 illustrates the distribution of the strains along the lowest layer of the main tension reinforcement. Reinforcement strains close to the support are larger than the strains near the mid-point of the shear span for beams with *a/d*≤ 1.8 in this study. For the specimen with *a/d*=2.4, a gradual reduction in the strains along the bar was measured. Strains close to the supports became larger than strains at midspan at earlier stages of loading for smaller *a/d* ratios. The strain distribution shape changed from a relatively uniform strain magnitude along the entire span with increase of strains close to the supports for the small *a/d* ratio of beam MS1-2, to a gradual decrease in strain between mid-span and support locations for beam MS3-2 with large *a/d* ratio. No strains were measured beyond 400 mm from the exterior edge of the bearing plate for all the specimens in this set.

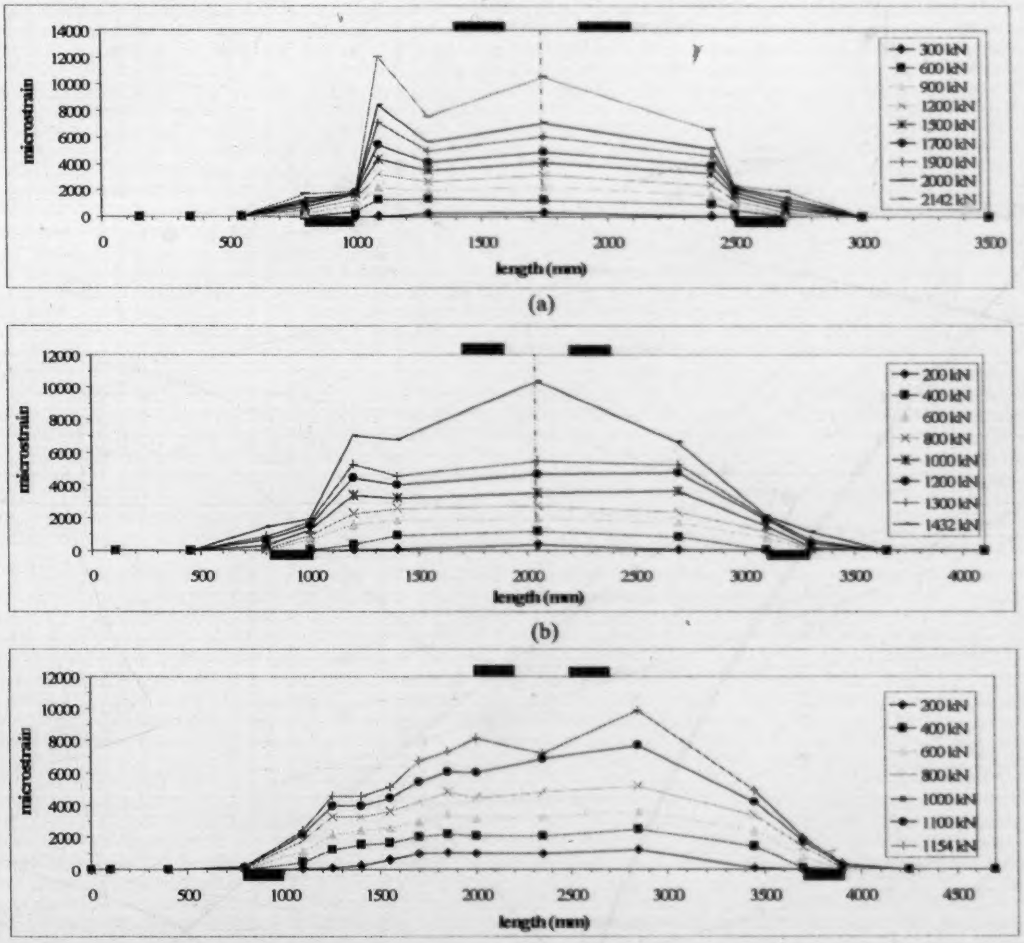

(a)

(b)

(c)

Figure 5-4 Strain distribution along the lowest reinforcement bar for specimens (a) MS1-2, (b) MS2-2 and (c) MS3-2 at different loading stages

The first flexural cracks were observed at an average of 12.5 % of P_{max} for all the beams in the set. The first diagonal strut cracks were observed to develop at an average of 20.2% of P_{max} for MS1-2, 26.7% of P_{max} for MS2-2 and 24.1% of P_{max} for MS3-2 (see Table 5-3).

Table 5-3 Loads at first flexural and strut cracks and percentage of P_{max} for specimens MS1-2, MS2-2 and MS3-2

Specimen	*a/d*	P_{max} *(kN)*	First flexural crack		First Strut crack at side A		First Strut crack at side B	
			P *(kN)*	% of P_{max}	P *(kN)*	% of P_{max}	P *(kN)*	% of P_{max}
MS1-2	1.19	2142	271	12.6	410	19.1	456	21.3
MS2-2	1.79	1432	192	13.4	376	26.3	387	27.0
MS3-2	2.38	1154	130	11.3	258	22.4	298	25.8

For specimen MS1-2, the main diagonal strut crack in both shear spans went from the interior edges of the support plates toward the interior edges of the loading plates. For specimen MS2-2 the diagonal strut crack trajectories pointed to the middle of the loading plates and for specimen MS3-2, the diagonal strut crack directions were pointed approximately 200 mm away from the exterior edge of the loading plate. These crack patterns indicated that for large *a/d* ratios, no direct strut from the loading points to the supports are developed. Figure 5-5 illustrates the crack pattern for the three specimens at approximately 84% of P_{max}.

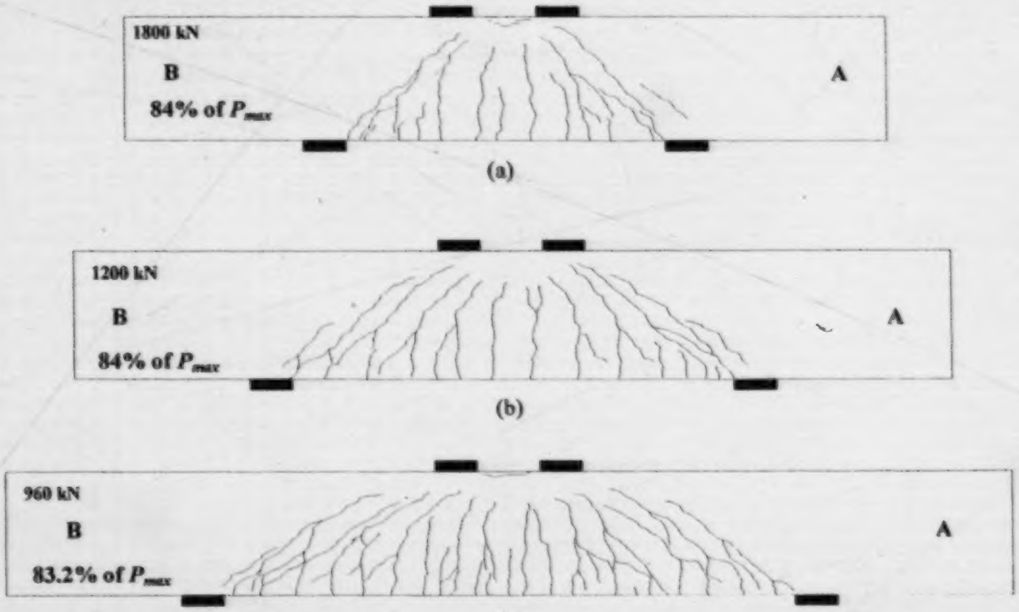

(a)

(b)

(c)

Figure 5-5 Crack development of (a) MS1-2 at 1800 kN , (b) MS2-2 at 1200 kN and (c) MS3-2 at 960 kN

5.1.1.2 Specimens with different *a/d* and constant ρ of 2.29%

The specimens considered in this set are specimens MS1-3 and MS2-3. Table 5-4 shows ρ, *a/d*, vertical web reinforcement arrangement, failure mode, maximum load reached during the test, deflection at maximum load and secant stiffness of the beams at 60% of P_{max}.

Table 5-4 Comparison of specimens MS1-3 and MS2-3

Beam	ρ (%)	*a/d*	vertical web reinforcement	f'_c (MPa)	Mode of failure	P_{max} (kN)	Deflection at midspan for P_{max} (mm)	Stiffness at 60% of P_{max} (kN/mm)
MS1-3	2.29	1.18	10M@200mm	44	Splitting Strut	2747	7.86	504
MS2-3	2.29	1.78	10M@200mm	43	Flexure-Splitting Strut	2055	12.49	174

Comparing MS1-3 and MS2-3, a decrease in capacity of 25% occurred due to an increase in the *a/d* ratio of 50%.

A brittle diagonal strut failure was observed for both specimens, resulting from cracks that went from the exterior edge of the loading plate to the interior edge of the support. At the time of maximum load, no cracking of the top strut between the loading plates was detected in specimen MS1-3. For specimen MS2-3, however, some horizontal cracking of the top strut between the loading plates was observed at approximately 95% of P_{max}. For specimens MS1-3 and MS2-3, no strains in the main tension reinforcement larger than the effective yield strain ε_y, (see Table 3.1) were measured prior to P_{max}. The strain in the lowest layer of the main tension reinforcement at P_{max} was 0.0035 mm/mm and 0.0042 mm/mm (54% and 65% of ε_y) for specimens MS1-3 and MS2-3 respectively.

The load-deflection response for the two specimens in the set is illustrated in Figure 5-6. Figure 5-6a shows that for smaller *a/d* ratios the stiffness of the beams increases. A similar trend was reported from Figure 5-2. The moment-deflection response, shown in Figure 5-6b, was plotted to normalize the effect of different clear spans between the two specimens. This figure also shows that for smaller *a/d* ratios, the stiffness increases.

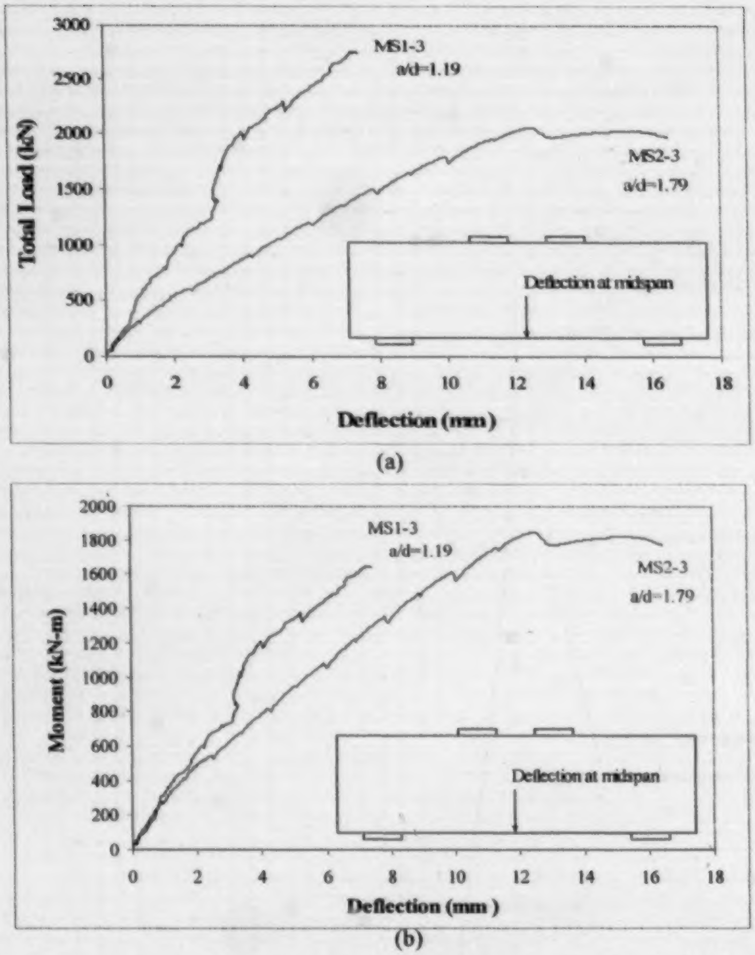

(a)

(b)

Figure 5-6 (a) Load-deflection and (b) moment-deflection response for specimens MS1-3 and MS2-3

Using the method described in Section 5.1.1.1., the secant stiffness of each specimen was determined between the point corresponding to first flexural cracking and the point on the curve at 60% of P_{max}. The reduction in the secant stiffness at 60% of P_{max} was 65.5% from MS1-3 to MS2-3. This reduction in secant stiffness was similar to the reduction observed for the same variation of *a/d* from 1.19 to 1.79 in beams with constant ρ of 1.13% (i.e. MS1-2 and MS2-2) in Section 5.1.1.1.

Comparisons of the deflections at maximum loads and at common serviceability limits for specimens with ρ=2.29% are shown in Table 5-5. The deflection limits of *l/360* and *l/180* were reached at larger percentages of P_{max} for larger *a/d* ratios. Specimen MS1-

3 reached the *l/360* limit at 79% of P_{max}, but failed in a sudden manner due to splitting of the diagonal strut before reaching the *l/180* limit. Specimen MS2-3 reached the *l/360* limit at 61.4% of P_{max}, but reached the maximum load before reaching the *l/180* limit. At P_{max}, the midspan deflection corresponded to *l*/216 and *l*/184 for specimens MS1-3 and MS2-3 respectively.

Table 5-5 Deflections and P_{max} for specimens MS1-3 and MS2-3

Specimen	*a/d*	ρ *(%)*	P_{max} *(kN)*	Δ @ P_{max} * at midspan *(mm)*	load at deflection *(kN)*		% P_{max} *(kN)*	
					l/180	*l/360*	*l/180*	*l/360*
MS1-3	1.19	2.29	2747	7.9	N/A	2166	N/A	78.8
MS2-3	1.78	2.29	2055	12.5	N/A	1261	N/A	61.4

*Deflection at the maximum load reached by the specimen

Figure 5-7 illustrates the load-strain response of the lowest layer of the main tension reinforcement at mid-span. Strains less than the strain corresponding to the effective yield stress (i.e., ε_y=0.0065) were measured prior to reaching P_{max}. A linear strain response with load was observed for both beams up to P_{max}.

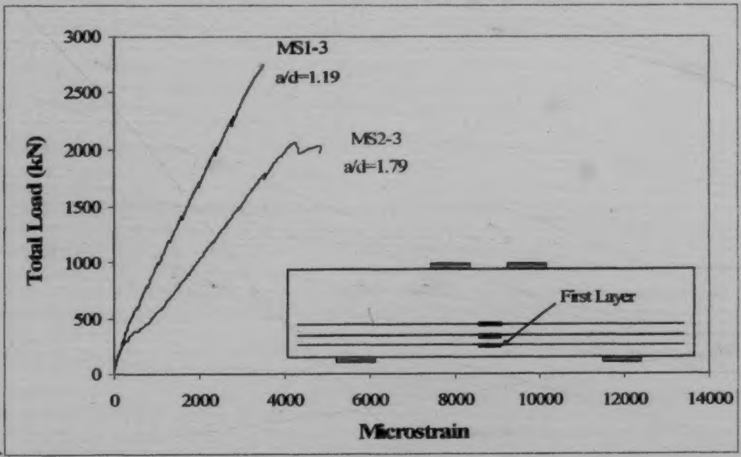

Figure 5-7 Load-strain response for the first (lowest) layer of specimens MS1-3 and MS2-3

Figure 5-8 illustrates the strain distribution along one bar of the lowest layer of the main tension reinforcement for different applied loads. The variation in reinforcement strain along the member length was different for the two specimens. For specimen MS1-3 with smaller *a/d* ratio, a more uniform magnitude of strain along the span was observed compared to specimen MS2-3 with larger *a/d* ratio. A gradual reduction in the strain magnitude between mid-span and the supports was observed for specimen MS2-3. No strains were measured at 400 from the exterior edge of the bearing plate for both specimens. The shape of the strain distribution of each specimen remained similar for all the stages of loading.

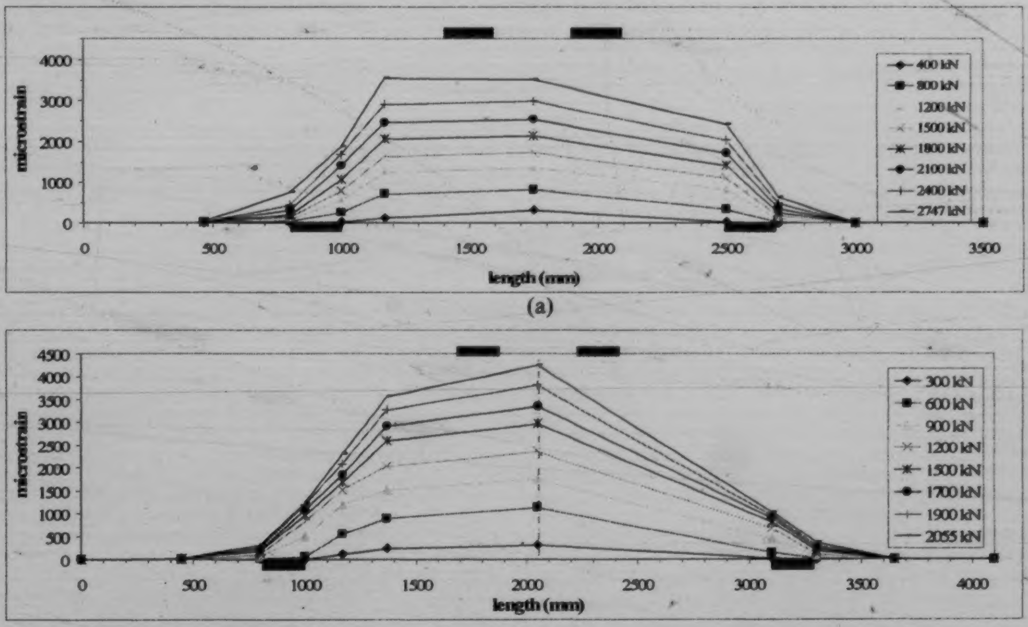

(b)

Figure 5-8 Strain distribution along the lowest bar of main tension reinforcement for specimens (a) MS1-3 and (b) MS2-3

The first flexural cracks were observed at an average of 14.2 % of P_{max} for both specimens. The first diagonal strut cracks developed on average at 24.2% of P_{max} for specimen MS1-3 and at 27.7% of P_{max} for specimen MS3-2.

Table 5-6 Loads at first flexural and strut cracks and percentage of P_{max} for specimens MS1-2 and MS2-3

Specimen	a/d	P_{max} (kN)	First flexural crack		First Strut crack at side A		First Strut crack at side B	
			P (kN)	% of P_{max}	P (kN)	% of P_{max}	P (kN)	% of P_{max}
MS1-3	1.19	2747	389	14.16	640	23.3	688	25.0
MS2-3	1.79	2055	293	14.25	560	27.25	580	28.2

For specimen MS1-3, two main diagonal strut cracks developed in each shear span. One of these cracks developed at mid depth of the specimen and extended along a line joining the centerline of the support and the centerline of the loading points. The other crack developed from the interior edge of the support plate towards the interior edge of the loading plates. A similar pattern occurred for both shear spans. Specimen MS2-3 with larger *a/d* ratio developed different patterns of diagonal strut cracks. For this specimen, two main diagonal struts cracks developed at each shear span. One of the cracks at each shear span went from the interior edge of the support toward the interior edge of the loading plate. The other diagonal strut crack went from the centerline of the support plate to the exterior edge of the loading plate. Figure 5-9 illustrates the crack patterns of specimen MS1-3 and MS2-3 at approximately 73% of P_{max}.

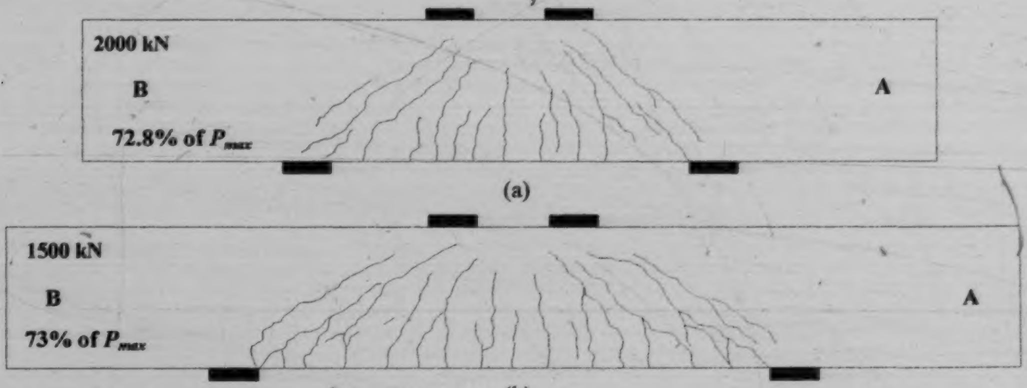

(b)

Figure 5-9 Crack development at 73% of P_{max} for (a) Specimen MS1-3 (b) Specimen MS2-3

A comparison was made between the crack patterns for specimens reinforced with ρ of 1.13% (from Section 5.1.1.1) and the corresponding specimen with ρ of 2.29%. It was observed that for the same *a/d* ratio, similar crack patterns developed.

5.1.2 Influence of main reinforcement ratio

Two sets of specimens were studied to compare the effects of the main reinforcement ratio, *ρ*, on the behavior of deep beams longitudinally reinforced with ASTM A1035 reinforcing steel. The first set of specimens is composed of members with *a/d*=1.2, and includes specimens MS1-1, MS1-2 and MS1-3. The second set is composed of members with *a/d*=1.8, which includes specimens MS2-2 and MS2-3.

Figure 5-10 shows the relationship between maximum total load and reinforcement ratio ρ for specimens with *a/d* of 1.2 and 1.8. For members having the same *a/d* ratio, the capacity increases as the reinforcement ratio ρ increases.

Comparison of member performance within each set is provided in Sections 5.1.2.1 and 5.1.2.2.

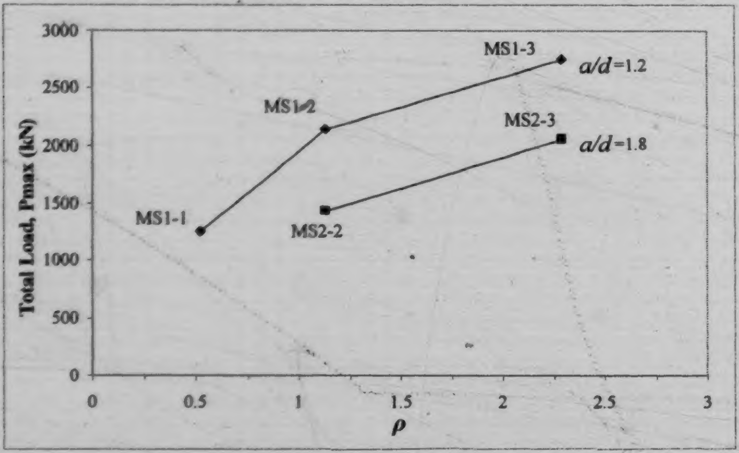

Figure 5-10 Load-ρ relationship for specimens with *a/d*=1.2 and 1.8

5.1.2.1 Specimens with *a/d* of 1.2 and different ρ

The specimens considered in this set are specimens MS1-1, MS1-2 and MS1-3. Table 5-7 shows ρ, *a/d*, vertical web reinforcement arrangement, failure mode, maximum load reached during the test, deflection at maximum load, secant stiffness of the beams and 60% of P_{max}.

Table 5-7 Comparison of specimens MS1-1, MS1-2 and MS1-3

Specimen	*a/d*	ρ	vertical web reinforcement	f'_c *(MPa)*	Mode of failure	P_{max} *(kN)*	Deflection at midspan for P_{max} *(mm)*	Stiffness at 60% of P_{max} *(kN/mm)*
MS1-1	1.19	0.52	10M@200mm	46	Flexure	1252	13.7	158
MS1-2	1.19	1.13	10M@200mm	44	Flexure	2142	14.9	235
MS1-3	1.19	2.29	10M@200mm	44	strut	2747	7.9	504

A reduction of 78% in ρ from specimen MS1-3 to specimen MS1-1 reduced the capacity by 55%. From specimen MS1-3 to specimen MS1-2, a reduction of 51% in ρ decreased the capacity by 20 %.

The behavior prior to P_{max} for each of the specimens in this group was different. For specimen MS1-1, strains corresponding to the effective yield strains were measured at midspan for the three layers of main tension reinforcement at approximately 90% of P_{max}. At the time of failure, crushing of the top strut of specimen MS1-1 also occurred. For specimen MS1-2, cracking of the top strut was observed prior to strains reaching the effective yield strain in the layers of main tension reinforcement. Once the strains exceeded the effective yield strain in the main tension reinforcement, specimen MS1-2 reached P_{max}. After P_{max}, the applied load for specimen MS1-2 started to drop for increasing applied displacement and then a splitting failure of the diagonal strut occurred suddenly. For specimen MS1-3, a splitting strut failure occurred before the strains in the main tension reinforcement reached the effective yield strain and before cracking of the top horizontal strut was observed.

The different behavior of the specimens is illustrated in the load-deflection curves of Figure 5-11. This figure shows that for larger values of ρ, the specimen stiffness increases. Secant stiffness values to 60% of P_{max} are shown in Table 5-7. A reduction of 53.4% in stiffness for specimen MS1-2 with respect to specimen MS1-3 and a reduction of 32.8% in stiffness for specimen MS1-1 with respect to specimen MS1-2 were observed.

The ductile behavior of this set was analyzed using a deflection ductility parameter (μ) as explained in section 5.1.1.1. The deflection ductility evaluates the ratio of the deflection at the maximum load divided to the deflection at yielding of the system. Effective yield strains were measured on the lowest layer of main longitudinal reinforcement at 79% and 90% of P_{max} for specimens MS1-1 and MS1-2, respectively, giving deflection ductility ratios μ of 2.19 for specimen MS1-1 and 1.65 for specimen MS1-2. A brittle failure was observed for specimen MS1-3. The study of deflection ductility (μ) for this set shows that μ increased for smaller main longitudinal reinforcement ratios, ρ.

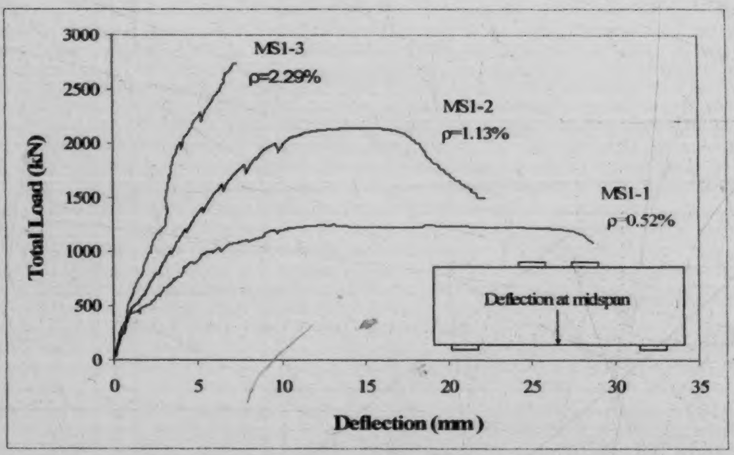

Figure 5-11 Load-deflection response for specimens MS1-2, MS2-2 and MS3-2

The common deflection limits of *l/360* and *l/180* were reached at approximately 60% and 90% of P_{max} respectively for specimens MS1-1 and MS1-2. Specimen MS1-3 reached the *l/360* limit at 79% of P_{max}, but failed in a sudden manner before reaching the *l/180* limit. At failure, the deflection corresponded to *l*/216. Deflections at P_{max} and at serviceability limits are shown in Table 5-8.

Table 5-8 Deflections and P_{max} for specimens MS1-1, MS1-2 and MS1-3

Specimen	ρ (%)	P_{max} (kN)	Δ @ P_{max}* midspan (mm)	load at deflection (kN)		% P_{max} (kN)	
				l/180	*l/360*	*l/180*	*l/360*
MS1-1	0.52	1252	13.7	1128	804	90.1	64.2
MS1-2	1.13	2142	14.9	1978	1278	92.3	59.7
MS1-3	2.29	2747	7.9	N/A	2166	N/A	78.8

*Deflection at the maximum load reached by the specimen

Figure 5-12 illustrates the load-strain response of the lowest layer of the main tension reinforcement at mid-span. Different ρ resulted in different load-strain relationships for the main tension reinforcement. For specimens MS1-1 and MS1-2, strains exceeding the effective yield strain were detected at approximately 80% and 90% of P_{max}. For specimen MS1-3, the midspan strain reading at P_{max} was approximately 50% of the effective yielding strain.

The variation in strain magnitude along the lowest layer of the main longitudinal reinforcement at 90% of P_{max} for the three specimens is shown in Figure 5-13. Similar behavior is observed for specimens MS1-1 and MS1-2, where the strains close to the supports were larger than the strains at mid-length of the shear span. Specimen MS1-3 showed more uniform variation in strain magnitude along the clear span.

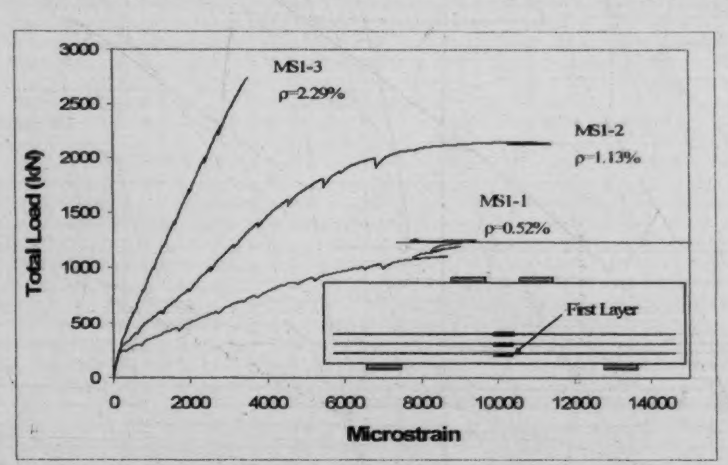

Figure 5-12 Load-strain response for the first layer of the main tension reinforcement for specimens MS1-1, MS1-2 and MS1-3

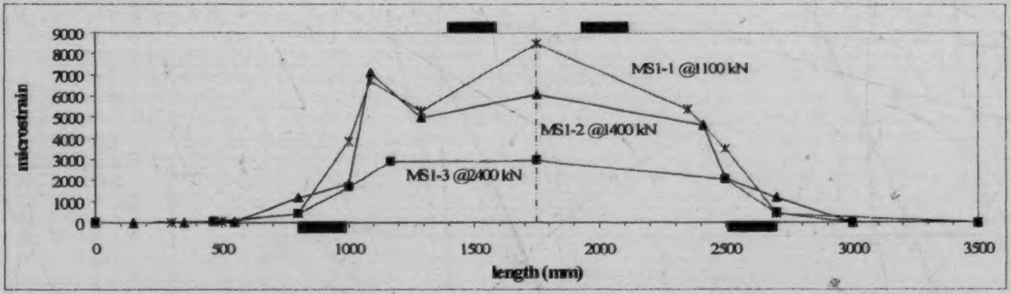

Figure 5-13 Strain distribution along the bottom reinforcing bar at approximately 90 % of P_{max}

Table 5-9 shows the loads corresponding to first flexural cracking and the formation of the diagonal strut cracks. The percentage of P_{max} when these cracks occurred is also indicated. The first flexural cracks occurred at approximately 14 % of P_{max} and the diagonal strut cracks were detected at approximately at 24% of P_{max}.

Very similar crack development was observed in specimens MS1-1 and MS1-2. For these specimens, the main diagonal strut crack at the shear spans went from the interior edges of the support towards the interior edges of the loading plates (see Figure

5-14). The same crack patterns were also observed in specimen MS1-3, however, other important diagonal strut cracks were also observed. At shear span A, this crack developed along the line between the centerlines of the support and loading points. At shear span B, this crack went from the centerline of the support towards the interior edge of the loading point. In the zone with constant moment between the loading plates, flexural cracks for the specimens from this set reached different heights at similar fraction of P_{max} (see Figure 5-14).

Table 5-9 Load at first flexural and strut cracks and percentage of P_{max} at the occurrence of the cracks

Specimen	P_{max} (kN)	ρ (%)	First flexural crack		First Strut crack at side A		First Strut crack at side B	
			P (kN)	% of P_{max}	P (kN)	% of P_{max}	P (kN)	% of P_{max}
MS1-1	1252	0.52	200	16	365	29.2	354	28.32
MS1-2	2142	1.13	271	12.6	410	19.1	456	21.30
MS1-3	2747	2.29	389	14.16	640	23.3	688	25.04

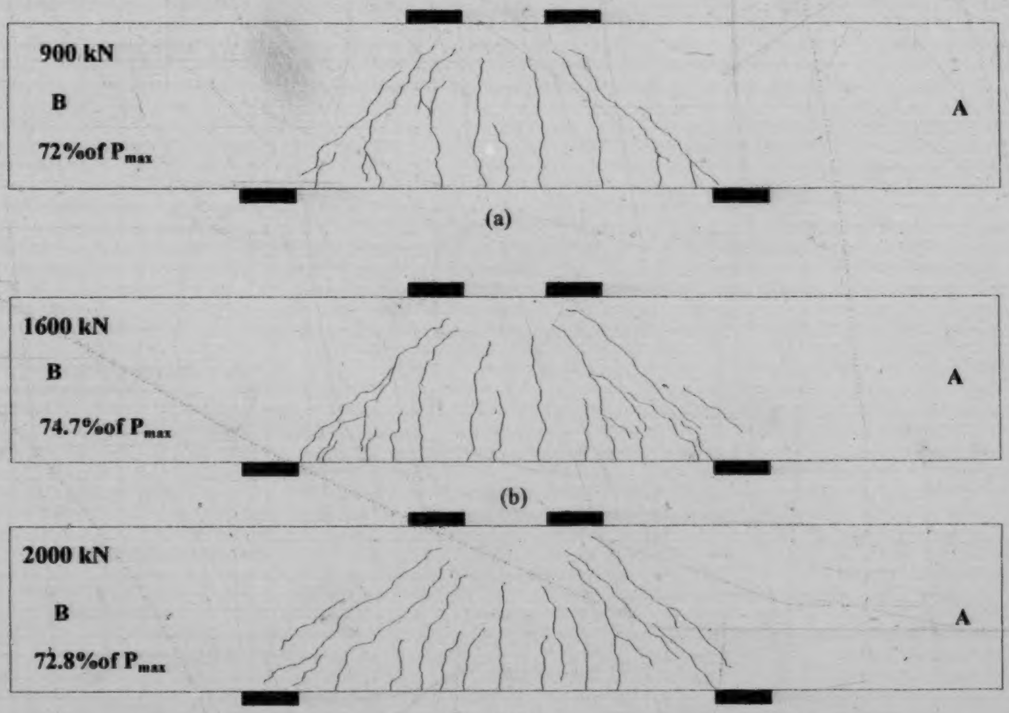

(a)

(b)

(c)

Figure 5-14 Crack development of (a) MS1-1 at 900 kN , (b) MS1-2 at 1600 kN and (c) MS1-3 at 2000 kN

5.1.2.2 Specimens with *a/d* of 1.8 and different ρ

The specimens considered in this set are specimens MS2-2 and MS2-3. Table 5-10 shows ρ, *a/d*, vertical web reinforcement arrangement, failure mode, maximum load reached during each test, deflection at P_{max} and secant stiffness of the specimens at 60% of P_{max}.

Table 5-10 Comparison of specimens MS2-2 and MS2-3

Specimen	*a/d*	ρ (%)	vertical web reinforcement	f'_c (MPa)	Mode of failure	P_{max} (kN)	Deflection at midspan for P_{max} (mm)	Stiffness at 60% of P_{max} (kN/mm)
MS2-2	1.79	1.13	10M@200mm	47	Flexure	1432	24.6	118
MS2-3	1.78	2.29	10M@200mm	43	Flexure-splitting Strut	2055	12.5	174

A reduction of 51% in ρ from specimen MS2-3 to specimen MS2-2 resulted in a reduction in capacity of 30%. This reduction in capacity was 10% higher than observed for the same change in reinforcement ratio when $a/d = 1.19$, where the reduction of 51% in ρ decreased the capacity by 20 % (see Section 5.1.2.1).

Prior to P_{max}, some cracking of the top horizontal strut between the load points was observed for both specimens in the set. Strains exceeding the effective yield strain of the main tension reinforcement were measured, followed by crushing of the compression zone between the loading points, for specimen MS2-2. Specimen MS2-3 suffered brittle failure caused by splitting of the diagonal strut soon after reaching P_{max} which was governed by weakening of the compression zone between the loading points due to cracking of the concrete. Strains measured for the main longitudinal reinforcement at midspan showed that the steel did not reach the effective yield strain for MS2-3.

The load-deflection response for specimens MS2-2 and MS2-3 is illustrated in Figure 5-15. This figure shows the influence of the reinforcement on the stiffness of the specimens, after the first flexural crack. The slope of the load-deflection curve for specimen MS2-3 was steeper than for specimen MS2-2. Using the 60% secant stiffness approach (described in section 5.1.1.1) to compare the stiffness of the specimens, a reduction of 40% in stiffness for specimen MS2-2 with respect to specimen MS2-3 was observed. The deflection ductility of specimen MS2-2, as defined in Section 5.1.1.1, was much larger than the corresponding ductility of specimen MS2-3. The strain readings for specimen MS2-2 reached the effective yield strain value at 93% of P_{max} and the deflection ductility μ was 1.56. Specimen MS2-3 had a linear strain response prior to P_{max}. While there was some additional displacement after P_{max}, there was no "yielding" of the main reinforcement, and thus the displacement ductility as defined in Section 5.1.1.1 cannot be determined. The ratio of deflection when the slope of load-deflection curve started to change to the deflection at failure was approximately 0.8, indicating that the failure occurred with minimal warning.

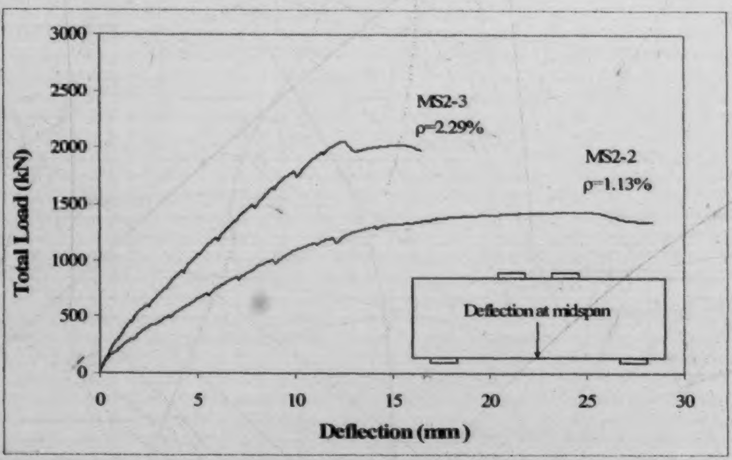

Figure 5-15 Load-deflection response for specimens MS2-2 and MS2-3

Comparison of the deflections at maximum loads and at common serviceability limits for specimens MS2-2 and MS2-3 are shown in Table 5-11. The first deflection limit of *l/360* was reached at loading stages larger than half of P_{max} and the second limit of *l/180* was reached close to P_{max} for both specimens. The deflection limits of *l/*360 and *l/180* were reached at larger percentages of P_{max} for larger reinforcement ratios.

Table 5-11 Deflections and Pmax for specimens MS2-2 and MS2-3

Specimen	a/d	ρ *(%)*	P_{max} *(kN)*	Δ @ P_{max}* at midspan *(mm)*	load at deflection *(kN)*		% P_{max}	
					l/180	*l/360*	*l/180*	*l/360*
MS2-2	1.79	1.13	1432	24.62	1236	796	86.3	55.6
MS2-3	1.78	2.29	2055	12.50	2003	1261	97.5	61.4

*Deflection at the maximum load reached by the specimen

Figure 5-16 illustrates the load-strain response of the lowest layer of the main tension reinforcement at mid-span. Different load-strain relationships were observed based on the reinforcement ratio, ρ. For specimen MS2-2, strains exceeding the effective yield strain were detected, however, for beam MS2-3, the strain readings at P_{max} were approximately 64% of the effective yielding strain.

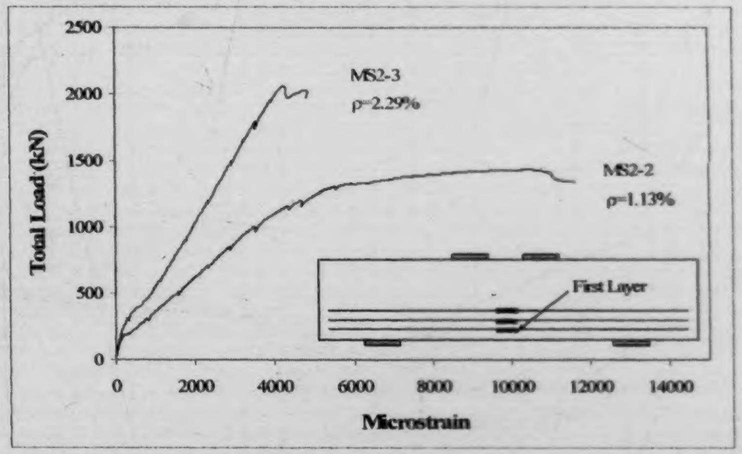

Figure 5-16 Load-strain response for the first layer of the main tension reinforcement

The variation in strain along the lowest layer of the main longitudinal reinforcement for the specimens at 90% of P_{max} is shown in Figure 5-17. While in specimen MS2-2, strains close to the support were larger than in the mid span, specimen MS2-3 showed a gradual reduction of the strains in the clear span along the bottom rebar.

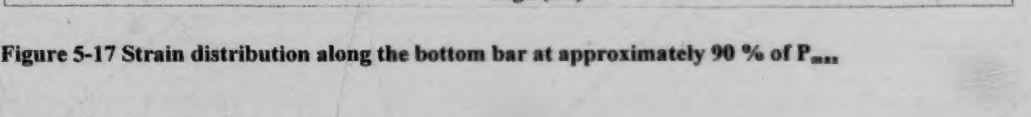

Figure 5-17 Strain distribution along the bottom bar at approximately 90 % of P_{max}

For shear span A of specimens MS2-2 and MS2-3, the crack development was similar, as shown in Figure 5-18. The main diagonal strut crack went from the interior edge of the support toward the interior edge of the loading point. The other diagonal cracks were parallel to the main diagonal strut crack. For shear span B of these specimens, the crack development was different. For specimen MS2-2, one diagonal strut crack went from the interior edge of the support to the exterior edge of the loading point and a shorter parallel crack went towards the centerline of the loading point. At shear span B of specimen MS2-3, one strut crack went from the interior edge of the support to the interior edge of the loading point. Another crack parallel to this diagonal strut crack was developed.

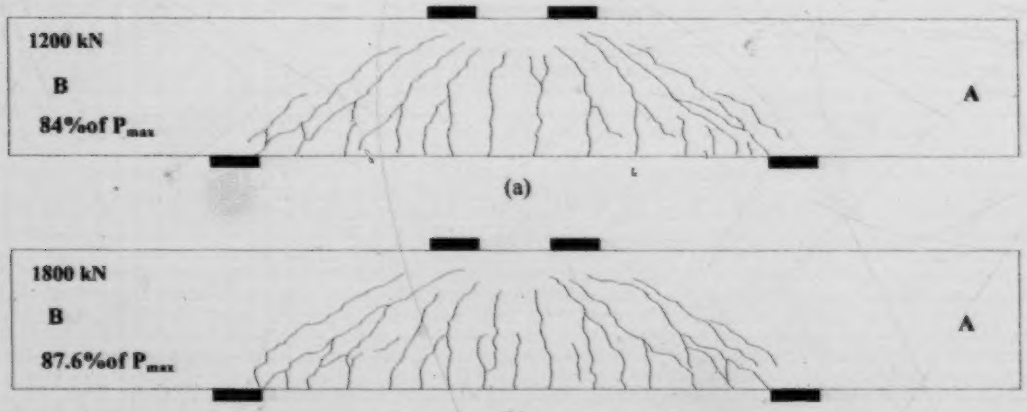

Figure 5-18 Crack development of (a) MS2-2 at 1200 kN and (b) MS2-3 at 1800 kN

Table 5-12 shows the load corresponding to the first flexural crack, first diagonal strut cracks and the respective percentage of P_{max}. For both specimens, the first flexural crack occurred at approximately 14 % of P_{max} and the diagonal strut cracks were detected at approximately at 26% of P_{max}.

Table 5-12 Load at first flexural and strut cracks and percentage of P_{max} at the occurrence of the cracks for specimens MS2-2 and MS2-3

Specimen	P_{max} (kN)	ρ (%)	First flexural crack		First Strut crack at side A		First Strut crack at side B	
			P (kN)	% of P_{max}	P (kN)	% of P_{max}	P (kN)	% of P_{max}
MS2-2	1432	1.13	192	13.4	376	26.3	387	27.0
MS2-3	2055	2.29	293	14.3	560	27.3	580	28.2

5.2 Specimens without web reinforcement

The specimens constructed without web reinforcement are specimens MW1-2 and MW3-2. These two specimens had the same cross section and reinforcement arrangements. The only parameter that varied between the specimens was the shear span to depth ratio. The comparison between both specimens allowed evaluation of the influence of shear span to depth ratio on their behavior. The failure mode observed for both beams was diagonal strut failure. No yielding of main longitudinal reinforcement or crushing of the compression zone between the loading plates was observed. Even though both specimens failed by splitting of the diagonal strut, only specimen MW1-2 suffered a brittle failure. At the peak load for MW3-2, a small sudden drop in applied force occurred, followed by a gradually decreasing force for increased applied displacement. The loading process for specimen MW3-2 was stopped after the diagonal strut crack width was approximately 15 mm, but no total collapse of the system had occurred.

Table 5-13 shows ρ, a/d, failure mode, maximum load reached during the test, deflection at maximum load and secant stiffness of the beams at 60% of P_{max}.

Table 5-13 Comparison of specimens MW1-2 and MW3-2

Specimen	ρ (%)	a/d	f'_c (MPa)	Mode of failure	P_{max} (kN)	Deflection at midspan for P_{max} (mm)	Stiffness at 60% of P_{max} (kN/mm)
MW1-2	1.13	1.19	39	Splitting Strut	1568	7.50	242
MW3-2	1.13	2.38	43	Splitting Strut	411	9.08	79

For the specimens without web reinforcement, the increment in a/d from 1.19 to 2.38 reduced the maximum force capacity by 73.7%. The secant stiffness at 60% of P_{max}, was reduced by 67.3% from specimen MW1-2 to specimen MW3-2. Secant stiffness was evaluated using the method described in Section 5.1.1.1.

The load-deflection and moment-deflection response for the two specimens is described in Figure 5-19. The moment-deflection response was plotted to normalize the effect of different clear span between the specimens. The figure shows that for smaller a/d ratio, the stiffness of the beams increased. After initial flexural cracking, the load-deflection response of specimen MW1-2 remained essentially linear up to 97% of P_{max}. After that load level, the deflection and crack width rates increased until the loading on specimen MW1-2 reached P_{max}. Specimen MW3-2 showed approximately linear load-deflection behavior after cracking up to 80% of P_{max}. After that load, the capacity of specimen MW3-2 decreased 12.8 % and then recovered with increasing applied deflection until P_{max} was reached.

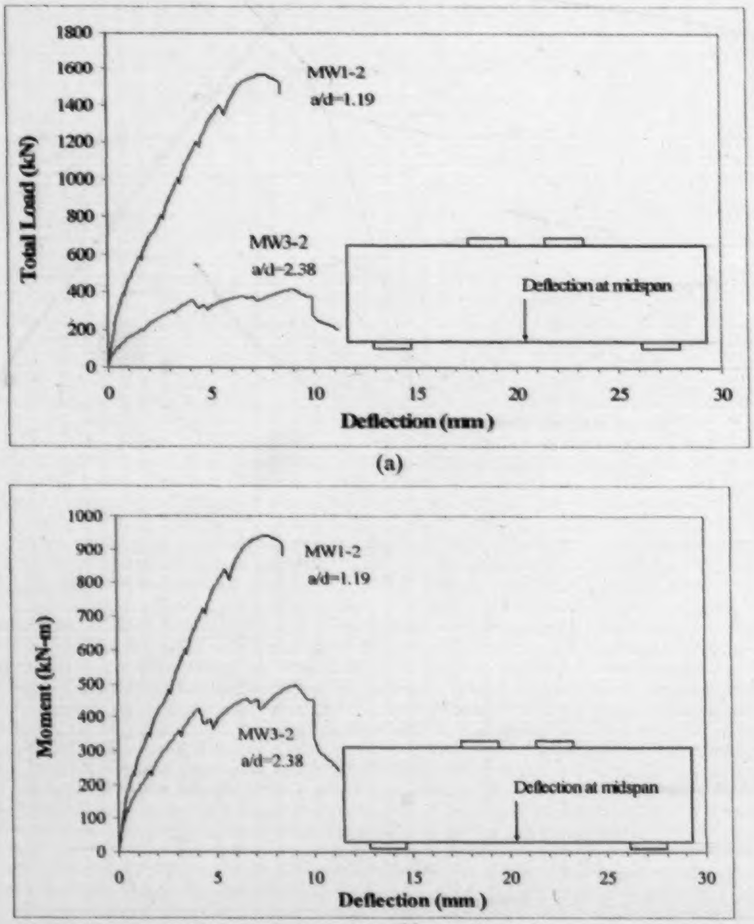

(a)

(b)

Figure 5-19 (a) Load-deflection response and (b) moment-deflection response for specimens MW1-2 and MW3-2

Details of the deflections at maximum loads and at common serviceability limits are shown in Table 5-2. Both specimens failed prior to reaching the deflection limit of *l/180*. At P_{max}, the deflections corresponded to *l*/226 and *l*/253 for specimens MW1-2 and MW3-2, respectively.

Table 5-14 Deflections and P_{max} for specimens MW1-2 and MW3-2

Specimen	a/d	ρ (%)	P_{max} (kN)	Δ @ P_{max} * at midspan (mm)	load at deflection (kN)		% P_{max}	
					$l/180$	$l/360$	$l/180$	$l/360$
MW1-2	1.19	1.13	1568	7.50	NA	1251	NA	79.8
MW3-2	2.38	1.13	411	9.08	NA	389	NA	94.6

*Deflection at the maximum load reached by the specimen

The midspan strain in the lowest layer of the main tension reinforcement for specimen MW1-2 at P_{max} was 0.0042. This strain is only 66% of the effective yield strain, ε_y, and 11% of the strain at the maximum stress, ε_u. For specimen MW3-2, the midspan strain in the lowest layer of main tension reinforcement at P_{max} was 0.002, which represents 31% of the effective yield strain, ε_y, and only 5% of the strain at maximum stress, ε_u (see Table 3.4). The strains of 0.0042 and 0.002 correspond to stresses of 732 MPa and 408 MPa respectively. Figure 5-20 illustrates the load-strain response of the lowest layer of the main tension reinforcement at mid-span.

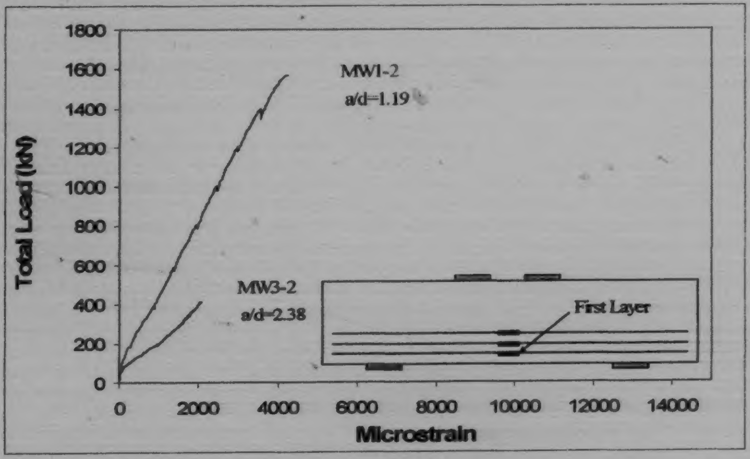

Figure 5-20 Load-strain response for MW1-2 and MW3-2

Figure 5-21 illustrates the distribution of the strains along the lowest layer of the main tension reinforcement for specimens MW1-2 and MW3-2. The increment rates for reinforcement strains close to the support are larger than the strains near the mid-point of the shear span for specimen MW1-2. For specimen MW3-2, the increment rates were larger close to the mid-point of the shear span than close to the supports. The large increase in strains near the supports at the last load level shown for each specimen correspond to the increase in crack width in this region close to failure.

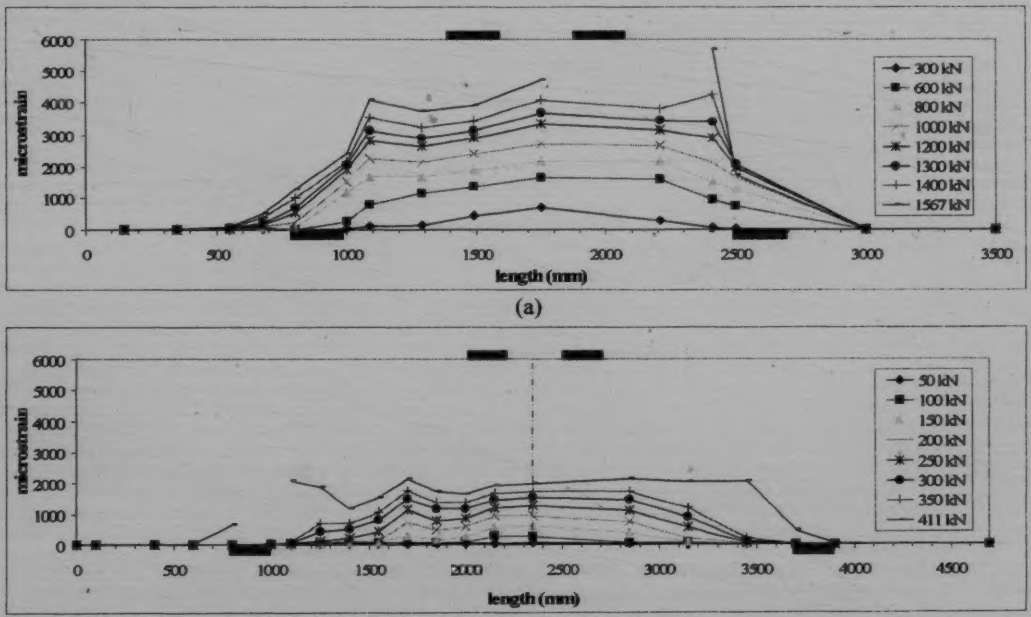

(a)

(b)

Figure 5-21 Strain distribution along the bottom bar for (a) MW1-2 and (b) MW3-2 at different loading stages

Table 5-15 shows the load corresponding to the first flexural crack, first diagonal strut cracks and the respective percentage of P_{max}. This table shows that an increment of *a/d* from 1.19 to 2.38 reduced the load at first flexural crack by 61%. The load of first diagonal strut crack was reduced 37% from MW1-2 to MW3-2.

Table 5-15 Loads at first flexural and strut cracks and percentage of maximum load for specimens MW1-2 and MW3-2

Specimen	a/d	P_{max} (kN)	First flexural crack		First Strut crack at side A		First Strut crack at side B	
			P (kN)	% of P_{max}	P (kN)	% of P_{max}	P (kN)	% of P_{max}
MW1-2	1.19	1568	257	16.4	393	25.1	450	28.7
MW3-2	2.38	411	99	24.1	247	60.1	283	68.8

Figure 5-22 illustrates the crack development of specimens MW1-2 and MW3-2. Strut cracks propagated very fast at small applied loads for both specimens. Specimen MW1-2 developed symmetric cracks at both ends. On the other hand, specimen MW3-2 developed strut cracks mainly on shear span A.

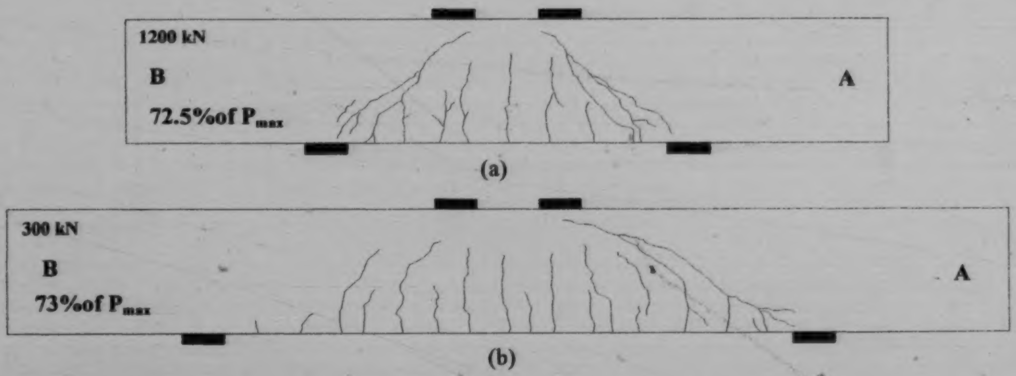

Figure 5-22 (a) Crack development of MW1-2 at 1200 kN (72.5%of P_{max}) and (b) Crack development of MW3-2 at 300 kN (73%of P_{max})

5.3 Strength contribution of web reinforcement

In this section, the influence of the web reinforcement on the strength of deep beams was examined. For this purpose, two sets of companion beams are compared. Each specimen in a companion set had the same dimensions and ρ, but one specimen did not include horizontal or vertical web reinforcement.

Figure 5-23 shows the influence of the web reinforcement on the strength of the specimens. Comparison of member performance between members with similar *a/d* ratio from each set is provided in Sections 5.3.1 and 5.3.2.

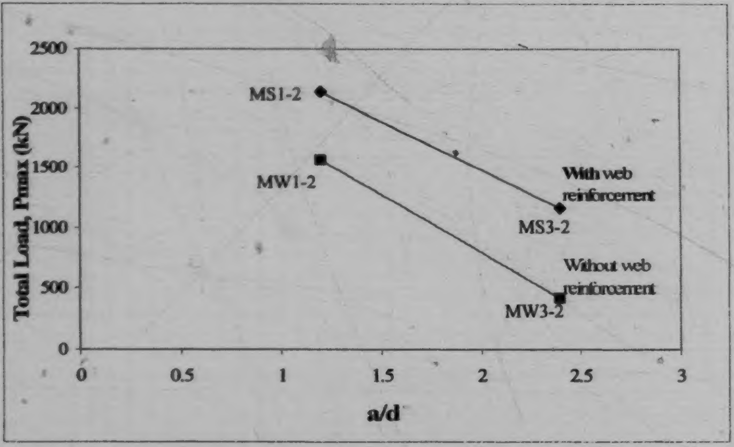

Figure 5-23 Influence of web reinforcement on member strength

5.3.1 Specimens MS1-2 and MW1-2

Table 5-16 shows ρ, a/d, vertical web reinforcement arrangement, maximum load reached at test, deflection at P_{max} and the secant stiffness of the specimens at 60% of P_{max}.

Table 5-16 Comparison of specimens MS1-2 and MW1-2

Specimen	ρ (%)	a/d	vertical web reinforcement	f'_c (MPa)	Mode of failure	P_{max} (kN)	Deflection at midspan for P_{max} (mm)	Stiffness at 60%P_{max} (kN/mm)
MS1-2	1.13	1.19	10M@200mm	44	Flexure	2142	14.90	235
MW1-2	1.13	1.19	-	39	Strut	1568	7.50	242

The inclusion of the web reinforcement increased the overall strength of specimen MS1-2 by 37% compared to specimen MW1-2.

Prior to reaching P_{max}, crushing of the top strut of specimen MS1-2 was observed and strains exceeding the effective yield strain were measured in the main tension reinforcement. On the other hand, specimen MW1-2 failed in a brittle manner due to splitting of the diagonal strut. No yielding of the main tension reinforcement was detected in specimen MW1-2.

The load-deflection response for the specimens is illustrated in Figure 5-24. The figure indicates that there was no significant influence on load-deflection response up to an applied load of 1350 kN, which represents 63% of P_{max} for the beam with vertical web reinforcement (MS1-2). After that point, the influence of web reinforcement is noticeable. Specimen MS1-2 continued to resist significant additional load with similar stiffness. A flexural failure eventually occurred at P_{max} of 2142 kN. There was considerable additional deflection prior to failure. For Specimen MW1-2, the slope of the load-deflection curve, started to change at the load of 1350 kN, and only moderate further increase in load capacity was observed. Due to the lack of web reinforcement to control cracking, diagonal strut cracks in specimen MW1-2 increased suddenly and brittle failure occurred.

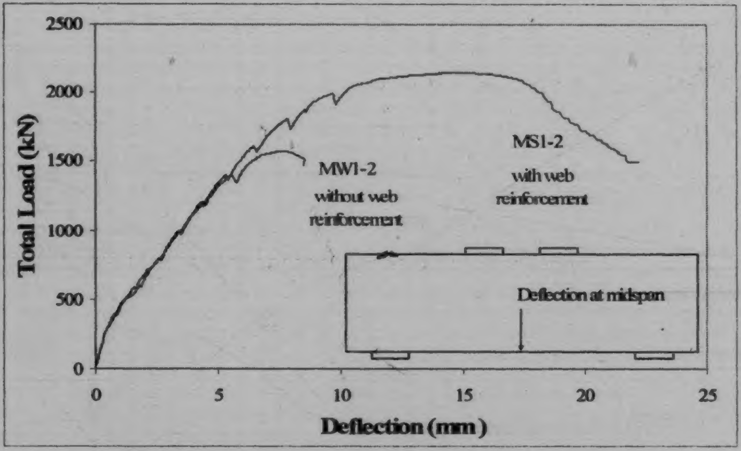

Figure 5-24 Load-deflection response for specimens MS1-2 and MW1-2

Deflections at maximum loads and at common serviceability limits are shown in Table 5-17. At P_{max}, the deflection corresponded to $l/114$ and $l/226$ for specimens MS1-2 and MW1-2, respectively.

Table 5-17 Deflections and P_{max} for specimens MS1-2 and MW1-2

Specimen	a/d	ρ (%)	P_{max} (kN)	Δ @ P_{max}* at midspan (mm)	load at deflection (kN)		% P_{max}	
					$l/180$	$l/360$	$l/180$	$l/360$
MS1-2	1.19	1.13	2142	14.90	1978	1278	92.3	59.7
MW1-2	1.19	1.13	1568	7.50	N/A	1251	N/A	79.8

*Deflection at the maximum load reached by the specimen

Figure 5-25 illustrates the load-strain response of the lowest layer of the main tension reinforcement at mid-span. While specimen MS1-2 developed strains in the main tension reinforcement larger than the effective yield strains at failure, specimen MW1-2 developed only 74% of the effective yield strain. Note that 74% of the effective yield strain corresponded to a stress level (750 MPa) higher than the permitted design stress in current design codes (e.g., ACI 318-05, CSA A23.3-04, Eurocode 2). Strains for given magnitudes of applied loads were similar for both specimens prior to failure of specimen MW1-2, indicating that the presence of web reinforcement did not create significant difference in strength demand in the main tension reinforcement at mid-span.

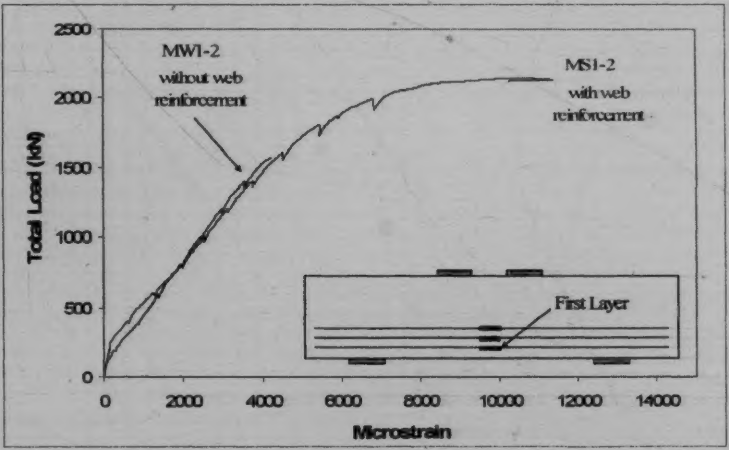

Figure 5-25 Load-strain response for the first layer of the main tension reinforcement

Strain distributions along the lowest layer of the main longitudinal reinforcement at a similar load stage (1400 kN) and at 90% of P_{max} (1900 kN for specimen MS1-2 and 1400 kN for specimen MW1-2) are shown in Figure 5-26. At the same stage of loading (1400 kN), the strains along the reinforcing bar were similar for both specimens, but the strains near the edge of the support plate were slightly smaller for the specimen with web reinforcement.

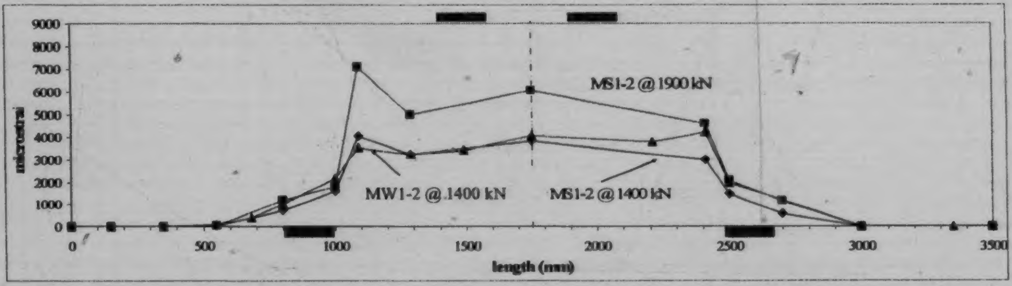

Figure 5-26 Strain distribution along the bottom reinforcing bars for specimens MS1-2 and MW1-2

Figure 5-27 and Figure 5-28 show the crack patterns for specimens MS1-2 and MW1-2, respectively, at several loading stages. Even though the locations of flexural cracks were different for the two specimens, the spacing between these cracks along the longitudinal axis remained at approximately 200 mm for both cases. The diagonal strut crack development was similar for both specimens, but the rate of crack width increase was larger for specimen MW1-2 than for specimen MS1-2. The loading corresponding to initial formation of flexural cracks were similar. Table 5-18 shows the load at the first flexural and strut cracks and the percentage of P_{max} when these cracks occurred

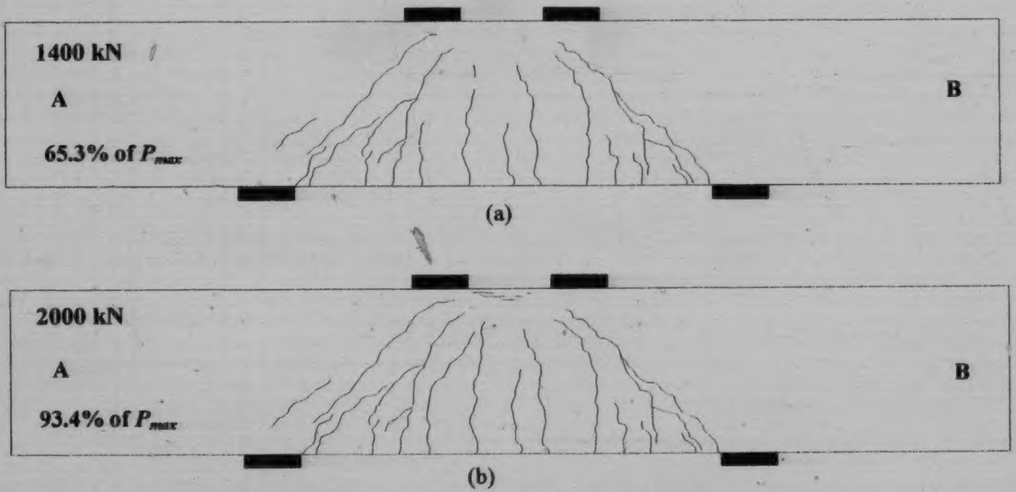

Figure 5-27 Crack development of MS1-2 at (a) 1400 kN and (b) 2000 kN

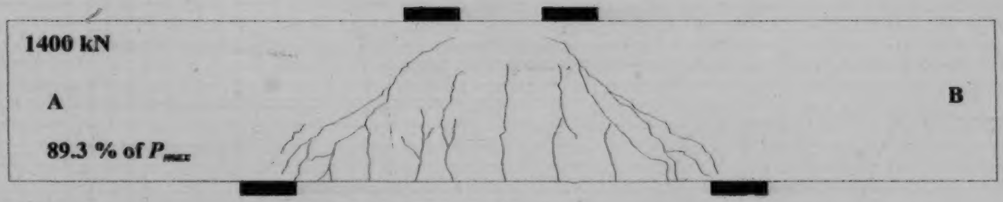

Figure 5-28 Crack development and crack width of MW1-2 at 1400 kN

Table 5-18 Load at first flexural and strut cracks and percentage of P_{max} at the occurrence of the cracks for specimens MS1-2 and MW1-2

Specimen	*a/d*	P_{max} *(kN)*	First flexural crack		First Strut crack at side A		First Strut crack at side B	
			P *(kN)*	% of P_{max}	P *(kN)*	% of P_{max}	P *(kN)*	% of P_{max}
MS1-2	1.19	2142	271	12.6	410	19.1	456	21.3
MW1-2	1.19	1568	257	16.4	393	25.1	450	28.7

5.3.2 Specimens MS3-2 and MW3-2

Table 5-19 shows vertical web reinforcement arrangement, maximum load reached during the test, deflection at maximum load and the secant stiffness of the beams at 60% of P_{max}.

Table 5-19 Comparison of specimens MS3-2 and MW3-2

Specimen	ρ *(%)*	*a/d*	vertical web reinforcement	f'_c *(MPa)*	Mode of failure	P_{max} *(kN)*	Deflection at midspan for P_{max} *(mm)*	Stiffness at 60%P_{max} (kN/mm)
MS3-2	1.13	2.38	10M@150mm	48	Flexure	1154	35.06	118
MW3-2	1.13	2.38	-	43	Strut	411	9.08	79

The use of vertical web reinforcement in MS3-2 increased the overall strength of the specimen by 280% in comparison to specimen MW3-2. Both specimens were reinforced with ρ of 1.13 % and had the same shear span to depth ratio of 2.38. Prior to reaching P_{max}, crushing of the top horizontal strut of specimen MS3-2 was observed and strains exceeding the effective yield strain were measured in the main tension reinforcement. On the other hand, specimen MW3-2 failed in a brittle manner due to splitting of the diagonal strut and no yielding in the main tension reinforcement was detected.

The load-deflection response of the specimens is illustrated in Figure 5-29. As shown in the figure, there was no influence on load-deflection response due to the presence of the web reinforcement up to an applied load of 350 kN. This load level represents a magnitude 29% of P_{max} for the specimen with vertical web reinforcement (MS3-2). Up to that point, the load-deflection curves were similar. However, after the load of 350 kN, the influence of web reinforcement is noticeable. Specimen MS3-2 continued to resist significant additional load with similar stiffness. A flexural failure eventually occurred at P_{max} of 1154 kN. There was considerable additional deflection prior to failure. For Specimen MW3-2, the slope of the load-deflection curve suddenly changed at the load level of 350 kN, when the load dropped. After that drop in applied load, moderate increase in load capacity was observed prior to the next drop in load. Finally, after additional displacement was applied, specimen MW3-2 reached the maximum load governed by splitting of the diagonal strut.

Deflections corresponding to maximum loads and at common serviceability limits are shown in Table 5-20. At P_{max}, the midspan deflection corresponded to *l/82* and *l/*253 for specimens MS3-2 and MW3-2, respectively.

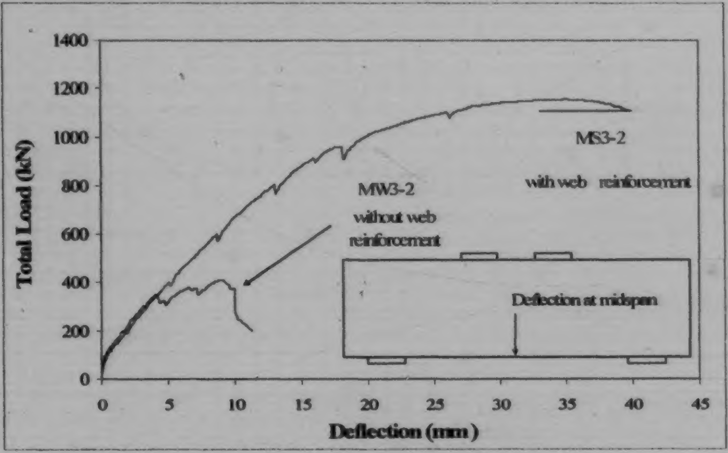

Figure 5-29 Load-deflection response for specimens MS3-2 and MW3-2

Table 5-20 Deflections and P_{max} for specimens MS3-2 and MW3-2

Specimen	a/d	P_{max} *(kN)*	Δ @ P_{max} at midspan *(mm)*	load at deflection *(kN)*		% P_{max}	
				l/180	*l/360*	*l/180*	*l/360*
MS3-2	2.38	1154	35.06	896	564	79.5	50.0
MW3-2	2.38	411	9.08	N/A	389	N/A	94.6

Figure 5-30 illustrates the load-strain response of the lowest layer of the main tension reinforcement at mid-span. While specimen MS3-2 developed strains in the main tension reinforcement larger than the effective yield strain, specimen MW3-2 developed strains of only 32% of the effective yield strain, which corresponded to the yielding strain of normal strength reinforcement (0.002 mm/mm). As it was observed for specimens MS1-2 and MW1-2 (see Section 5.3.1), the strains at midspan were similar for given load levels prior to the failure of the specimen without web reinforcement (MW3-2). The small differences in strain may have resulted from the proximity of cracks to the strain gauge locations.

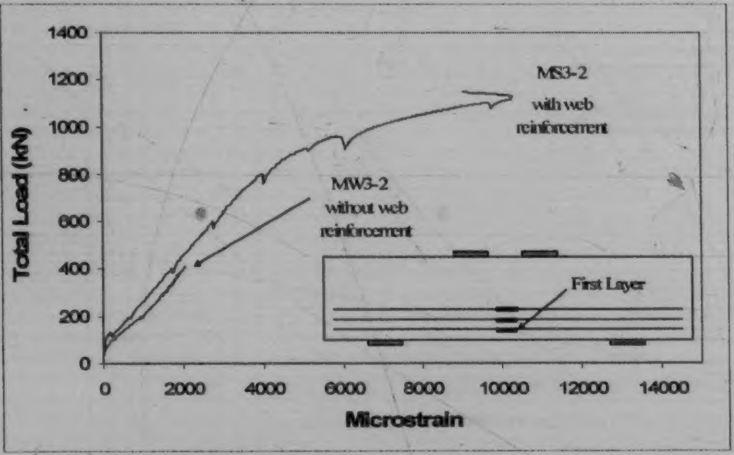

Figure 5-30 Load-strain response for the first layer of the main tension reinforcement

The strain distribution in the lowest layer of the main longitudinal reinforcement at 350 kN for both specimens and at 90% of P_{max} for specimen MS3-2 are shown in Figure 5-31. At the same stage of loading (350 kN), the strains along the reinforcing bar were similar for both specimens. The shape of the distribution for loading stages close to P_{max} remained similar to the shape in the early load stages for specimen MS3-2. The shape of strain distribution along the bottom rebar of specimens with a/d=2.4 was different than the strain distribution in the same bar for specimens with *a/d*=1.2, studied in section 5.3.1. There was more variation in strain magnitude between the midspan and support locations as *a/d* increased.

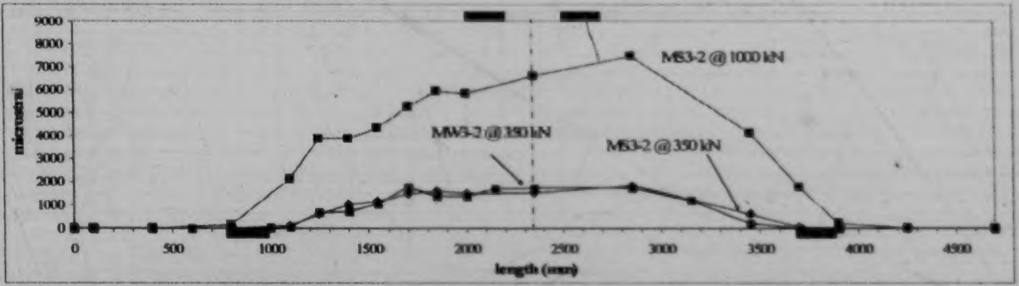

Figure 5-31 Strain distribution along the bottom bar at approximately 90 % of P_{max} for specimens MS3-2 and MW3-2 and at 350 kN for specimen MS3-2.

Figure 5-32 and Figure 5-33 show the crack patterns for specimens MS3-2 and MW3-2, respectively. Even though approximately the same number of main flexural and flexural shear cracks developed in both specimens at similar load levels, the crack behavior was different. In specimen MW3-2, the diagonal strut cracks developed toward the compression zone between loading plates (see Figure 5-33). For specimen MS3-2 (see Figure 5-32), some of the diagonal strut cracks developed toward zones outside of the loading plates. Small cracks, additional to the main cracks, developed in specimen MS3-2 at higher load levels but these small cracks were not observed in specimen MW3-2. Near failure, a strut crack was developed in specimen MW3-2 forming a gradual curve and reaching the compression zone very quickly.

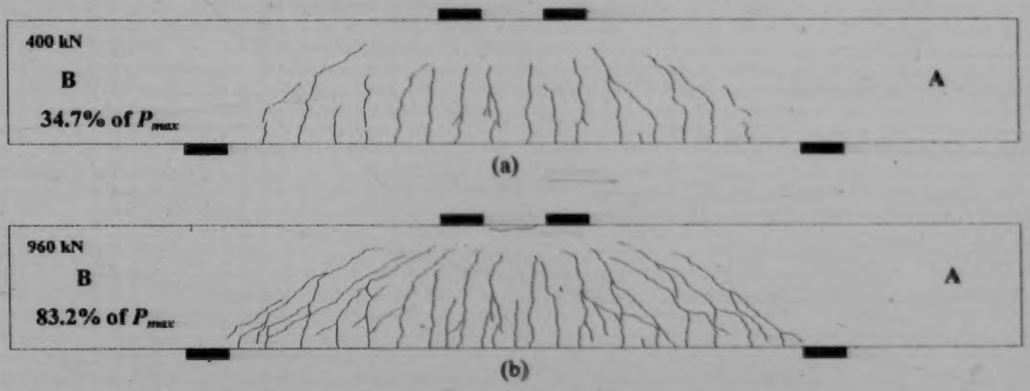

Figure 5-32 Crack development of specimen MS3-2 at (a) 400 kN and (b) 960 kN

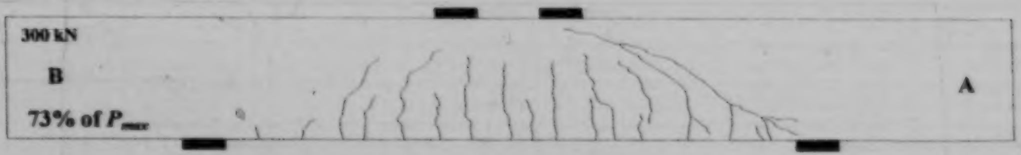

Figure 5-33 Crack development of specimen MW3-2 at 300 kN

Table 5-21 shows the loads corresponding to formation of the first flexural cracks and diagonal strut cracks and the equivalent percentage of P_{max}. The first flexural crack and diagonal strut cracks occurred at similar loads for both specimens.

Table 5-21 Load at first flexural and strut cracks and percentage of P_{max} at the occurrence of the cracks

Specimen	P_{max} (kN)	a/d	First flexural crack		First Strut crack at side A		First Strut crack at side B	
			P (kN)	% of P_{max}	P (kN)	% of P_{max}	P (kN)	% of P_{max}
MS3-2	1154	2.38	130	11.3	258	22.4	298	25.8
MW3-2	411	2.38	99	24.1	247	60.1	283	68.8

5.4 Summary

This chapter evaluated the influence of shear span to depth ratios, main longitudinal reinforcement ratio and web reinforcement in the performance of deep beams longitudinally reinforced with ASTM A1035 steel.

A comparison was made between members with similar geometry and/or reinforcement details for members with web reinforcement. The maximum load capacity of deep beams reinforced with ASTM A1035 reinforcing steel increased for smaller *a/d* ratios. For members having the same *a/d* ratio, the capacity increased as the reinforcement ratio ρ increased. For smaller *a/d* ratios and same reinforcement ratios, ρ, the member stiffness was observed to increase and smaller deflections occurred at the maximum applied force. Deflection ductility (μ) increased for larger *a/d* ratios and same reinforcement ratios, ρ. For larger values of ρ and same *a/d* ratio the stiffness of the beams increased and the ductility decreased. Crack patterns changed for specimens with same ρ and different *a/d* ratios. No significant influence in crack patterns was observed for different ρ. Crack patterns indicated that for specimens with *a/d* ratios of 2.4, no struts were formed directly from the loading points to the supports.

For members without web reinforcement, a comparison of behaviour was completed for specimens with similar transversal dimensions but different *a/d*. For these specimens without web reinforcement, the increment in *a/d* from 1.19 to 2.38 reduced the maximum force capacity by 73.7%. The secant stiffness at 60% of P_{max}, was reduced by 67.3% from specimen MW1-2 to specimen MW3-2.

For members with or without web reinforcement, it was observed that the shape of the strain distribution along the bottom bar of the main tension reinforcement was influenced by the *a/d* ratio. There was no influence on this distribution from ρ.

Specimens with web reinforcement behaved differently than specimens without web reinforcement. The inclusion of the web reinforcement increased the overall strength of the specimens; 37% for the specimen with a/d=1.2 and ρ of 1.13% and 280% for the specimen with a/d=2.4 and ρ of 1.13%. The deflection ductility also increased. The crack distribution was more symmetric for specimens with web reinforcement. The presence of web reinforcement did not create significant difference in demand in the main tension reinforcement at given load levels.

6. VALIDATION OF DESIGN CODE ANALYTICAL MODELS

6.1 General

In this chapter, the adequacy of existing code provisions for the design of reinforced concrete deep beams was studied for the case of members longitudinally reinforced with ASTM A1035 reinforcing steel. The effective yield strength of ASTM A1035 exceeds the maximum permitted design value for reinforcement strength according to the code provisions. In order to validate the design provisions for deep beams (i.e. Strut and Tie Method), comparisons were made between the maximum load achieved during the laboratory tests and the predicted capacity according to the different code provisions examined. The predicted failure loads were calculated using the Strut and Tie Method provisions according to three codes applicable for the design of building-type structures: ACI 318-05, CSA A23.3-04 and Eurocode2 (published as BS EN1992-1-1, 2004). For this purpose, the design codes were applied with relaxation of the maximum limits for reinforcement strength.

Two analysis models were used to predict the strength of the deep beam specimens using the Strut and Tie Method. These models were the Direct Strut and Tie Model (STM-D), described in Section 2.4.3.1, and the Combined Strut and Tie Model (STM-C), described in Section 2.4.3.3. In addition to these two Strut and Tie models for analysis, the specimen capacities were also evaluated using the traditional Sectional Method (Sectional Flexure Analysis and Sectional Shear Analysis) provisions from CSA A23.3-04 and ACI 318-05 as a comparison against the Strut and Tie Method. The Sectional Shear Analysis is generally viewed as a more appropriate analytical model if *a/d* > 2.5 (e.g, Kani et al, 1979), but the specific *a/d* limit to separate analysis model usage has not been previously validated for members with high strength longitudinal reinforcement.

All calculations using code provisions were completed with load and resistance factors of unity. Measured material properties as reported in Chapter 3 were utilized. Thus, calculations represent the actual predicted strength of the specimens according to the analytical models considered. Self weight of the specimens was ignored, but it represented a minor part of the final failure load.

For analysis, the specimens were divided into two groups: specimens with web reinforcement and specimens without web reinforcement. For each group, the predicted capacities using the traditional Sectional Method and the Strut and Tie Method provisions are compared against the measured capacities from the tests. Predicted failure modes, strains in the main tension reinforcement and the angle of principal strains in the shear span were also compared against the values obtained from the tests.

The analysis of the specimens using the traditional Sectional Method and Strut and Tie Method were carried out using a spreadsheet implementing an iterative solution process. With member dimensions, material properties and the analysis models defined, the load was gradually incremented until the first predicted failure mode was reached. The failure modes considered for the Strut and Tie Method analysis were "yielding" of the main tension reinforcement (centroid of main tension reinforcement), diagonal strut failure and node failure. The top horizontal strut was assumed to be at its limiting stress value. The "yielding" failure mode corresponded to predicted strains in the reinforcement equal to the effective yield strain. The failure modes considered for the Sectional Method analysis were established when the applied shear force on the cross-section reached the shear force capacity of the section according to the model or when the moment produced at midspan reached the moment capacity of the cross section. The moment capacity of specimens using the Sectional Method was obtained using the procedure described in Appendix B.

The Sectional Method, Direct Strut and Tie (STM-D) and Combined Strut and Tie (STM-D) analysis results are presented in Sections 6.2 to 6.4. The predicted loads shown in Table 6-1, Table 6-3 and Table 6-5 within these sections represent the predicted loads corresponding to reaching the first failure mode in the calculations, even when this mode was different from the failure mode observed during the test. A combined discussion of loads and failure mode predictions for each specimen are provided in Section 6.5.

For comparison between the predicted angles of the principal strains and the angles measured during the tests using the LVDT rosettes, load conditions 20% before the peak loads were selected. The selection of this load level prevented inclusion of potentially inaccurate average concrete strain measurements from LVDTs in the rosettes due to excessive specimen deformations during the final stages of loading. The LVDT rosette location was at mid-height of each specimen, along the line of action of the direct diagonal strut between the load and support. This is approximately the same line of action of the direct diagonal strut in the STM-D model, with minor variation due to the exact nodal coordinates of the truss model at failure.

6.2 Sectional Method

The predicted capacities of the specimens were determined using the Sectional Method provisions for slender beams in CSA A23.3-04 and ACI 318-05 (see Appendix B). In general, the predicted capacities of the specimens obtained by this method were significantly lower than the measured capacities (see Table 6-1).

Table 6-1 shows the ratio of maximum total load at test to predicted failure (P_{max}/P_{pv}) for the specimens using the Sectional Shear Method. The mean P_{max}/P_{pv} ratios for all of the specimens were 2.22 and 2.29 for CSA A23.3-04 and ACI 318-05 respectively, indicating that the code provisions predicted significantly lower capacities than the ones achieved during the test when applied to the specimen configurations in this study. The high coefficient of variation (44.2% and 44.8% for CSA A23.3-04 and ACI 318-05 respectively) indicate that the models do not adequately capture all significant design parameters, leading to very large scatter of test prediction quality. The best predictions using the Sectional Shear Analysis Method for specimens with ASTM A1035 reinforcing steel were for specimens MS3-2 and MW3-2, for both CSA A23.3-04 and ACI 318-05 codes. According to ACI 318-05, specimens MS3-2 and MW3-2, each with a/d=2.38, would not be considered as deep beams since $a/d > 2$. For these reason, the sectional method was considered an adequate method of design for these two specimens. A more detailed study of these predictions for each specimen is presented in Section 6.5.

Table 6-2 shows the maximum total load at test to predicted failure load ratio (P_{max}/P_{pm}) for the specimens using the Sectional Flexure Analysis Method. The ratios for specimens that suffered diagonal strut failure were omitted from this table (specimens MS1-3, MW1-2 and MW3-2). The mean P_{max}/P_{pm} ratios for all of the specimens considered in this table were 1.04 and 1.06 for CSA A23.3-04 and ACI 318-05 codes provisions, with a smaller coefficient of variation for predictions using CSA A23.3-04 provisions (see Table 6-2). These results indicate that flexural capacity of deep beams reinforced with high strength reinforcing steel can be accurately predicted.

Table 6-1 Failure load at test and predicted loads using Sectional Shear Analysis

Beam	a/d	ρ (%)	P_{max} (kN)	Sectional Shear Analysis			
				CSA A23.3-04		ACI 318-05	
				$P_{pv(CSA)}$ (kN)	$P_{max}/P_{pv(CSA)}$	$P_{p(ACI)}$ (kN)	$P_{max}/P_{pv(ACI)}$
MS1-1	1.19	0.52	1252	596	2.10	750	1.67
MS1-2	1.19	1.13	2142	772	2.77	764	2.80
MS1-3	1.18	2.29	2747	942	2.92	830	3.31
MS2-2	1.79	1.13	1432	786	1.82	768	1.86
MS2-3	1.78	2.29	2055	936	2.20	790	2.60
MS3-2	2.38	1.13	1154	828	1.39	896	1.29
NS1-4	1.18	1.77	1567	806	1.94	720	2.18
NS2-4	1.80	1.77	1065	816	1.31	702	1.52
MW1-2	1.19	1.13	1568	350	4.48	352	4.45
MW3-2	2.38	1.13	411	332	1.24	342	1.20
Mean					2.22		2.29
COV					0.442		0.448

Table 6-2 Failure load at test and predicted loads using Sectional Flexural Analysis

Beam	a/d	ρ (%)	P_{max} (kN)	Sectional Flexure Analysis			
				CSA A23.3-04		ACI 318-05	
				$P_{pm(CSA)}$ (kN)	$P_{max}/P_{pm(CSA)}$	$P_{pm(ACI)}$ (kN)	$P_{max}/P_{pm(ACI)}$
MS1-1	1.19	0.52	1252	1220	1.03	1214	1.03
MS1-2	1.19	1.13	2142	2127	1.01	2026	1.06
MS1-3	1.18	2.29	2747	-	-	-	-
MS2-2	1.79	1.13	1432	1457	0.98	1382	1.04
MS2-3	1.78	2.29	2055	1912	1.07	1823	1.13
MS3-2	2.38	1.13	1154	1095	1.05	1039	1.11
NS1-4	1.18	1.77	1567	1489	1.05	1503	1.04
NS2-4	1.80	1.77	1065	997	1.07	1016	1.05
MW1-2	1.19	1.13	1568	-	-	-	-
MW3-2	2.38	1.13	411	-	-	-	-
Mean					1.04		1.06
COV					0.033		0.036

6.3 Direct Strut and Tie Model (STM-D)

As described in Section 2.4.1.4 of Chapter 2, the strength of the overall system depends on the direct diagonal strut developed between the loading points and the supports, and a tension tie between the supports. To take into consideration the compression capacity of the struts within the overall truss model used, CSA A23.3-04, ACI318-05 and Eurocode 2 each assign different stress reduction factors for specific conditions of strut geometry or other model characteristics. These were presented in Section 2.5 of Chapter 2. Figure 6-1 shows the direct strut model (STM-D) used to analyze the specimens.

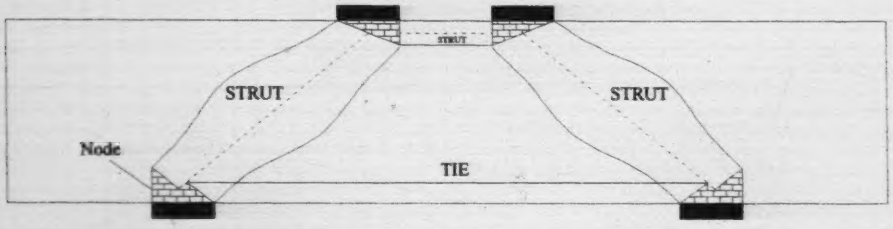

Figure 6-1 Direct Strut and Tie Model

For STM-D, the failure modes considered in the analysis were yielding of the main longitudinal reinforcement (at the centroid of main longitudinal reinforcement location), diagonal strut failure and node failure. Since the high strength reinforcement (ASTM A1035) does not have a well defined yielding point, the 'yielding' condition was established based on the effective yield strength according to the 0.2% offset method and given in Table 3.1. To determine the geometry of the Direct Strut-and-Tie Model, the horizontal prismatic top strut was considered to be at its strength limit of $0.85\Phi_c f'_c$ for CSA A23.3-04, $\Phi_{STM}0.85\beta_s f'_c$ with β_s=1.0 for ACI 318-05 and νf_{cd} for Eurocode 2. Φ_c and Φ_{STM} were taken as unity. For a given applied load, a spreadsheet was used to calculate the height of the horizontal top strut needed to resist the force given by the bending moment at mid-span. Once this height was obtained, the forces and/or dimensions of the tie, nodes and diagonal struts were calculated.

During the analysis of the specimens using ACI 318-05 provisions, diagonal struts were considered as bottle shaped struts with β_s=0.75. In the analysis of struts, Equations

(2.1) and (2.14) were used to calculate the strength of the diagonal struts for CSA A23.3-04 and Eurocode 2 capacity predictions.

For specimens with ASTM A1035 reinforcing steel as the main longitudinal reinforcement, Equations (3.1) to (3.3) were used to model the non-linear stress-strain response of the reinforcement up to values of f_u when necessary (i.e. tension failure of specimen MS1-1). Tension failure of specimen MS1-1 occurred when the main longitudinal reinforcement reached the strain corresponding to f_u (see Table 3.4).

In calculations for diagonal strut capacity according to the CSA A23.3-04 provisions, the maximum strut strength was obtained using the parameter ε_s, which is a measure of the tie strain in the region of the diagonal strut (see Equation (2.2)). The tie strain was determined from the corresponding stress level using Equations (3.1) to (3.3) when ASTM A1035 reinforcing steel was used. For Grade 400R steel, a constant Young's modulus of E_s = 200,000 MPa was assumed. At the supports, it is recognized that for the specimen configurations studied, the tie would be anchored at the outside edge of the support, with an increase in strain in the tie across the nodal region. Two methods were used to determine ε_s. In the first case, the value of ε_s was determined from Equation (3.1) to (3.3) when ASTM A1035 reinforcing steel was used, by assuming that the tie strain was constant across the node, with a value equal to the tie strain determined by the tie force to the interior of the nodal region. In the second case, the value of ε_s was taken as one-half of the value from the first case, by considering that the tie strain parameter in Equation (2.2) should approximate the average strain near the center of the node. The assumption of the second case has been used previously in design examples published by the Cement Association of Canada (Concrete Design Handbook, 2004). In this project, the approximate average strain in the tie near the center of the node for the second case is denoted as ε_{as}.

The failure loads and corresponding predicted capacities for diagonal splitting strut and flexural failure modes for each specimen were analyzed. Thus, two test-to-predicted load ratios were completed using each code method. P_{max}/P_p represents the ratio between P_{max} and the lowest predicted capacity of all modes considered. P_f/P_c represents the ratio between the measured load corresponding to the first failure mode reached during the test (i.e. "yielding" of main tension reinforcement, crushing of strut between loading plates or splitting of the diagonal strut) and the predicted load for the same mode. Additional subscripts are used with these ratios to differentiate between each set of code provisions.

Table 6-3 shows the ratio between P_{max} and the lowest predicted capacity of all modes considered (P_{max}/P_p) for all specimens using STM-D. From this table, the mean P_{max}/P_p values for the CSA A23.3-04 were 1.63 and 1.44 using the approach with nodal tie strains of ε_s and ε_{as} respectively. There was a slightly higher coefficient of variation for the predictions using nodal tie strains of ε_s. These results show that predictions using ε_{as} provide better estimates of capacity for the configuration studied. The mean value for P_{max}/P_p ratio using the ACI 318-05 code provisions was 1.09 with a coefficient of variation of 0.195. This average includes the specimens MW1-2 and MW3-2, since the ACI 318-05 code is the only design standard considered in the current study that allows the use of deep beams that do not contain distributed web reinforcement. The ACI 318-05 model provided an accurate prediction of the capacity of MW1-2. While the capacity of MW3-3 was overestimated by the ACI318-05 model, this specimen would not typically be analyzed using the Strut and Tie Method according to the ACI 318-05 code provisions because the angle developed between the diagonal strut and the tie was smaller than 25°. Eliminating the predictions for specimens with $a/d>2$, the mean P_{max}/P_p ratio changes from 1.09 to 1.16 and a COV of 0.111 was calculated. The mean P_{max}/P_p ratio using the Eurocode 2 model was 1.59, with a coefficient of variation of 0.170. Of the three codes, the best predictions of the specimens in Table 6-3 were obtained using the ACI 318-05 code.

Table 6-4 shows the ratio between the measured load corresponding to the first failure mode reached during the test and the predicted load for the same mode (P_f/P_c) for all specimens using STM-D. From this table, the mean P_f/P_c value for the CSA A23.3-04 provisions was 1.02 and 1.00 using the approach with tie strains in the nodal region of ε_s and ε_{as} respectively. The two mean values were very similar because only specimen MS1-3 had different P_f/P_c ratios for the cases with nodal tie strains of ε_s and ε_{as} according to the CSA A23.3-04 provisions. This occurred since failures by yielding of the main tension reinforcement were predicted for the other specimens, which would be unaffected by the choice of nodal tie strains of ε_s or ε_{as}. The mean value for P_f/P_c ratio using the ACI 318-05 code provisions was 0.96 with a coefficient of variation of 0.172. Eliminating the predictions for specimens with a/d>2, the mean changes from 0.96 to 1.01, with a coefficient of variation of 0.111. The mean P_f/P_c ratio using the Eurocode 2 model was 1.06, with a coefficient of variation of 0.273.

Table 6-3 Maximum applied load versus predicted load (P_{max}/P_p) using STM-D

Beam	a/d	ρ (%)	P_{max} (kN)	STM –D							
				CSA A23.3-04 (ε_s)		CSA A23.3-04 (ε_{as})		ACI 318-05		Eurocode 2	
				P_p (CSA) (kN)	P_{max}/P_p (CSA)	P_p (CSA) (kN)	P_{max}/P_p (CSA)	P_p (ACI) (kN)	P_{max}/P_p (ACI)	P_p (EN) (kN)	P_{max}/P_p (EN)
MS1-1	1.19	0.52	1252	1024	1.22	1024	1.22	1024	1.22	1020	1.23
MS1-2	1.19	1.13	2142	1598	1.34	1866	1.15	2160	0.99	1546	1.39
MS1-3	1.18	2.29	2747	1930	1.42	2212	1.24	2296	1.20	1558	1.76
MS2-2	1.79	1.13	1432	900	1.59	1056	1.36	1454	0.98	1080	1.33
MS2-3	1.78	2.29	2055	980	2.10	1114	1.84	1560	1.32	1006	2.04
MS3-2	2.38	1.13	1154	530	2.18	626	1.84	1092	1.06	748	1.54
NS1-4	1.18	1.77	1567	1100	1.42	1230	1.27	1198	1.31	896	1.75
NS2-4	1.80	1.77	1065	602	1.77	672	1.58	906	1.18	632	1.69
MW1-2	1.19	1.13	1568					1414	1.11		
MW3-2	2.38	1.13	411					700	0.59		
Mean					1.63		1.44		1.09		1.59
COV					0.217		0.195		0.195		0.170

Table 6-4 First measured failure load versus predicted load (P_f/P_c) using STM-D

Beam	P_{max}	P at effective yielding (kN)	observed failure mode*	P_f (kN)	STM-D							
					CSA A23.3-04 (ε_s)		CSA A23.3-04 (ε_{as})		ACI 318-05		Eurocode 2	
					P_c (CSA) (kN)	P_f/P_c (CSA)	P_c (CSA) (kN)	P_f/P_c (CSA)	P_c (ACI) (kN)	P_f/P_c (ACI)	P_c (EN) (kN)	P_f/P_c (EN)
MS1-1	1252	1082	F	1082	1024	1.06	1024	1.06	1024	1.06	1020	1.06
MS1-2	2142	2124	F	2124	2158	0.98	2158	0.98	2158	0.98	2148	0.99
MS1-3	2747	-	DS	2747	1930	1.42	2212	1.24	2296	1.20	1558	1.76
MS2-2	1432	1381	F	1381	1454	0.95	1454	0.95	1454	0.95	1444	0.96
MS2-3	2055	-	TS-DS	2055	1912	1.07	1912	1.07	1978	1.04	1952	1.05
MS3-2	1154	1031	F	1031	1092	0.94	1092	0.94	1092	0.94	1084	0.95
NS1-4	1567	1323	F	1323	1496	0.88	1496	0.88	1496	0.88	1518	0.87
NS2-4	1065	892	F	892	1012	0.88	1012	0.88	1012	0.88	1024	0.87
MW1-2	1568	-	DS	1568					1414	1.11		
MW3-2	411	-	DS	411					700	0.59		
Mean						1.02		1.00		0.96		1.06
COV						0.172		0.120		0.172		0.273

* F =Flexure, DS=splitting of diagonal strut and TS =crushing of top strut between loading points

From Table 6-3 and Table 6-4, it is observed that the diagonal strut capacity is safely predicted by all three codes. However, the predicted load corresponding to the effective stress in the main tension reinforcement was slightly higher than the test values for specimens MS1-2, MS2-2 and MS3-2, which were all reinforced with high strength steel. Also, higher loads at yielding of the main longitudinal reinforcement were predicted for specimens NS1-4 and NS2-4 reinforced longitudinally with Grade 400R steel. The ACI 318-05 code provisions correctly predicted all failure modes except for specimens MS2-3, NS1-4 and NS2-4. On the other hand, CSA A23.3-04 and Eurocode 2 only correctly predicted the modes of failure for MS1-1 and MS1-3.

6.4 Combined strut and tie Model (STM-C)

In the Combined Strut and Tie Model described in Section 2.4.1.6 of Chapter 2, the strength of the specimens comes from the combination of a truss developed to use the indirect force flow path through the vertical web reinforcement and from direct diagonal struts going from the loading points to the supports. Figure 6-2 illustrates the Combined Strut and Tie Model used for the analysis of the specimens.

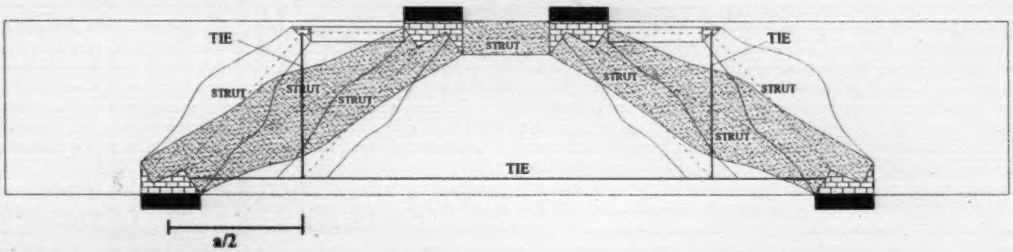

Figure 6-2 Combined Strut and Tie Method

During the design of deep beams, reinforcement in the form of vertical ties can be placed to carry load in an indirect path and thereby contribute towards the total strength of the system. For the deep beams used in this project, web reinforcement consistent with minimum code requirements for distributed reinforcement was provided. During initial specimen design, only a small load was assumed to be carried by the stirrups. For post-test analysis, the force carried by the vertical tie was assumed to be equal to the force needed to reach the yielding stress of the vertical reinforcement (405 MPa). Strain hardening in the vertical ties was ignored. Since multiple stirrup legs exist between the load and the support, these were considered by placing the force equivalent of two stirrups for specimens with *a/d* of 1.2, three stirrups for specimens with *a/d* of 1.8 and five stirrups for specimens with *a/d* of 2.4 in a truss position mid-way between the load and support (see Figure 6-2)

Note that in the truss model shown in Figure 6-2, there are regions where overlapping struts are present. This overlapping of the struts must be checked to ensure that the combined stress condition in the concrete does not exceed the limiting concrete compressive strength. Clause RA.2.3 in the Commentary of ACI 318-05 suggests that a resultant load could be considered in the overlapping region, to verify the strength of the struts and nodes. This approach was also used for analysis by the CSA A23.3-04 and Eurocode2 provisions as well as for ACI318-05, since no guidelines are provided in the former two documents.

Table 6-5 shows a comparison between the failure loads from the tests and the predicted loads using the Combined Strut and Tie Model (STM-C). Only members with vertical web reinforcement are consistent with the model, so specimens MW1-1 and MW1-3 are excluded from this analysis. The predicted loads were determined using the three design codes. The failure loads during tests (P_{max}) were obtained from the maximum load recorded by the load cells.

The only code that gave different results than analysis according to the STM-D model (see Section 6.3) was the CSA A23.3-04 code. The STM-C model considers the reduction in the strain of the main tension steel between the midpoint of shear span and the support due to the effect of the compression strut that goes from the loading plate to the mid-point of the shear span. This reduction in tie strain in the support nodal region (i.e. ε_s or ε_{as}) contributes to the increase in strength of the direct strut going from the loading points to the supports when using CSA A23.3-04 provisions, thereby altering the predicted capacity. The ACI 318-05 and Eurocode 2 code provisions gave the same predicted loads for the STM-C model as the STM-D model since the reduction in the strain of the main tension steel in the support nodal zone due to the development of an indirect strut is not taken into consideration for these code provisions. For this reason, for a beam reinforced with minimum web reinforcement, the STM-D model is easier and more practical for the analysis of deep beams using ACI 318-05 and Eurocode 2. If the failure prediction is by yielding of the main tension reinforcement, the results using STM-D and STM-C are the same for each code considered since a constant quantity of reinforcement was provided along the entire span. However, if the failure prediction is by diagonal strut failure, the change in strain of the reinforcement may give different results between the STM-D and STM-C only for CSA A23.3-04.

From Table 6-5, the mean P_{max}/P_p value for CSA A23.3-04 was 1.23 and 1.14 using the approach with ε_s and ε_{as} respectively. The predictions using STM-C for CSA A23.3-04 were more accurate than predictions using STM-D for the same code reported in Section 6.3. The P_{max}/P_p ratios using the ACI 318-05 and Eurocode 2 code provisions remained similar as predictions using STM-D. However, the mean value for P_{max}/P_p ratio using the ACI 318-05 in Table 6-4 is different from the ratio in Table 6-3 because specimens without web reinforcement were not considered in Table 6-5.

Table 6-5 Maximum applied load at test versus predicted load (P_{max}/P_p) using STM-C

Beam	a/d	ρ (%)	P_{max} (kN)	STM-C							
				CSA A23.3-04 (ε_s)		CSA A23.3-04 (ε_{as})		ACI 318-05		Eurocode 2	
				P_p (CSA) (kN)	P_{max}/P_p (CSA)	P_p (CSA) (kN)	P_{max}/P_p (CSA)	P_p (ACI) (kN)	P_{max}/P_p (ACI)	P_p (EN) (kN)	P_{max}/P_p (EN)
MS1-1	1.19	0.52	1252	1024	1.22	1024	1.22	1024	1.22	1020	1.23
MS1-2	1.19	1.13	2142	1786	1.20	2048	1.05	2160	0.99	1546	1.39
MS1-3	1.18	2.29	2747	2122	1.29	2400	1.14	2296	1.20	1558	1.76
MS2-2	1.79	1.13	1432	1232	1.16	1386	1.03	1454	0.98	1080	1.33
MS2-3	1.78	2.29	2055	1322	1.55	1456	1.41	1560	1.32	1006	2.04
MS3-2	2.38	1.13	1154	1092	1.06	1092	1.06	1092	1.06	748	1.54
NS1-4	1.18	1.77	1567	1286	1.22	1342	1.17	1198	1.31	896	1.75
NS2-4	1.80	1.77	1065	928	1.15	996	1.07	906	1.18	632	1.69
MW1-2	1.19	1.13	1568								
MW3-2	2.38	1.13	411								
Mean					1.23		1.14		1.16		1.59
CV					0.118		0.110		0.115		0.169

Table 6-6 shows the ratio between the measured load corresponding to the first failure mode reached during the test and the predicted load for the same mode (P_f/P_c) for all specimens using STM-C. From this table, the mean P_f/P_c value for the CSA A23.3-04 code provisions was 0.99 and 0.97 using the approach with for ε_s and ε_{as} respectively.

These results are very similar to Table 6-4 because the predicted capacities only changed for specimen MS1-3, as it was the only specimen that failed by diagonal strut failure. All other specimens failed by yielding of the main tension reinforcement or by crushing of the compression zone between the loading points. For these two modes of failure, STM-D and STM-C give the same results. Specimens MW1-2 and MW3-2 also failed by diagonal strut failure, but they can not be analyzed with CSA A23.3-04 since they do not contain web reinforcement.

Table 6-6 First measured failure load versus predicted load (P_f/P_c) for STM-C

Beam	P_{max}	P at effective yielding (kN)	observed failure mode*	P_f	STM-C							
					CSA A23.3-04 (ε_s)		CSA A23.3-04 (ε_{ss})		ACI 318-05		Eurocode 2	
					P_c (CSA)	P_f/P_c (CSA)	P_c (CSA)	P_f/P_c (CSA)	P_c (ACI)	P_f/P_c (ACI)	P_c (EN)	P_f/P_c (EN)
MS1-1	1252	1082	F	1082	1024	1.06	1024	1.06	1024	1.06	1020	1.06
MS1-2	2142	2124	F	2124	2158	0.98	2158	0.98	2158	0.98	2148	0.99
MS1-3	2747	-	DS	2747	2122	1.29	2400	1.14	2296	1.20	1558	1.76
MS2-2	1432	1381	F	1381	1454	0.95	1454	0.95	1454	0.95	1444	0.96
MS2-3	2055	-	TS-DS	2055	1912	1.07	1912	1.07	1978	1.04	1952	1.05
MS3-2	1154	1031	F	1031	1092	0.94	1092	0.94	1092	0.94	1084	0.95
NS1-4	1567	1323	F	1323	1496	0.88	1496	0.88	1496	0.88	1518	0.87
NS2-4	1065	892	F	892	1012	0.88	1012	0.88	1012	0.88	1024	0.87
MW1-2	1568	-	DS	1568								
MW3-2	411	-	DS	411								
Mean						1.01		0.97		0.99		1.06
CV						0.135		0.095		0.108		0.273

* F =Flexure, DS=splitting of diagonal strut and TS =crushing of top strut between loading points

6.5 Individual Analysis and discussion of specimens

6.5.1 Specimens with web reinforcement

6.5.1.1 Beam with ρ=0.52% and a/d=1.19

For specimen MS1-1, the total load capacity predicted using the **Sectional Method** was 596 kN for CSA A23.3-04 and 750 kN for ACI-318-05. Both codes predicted shear failure, however, flexural failure occurred at P_{max} =1252 kN. Analyzing this specimen with the **Sectional Flexure Analysis**, the flexural capacity was reached at a total applied load of 1220 kN and 1214 kN according to CSA A23.3-04 and ACI 318-05 provisions, giving test/predicted ratios (P_{max}/P_{pm}) of 1.03 for both CSA A23.3-04 and

ACI 318-05 codes. When the beam reached P_{max}, 110% and 67% more shear capacity that the values predicted using CSA A23.3-04 and ACI 318-05 respectively had been developed.

According to the **Direct Strut and Tie Model and Combined Strut and Tie Model** predictions, the main tension reinforcement should reach the effective yield strain before diagonal strut failure occurred. The predicted failure load according to the CSA-A23.3-04, ACI 318-05 and Eurocode 2 provisions was approximately 1023 kN based on the main tension reinforcement reaching the effective yield stress. Using the ASTM A1035 stress-strain relations (see Equation 3.1), a predicted total capacity of 1225 kN would apply for the case of tension rupture of the main reinforcement, at reinforcement stress of 1067 MPa. Yielding of the main tension reinforcement was not directly monitored during this test because the strain gauge located at the centroid of the reinforcement was damaged. Taking as reference the strain in the first and third layer of the main reinforcement, the strain at the centroid reached the effective yield strain at a total applied load of approximately 1082 kN. The maximum load reached during the test was 1252 kN. The predictions for yielding of main reinforcement were very accurate with a test/predicted (Pt/Pc) ratio of 1.06. For the maximum load, the test/predicted (P_{max}/P_p) ratio was 1.22.

The angle of principal compression strains on the concrete surface at the middle of the direct strut location were calculated at an applied load of 1000 kN (80%P_{max}), based on the LVDTs readings from the rosette. The angles measured to the principal compression direction from the horizontal axis, were 39.2° for shear span A and 42.5° for shear span B. The angle predicted for that load based on the geometry of the Direct Strut and Tie Model was 38.3°.

6.5.1.2 Beams with ρ=1.13% and different shear span

For a better understanding of the accuracy of the predictions using the STM-D and STM-C models, the results are illustrated in Figure 6-3. This figure shows the maximum load at test to predicted load ratios (P_{max}/P_p) for different a/d ratios and ρ=1.13% according to the different code provisions.

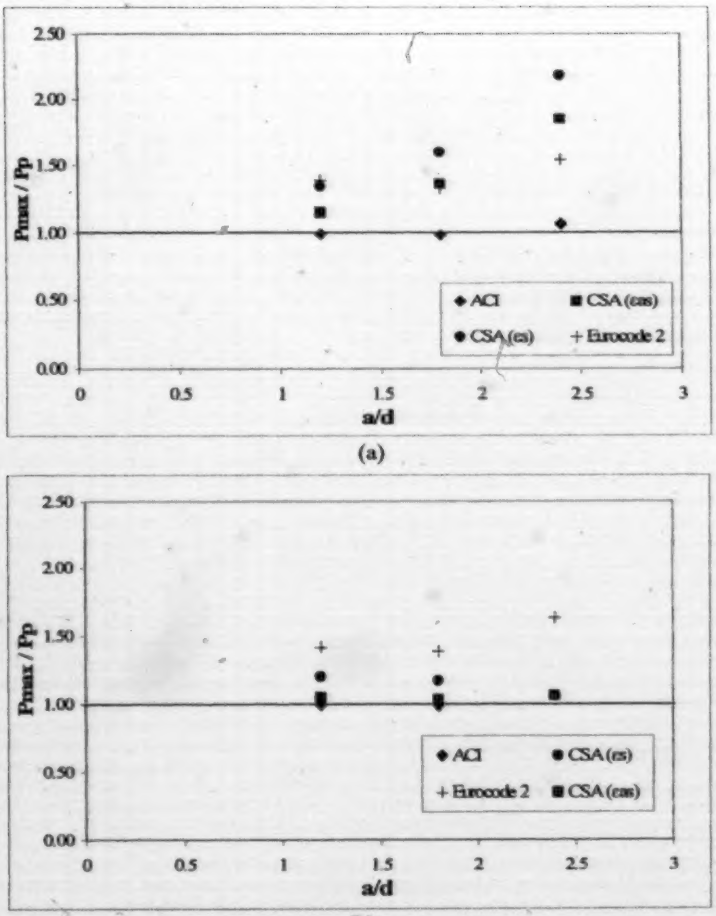

(a)

(b)

Figure 6-3 P_{max}/P_p for three different *a/d* and ρ=1.13% using (a) STM-D and (b) STM-C

Using the Direct Strut and Tie Model (STM-D) and CSA A23.3-04 provisions, the test to predicted capacity (P_{max}/P_p) ratio increases for higher *a/d* ratios, with all values above 1.0 for the specimens in this study. Eurocode 2 provisions gave test to predicted capacity (P_{max}/P_p) ratio values closer to 1.0 for *a/d*=1.8 than the values obtained for *a/d*=1.2 or 2.4. ACI 318-05 provisions with the STM-D model gave very good predictions of the failure load for the three different *a/d* ratios studied. Using the Combined Strut and Tie Model (STM-C), the test to predicted capacity ratios were closer to one for the three different *a/d* using CSA A23.3-04 using tie strains in the nodal region of ε_{as} compared to ε_s, as illustrated in Figure 6-3b. The same results were obtained for both the STM-D and STM-C models when using ACI 318-05 and Eurocode 2 provisions.

6.5.1.2.1 Specimen MS1-2

For specimen MS1-2, the total capacity predicted using the **Sectional Method** was 774 kN for CSA A23.3-04 and 764 kN for ACI 318-05. Both codes predicted shear failure, however, flexural failure occurred at P_{max} = 2142 kN. Analyzing this specimen with the **Sectional Flexure Analysis**, the flexure capacity was accurately predicted at 2127 kN and 2026 kN according to CSA A23.3-04 and ACI 318-05 provisions, giving test/predicted ratios (P_{max}/P_{pm}) of 1.01 and 1.06 for CSA A23.3-04 and ACI 318-05 codes.. When the specimen reached P_{max}, 177% and 180% more shear capacity than predicted using CSA A23.3-04 and ACI 318-05 sectional shear provisions respectively had been developed.

Using the **Direct Strut and Tie Model**, the predicted failure mode was diagonal strut failure for CSA A23.3-04 and Eurocode 2. ACI 318-05 predicted yielding of the main tension reinforcement prior to diagonal strut failure. According to the CSA A23.3-04 provisions, the predicted load for diagonal strut failure was 1598 kN using tie strains in the nodal region of ε_s and 1866 kN using ε_{as}. Eurocode 2 predicted failure of the diagonal strut at a load of 1546 kN. ACI 318-05 predicted yielding of the main tension reinforcement at a load of 2160 kN. If the strut stress limit was ignored during the analysis, the main tension reinforcement was predicted to reach the effective yield stress at 2160 kN according to CSA A23.3-04 and ACI 318-05 provisions, and at 2148 kN according to Eurocode 2 provisions. These predictions were 1.7% and 1.2% higher than the capacity obtained at test (2124 kN).

The angle of principal compression strains on the concrete surface at the middle of the direct strut location were calculated at an applied load of 1722 kN (80%P_{max}), based on the LVDTs readings from the rosette. The angles measured to the principal compression direction from the horizontal axis were 31.4° for shear span A and 31.8° for shear span B. The angle predicted for that load based on the geometry of the Direct Strut and Tie Model was 37.0°.

By analyzing the deep beams with the **Combined Strut and Tie Model (STM-C)**, more accurate predictions were obtained than for the STM-D model when using the CSA A23.3-04 code provisions. The predicted strength of the STM-C model using tie strains in the nodal region of ε_s, was 1786 kN and 2048 kN when using ε_{as}. These results gave P_{max}/P_p ratios of 1.20 and 1.05 respectively. Thus, the STM-C model predicted a failure load approximately 10% higher than the STM-D model according to CSA A23.3-04. This increment for the predicted failure load occurs because the strains in the support nodal region are smaller for STM-C than for STM-D.

6.5.1.2.2 Specimen MS2-2

For specimen MS2-2, the total load capacity predicted using the **Sectional Method** was 786 kN for CSA A23.3 and 768 kN for ACI 318-05. Both codes predicted shear failure, however, flexural failure occurred at P_{max} = 1432 kN. When the specimen reached P_{max}, 82% and 86% more shear capacity than predicted using CSA A23.3-04 and ACI 318-05 provisions respectively had been developed. Analyzing this specimen with the **Sectional Flexure Analysis**, the flexure capacity was reached at 1457 kN and 1382 kN according to CSA A23.3-04 and ACI 318-05 provisions. The flexural capacity predicted using the Sectional Flexure Analysis and CSA A23.3-04 provisions was 2% smaller than the capacity obtained at test. ACI 318-05 predicted 4% more capacity that the one obtained during the test.

Using the **Direct Strut and Tie Model**, the predicted failure total load according to the CSA A23.3 was 900 kN using tie strains in the nodal region of ε_s and 1056 kN using ε_{as}. The predicted failure mode was for CSA A23.3-04 code was diagonal strut failure. ACI 318-05 predicted flexural failure (yielding of main tension reinforcement) at a total load of 1454 kN. Eurocode 2 predicted a failure load of 1080 kN by diagonal strut failure. The only code that predicted a failure load higher than P_{max} was the ACI 318-05 code. The predicted load when the main tension reinforcement reached the effective yield strain were larger that the loads measured at yielding (5% more).

The angle of principal compression strains on the concrete surface at the middle of the direct strut location were calculated at an applied load of 1146 kN (80%P_{max}), based on the LVDTs readings from the rosette. The angles measured to the principal compression direction from the horizontal axis were 30.7° for shear span B. The angle predicted for that load based on the geometry of the Direct Strut and Tie Model was 26.8°. No data was obtained from the LVDTs rosettes for side A.

By analyzing the specimens with the **Combined Strut and Tie Model (STM-C)**, more accurate predictions were obtained than for the STM-D model when using the CSA A23.3 code provisions. The predicted strength of the STM-C model using tie strains in the nodal region of ε_s, was 1232 kN and 1386 kN when using ε_{as}. These results gave P_{max}/P_P ratios of 1.16 and 1.03 respectively. Thus, the STM-C model predicted a failure load approximately 37% and 31% higher than the STM-D model according to CSA A23.3-04. This increment for the predicted failure load occurs because the strains in the support nodal region are smaller for STM-C than for STM-D. The Combined Strut and Tie Model predictions were the same to the predictions obtained using Direct STM for the ACI 318-05 and Eurocode 2 codes, with 1454 kN and 1080 kN. The flexural capacities of the beams according to STM-C remained similar to those obtained using STM-D.

At P_{max}, the predicted strain in the main tension reinforcement at midspan was 0.006 according to the STM. The measured strain at P_{max} was 0.0086.

6.5.1.2.3 Specimen MS3-2

For specimen MS3-2, the total capacities predicted using the **Sectional Method** were 828 kN for CSA A23.3-04 and 896 kN for ACI 318-05. Even though the sectional method typically underestimates the failure load of deep beams, good predictions were obtained for this specimen since its *a/d* ratio of 2.38 is close to the limit of 2.5 for deep beams (see Section 2.3). Both codes predicted shear failure, however, flexural failure occurred at $P_{max} = 1154$ kN. When the specimen reached P_{max}, 39% and 29% more shear capacity than predicted using CSA A23.3-04 and ACI 318-05 provisions respectively had been developed. Analyzing this specimen with the **Sectional Flexure Analysis**, the flexure capacity predicted with CSA A23.3-04 and ACI 318-05 codes was 5% and 11% higher, respectively, than the maximum applied load in the test.

Using the **Direct Strut and Tie Model**, the code with the smallest predicted capacities was the CSA A23.3-04 code, with P_{max}/P_P ratios of 2.18 and 1.84 using tie strains in the nodal region of ε_s and ε_{as} respectively. Eurocode 2 also predicted a smaller capacity (748 kN) than the test value giving P_{max}/P_P of 1.54. For ACI 318-05, flexural failure was predicted for this specimen. Effective yielding of the main tension reinforcement was predicted at 1092 kN, only 5.6 % more that the load at effective yielding measured during the test (1031 kN). As it was observed in the previous two beams, CSA A23.3 and Eurocode predicted diagonal strut failure and ACI 318-05 predicted yielding in the tension ties. The mode of failure at test was flexural failure.

The angle of principal compression strains on the concrete surface at the middle of the direct strut location were calculated at an applied load of 923 kN (80%P_{max}), based on the LVDTs readings from the rosette. The angles measured to the principal compression direction from the horizontal axis were 28.9° for shear span A and 35.9° for shear span B. The angle predicted for that load based on the geometry of the Direct Strut and Tie Method was 20.0°.

Analyzing this specimen with the **Combined Strut and Tie Model**, the CSA A23.3 and ACI 318-05 code predicted failure by yielding of the tension tie at 1092 kN with a P_{max}/P_p of 1.05. Eurocode 2 predicted diagonal strut failure at a load of 748 kN, giving a P_{max}/P_p ratio of 1.54.

6.5.1.3 Beams with ρ=2.29% and different shear span to depth ratio

The maximum load at test to total predicted load (P_{max}/P_p) ratios for different *a/d* and ρ=2.29% according to different code provisions are illustrated in Figure 6-4. Using the Direct Strut and Tie Model (STM-D) for all three codes used in this project, the test to predicted capacity (P_{max}/P_p) ratios increase for higher *a/d* ratios, with all values above 1.0 for the specimens in this study. All the codes provisions gave test to predicted capacity (P_{max}/P_p) ratio values closer to 1.0 for *a/d*=1.2 than the values obtained for *a/d*=1.8. ACI 318-05 provisions with the STM-D model gave better predictions of the failure load than CSA A23.3-04 and Eurocode 2 codes for the two different *a/d* ratios studied. Using the Combined Strut and Tie Model (STM-C), the test to predicted capacity ratios were closer to one for the three different *a/d* ratios using CSA A23.3-04 as illustrated in Figure 6-4b. The same analysis of results was obtained for STM-D and STM-C using ACI 318-05 and Eurocode 2.

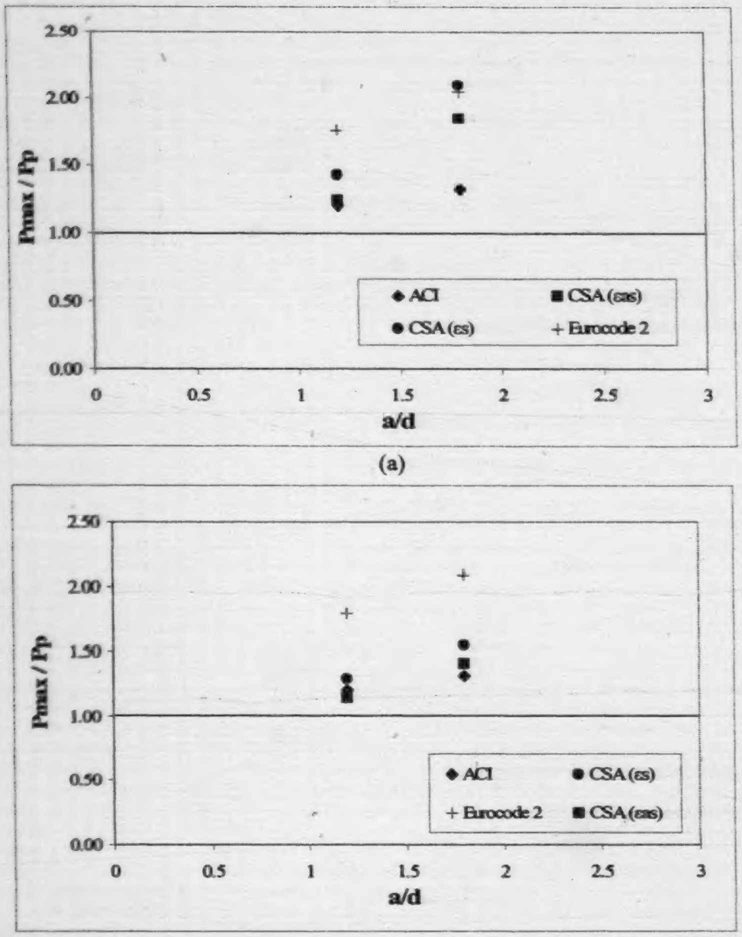

(a)

(b)

Figure 6-4 P_{max}/P_p for two different a/d and ρ=2.29% using (a) STM-D and (b) STM-C

6.5.1.3.1 Specimen MS1-3

The total load capacity predicted using the **Sectional Method** for specimen MS1-3 was 942 kN for CSA A23.3-04 and 830 kN for ACI 318-05. Both codes predicted the correct failure mode, shear failure. However, very inaccurate load capacity was predicted, with P_{max}/P_{pv} ratios of 2.92 and 3.31 for CSA A23.3-04 and ACI 318-05 codes respectively.

Using the **Direct Strut and Tie Model**, the predicted failure load according to CSA A23.3-04 was 1930 kN using tie strains in the nodal region of ε_s and 2212 kN using ε_{as}, giving a P_{max}/P_p ratio of 1.42 and 1.24 respectively. The ACI 318-05 predicted a failure load of 2296 kN while for Eurocode 2, the predicted failure load was 1558 kN, giving P_{max}/P_p ratios of 1.20 and 1.76 respectively. All three codes used predicted the correct failure mode.

The angle of principal compression strains on the concrete surface at the middle of the direct strut location were calculated at an applied load of 2198 kN (80%P_{max}), based on the LVDTs readings from the rosette. The angles measured to the principal compression direction from the horizontal axis were 32.3° for shear span A and 28.0° for shear span B. The angle predicted for that load based on the geometry of the Direct Strut and Tie Model was 36.2°.

By using the **Combined Strut and Tie Model** to analyze specimen MS1-3, approximately 10 % bigger capacities than for the STM-D model were obtained when using the CSA A23.3-04 code provisions. The predicted strength of the STM-C model using tie strains in the nodal region of ε_s, was 2122 kN and 2400 kN when using ε_{as}. These results gave P_{max}/P_p ratios of 1.29 and 1.14 respectively.

At P_{max} of (2747 kN), the strain in the main tension reinforcement at mid-span was 0.0031. The predicted strain in the main tension reinforcement for that load of 2747 kN was 0.0030 according to the STM.

6.5.1.3.2 Specimen MS2-3

The mode of failure observed in this specimen was a combination of crushing of the compression zone between loading plates and diagonal strut failure. Considering the way it failed, with an independent diagonal strut between the interior edge of the support plate and the exterior edge of the loading plate (see Figure 4.26), it was assumed that the maximum diagonal strut strength was near its capacity at P_{max}.

The total capacity predicted using the **Sectional Shear Analysis** for specimen MS2-3 was 936 kN for CSA A23.3-04 and 790 kN for ACI 318-05, giving P_{max}/P_p ratios of 2.20 and 2.60 respectively. Analyzing this specimen with the **Sectional Flexure Analysis**, the flexural capacity predicted with CSA A23.3-04 and ACI 318-05 codes was 7% and 13% higher than the maximum test load, respectively.

Using the **Direct Strut and Tie Model**, the predicted failure load according to CSA A23.3-04 was 980 kN using tie strains in the nodal region of ε_s and 1114 kN using ε_{as}, giving P_{max}/P_p ratios of 1.84 and 1.32 respectively. The ACI 318-05 predicted a failure load of 1560 kN while for Eurocode 2, the predicted load was 1006 kN. The P_{max}/P_p ratio for ACI 318-05 was 1.32 while for Eurocode 2 the ratio was 2.04.

The angle of principal compression strains on the concrete surface at the middle of the direct strut location were calculated at an applied load of 1644 kN (80%P_{max}), based on the LVDTs readings from the rosette. The angles measured to the principal compression direction from the horizontal axis were 22.0° for shear span A and 30.0° for shear span B. The angle predicted for that load based on the geometry of the Direct Strut and Tie Method was 25.3°.

By analyzing specimen MS2-3 with the **Combined Strut and Tie Model** to predict the failure loads, the CSA A23.3-04 code predicted capacities approximately 30 % higher than the ones predicted by STM-D for the same code. The loads predicted and the P_{max}/P_p ratios are shown in Table 6-5. The STM-C gave the same predictions as STM-D for the ACI 318-05 and Eurocode 2 codes.

The predictions shown in Table 6-4 and Table 6-6 for Specimen MS2-3 are based on failure of the top strut between the loading plates. Failure of the top strut was considered when strains at the top concrete fiber of the beam at midspan reached 0.0035 for CSA A23.3-04 and Eurocode 2 and 0.003 for ACI 318-05 code. The strain at the top concrete fiber was calculated using the strain in the main tension reinforcement and the neutral axis. The neutral axis was obtained assuming that the width of the top horizontal strut developed between loading points, and calculated using the STM, is equal to the corresponding depth of equivalent rectangular stress block (a). Once a was calculated, the deep of the neutral axis was obtained using the relationship $a = \beta_1 c$ (see Appendix B) for CSA A23.3-04 and ACI 318-05, and $a = \lambda c$ for Eurocode 2, where $\lambda = 0.8$.

At P_{max} (2055 kN), the strain in the main tension reinforcement at mid-span was 0.0033. The predicted strain for that load of 2055 kN was 0.0037 according to the STM.

6.5.1.4 Specimen with same *a/d* and different *ρ*

Specimens in this group are MS1-1, MS1-2 and MS1-3. These specimens were analyzed in previous sections and only the curves that compare the change in maximum capacity over prediction ratio for three different ρ are shown. ACI 318-05 and Eurocode 2 do not consider the contribution of main tension reinforcement in the predicted strength of beams failing in shear, even though previous research [e.g. Oh and Shin, 2001; Watstein, 1958] indicates that increases in ρ contribute to the shear capacity due to dowel action. Unfortunately, two of the beams in this set failed by flexure and one by shear; with this information, no conclusions about the influence of main tensile reinforcement in the shear strength of deep beams reinforced with ASTM A1035 steel can be made.

Figure 6-5 shows the maximum load at test to predicted load (P_{max}/P_p) for different values of ρ ratios and constant a/d =1.2%. Approximately the same (P_{max}/P_p) ratios were obtained for specimen MS1-1 using both Strut and Tie Models (STM-D, STM-C) and the three code provisions. Analyzing (P_{max}/P_p) for specimens MS1-2 and MS1-3, it is observed that using the Direct Strut and Tie Model (STM-D) and CSA A23.3-04 provisions, the test to predicted capacity (P_{max}/P_p) ratio increases for higher ρ, with all values above 1.0 for the specimens in this study. Eurocode 2 provisions gave test to predicted capacity (P_{max}/P_p) ratio values closer to 1.0 for ρ=1.13% than the values obtained for ρ=2.29%. ACI 318-05 provisions with the STM-D model gave predictions values slightly below 1.0 for specimen MS2-2. Using the Combined Strut and Tie Model (STM-C), the test to predicted capacity ratios were closer to one for ρ of 1.13% and 2.29% using CSA A23.3-04 as illustrated in Figure 6-5b. The same results were obtained for either STM-D or STM-C using ACI 318-05 and Eurocode 2.

Figure 6-6 shows the maximum load at test to predicted load (P_{max}/P_p) for different values of ρ ratios and constant a/d =1.8%. This figure illustrates that better predictions for smaller ρ were obtained. However, the conservatism was reduced using Combined Strut and Tie Model for CSA A23.3-04. ACI 318-05 and Eurocode 2 predictions did not change.

From Figure 6-5 and Figure 6-6, it was observed that for CSA A23.3-04, more uniform P_{max}/P_p ratios for a/d=1.2 and different ρ than for a/d=1.8 and different ρ. For

ρ=1.13%, ACI 318-05 and Eurocode 2 gave similar P_{max}/P_p ratios in both *a/d*=1.2 and *a/d*=1.8. However, for ρ=2.29%, the P_{max}/P_p ratios were closer to 1.0 for *a/d*=1.2 than for *a/d*=1.8.

These results show that for this group of beams, the predictions were safe. Analysis of deep beams longitudinally reinforced with ASTM A1035 steel in the studied configuration can be carried out using the existing code provisions with ε_y determined according to the 0.2% offset method.

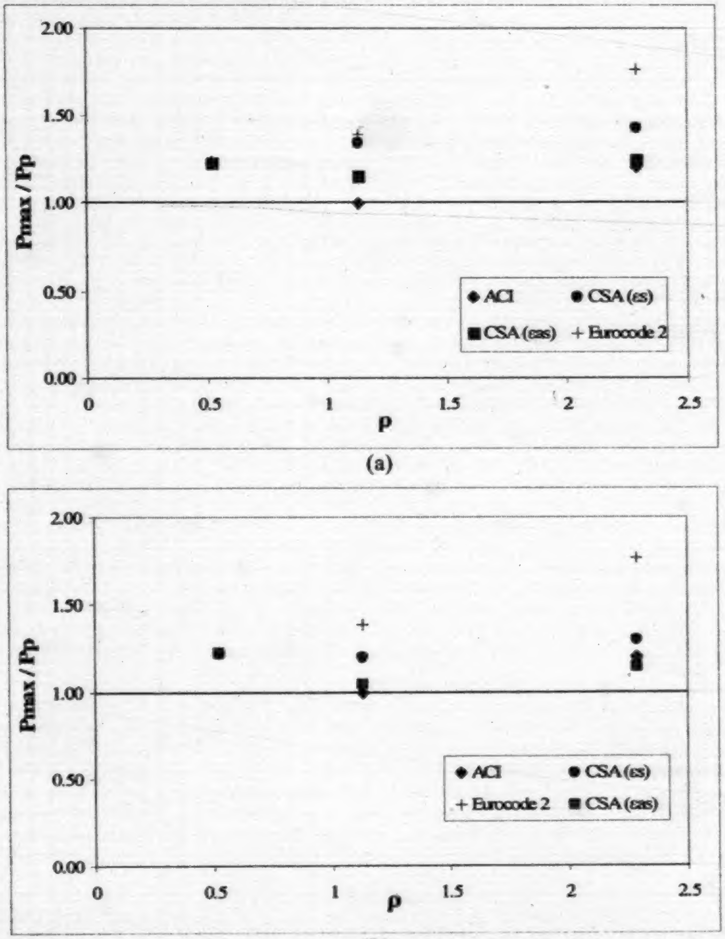

Figure 6-5 P_{max}/P_p for three different ρ and *a/d*=1.2 using (a) STM-D and (b) STM-C

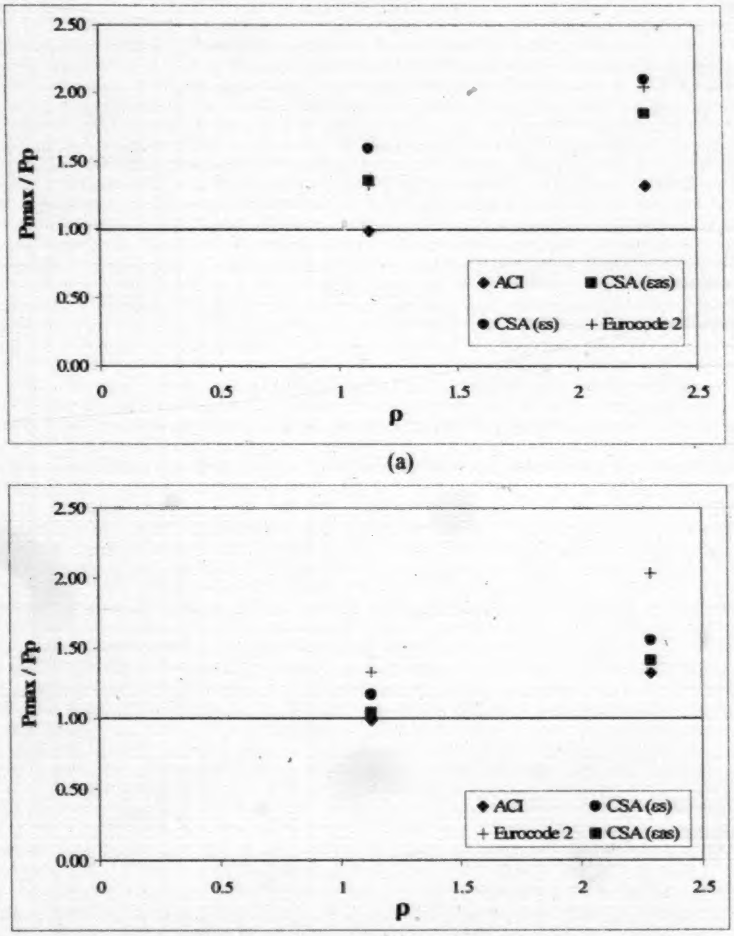

(a)

(b)

Figure 6-6 P_{max}/P_p for three different ρ and a/d=1.8 using (a) STM-D and (b) STM-C

6.5.1.5 Beams reinforced with normal strength steel

6.5.1.5.1 Specimen NS1-4

Prior to the final failure due to diagonal strut failure, yielding of the main longitudinal reinforcement was observed.

For specimen NS1-4, the total load capacity predicted using the **Sectional Method** was 806 kN for CSA A23.3-04 and 720 kN for ACI 318-05 respectively. The **Sectional Shear Analysis** underestimated the capacity of the specimen by 49% and 54% for CSA A23.3-04 and ACI 318-05 provisions respectively. Analyzing this specimen with the

Sectional Flexure Analysis, the flexure capacity was accurately predicted at 1489 kN and 1503 kN according to CSA A23.3-04 and ACI 318-05 provisions, giving test/predicted ratios (P_{max}/P_{pm}) of 1.05 and 1.04 for CSA A23.3-04 and ACI 318-05 codes.

Using the **Direct Strut and Tie Model**, the predicted failure mode for the three codes was diagonal strut failure. According to the CSA A23.3-04 provisions, the predicted strut failure was at a total load of 1100 kN using tie strains in the nodal region of ε_s and 1230 kN using ε_{as}. ACI 318-05 predicted a strut failure at 1196 kN while for Eurocode 2, strut failure was predicted to occur at 896 kN. The ratios of predicted load to measured capacity are shown in Table 6-3.

The angle of principal compression strains on the concrete surface at the middle of the direct strut location were calculated at an applied load of 1253 kN (80%P_{max}), based on the LVDTs readings from the rosette. The angles measured to the principal compression direction from the horizontal axis were 33.3° for shear span A and 34.4° for shear span B. The angle predicted for that load based on the geometry of the Direct Strut and Tie Method was 35.8°.

By analyzing specimen NS1-4 with the **Combined Strut and Tie Model (STM-C)**, more accurate predictions were obtained than for the STM-D model when using the CSA A23.3-04 code provisions. The predicted strength using the STM-C model was 1286 kN for tie strains in the nodal region of ε_s and 1342 kN when using ε_{as}. These results correspond to P_{max}/P_p ratios of 1.22 and 1.17 respectively.

The Combined Strut and Tie Model predictions were the same to the predictions obtained using STM-D for the ACI 318-05 and Eurocode 2 codes, with 1198 kN and 896 kN.

6.5.1.5.2 Specimen NS2-4

Flexural failure was observed for specimen NS2-4.

For specimen NS2-4, the total load capacity predicted using the **Sectional Method** was 816 kN for CSA A23.3-04 and 702 kN for ACI 318-05. Both codes predicted shear failure. Flexural failure occurred at P_{max} =1065 kN. When the beam reached P_{max}, 23%

and 58% more shear capacity that the values predicted using CSA A23.3-04 and ACI 318-05 respectively had been developed. When analyzing this specimen with the **Sectional Flexure Analysis**, the flexural capacity was accurately predicted as 997 kN and 1016 kN according to CSA A23.3-04 and ACI 318-05 provisions, giving test to predicted capacity ratios (P_{max}/P_{pm}) of 1.07 and 1.05 for CSA A23.3-04 and ACI 318-05 codes.

Using the **Direct Strut and Tie Model**, the predicted failure mode for all three codes was diagonal strut failure. According to the CSA A23.3-04 provisions, the predicted strut failure was at 602 kN using tie strains in the nodal region of ε_s and 672 kN using ε_{as}. ACI 318-05 predicted a strut failure at 904 kN while for Eurocode 2, the predicted strut failure was 632 kN. The ratios of predicted over capacity are shown in Table 6-3.

The angle of principal compression strains on the concrete surface at the middle of the direct strut location were calculated at an applied load of 852 kN (80%P_{max}), based on the LVDTs readings from the rosette. The angles measured to the principal compression direction from the horizontal axis were 22.1° for shear span A and 23.8° for shear span B. The angle predicted for that load based on the geometry of the Direct Strut and Tie Method was 25.9°.

When analyzing the deep beams with the **Combined Strut and Tie Model**, more accurate predictions were obtained for the CSA A23.3 code compared with the STM-D. For analysis using ε_s, the predicted strut failure was 928 kN and using ε_{as}, the predicted strut failure was 996 kN. These results correspond to P_{max}/P_p of 1.15 and 1.07 respectively. The predictions using STM-C were the same to the predictions obtained using STM-D for the ACI 318-05 and Eurocode 2 codes, with 906 kN and 632 kN.

6.5.2 Beams without web reinforcement

The ACI 318-05 code is the only design code considered in the current study that allows for analysis and design of deep beams that do not contain distributed web reinforcement. In this project, Specimens MW1-2 and MW3-2 are specimens that were designed without web reinforcement. Note that the sectional methods in ACI 318-05 and

CSA A23.3 both allow the design of slender beams without web reinforcement. The two specimens considered in this group are analyzed by the Sectional Method according to the ACI 318-05 and CSA A23.3-04 and the Strut and Tie Method using ACI 318-05 code provisions.

6.5.2.1 Specimen MW1-2

Using the **Sectional Method** of analysis, CSA A23.3-04 provisions predicted a total load at failure of 350 kN. This corresponded to a very high P_{max}/P_{pv} ratio of 4.48. The ACI 318-05 provisions predicted a total load at failure of 352 kN, giving a P_{max}/P_{pv} ratio of 4.45.

The use of Strut and Tie Method for the analysis of deep beams without web reinforcement is not permitted by CSA A23.3-04 and Eurocode 2 provisions. This restriction is in place because the design formulas in these codes are based on the presence of minimum web reinforcement. On the other hand, ACI 318-05 provides strut strength reduction factors for deep beams without web reinforcement. For specimen MW1-2, the capacity predicted using ACI 318-05 provisions was 1414 kN, very close to the failure load at test of 1568 kN. This corresponded to a P_{max}/P_p ratio of 1.11. The failure mode (diagonal strut failure) was predicted correctly.

The strain measured in the main reinforcement at P_{max} (1568 kN) was 0.0036. The strain predicted at that load was 0.0032 according to the STM.

The angle of principal compression strains on the concrete surface at the middle of the direct strut location were calculated at an applied load of 1255 kN (80%P_{max}), based on the LVDTs readings from the rosette. The angles measured to the principal compression direction from the horizontal axis were 47.9° for shear span A and 46.2° for shear span B. The angle predicted for that load based on the geometry of the Direct Strut and Tie Method was 37.6°.

6.5.2.2 Specimen MW3-2

The **Sectional Method** predicted a beam capacity of 332 kN using CSA A23.3-04 and 342 kN using ACI 318-05, corresponding to P_{max}/P_{pv} ratios of 1.24 and 1.20 respectively. The failure mode (shear failure) for this specimen was correctly predicted.

Considering all the restriction for the design of deep beams provided in the codes, this specimen cannot be designed or analyzed using any code by STM. For CSA A23.3-04 and Eurocode 2 codes it is necessary to provide minimum web reinforcement and for ACI 318-05 the angle between the main tension reinforcement must be bigger than 25°. Even though this specimen is outside the limits of ACI 318-05, analysis using STM was carried out. The predicted failure load was 700 kN, significantly overestimating the measured failure load of 411 kN.

The strain measured in the main reinforcement at P_{max} (411 kN) was 0.0016. The strain in main reinforcement predicted at that load was 0.0015 according to the STM.

6.6 Summary

The adequacy of CSA A23.3-04, ACI 318-05 and Eurocode 2 code provisions for the design of reinforced concrete deep beams was studied for the case of members longitudinally reinforced with ASTM A1035 reinforcing steel. Traditional sectional methods and Strut and Tie Methods were used in the predictions of the failure loads.

The predicted capacities of the specimens obtained by Sectional Shear Analysis from CSA A23.3-04 and ACI 318-05 were significantly lower than the measured capacities for the specimen configurations used in this project with $a/d \leq 1.8$. For specimens with a/d=2.4 tested in this project, good predictions were obtained using the Sectional Shear Analysis provisions. Sectional Flexure Analysis Methods in CSA A23.3-04 and ACI 318-05 gave good predictions of the moment capacity of the specimens.

The predicted load capacities for diagonal strut splitting strut and flexural failure modes for each specimen were analyzed using the Strut and Tie Method provisions from CSA A23.3-04, ACI 318-05 and Eurocode 2. Two Strut and Tie Models of analysis were used: the Direct Strut and Tie Model and the Combined Strut and Tie Model. Two test-to-predicted load ratios were completed using each code: P_{max}/P_p and P_f/P_c represented the maximum measured load to failure prediction, and the measured load corresponding to the first failure mode reached during the test and the predicted load for the same mode.

Of the three code provisions studied to predict the failure loads using the Direct Strut and Tie Model, the best results were obtained using the ACI 318-05 code provisions. Predictions using Combined Strut and Tie Model for CSA A23.3-04 were more accurate than predictions using STM-D for the same code. For ACI 318-05 and Eurocode 2 code provisions, the predictions using the STM-C remained similar to those obtained using STM-D. The ACI 318-05 provisions correctly predicted all failure modes except for specimens MS2-3, NS1-4 and NS2-4. On the other hand, CSA A23.3-04 and Eurocode 2 only correctly predicted the modes of failure for MS1-1 and MS1-3.

For specimens with same reinforcement ratio ρ, the test to predicted capacity (P_{max}/P_p) ratio, using the Strut and Tie Method and CSA A23.3-04 provisions, increased for higher a/d ratios, with all values above 1.0. The test to predicted capacity ratios (P_{max}/P_p) were closer to one using tie strains in the nodal region of ε_{sa} for CSA A23.3-04 than using ε_s. Eurocode 2 provisions gave test to predicted capacity (P_{max}/P_p) ratio values closer to 1.0 for a/d=1.8 than the values obtained for a/d= 2.4. ACI 318-05 provisions gave very good predictions of the failure load for the three different a/d ratios studied..

Using the Strut and Tie Method and the three codes provisions, the test to predicted capacity (P_{max}/P_p) ratio, for specimens with same a/d, increases for higher reinforcement ratios ρ. However, the P_{max}/P_p ratios for MS1-1 (a/d=1.2 and ρ=0.52%) using CSA A23.3-04 and ACI 318-05 were higher than for MS1-2 (a/d=1.2 and ρ=1.13%).

Results show that for deep beams with ASTM A1035 reinforcing steel which contain web reinforcement, the diagonal strut strength is safely predicted. However, the predictions of flexural strength were slightly higher than the one obtained at test.

7. SUMMARY AND CONCLUSIONS

Ten large-scale specimens were tested under four point bending to evaluate the behaviour of reinforced concrete deep beams containing high strength steel reinforcement. The adequacy of CSA A23.3-04, ACI 318-05 and Eurocode 2 design models for these deep beams was examined. The main variables in the test program were the shear span to depth ratio, main longitudinal steel ratio, and the type of longitudinal reinforcement. Eight deep beam specimens contained Grade 400R vertical web reinforcement and two specimens omitted vertical web reinforcement.

7.1 Experimental Program

The experimental program was successfully carried out and new test data was obtained for the behaviour of non-slender deep beams containing ASTM A1035 steel as the main tension reinforcement. Three different failure modes were observed in specimens that contained web reinforcement: yielding of the main longitudinal reinforcement, crushing of the top horizontal strut between the loading points and diagonal strut failure. All specimens that did not contain web reinforcement failed by diagonal strut failure.

The maximum load capacity of deep beams reinforced with ASTM A1035 reinforcing steel increased as the shear span to depth ratio *(a/d)* decreased. For smaller *a/d* ratios and constant reinforcement ratio ρ, the stiffness of the deep beams increased and smaller deflections at failure were obtained. Deflection ductility (μ), defined as the ratio between maximum deflection and the deflection at first yield of the main reinforcement, increased for larger *a/d* ratios when the reinforcement ratio ρ was constant. For members having constant *a/d* ratios, the capacity of the beams increased as the reinforcement ratio ρ increased. For larger values of ρ and constant *a/d* ratio, the stiffness of the beams increased and the deflection ductility decreased.

For specimens containing web reinforcement and ASTM A1035 steel as the main tension reinforcement, the common serviceability deflection limits of *l/360* and *l/180* were reached at loads greater than 60% and 90% of P_{max}, respectively. At these load levels, strains in the main tension reinforcement were higher than the yield strain of normal strength reinforcement having f_y = 400 MPa. The average stresses reached in the main tension reinforcement for these specimens at the *l/360* and *l/180* serviceability limits were 590 MPa and 840 MPa, respectively.

The crack patterns and failure mechanisms for deep beams reinforced with high strength reinforcing steel were similar to those reinforced with normal strength reinforcing steel tested in this project and in test programs previously reported by other researchers. For beams containing web reinforcement and ASTM A1035 steel as the main tension reinforcement, the common crack width limits of 0.33mm and 0.4 mm were reached on average at 40% and 45% of P_{max}, respectively, for cracks which developed at midspan. For diagonal struts cracks, these crack width limits of 0.33 mm and 0.4 mm were reached on average at 42% and 46% of P_{max}, respectively. At these load levels, strains in the main tension reinforcement were close to the yield strain of normal strength reinforcement having f_y = 400 MPa. The stresses reached in the main tension reinforcement for these specimens were on average 350 MPa and 390 MPa, for the 0.33 mm and 0.4 mm crack width serviceability limits at midspan, respectively. For diagonal struts cracks, the stress in the main tension reinforcement was 390 MPa and 430 MPa for the 0.33 mm and 0.4 mm serviceability crack width limits, respectively.

The shape of the strain distribution along the bottom bar of main tension reinforcement varied for different *a/d* ratios. The strain distribution along the beam span was relatively uniform at early stages of loading for beams with $a/d \leq 1.8$. For higher load levels in these specimens, strains close to the supports became larger than the strains at midspan due to the development of wider cracks near to the supports. For specimens with a/d=2.4, a gradual decrease in reinforcement strains between midspan and the supports was observed for all stages of loading. Reinforcement strains at the exterior edges of the supports were small compared with the strains developed in the clear span due to the bar anchorage resulting from the influence of the diagonal compression struts formed between the loading points to the supports. No anchorage failure at beam-ends was observed in the specimens, indicating that the current ACI 318-05 and CSA A23.3-04 code provisions for reinforcement development length are viable for the design of deep beams reinforced with ASTM A1035 using the Strut and Tie Method.

The use of web reinforcement in deep beams is recommended to obtain higher capacity and improve the deflection ductility. Specimens with web reinforcement resisted significantly more load prior to failure and the crack distribution was observed to be more symmetric than companion specimens without web reinforcement. Load deflection response of beams without web reinforcement remained similar to geometrically identical beams with web reinforcement until an increase in crack width rates occurred in the diagonal strut, followed by splitting of the diagonal strut in the specimens without web reinforcement. The load-deflection responses of specimens with and without web reinforcement remained similar up to 63% of P_{max} for beams with web reinforcement and a/d=1.2 and similar up to 29% of P_{max} for beams with web reinforcement and a/d of 2.4 in the current study.

7.2 Analytical Methods

Predictions of capacity for the new experimental tests were completed using existing design code provisions for reinforced concrete, modified for the mechanical properties of the ASTM A1035 reinforcement. Both the Strut and Tie Method of analysis and Sectional Methods of analysis for shear and flexure were examined. These methods implemented the design provisions from CSA A23.3-04, ACI 318-05 and Eurocode 2. The stress-strain response of the ASTM A1035 reinforcement obtained from coupon tests was utilized.

The Sectional Shear Method of analysis from CSA A23.3-04 and ACI 318-05 predicted capacities significantly lower than the measured capacities for deep beams reinforced with high strength reinforcement and $a/d \leq 1.8$. The mean test to predicted capacity ratios (P_{max}/P_{pv}) for these specimens with a/d of 1.2 and 1.8 were 2.44 and 2.55 for CSA A23.3-04 and ACI 318-05 respectively. For specimen with a/d of 2.4, the sectional shear method of design was the most appropriate, with mean P_{max}/P_{pv} ratios of 1.32 and 1.24 for CSA A23.3-04 and ACI 318-05 respectively.

Using Sectional Flexure Analysis to predict the flexural capacity of the specimens, P_{max}/P_{pm} ratios of 1.04 and 1.06 for CSA A23.3-04 and ACI 318-05 codes, respectively, were obtained. The coefficient of variation was 0.033 and 0.036 for CSA A23.3-04 and ACI 318-05 codes respectively.

Two Strut and Tie Models were used for specimen analysis: the Direct Strut and Tie Model and the Combined Strut and Tie Model. The Direct Strut and Tie Model is the most practical technique for the analysis and design of deep beams reinforced with high strength steel using the ACI 318-05 and Eurocode 2 provisions. Strut reduction factors used in these codes were empirically obtained from test results for a wide variety of deep beam configurations. It is not necessary to consider a Combined Strut and Tie Model using these codes for the beam configurations tested, since the ACI 318 and Eurocode 2 provisions do not adjust the strut efficiency factors based on the strain in the main reinforcement that crosses the struts. Thus, for the beam configurations studied in this project, no change in capacity predictions from the Direct Strut and Tie Model would result by implementing the Combined Strut and Tie Model. On the other hand, the Combined Strut and Tie Model resulted in better predictions than the Direct Strut and Tie Model when using the CSA A23.3-04 code provisions, since the CSA A23.3-04 model considers the reduced strains of the main tension reinforcement in the area close to the support due to the altered truss model.

Of the three code provisions studied to predict the failure loads using the Direct Strut and Tie Model, the best results were obtained with the ACI 318-05 code provisions. Analysis according to ACI 318-05 resulted in test to predicted capacity P_{max}/P_p ratios closer to 1.0 with relatively low coefficient of variation. ACI 318-05 provisions correctly predicted the failure mode for more specimens than CSA A23.3-04 and Eurocode 2. For CSA A23.3-04 design provisions and the beam configurations studied, the assumption of using an average tie force in the nodal zone (i.e. ε_{as} from Equation (2.2)) when calculating the strength of the direct strut developed between the loading point and the support resulted in improved predictions of capacity than considering the maximum tie strain adjacent to the nodal zone (i.e. ε_s). Using CSA A23.3-04 provisions and the Direct Strut and Tie Model, the mean P_{max}/P_p ratios were 1.63 and 1.44 for the ε_s and ε_{as} assumptions, respectively. Predictions using the Combined Strut and Tie Model for CSA A23.3-04 were more accurate than predictions using the Direct Strut and Tie Model, with P_{max}/P_p ratios of 1.23 and 1.14 for the ε_s and ε_{as} assumptions, respectively. For the Direct Strut and Tie Model and the ACI 318-05 and Eurocode 2 provisions, the capacity prediction ratios were P_{max}/P_p =1.09 and P_{max}/P_p =1.59, respectively. For ACI 318-05 and

Eurocode 2 code provisions with the Combined Strut and Tie Model, the predictions remained similar to those using the Direct Strut and Tie Model.

ACI 318-05 correctly predicted all failure modes except for specimens MS2-3, NS1-4 and NS2-4. On the other hand, CSA A23.3-04 and Eurocode 2 only correctly predicted the modes of failure for specimens MS1-1 and MS1-3. Failure modes that were not correctly predicted resulted from design code provisions that underestimated the diagonal strut capacity.

The Strut and Tie Model can be used successfully for the design of deep beams with ASTM A1035 steel reinforcement if the design limits for reinforcement strength are set to the effective yield strength (approximately 860 MPa) according to the 0.2% offset method. Test-to-predicted ratios P_t/P_c were established between the measured load at first design limit reached during the test (P_t), such as occurrence of effective yield strains, and the model prediction for the same design limit (P_c). Even though some of the predicted loads for "yielding" of the main tension reinforcement were slightly higher than the loads obtained during testing (P_t/P_c ratios for MS2-2 and MS3-2 were less than 1.0), the specimens reached higher maximum loads than P_t. The P_t/P_c ratios for all specimens using the Direct Strut and Tie Model and CSA A23.3-04 provisions were 1.01 and 0.99 using the approach with tie strains in the nodal region of ε_s and ε_{as} respectively. The P_t/P_c ratios for all specimens using the Combined Strut and Tie Model and CSA A23.3-04 provisions were 0.99 and 0.97 using the approach with tie strains in the nodal region of ε_s and ε_{as} respectively. The mean value for P_t/P_c ratio using ACI 318-05 code provisions was 0.96 for both Direct and the Combined Strut and Tie Model. The mean P_t/P_c ratio using the Eurocode 2 model was 1.05 for both Direct and the Combined Strut and Tie Model.

For specimens with the same reinforcement ratio ρ, the test to predicted capacity (P_{max}/P_p) ratio, using the Direct Strut and Tie Method and CSA A23.3-04 provisions increased for higher *a/d* ratios, with all values above 1.0. Eurocode 2 provisions gave test to predicted capacity (P_{max}/P_p) ratio values closer to 1.0 for *a/d*=1.8 than the values obtained for *a/d*= 2.4. ACI 318-05 provisions gave very good predictions of the failure load for the three different *a/d* ratios studied. The test to predicted capacity (P_{max}/P_p)

ratios using the Combined Strut and Tie Method and CSA A23.3 provisions were very close to one for ρ=1.13%. For ρ=2.29%, the test to predicted capacity (P_{max}/P_p) ratios, using the Combined Strut and Tie Method and CSA A23.3 provisions, increased for higher *a/d*, but the values were closer to one than using the Direct Strut and Tie Method.

Using the Strut and Tie Method and the three code provisions, the test to predicted capacity (P_{max}/P_p) ratio for specimens with the same *a/d* increased as the reinforcement ratio ρ increased. However, the P_{max}/P_p ratios for MS1-1 (*a/d*=1.2 and ρ=0.52%) using CSA A23.3-04 and ACI 318-05 were higher than for MS1-2 (*a/d*=1.2 and ρ=1.13%).

Results show that for the beams with ASTM A1035 reinforcing steel with web reinforcement, the diagonal strut strength is safely predicted. On the other hand, predictions of capacities at yielding of the main tension reinforcement were slightly higher than the one obtained at test, with a P_t/P_c of 0.98.

7.3 Use of ASTM A1035 Reinforcement in Deep Beams

Capacity predictions made using the Strut and Tie Method provisions from the CSA A23.3-04, ACI 318-05 and Eurocode2 were in good agreement with the results from deep beam specimens constructed with ASTM A1035 reinforcing steel. In particular, prediction ratios close to 1.0 (0.98) with low coefficient of variation of 5.5% were obtained from comparison of applied load corresponding to tie strains at the effective yield strain and the magnitude of the model load condition with the same tie strain. Note that the effective yield strength values for these specimens were approximately 860 MPa according to the 0.2% offset method, which is significantly higher than current code limits for the design yield strength. Based on these results, the current design yield strength limits (500 MPa for CSA A23.3-04 and Eurocode 2 and 550 MPa for ACI 318-05) can be increased to magnitudes closer to the effective yield strength according to the 0.2% offset method. However, additional consideration is required of the resulting significances of crack width and member deflection during the design process.

8. RECOMMENDATIONS FOR FUTURE RESEARCH

Additional experimental work, analytical studies and finite element analysis are needed to allow the use in practice of design reinforcement strengths beyond the current limits established by the CSA A23.3-04, ACI 318-05 and Eurocode 2 design codes. While the beam configurations studied in this project could exploit the additional reinforcement strength beyond the code limits, consideration of other member configurations is warranted before permitting wide-spread adoption of ASTM A1035 steel in non-flexural members.

Due to the high effective yield strength of ASTM A1035 steel reinforcement, the current experimental program included several specimens that experienced concrete crushing in the top horizontal strut between the loading points. To better exploit the high strength of the main tension reinforcement and the capacity of the diagonal struts, additional research is needed to understand the influence of the top strut strength limits. To improve the structural efficiency of a reinforced concrete deep beam under four-point bending, reinforcement can be placed in the top strut region to obtain confinement of the concrete. The performance of deep beams containing high strength reinforcement and constructed from high strength concrete should also be examined. For deep beams constructed with normal strength concrete, a limit on width of the top strut should be considered, in order to prevent top strut failure in the Strut and Tie Method, prior to obtaining large strains in the main tension reinforcement.

Additional testing is required for specimens with sufficiently high top horizontal strut strengths and main tension reinforcement strength to achieve failure of the diagonal strut. These configurations, combined with variations of the reinforcement ratio ρ and the shear span to depth ratio a/d will help to further determine the influence of ρ and a/d on the diagonal strut capacity of deep beams reinforced with high strength reinforcement.

Specimens reinforced with high strength reinforcing steel, including vertical web reinforcement fabricated from ASTM A1035 steel, should be tested to determine the influence of high strength stirrups on the behavior or deep beams. The current test program only utilized Grade 400R vertical web reinforcement. The usage of high strength stirrups may make the assumption of "yielding of vertical web reinforcement" invalid within the analysis of deep beams using the Combined Strut and Tie Model for the calculation of member capacity.

Finite element analysis of specimens tested in this project is needed to compare the stress flow assumed in the STM against that established using a finite element model. Finite element analysis can be useful to further study the strain distribution at midspan to propose different reduction factors for the top strut. Current design techniques do not account for limits on maximum strain in the horizontal strut. Furthermore, development of a validated finite element analysis model will permit improved study of parametric influences from design configurations, including the use of high strength vertical web reinforcement and high strength concrete, as noted above.

Finally, additional study is required of non-flexural structural members (or regions) reinforced with ASTM A1035, where more complex truss analogies for the Strut and Tie Model are required. Member configurations should correspond to common arrangements in industry, including dapped-end beam connections, corbels, or beams with openings.

REFERENCES

ACI Committee 318, 2005, "Building Code requirements for Reinforced Concrete (ACI 318-05) and Commentary (ACI 318R-05)", *American Concrete Institute*, Farmington, Hills, Mich., 430 pp.

Adebar, P. and Zhou, Z., 1993, "Bearing strength of compressive struts confined by plain concrete", *ACI Structural Journal*, v 90, n 5, September-October, pp. 534-541.

Aguilar, G., Matamoros, A. B., Parra-Montesinos, G. J., Ramírez, J. A. and Wight, J. K. , 2002, "Experimental evaluation of design procedures for shear strength of deep reinforced concrete beams" *ACI Structural Journal*, v 99, n 4, July-August, pp. 539-548.

American Concrete Institute, 2002, "Examples for the design of Structural Concrete with Strut and Tie Models", January, American Concrete Institute. 242 pp.

Ansley, H. M., "Investigation into the structural performance of MMFX reinforcing", *MMFX Steel Corporation: Technical Resources*, August 13, 2002. 12 pp.

Bazant, Z. P., and Kim, J.-K., 1984, "Size Effect in Shear Failure of Longitudinally Reinforced Beams," *ACI Journal, Proceedings*, v 81, n 5, September-October, pp. 456-468.

Brown, M. D., Sankovich, C.L., Bayrak, O., Jirsa, J. O., Breen, J. E. and Wood, S. L., 2005, "Design for shear reinforced concrete using Strut-and-Tie Models", CTR *Research Report*, July, 330 pp.

Canadian Standards Association, 2004, "CAN/CSA A23.3-04 Design of Concrete Structures," CSA, Rexdale, Ontario, Canada.

Choi, K. K., Park H. G. and Wight J.K., 2007, "Unified Shear Strength Model for Reinforced Concrete Beams—Part I: Development" *ACI Structural Journal*, v 104, n 2, March-April, pp. 142-152.

Choi, K. K. and Park H. G., 2007, "Unified Shear Strength Model for Reinforced Concrete Beams—Part II: Verification and simplified method" *ACI Structural Journal*, v 104, n 2, March-April, pp. 153-161.

Collins, M.P. and Mitchell, D., 1991, "Prestressed Concrete Structures", *Prentice Hall*, 766 pp.

Darwin D., Browning J., Van Nguyen T. and Locke Jr C., 2002, "Mechanical and corrosion properties of high strength, high chrominium reinforcing steel for concrete". *Final Report, South Dakota, Department of transportation*, March, 142 pp.

El-Hacha, R and Rizkalla, S.H.., 2002, "Fundamental Material properties of MMFX steel Rebars", *NCSU-CFL Report*, July, 59 pp.

El-Hacha, R., El-Agroudy, H. and Rizkalla, S.H., 2006, “Bond Characteristics of high strength steel reinforcement”, *ACI Journal*, 103 No, 6, November-December, pp 771-782.

Eurocode 2, 1992, “—Design of Concrete Structures—Part 1-1: General Rules and Rules for Buildings,” EN 1992-1-1, 100 pp.

Foster, S. J., Gilbert, R. I., 1998, “Experimental studies on high-strength concrete deep beams”, *ACI Structural Journal*, v 95, n 4, July-August, pp 382-390.

Kani, M. W., Huggins, M. W., and Wittkopp, R. R., 1979, “Kani on Shear in Reinforced Concrete”, *University of Toronto Press*, 225 pp.

Lubell, A.S. 2006, "Shear in Wide Reinforced Concrete Members," *Ph.D. Dissertation*, Civil Engineering, University of Toronto, Toronto, Ontario, May 455 pp.

Malhas, A.F., 2002, “Preliminary experimental Investigation of the Flexural behavior of reinforced concrete Beams using MMFX Steel”, *MMFX Steel Corporation: Technical Resources*, July, 55 pp.

Marti, P., 1985, “Truss Models in Detailing”, *Concrete International*, v 7, n 12, pp. 66-73.

Matamoros, A B. and Wong, K H, 2003, “Design of Simply Supported Deep Beams Using Strut-and-Tie Models” *ACI Structural Journal*, v 100, n 6, November-December, pp. 704-712.

Nielsen, M.P., 1998, “Limit analysis and Concrete Plasticity”, 2nd Edition, CRC Press, Boca Raton, Fla., 908 pp.

Oh, J. K. and Shin, S. W., 2001, “Shear strength of reinforced high-strength concrete deep beams”, *ACI Structural Journal*, v 98, n 2, March-April, pp. 164-173.

Quintero-Febres, C. G., Parra-Montesinos, G. and Wight, J. K., 2006, “Strength of struts in deep concrete members designed using strut-and-tie method”, *ACI Structural Journal*, v 103, n 4, July-August, pp. 577-586.

Rogowsky, D. M. and MacGregor, J. G., “Design of reinforced concrete deep beams”, 1986, *Concrete International: Design and Construction*, v 8, n 8, August, pp. 49-58.

Rogowsky, D. M., MacGregor, J. G., Ong, S. Y., 1986, “Tests of reinforced concrete deep beams”, *Journal of The American Concrete Institute*, v 83, n 4, July-August, pp. 614-623.

Schlaich, J., Schäfer, K., and Jennewein, M., 1987, “Towards a Consistent Design of Structural Concrete,” *PCI Journal*, v 32, n 3, pp. 74-150.

Seliem H. M., Lucier G., Rizkalla S. H., and Zia P., 2008, "Behavior of Concrete Bridge Decks Reinforced with High-Performance Steel" *ACI Structural Journal*, V. 105, No. 1, January-February, pp 78-86.

Selvam, V. K. Manicka and Thomas, Kuruvilla, 1987, "shear strength of concrete deep beams" *Indian Concrete Journal*, v 61, n 8, August, pp. 219-222.

Subedi, N. K., Vardy, A. E. and Kubota, N., 1986, "Reinforced concrete deep beams - some test results", *Magazine of Concrete Research*, v 38, n 137, Dec, pp 206-219.

Tan, K.H. and Lu, H.Y., 1999, "Shear behavior of large reinforced concrete deep beams and code comparisons" *ACI Structural Journal*, v 96, n 5, September/October, pp. 836-845.

Tan, K.H. and Cheng, G.H., 2006, "Size effect on shear strength of deep beams: Investigating with strut-and-tie model" *Journal of Structural Engineering*, v 132, n 5, May, pp. 673-685.

Varghese, P.C. and Krishnamoorthy, C. S., 1966, "Strength and behavior of deep reinforced concrete beams", *The Indian concrete journal*, March, v 40, pp. 104-108.

Vecchio, F. J. and Collins, M. P., 1986, "The modified compression Field Theory for reinforced concrete elements Subjected to Shear"; *ACI Journal*, v 83, n 2, March-April, pp. 219-231.

Vijay, P.V.; Gangarao, V. S. and Prachasaree, W., 2002, "Bending Behavior of Concrete Beams Reinforced with MMFX Steel bars", *MMFX Steel Corporation: Technical Resources*, July, 33 pp.

Watstein, D. and Mathey, R.G., 1958, "Strains in Beams Having Diagonal Cracks", *ACI Journal*, v 55, n 12, pp. 717-728.

Yotakhong, P., 2003, "Flexural performance of MMFX reinforcing rebars in concrete structures". *Thesis*, November, 162 pp.

Zsutty, T. C., 1968, "Beam Shear Strength Prediction by Analysis of Existing Data," *ACI Journal, Proceedings*, v 65, n 11, November, pp. 943-951.

www.mmfx.com

APPENDIX A

A. Appendix A

A.1 Specimen MS1-1

Table A-1 Loads and deflections at important events during the test of specimen MS1-1

Load (kN)	Deflection (mm)	Event
200	0.95	First flexural crack
354	1.42	First diagonal strut crack B
365	1.47	First diagonal strut crack A
990	6.25	Yielding of the first layer of the main tension reinforcement
1174	9.70	Yielding of the third layer of the main tension reinforcement
1250	13.66	Maximum load

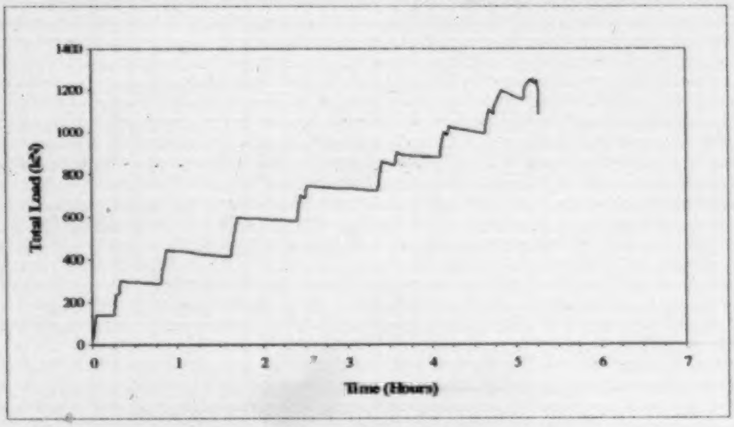

Figure A-1 Load-time response of specimen MS1-1

Table A-2 Flexural and diagonal crack widths at different loading stages of specimen MS1-1

Total Load (kN)	Maximum flexural crack width (mm)	distance to midspan (mm)	Diagonal crack width at A (mm)	Diagonal crack width at B (mm)
150	0	0	0	0
200	First flexural crack			
300	0.15	100	0	0
354	First diagonal strut crack B			
365	First diagonal strut crack A			
450	0.50	100	0.25	0.20
600	0.80	360	0.50	0.40
750	0.80	100	0.60	0.60
900	1.00	100	1.00	0.80
1020	1.25	100	1.25	1.00
1200	>1.50	100	>1.50	1.25
1250	Maximum load			

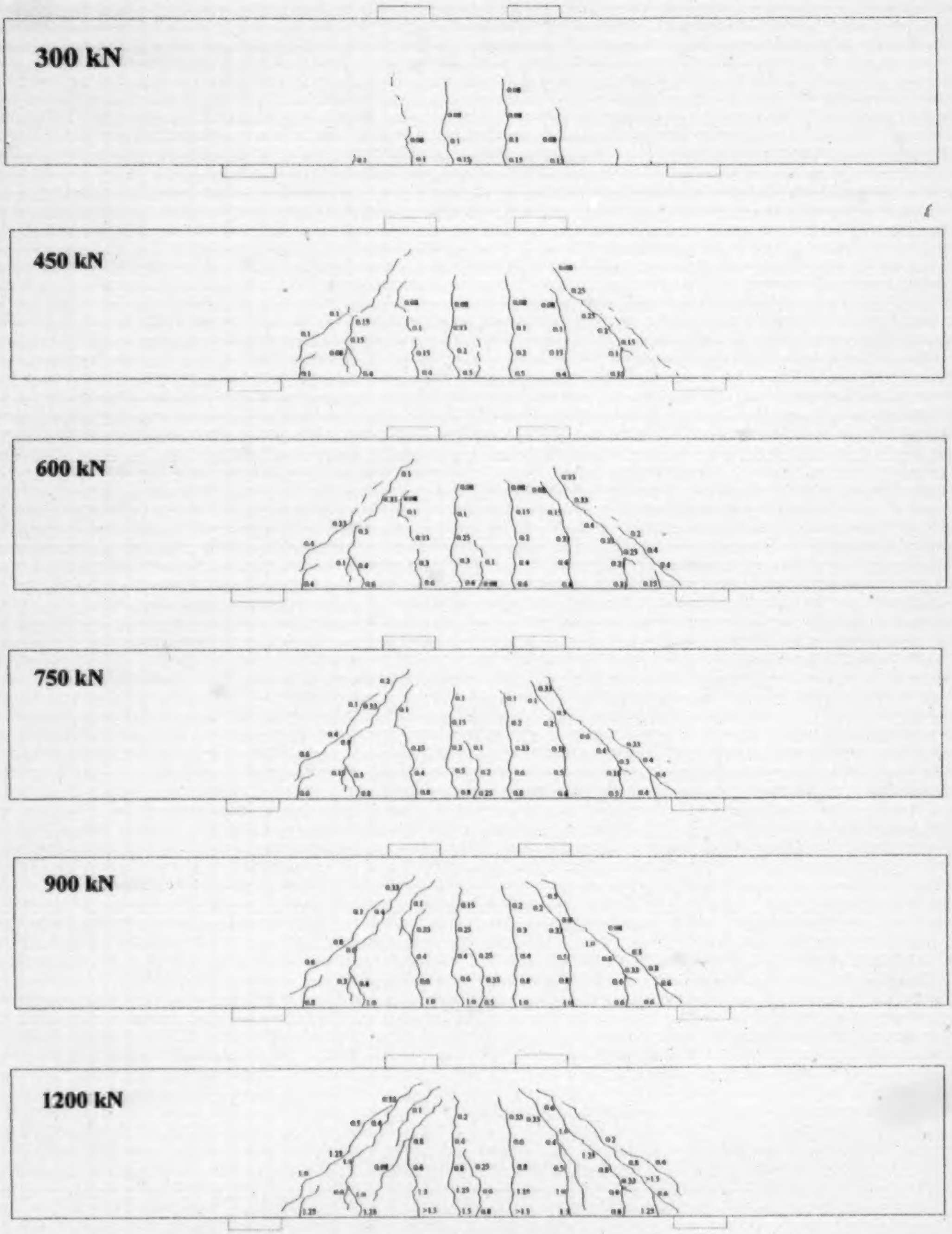

Figure A-2 Crack patterns at different loading stages of specimen MS1-1

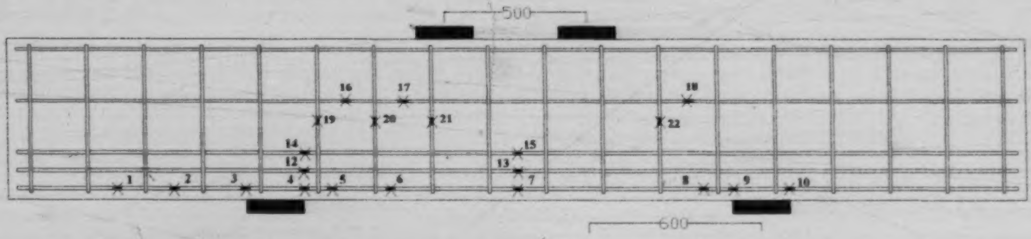

Figure A-3 Strain gages locations of specimen MS1-1

Table A-3 Location of strain gauges for specimen MS1-1

Strain Gauge	Distance from midspan (mm)	side	Strain Gauge	Distance from midspan (mm)	side
1	1450	A	12	750	A
2	1250	A	13	0	
3	950	A	14	750	A
4	750	A	15	0	
5	660	A	16	400	A
6	460	A	17	600	A
7	0		18	600	B
8	600	B	19	stirrup	A
9	750	B	20	stirrup	A
10	950	B	21	stirrup	A
11	0	B	22	stirrup	B

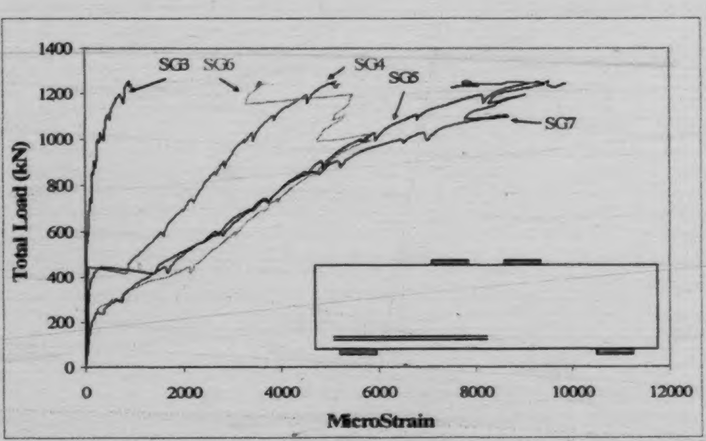

Figure A-4 Strains at a bar located in the lowest layer of main tension reinforcement of specimen MS1-1

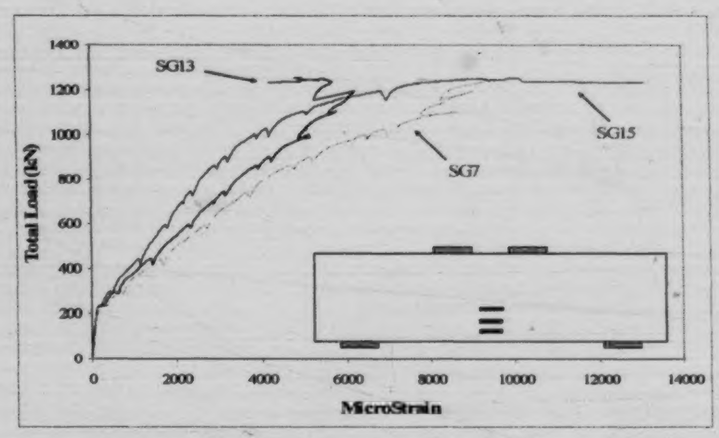

Figure A-5 Strains at midspan of the three layers of main tension reinforcement in specimen MS1-1

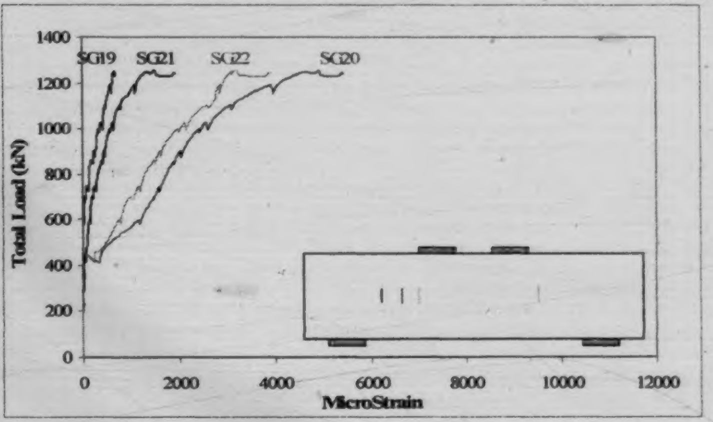

Figure A-6 Strains of stirrups located in the shear spans of specimen MS1-1

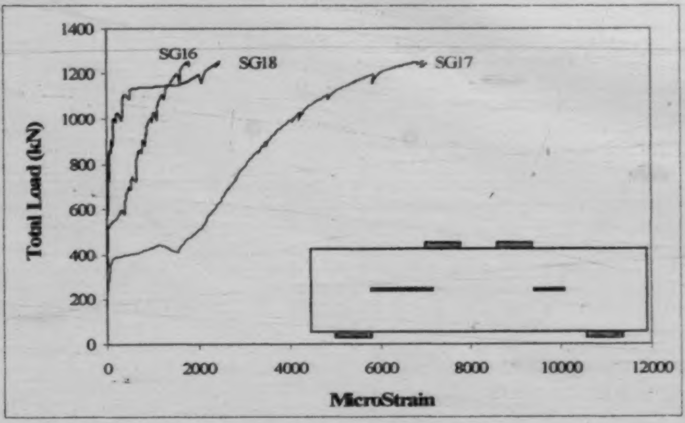

Figure A-7 Strains on the horizontal web reinforcement of specimen MS1-1

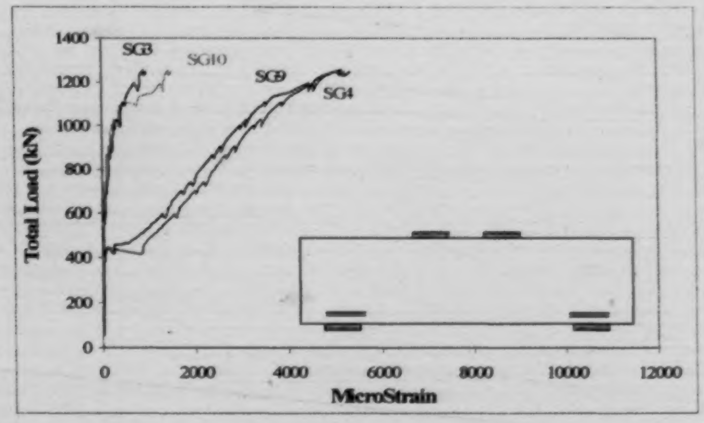

Figure A-8 Strains at the interior and exterior edges of the supports

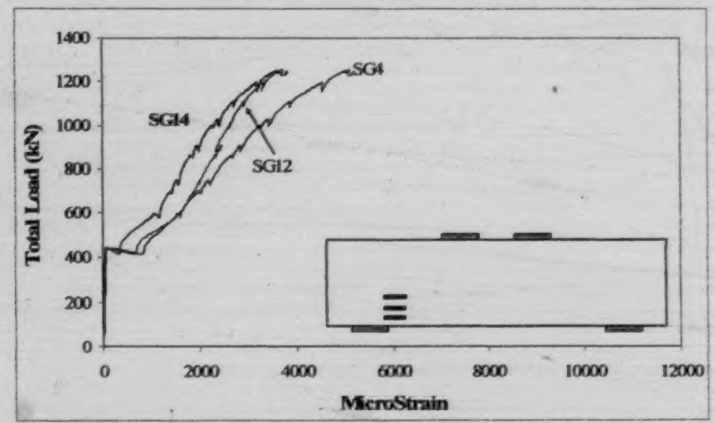

Figure A-9 Strain at the interior edge of one support for the three layers of tension reinforcement of specimen MS1-1

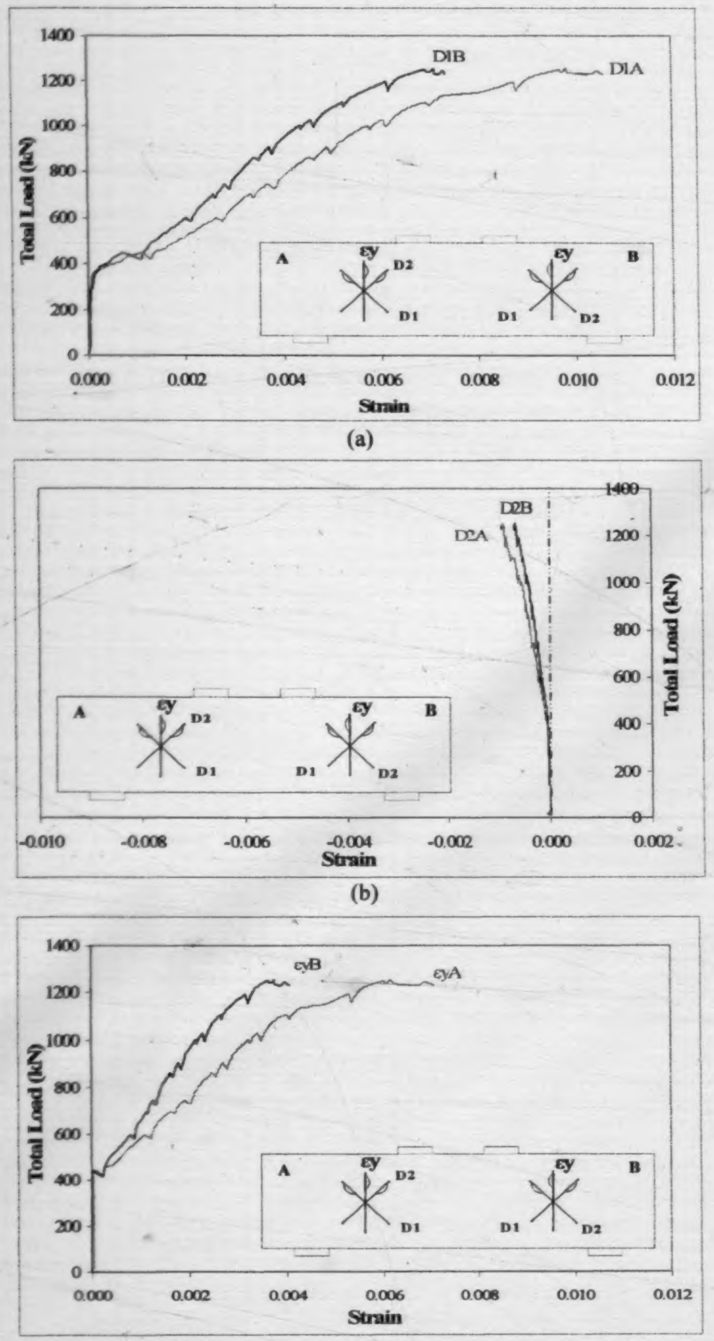

(a)

(b)

(c)

Figure A-10 Average Strains in the (a) diagonal strain D1, (b) diagonal strain D2 and (c) vertical strain of specimen MS1-1

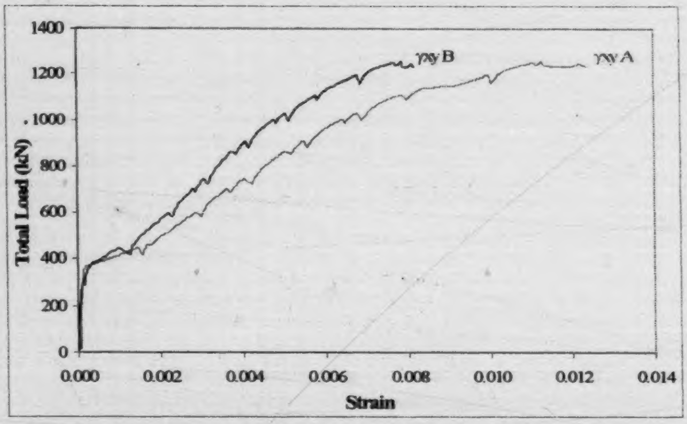

Figure A-11Maximum shear strain in diagonal struts of specimen MS1-1

Table A-4 Strains monitored by demec gages rosettes for specimen MS1-1

LOAD (kN)	εy B	εD2 B	εx B	εD1 B	εy A	εD1 A	εx A	εD2 A	Top
	I	II	III	IV	V	VI	VII	VIII	IX
0	0.00000	0.00000	0.00000	0.00000	0.00000	0.00000	0.00000	0.00000	0.00000
150	0.00003	-0.00002	0.00002	0.00002	0.00001	0.00002	0.00002	-0.00004	-0.00007
300	0.00000	-0.00005	0.00005	0.00012	-0.00001	0.00009	0.00004	-0.00005	-0.00030
450	0.00046	-0.00008	0.00019	0.00062	0.00006	0.00236	-0.00004	-0.00013	-0.00044
500	0.00160	-0.00027	0.00112	0.00217	0.00140	0.00308	0.00000	-0.00027	-0.00061
700	0.00221	-0.00037	0.00158	0.00296	0.00192	0.00345	0.00008	-0.00036	-0.00071
750	0.00247	-0.00040	0.00177	0.00315	0.00219	0.00365	0.00012	-0.00040	-0.00076
860	0.00321	-0.00054	0.00223	0.00417	0.00283	0.00411	0.00019	-0.00050	-0.00088
900	0.00349	-0.00057	0.00240	0.00451	0.00306	0.00430	0.00024	-0.00055	-0.00092
1000	0.00416	-0.00067	0.00291	0.00536	0.00366	0.00492	0.00043	-0.00061	-0.00100
1020	0.00438	-0.00070	0.00307	0.00568	0.00388	0.00518	0.00053	-0.00064	-0.00102
1100	0.00509	-0.00079	0.00362	0.00661	0.00470	0.00656	0.00152	-0.00072	-0.00111
1200	0.00616	-0.00092	0.00446	0.00810	0.00633	0.00920	0.00342	-0.00097	-0.00119

A.2 Specimen MS1-2

Table A-5 Deflections and important observations at different load stages for specimen MS1-2

Load (kN)	Deflection (mm)	Event
271	0.44	First flexural crack
410	0.96	First diagonal strut crack side A
456	1.06	First diagonal strut crack side B
1938	9.01	Yielding of the first layer of the main tension reinforcement
2124	12.83	Yielding of the second layer of the main tension reinforcement
2142	14.90	Maximum load

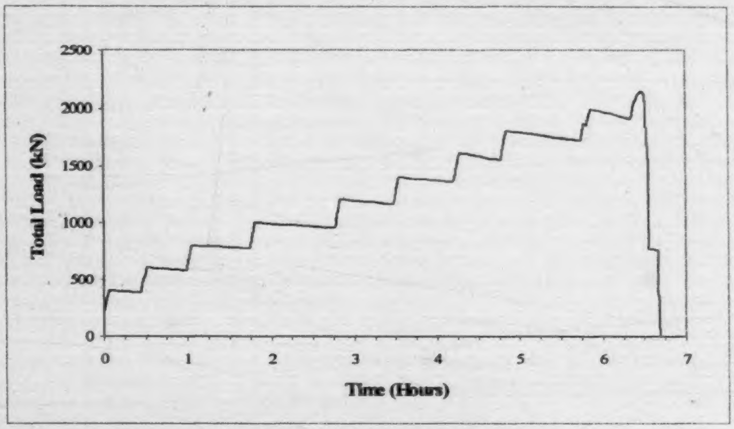

Figure A-12 Load-time response of specimen MS1-2

Table A-6 Flexural and diagonal crack widths at different loading stages of specimen MS1-2

Total Load MS1-2	Maximum flexural crack width (mm)	distance to midspan (mm)	Diagonal crack width at A (mm)	Diagonal crack width at B (mm)
200	0		0	0
271	First flexural crack			
400	0.1	100	0	0
410	First diagonal strut crack side A			
456	First diagonal strut crack side B			
600	0.25	100	0.15	0.15
800	0.30	100	0.33	0.30
1000	0.60	690	0.50	0.60
1200	0.80	690	0.80	0.80
1400	1.00	690	1.00	1.00
1600	1.00	690	1.00	1.25
1800	1.00	690	1.25	1.25
2000	1.25	690	1.5	1.5
2142	Maximum load			

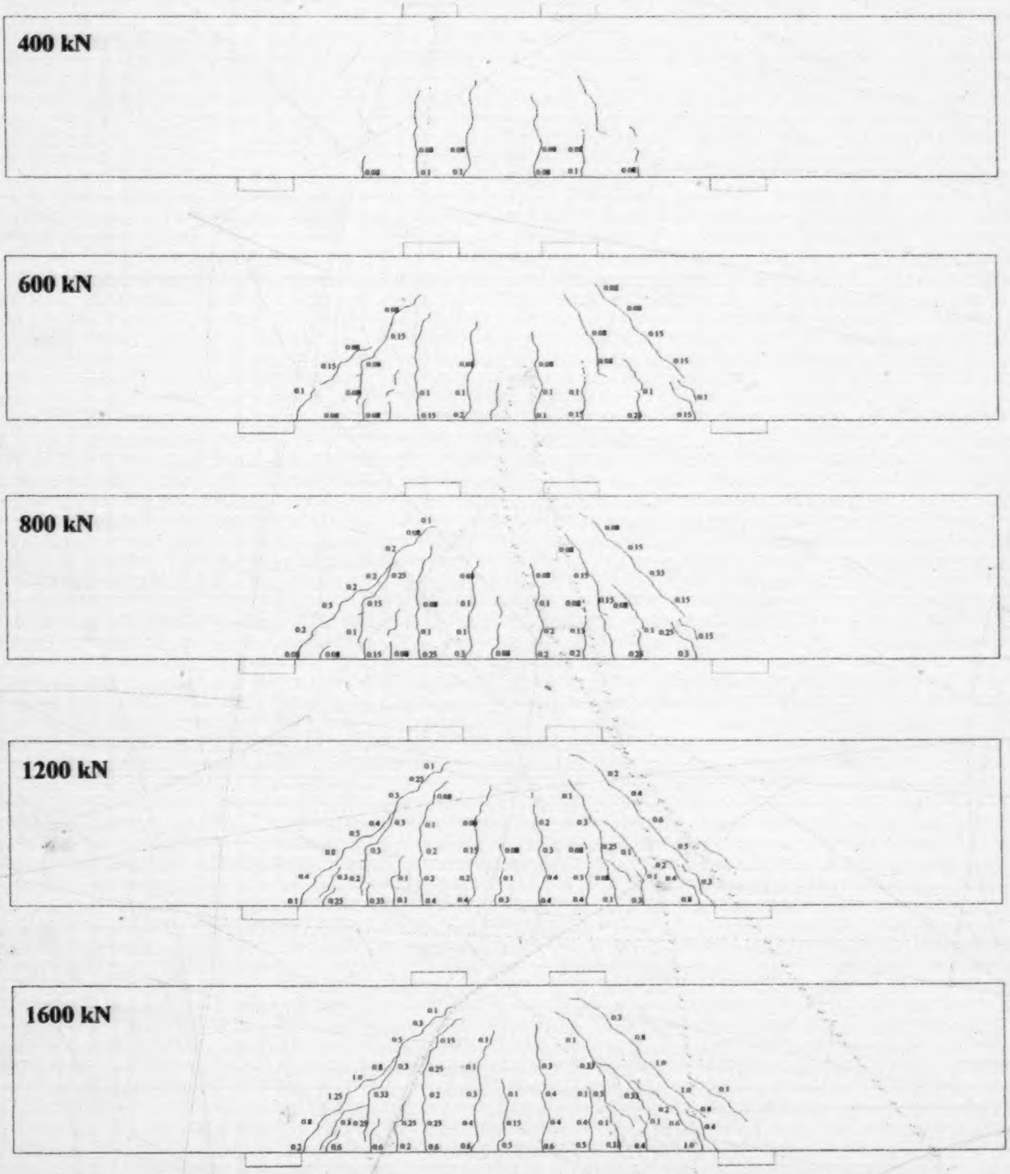

Figure A-13 Crack patterns at different loading stages from 400 kN to 1600 kN of specimen MS1-2

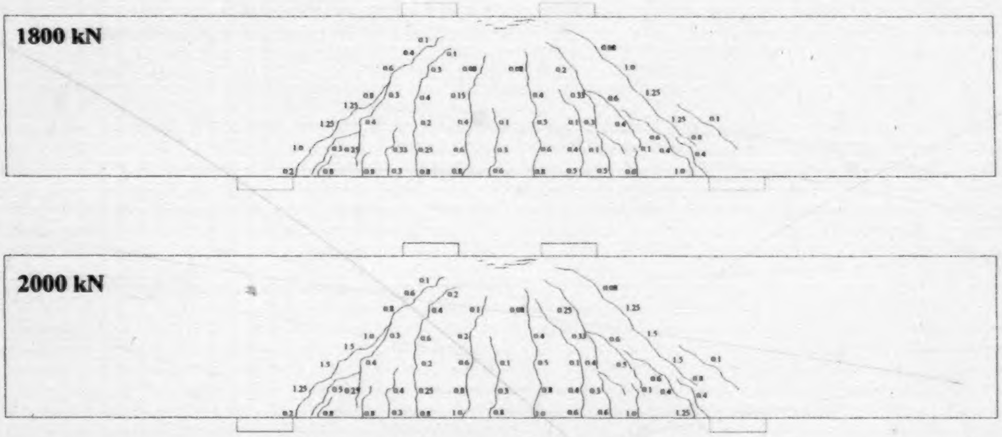

Figure A-14 Crack patterns at 1800 kN and 2000 kN for specimen MS1-2

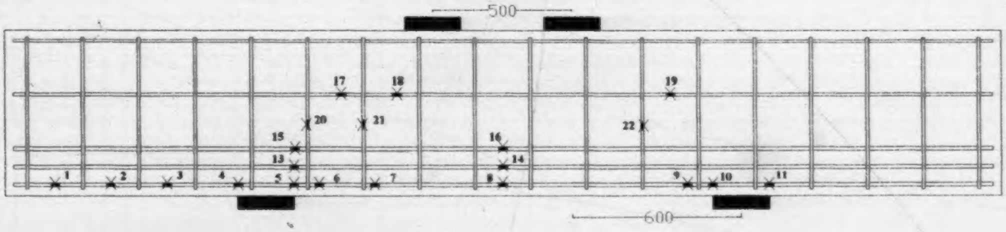

Figure A-15 Strain gages locations of specimen MS1-2

Table A-7 Location of strain gauges for specimen MS1-2

Strain Gauge	Distance from midspan (mm)	side	Strain Gauge	Distance from midspan (mm)	side
1	1600	A	12	0	
2	1400	A	13	750	A
3	1200	A	14	0	
4	950	A	15	750	A
5	750	A	16	0	
6	660	A	17	600	A
7	460	A	18	400	A
8	0		19	600	B
9	660	B	20	stirrup	A
10	750	B	21	stirrup	A
11	950	B	22	stirrup	B

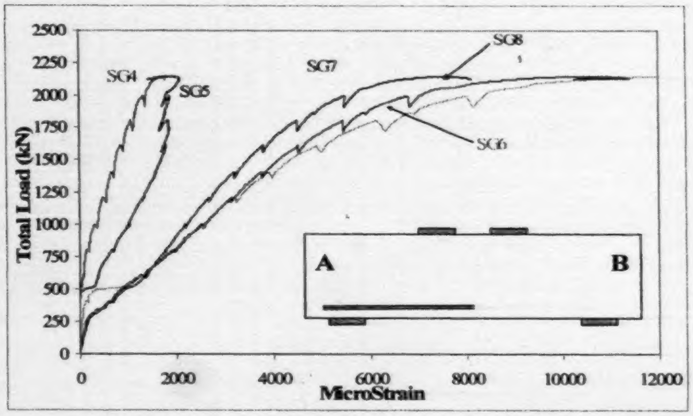

Figure A-16 Strains at a bar located in the lowest layer of main tension reinforcement of specimen MS1-2

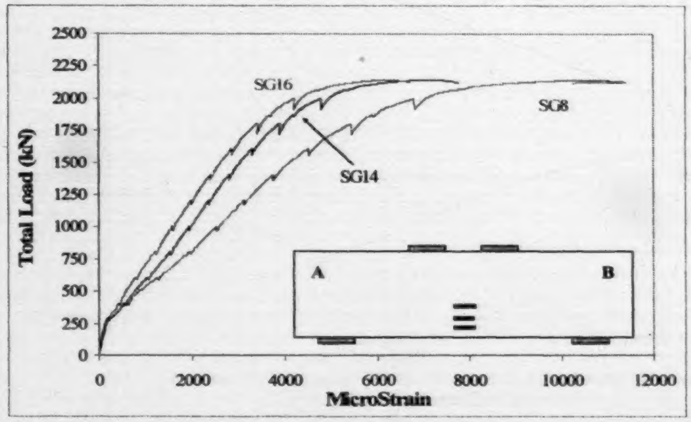

Figure A-17 Strains at midspan of the three layers of main tension reinforcement in specimen MS1-2

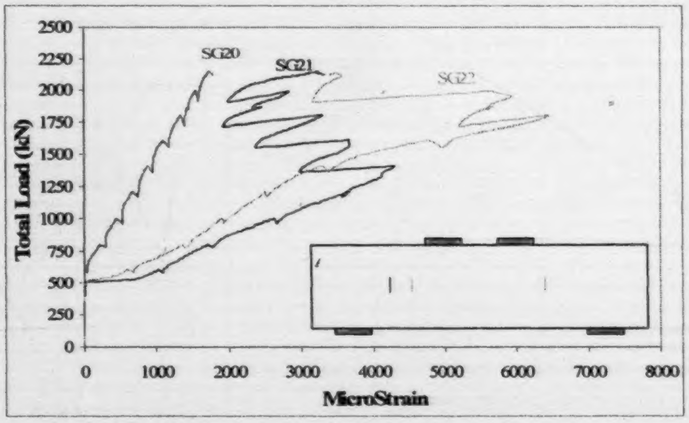

Figure A-18 Strains of stirrups located in the shear spans of specimen MS1-2

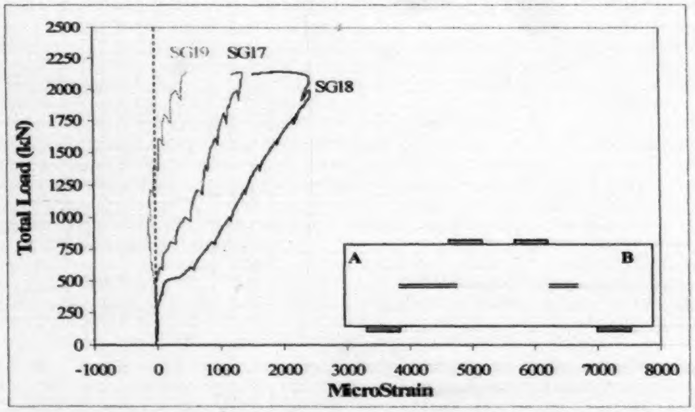

Figure A-19 Strains on the horizontal web reinforcement of specimen MS1-2

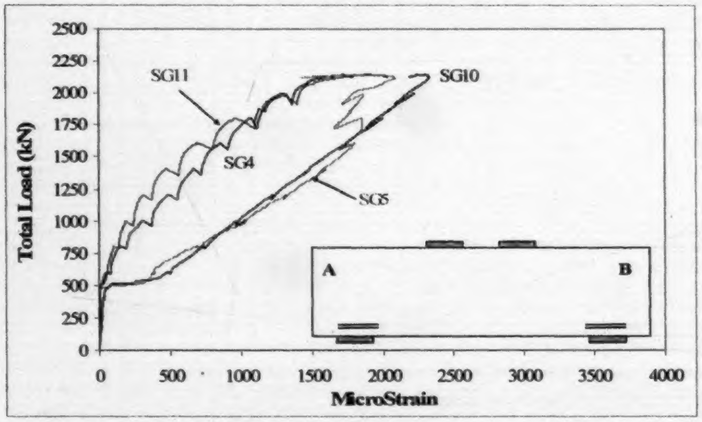

Figure A-20 Strains at the interior and exterior edges of the supports of specimen MS1-2

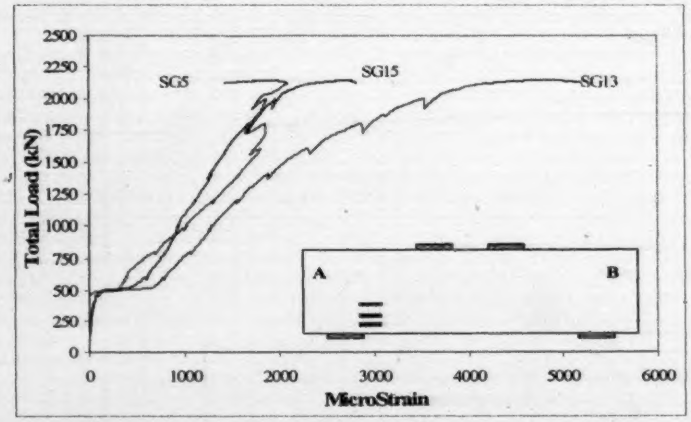

Figure A-21 Strain at the interior edge of one support for the three layers of tension reinforcement of specimen MS1-2

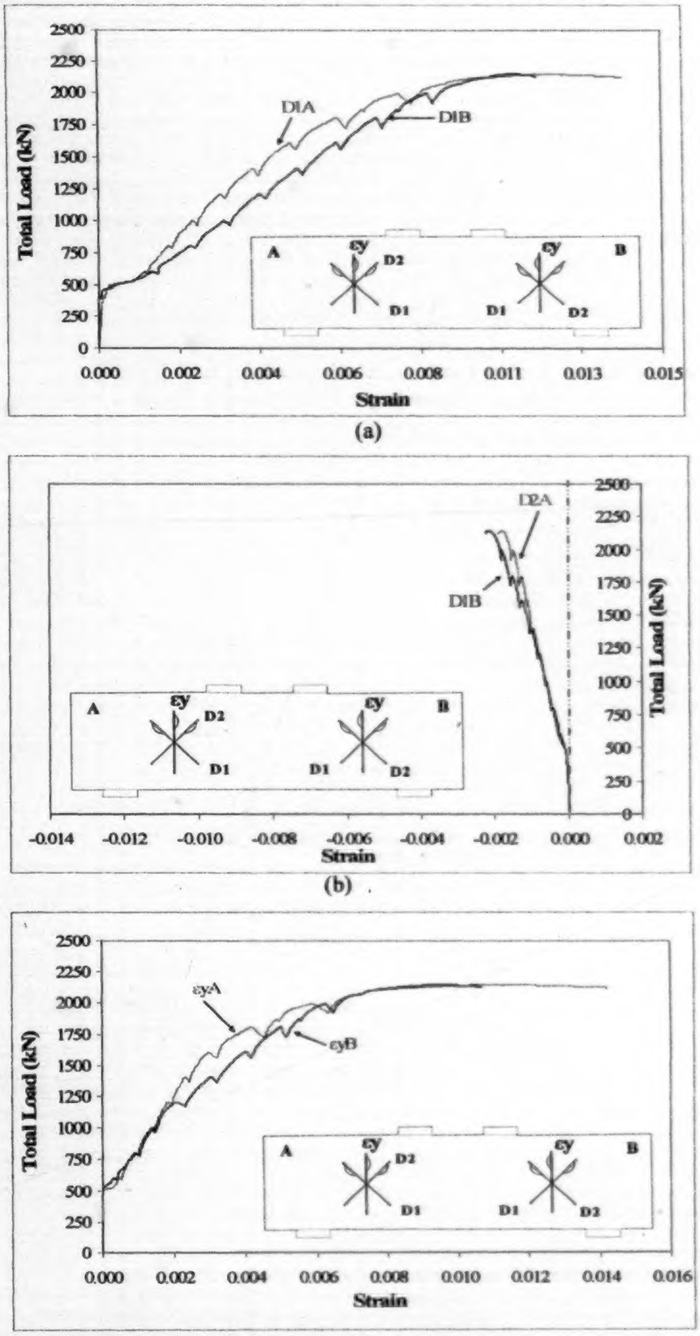

(a)

(b)

(c)

Figure A-22 Average Strains in the (a) diagonal strain D1, (b) diagonal strain D2 and (c) vertical strain of specimen MS1-2

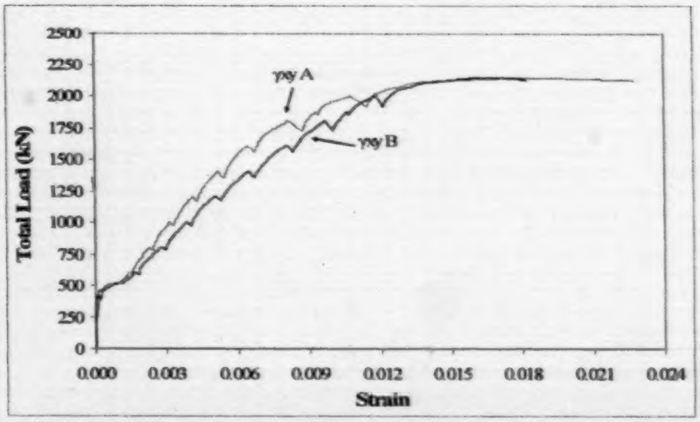

Figure A-23 Maximum shear strain in diagonal struts of specimen MS1-2

Table A-8 Concrete strains at the top of the specimen at last two manual readings

LOAD (kN)	ε_y B	ε_{D2} B	ε_x B	ε_{D1} B	ε_y A	ε_{D1} A	ε_x A	ε_{D2} A	Top
	I	II	III	IV	V	VI	VII	VIII	IX
0	0.0000	0.0000	0.0000	0.0000	0.0000	0.0000	0.0000	0.0000	0.0000
200	0.0000	-0.0001	0.0000	0.0001	0.0000	0.0000	0.0000	0.0000	-0.0001
400	0.0000	-0.0001	0.0001	0.0002	0.0000	0.0001	0.0000	-0.0001	-0.0003
600	0.0011	-0.0003	-0.0001	0.0025	0.0013	0.0018	0.0010	-0.0003	-0.0006
800	0.0021	-0.0004	-0.0001	0.0041	0.0021	0.0028	0.0016	-0.0004	-0.0008
1000	0.0024	-0.0006	0.0000	0.0054	0.0031	0.0039	0.0021	-0.0006	-0.0009
1200	0.0036	-0.0008	0.0001	0.0069	0.0040	0.0050	0.0025	-0.0008	-0.0012
1400	0.0046	-0.0011	0.0001	0.0085	0.0050	0.0062	0.0028	-0.0010	-0.0014
1600	0.0058	-0.0014	0.0002	0.0102	0.0061	0.0077	0.0034	-0.0013	-0.0017
1800	0.0073	-0.0016	0.0020	0.0122	0.0076	0.0094	0.0040	-0.0015	-0.0020
1870	0.0079	-0.0018	0.0026	0.0132	0.0086	0.0105	0.0043	-0.0014	-0.0022
2000	0.0089	-0.0019	0.0035	0.0146	0.0101	0.0121	0.0047	-0.0015	-0.0025

A.3 Specimen MS1-3

Table A-9 Loads and deflections at important events during the test of specimen MS1-3

Load (kN)	Deflection (mm)	Event
389	0.81	First flexural crack
640	1.23	First diagonal strut crack side B
688	1.32	First diagonal strut crack side A
2747	7.86	Maximum load

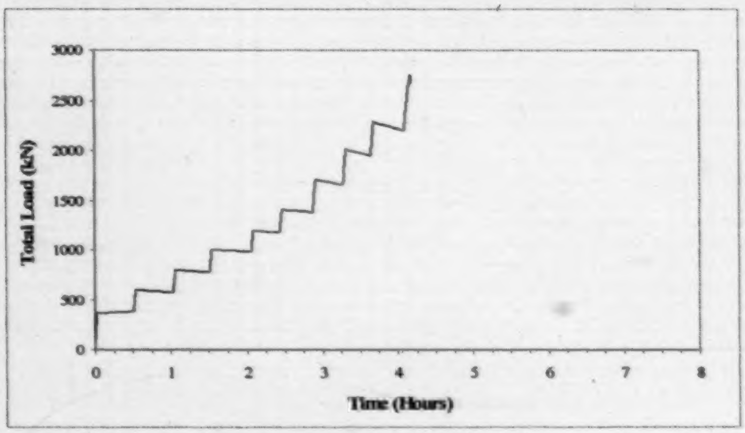

Figure A-24 Load-time response of specimen MS1-3

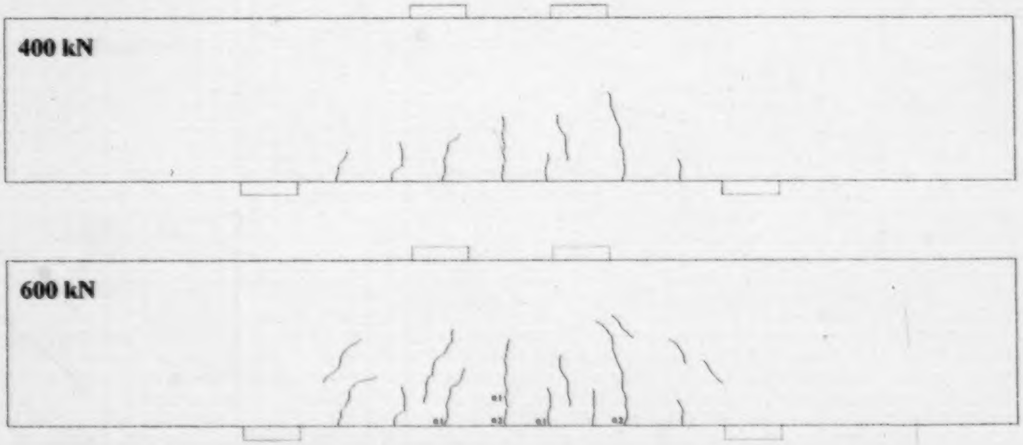

Figure A-25 Crack patterns at 400 kN and 800 kN of specimen MS1-3

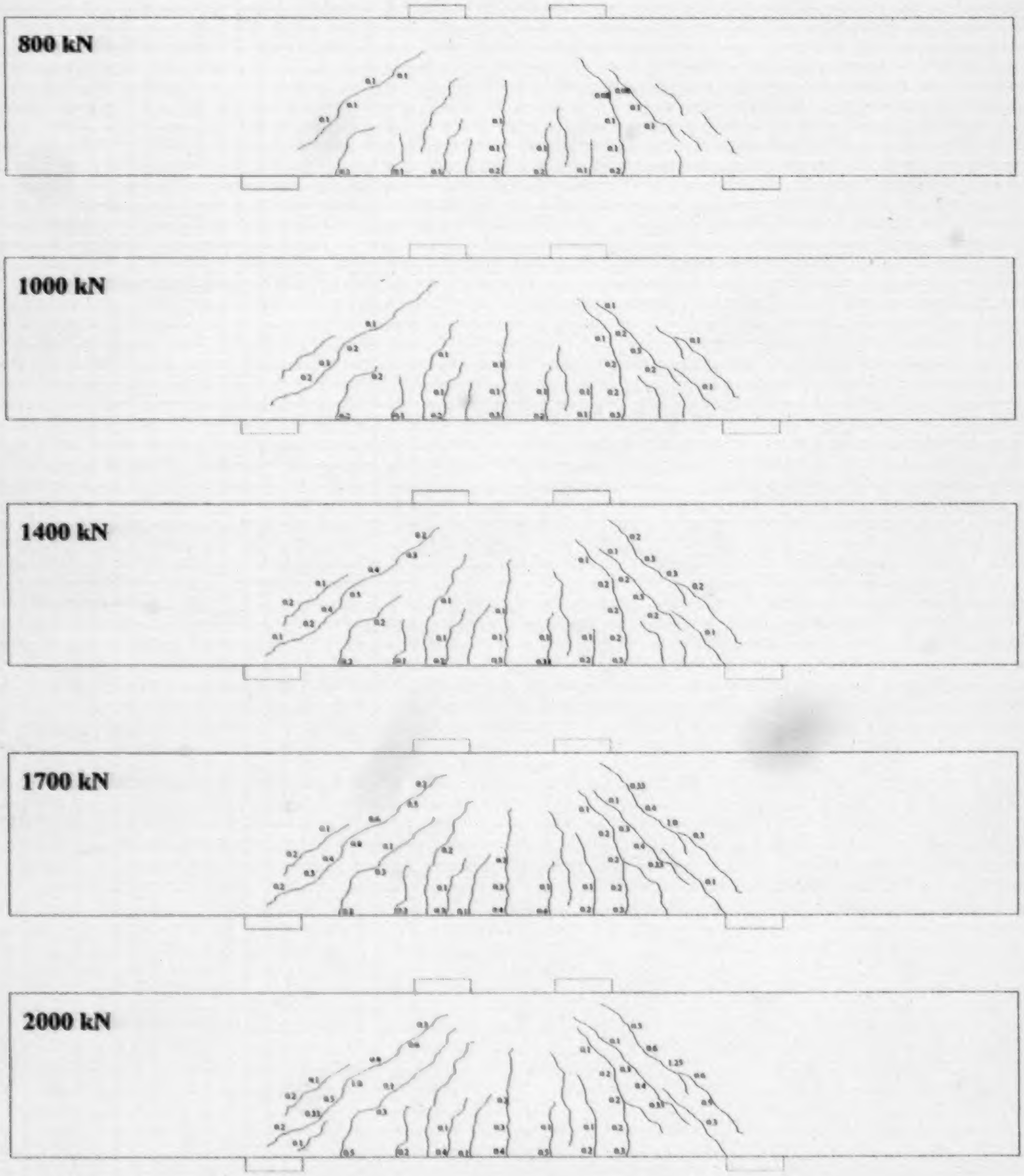

Figure A-26 Crack patterns at different loading stages from 800 kN to 2000 kN of specimen MS1-3

Table A-10 Flexural and diagonal crack widths at different loading stages of specimen MS1-3

Load MS1-3	Deflection (mm)	Maximum flexural crack width (mm)	distance to midspan (mm)	Diagonal crack width at A (mm)	Diagonal crack width at B (mm)
200	0.49	0		0	0
389	0.81	First flexural crack			
400	0.81	<0.08	0	0	0
600	1.12	0.20	0	<0.08	<0.08
640	1.23	First diagonal strut crack side B			
688	1.32	First diagonal strut crack side A			
800	1.78	0.20	0	0.10	0.10
1000	2.20	0.30	0	0.30	0.20
1200	2.95	0.30	0	0.33	0.30
1400	3.26	0.33	140	0.40	0.50
1700	3.42	0.40	0	1.00	0.80
2000	4.17	0.50	140	1.25	1.00
2300	5.55	0.50	140	1.25	1.25
2747	7.86	Maximum load			

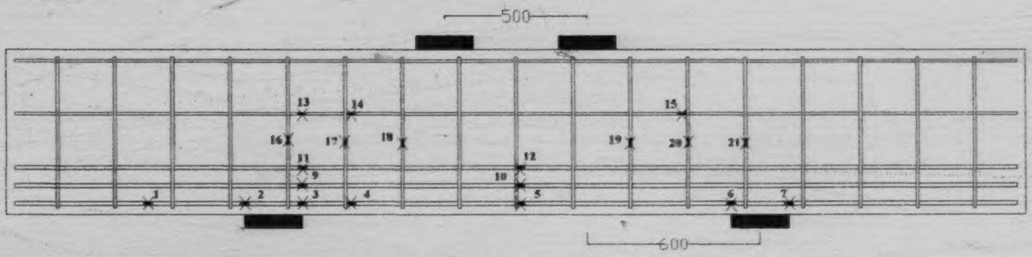

Figure A-27 Strain gages locations of specimen MS1-3

Table A-11 Location of strain gauges for specimen MS1-3

Strain Gauge	Distance from midspan (mm)	side	Strain Gauge	Distance from midspan (mm)	side
1	1285	A	12	0	
2	950	A	13	750	A
3	750	A	14	600	A
4	580	A	15	600	B
5	0		16	stirrup	A
6	750	B	17	stirrup	A
7	950	B	18	stirrup	A
8	0		19	stirrup	B
9	750	A	20	stirrup	B
10	0		21	stirrup	B
11	750	A			

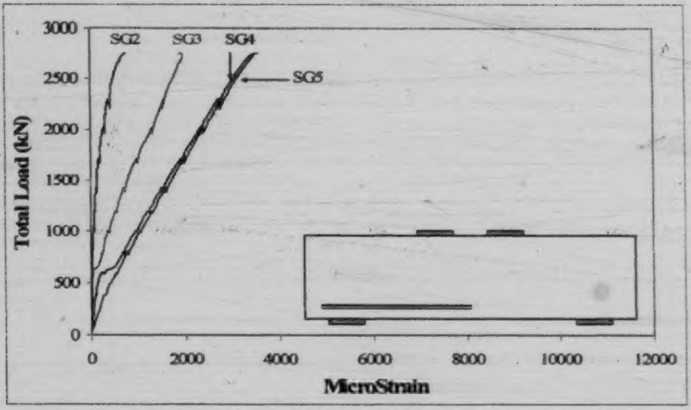

Figure A-28 Strains at a bar located in the lowest layer of main tension reinforcement of specimen MS1-3

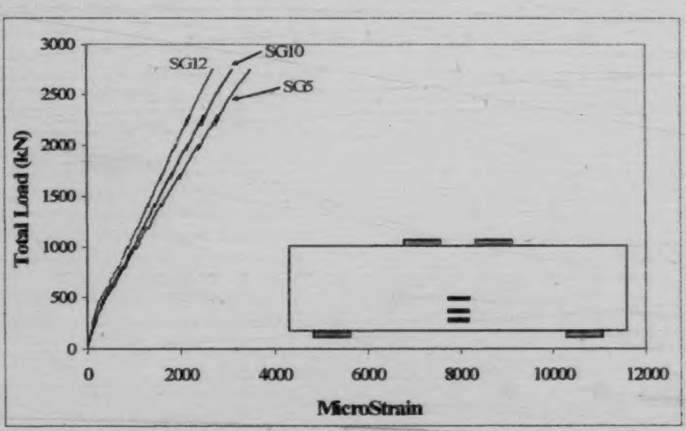

Figure A-29 Strains at midspan of the three layers of main tension reinforcement in specimen MS1-3

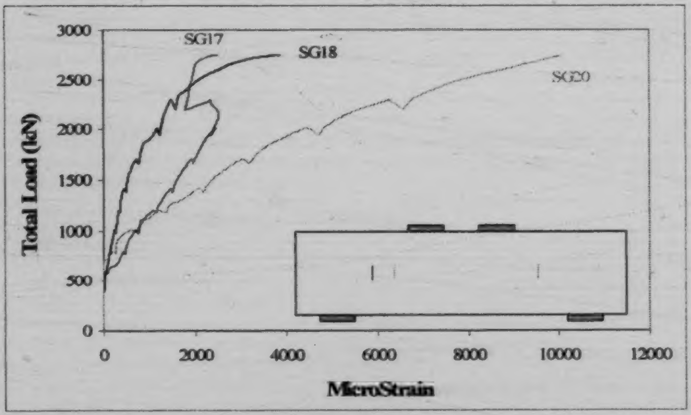

Figure A-30 Strains of stirrups located in the shear spans of specimen MS1-3

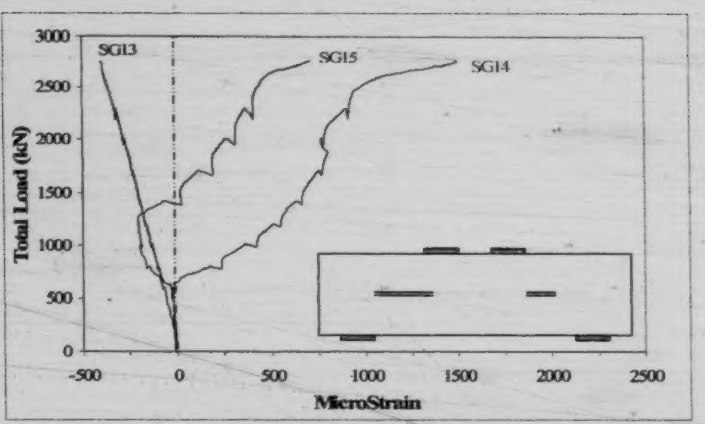

Figure A-31 Strains on the horizontal web reinforcement of specimen MS1-3

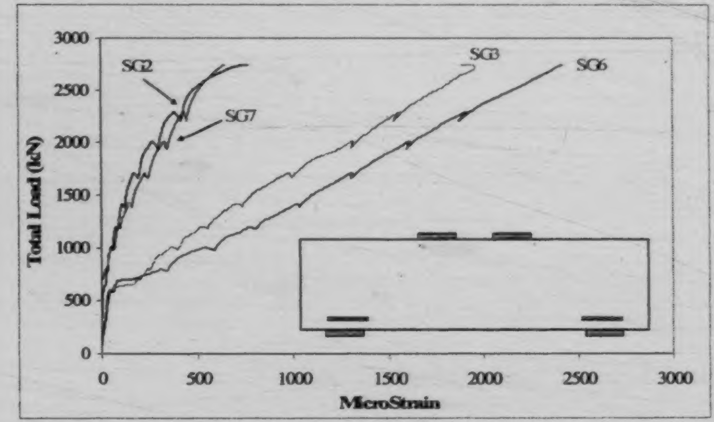

Figure A-32 Strains at the interior and exterior edges of the supports of specimen MS1-3

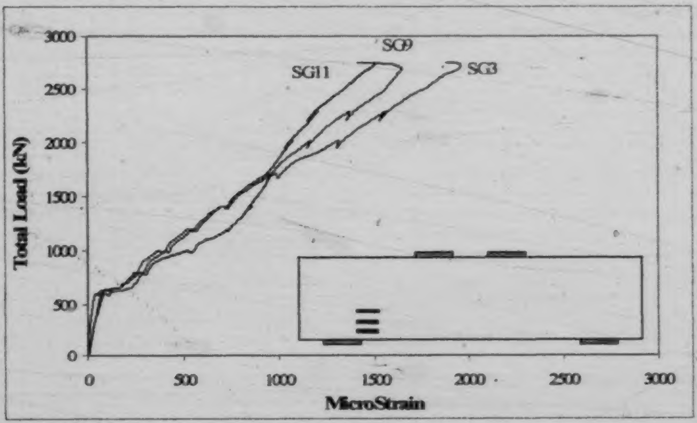

Figure A-33 Strain at the interior edge of one support for the three layers of tension reinforcement of specimen MS1-3

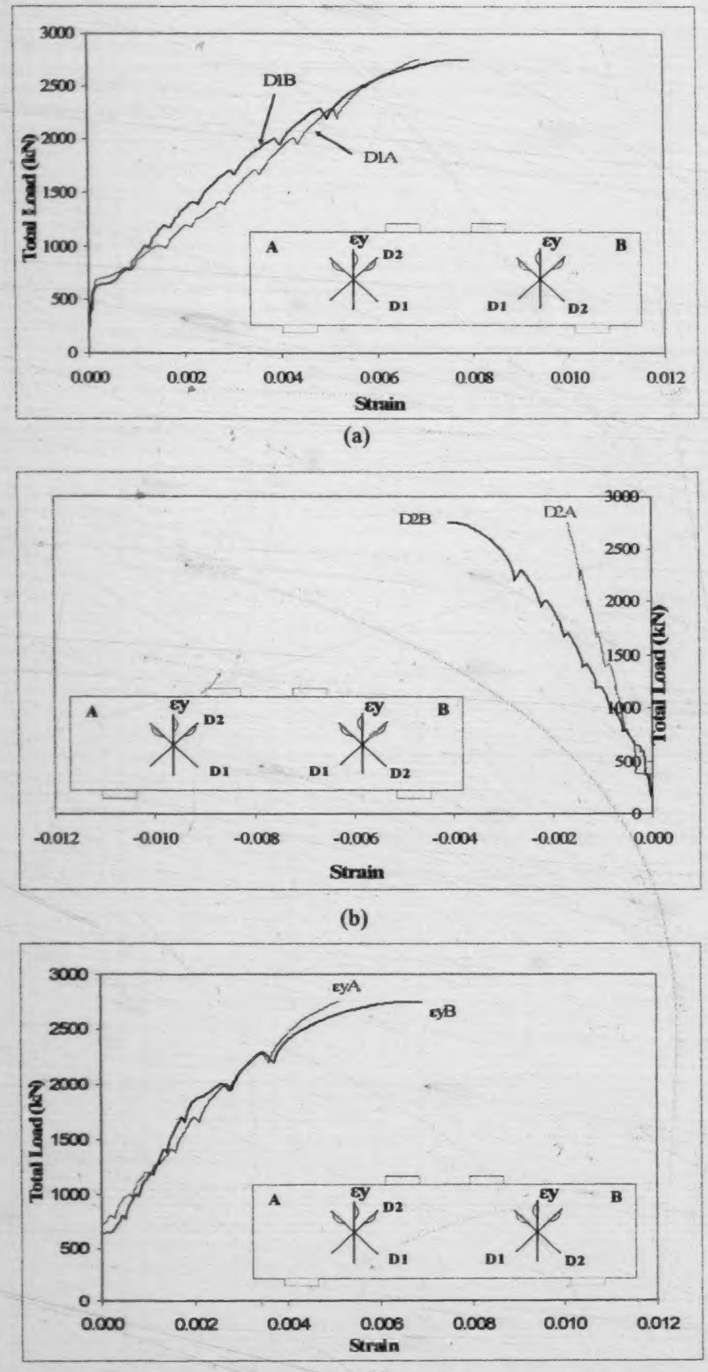

(a)

(b)

(c)

Figure A-34 Average Strains in the (a) diagonal strain D1, (b) diagonal strain D2 and (c) vertical strain of specimen MS1-3

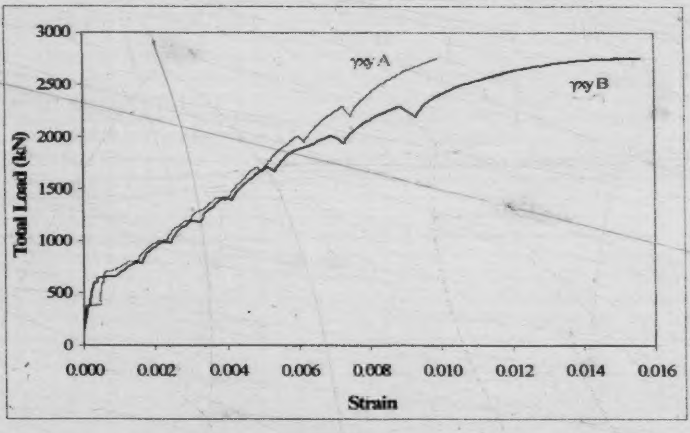

Figure A-35 Maximum shear strain in diagonal struts of specimen MS1-3

Table A-12 Strains monitored by demec gages rosettes for specimen MS1-3

LOAD (kN)	εy B	εD2 B	εx B	εD1 B	εy A	εD1 A	εx A	εD2 A	Top
	I	II	III	IV	V	VI	VII	VIII	IX
0	0.00000	0.00000	0.00000	0.00000	0.00000	0.00000	0.00000	0.00000	0.00000
200	0.00000	-0.00006	-0.00001	0.00004	-0.00001	0.00004	0.00002	-0.00004	-0.00016
400	-0.00001	-0.00012	0.00001	0.00008	-0.00002	0.00008	0.00000	-0.00014	-0.00030
600	0.00005	-0.00014	0.00005	0.00019	0.00000	0.00014	-0.00001	-0.00019	-0.00047
800	-0.00011	-0.00034	0.00091	0.00174	-0.00011	0.00147	-0.00010	-0.00026	-0.00064
1000	0.00170	-0.00054	0.00133	0.00250	0.00006	0.00250	0.00000	-0.00039	-0.00083
1200	0.00217	-0.00077	0.00169	0.00309	0.00088	0.00372	0.00078	-0.00063	-0.00100
1400	0.00263	-0.00094	0.00197	0.00367	0.00163	0.00492	0.00138	-0.00095	-0.00121
1700	0.00326	-0.00123	0.00221	0.00441	0.00247	0.00634	0.00189	-0.00123	-0.00150
2000	0.00420	-0.00158	0.00248	0.00525	0.00340	0.00794	0.00237	-0.00161	-0.00184
2300	0.00565	-0.00196	0.00278	0.00640	0.00441	0.00965	0.00277	-0.00198	-0.00218

A.4 Specimen MS2-2

Table A-13 Loads and deflections at important events during the test of specimen MS1-1 MS2-2

Load (kN)	Deflection (mm)	Event
192	0.84	First flexural crack
376	2.25	First diagonal strut crack side A
387	2.33	First diagonal strut crack side B
1332	15.78	Yielding of the first layer of the main tension reinforcement
1381	17.97	Yielding of the second layer of the main tension reinforcement
1429	23.67	Yielding of the third layer of the main tension reinforcement
1432	24.62	Maximum load

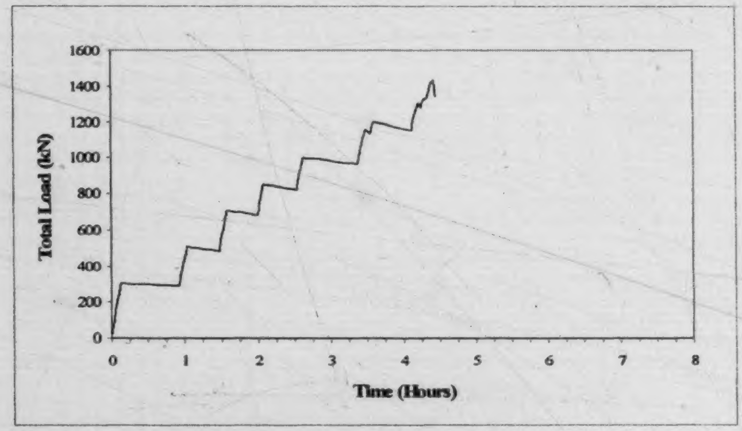

Figure A-36 Load-time response for specimen MS2-2

Table A-14 Crack width at different stages of loading for specimen MS2-2

load (kN)	Maximum flexural crack width (mm)	distance to midspan (mm)	Diagonal crack width at A (mm)	Diagonal crack width at B (mm)
192	First flexural crack			
300	0.15	100	0	0
376	First diagonal strut crack side A			
387	First diagonal strut crack side B			
500	0.33	100	0.2	0.2
700	0.60	100	0.6	0.5
850	0.80	100	0.60	0.80
1000	0.80	100	1.00	1.00
1200	1.25	100	1.25	1.25
1432	Maximum load			

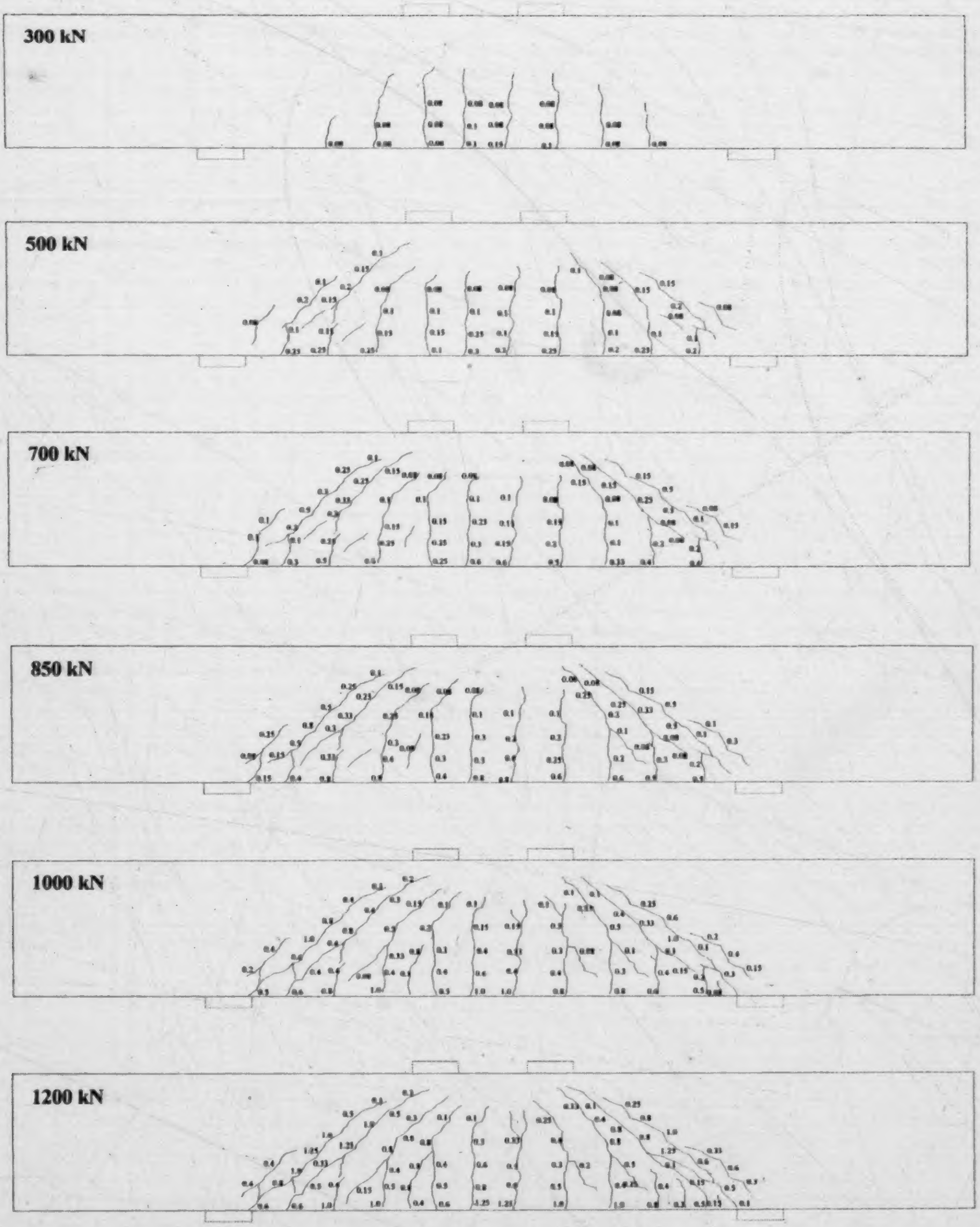

Figure A-37 Crack patterns at different loading stages of specimen MS2-2

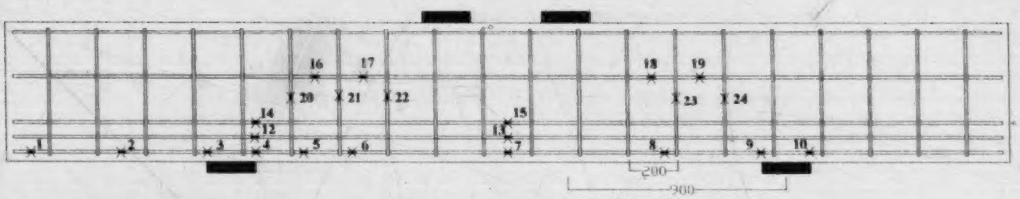

Figure A-38 Strain gages locations of specimen MS2-2

Table A-15 Location of strain gauges for specimen MS2-2

Strain Gauge	Distance from midspan (mm)	side	Strain Gauge	Distance from midspan (mm)	side
1	1940	A	13	0	
2	1600	A	14	1050	A
3	1250	A	15	0	
4	1050	A	16	800	A
5	850	A	17	600	A
6	650	A	18	600	B
7	0		19	800	B
8	650	B	20	stirrup	A
9	1050	B	21	stirrup	A
10	1250	B	22	stirrup	A
11	0		23	stirrup	B
12	1050	A	24	stirrup	B

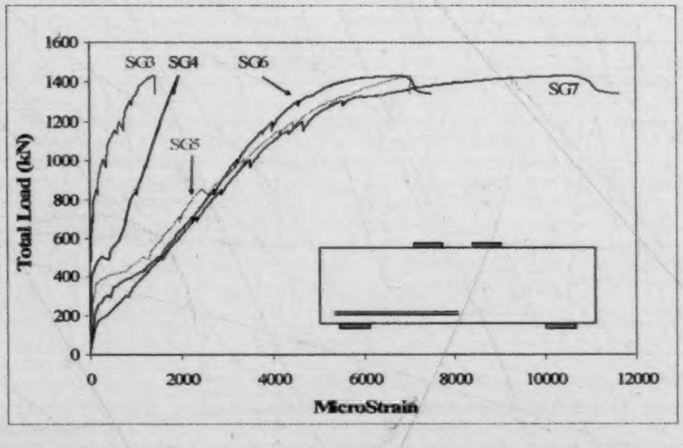

Figure A-39 Strains at a bar located in the lowest layer of main tension reinforcement of specimen MS2-2

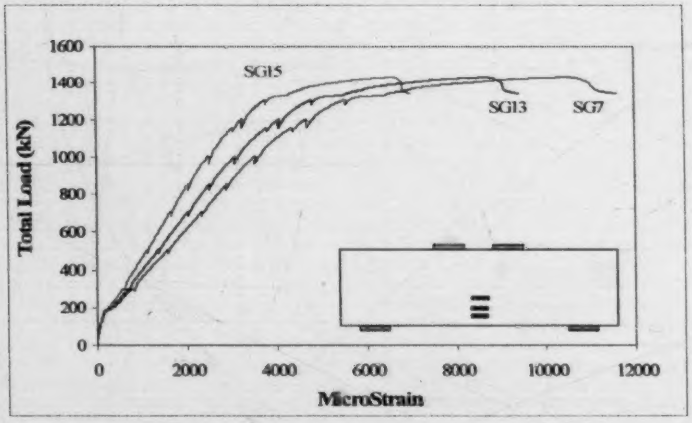

Figure A-40 Strains at midspan of the three layers of main tension reinforcement in specimen MS2-2

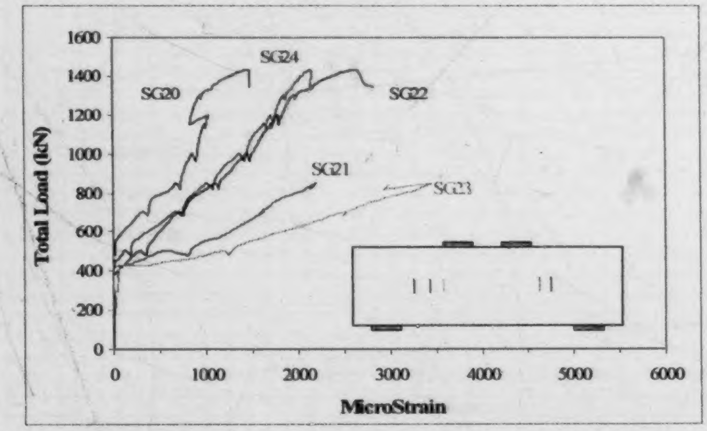

Figure A-41 Strains of stirrups located in the shear spans of specimen MS2-2

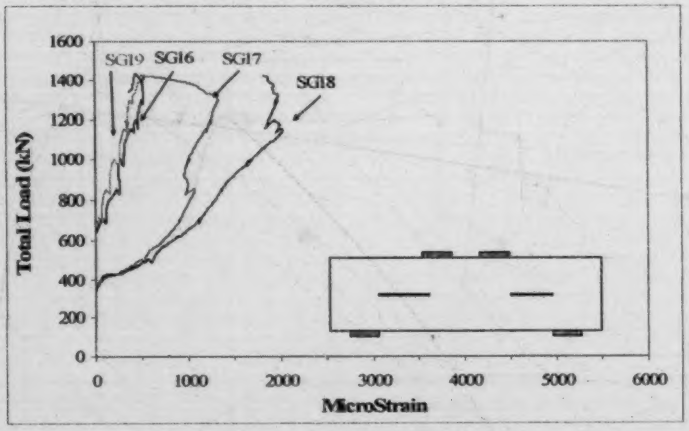

Figure A-42 Strains on the horizontal web reinforcement of specimen MS2-2

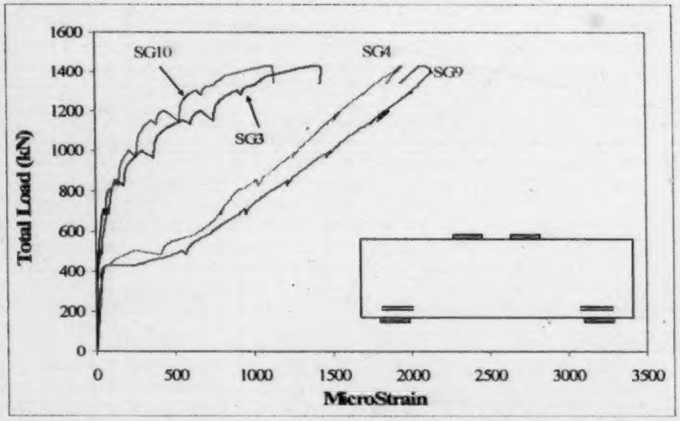

Figure A-43 Strains at the interior and exterior edges of the supports of specimen MS2-2

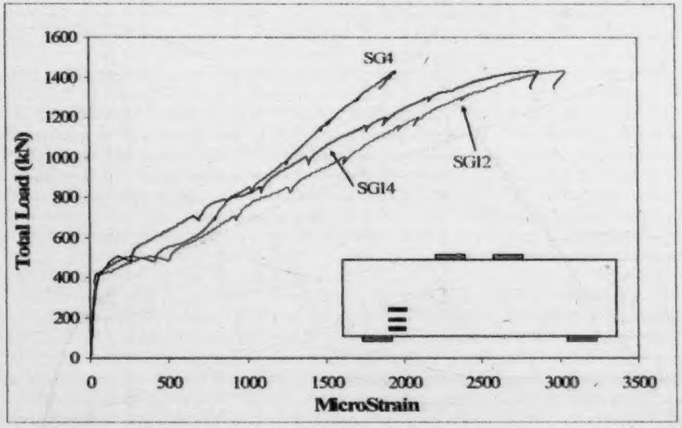

Figure A-44 Strain at the interior edge of one support for the three layers of tension reinforcement of specimen MS2-2

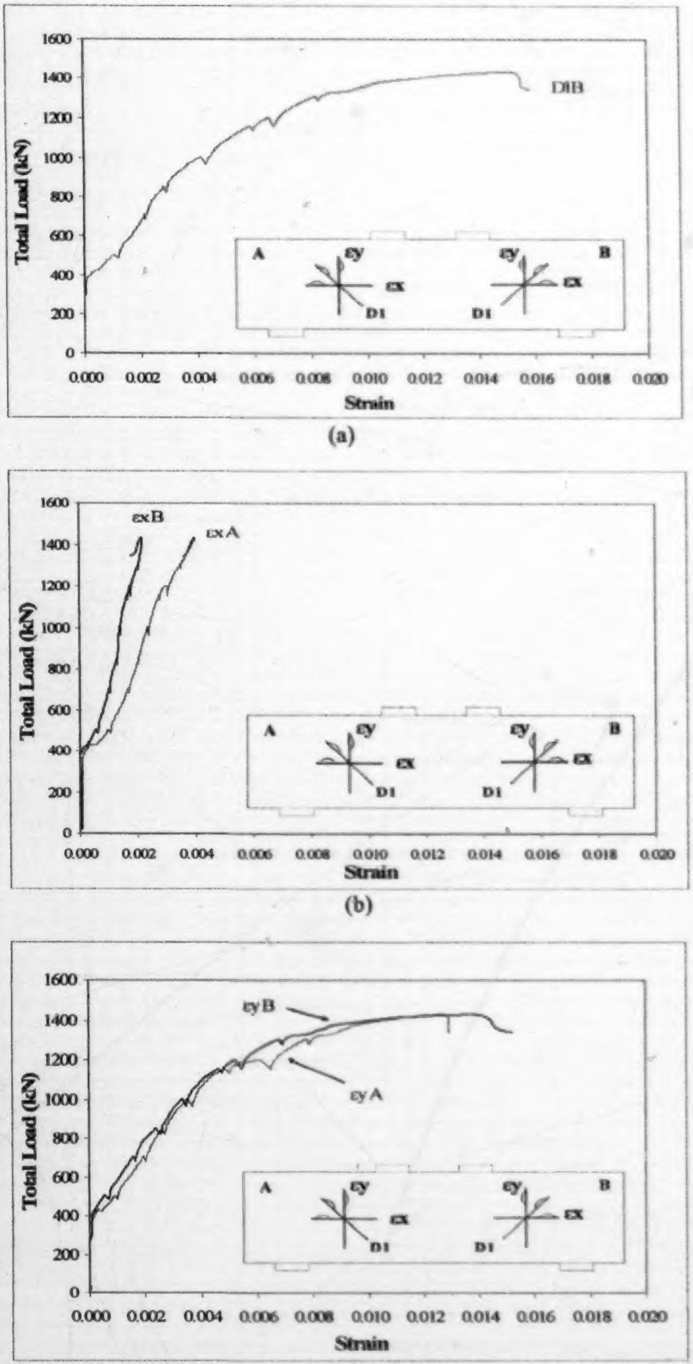

(a)

(b)

(c)

Figure A-45 Average Strains in the (a) diagonal strain D1, (b) horizontal strain and (c) vertical strain of specimen MS2-2

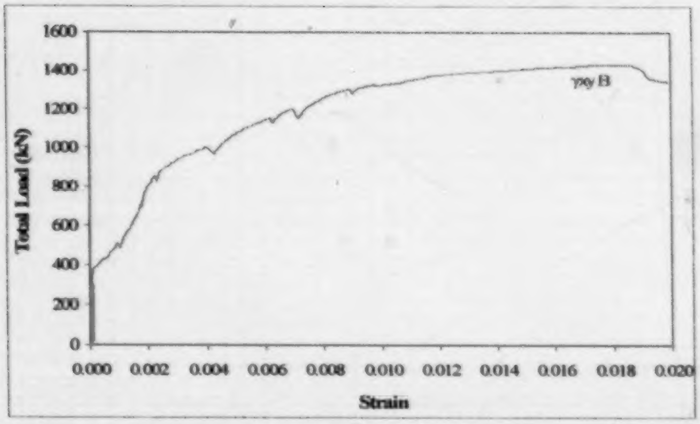

Figure A-46 Maximum shear strain in diagonal struts of specimen MS2-2

Table A-16 Concrete strains at the top of the specimen at last two manual readings

LOAD (kN)	εy B	εD2 B	εx B	εD1 B	εy A	εD1 A	εx A	εD2 A	Top
	I	II	III	IV	V	VI	VII	VIII	IX
0	0.00000	0.00000	0.00000	0.00000	0.00000	0.00000	0.00000	0.00000	0.00000
300	0.00002	-0.00006	0.00005	0.00012	0.00006	0.00012	0.00006	-0.00002	-0.00036
500	0.00095	-0.00017	0.00054	0.00311	0.00142	0.00246	0.00163	-0.00007	-0.00062
700	0.00255	-0.00026	0.00140	0.00600	0.00290	0.00463	0.00268	-0.00020	-0.00096
850	0.00355	-0.00030	0.00179	0.00839	0.00363	0.00597	0.00310	-0.00026	-0.00121
1000	0.00519	-0.00039	0.00207	0.01088	0.00471	0.00720	0.00343	-0.00034	-0.00154
1150	0.00754	-0.00049	0.00257	0.01436	0.00665	0.00936	0.00390	-0.00050	-0.00193
1200	0.00857	-0.00054	0.00277	0.01582	0.00884	0.01145	0.00451	-0.00065	-0.00208
1400	0.01131	-0.00066	0.00321	0.01129	0.01153	0.01141	0.00526	-0.00080	-0.00255

A.5 Specimen MS2-3

Table A-17 Deflections and important observations at different load stages for specimen MS2-3

load (kN)	Deflection (mm)	Observations
293	0.90	First flexural crack
560	2.13	First diagonal strut crack side A
580	2.29	First diagonal strut crack side B
2055	12.49	Maximum load

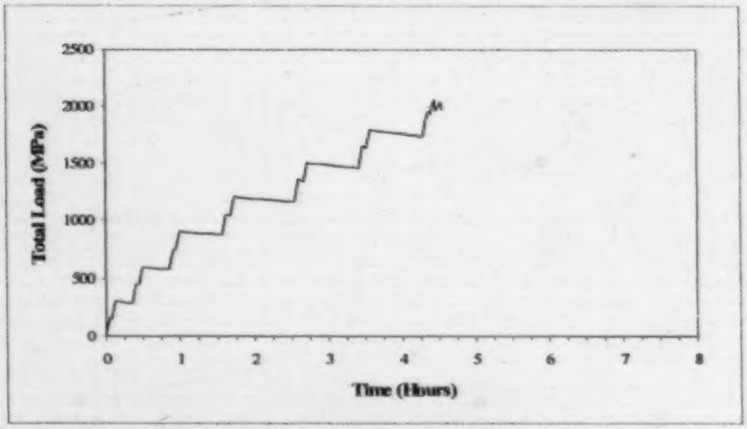

Figure A-47 Load-time response of specimen MS2-3

Table A-18 Crack width at different stages of loading for specimen MS2-3

load (kN)	Maximum flexural crack width (mm)	distance to midspan (mm)	Diagonal crack width at A (mm)	Diagonal crack width at B (mm)
293	First flexural crack			
300	0.08	100	0	0
560	First diagonal strut crack side A			
580	First diagonal strut crack side B			
600	0.2	100	0.1	0.1
900	0.33	100	0.4	0.4
1200	0.50	100	0.60	0.50
1500	0.60	100	0.80	0.80
1800	0.80	100	1.25	1.00
2055	Maximum load			

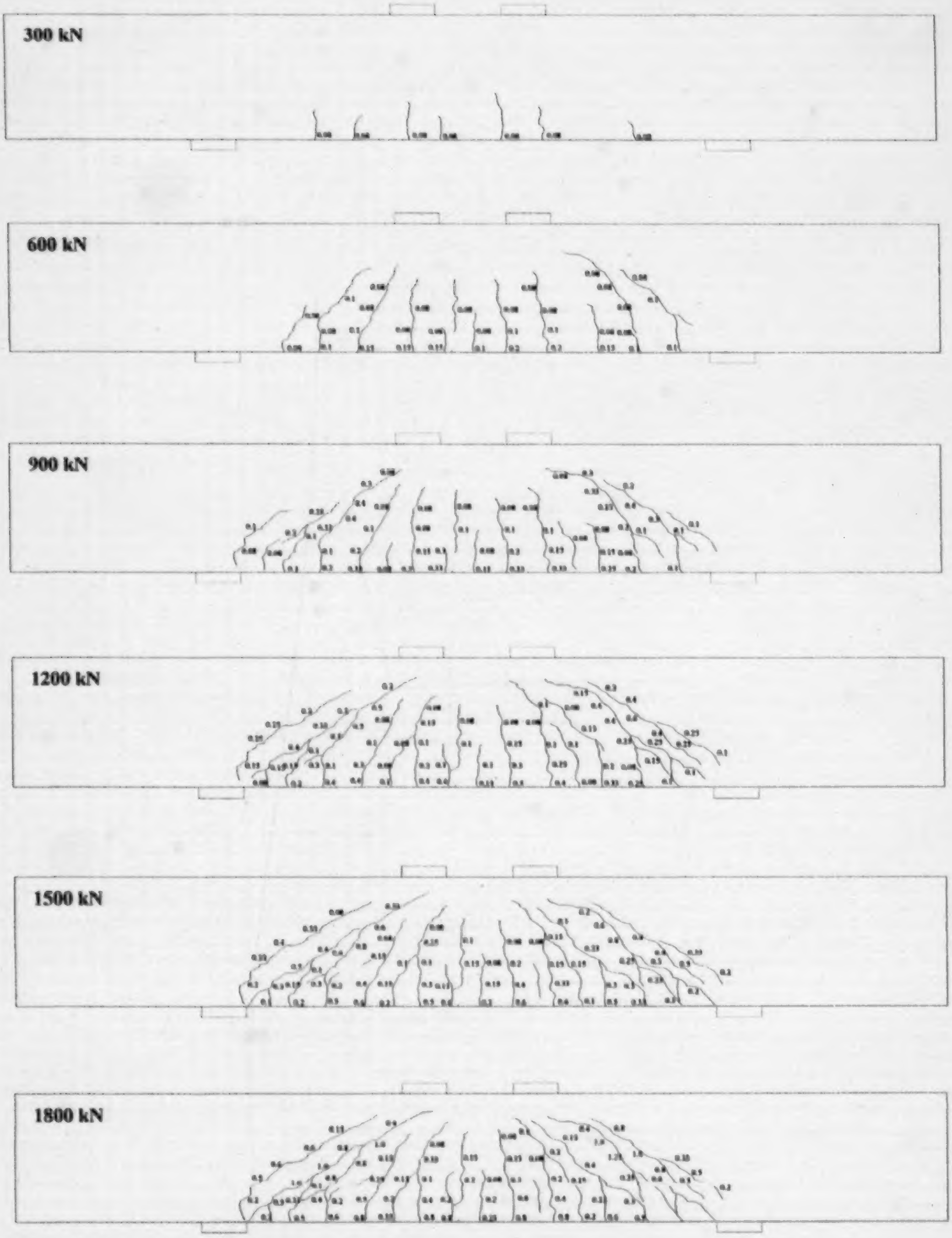

Figure A-48 Crack patterns at different loading stages of specimen MS2-3

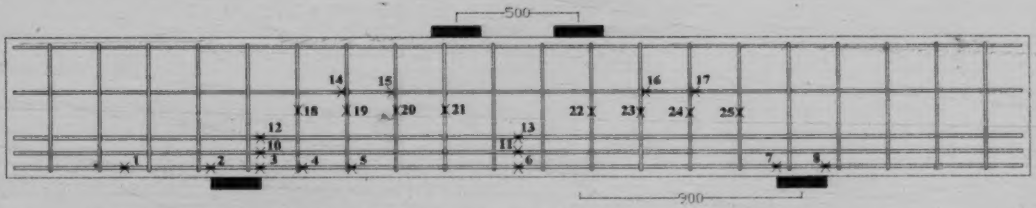

Figure A-49 Strain gages locations of specimen MS2-3

Table A-19 Location of strain gauges for specimen MS2-3

Strain Gauge	Distance from midspan (mm)	side	Strain Gauge	Distance from midspan (mm)	side
1	1600	A	14	720	A
2	1250	A	15	520	A
3	1050	A	16	520	B
4	880	A	17	720	B
5	680	A	18	stirrup	A
6	0		19	stirrup	A
7	1050	B	20	stirrup	A
8	1250	B	21	stirrup	A
9	0		22	stirrup	B
10	1050	A	23	stirrup	B
11	0		24	stirrup	B
12	1050	A	25	stirrup	B
13	0				

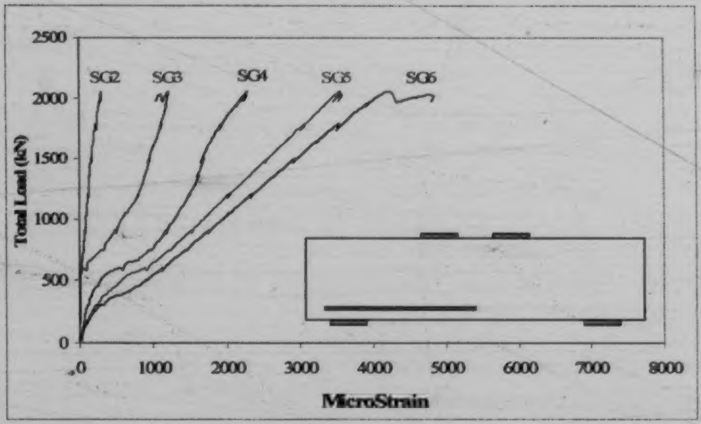

Figure A-50 Strains at a bar located in the lowest layer of main tension reinforcement of specimen MS2-3

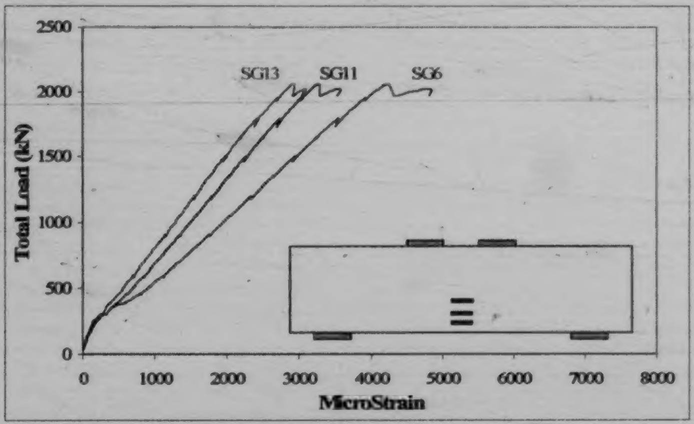

Figure A-51 Strains at midspan of the three layers of main tension reinforcement in specimen MS2-3

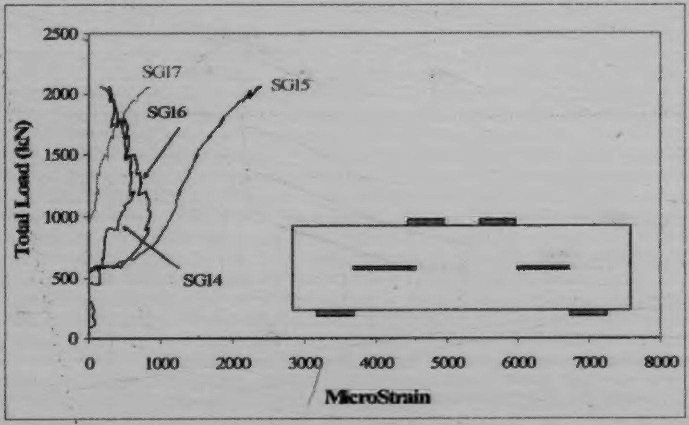

Figure A-52 Strains on the horizontal web reinforcement of specimen MS2-3

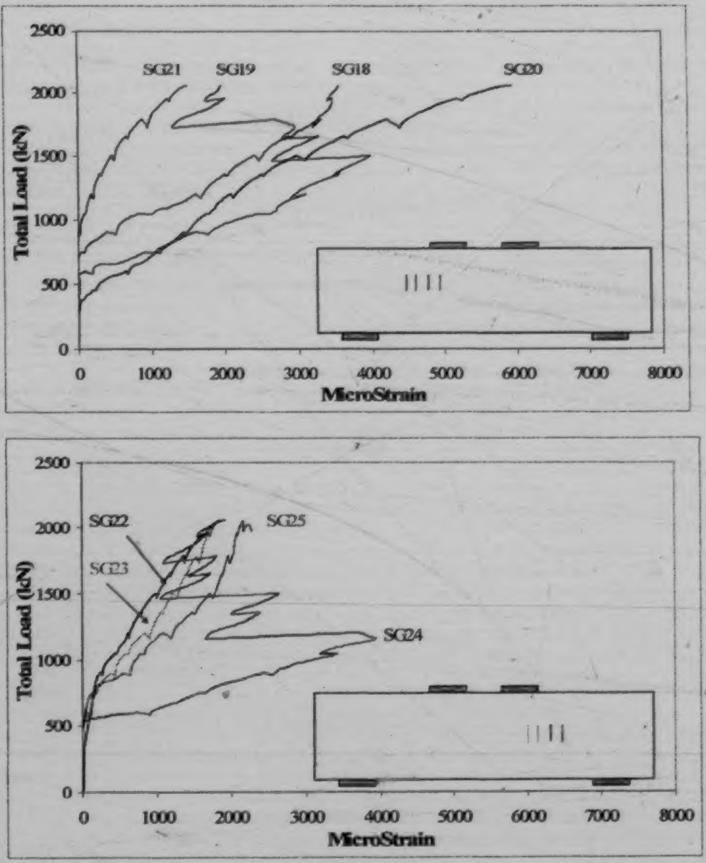

Figure A-53 Strains of stirrups located in the shear spans of specimen MS2-3

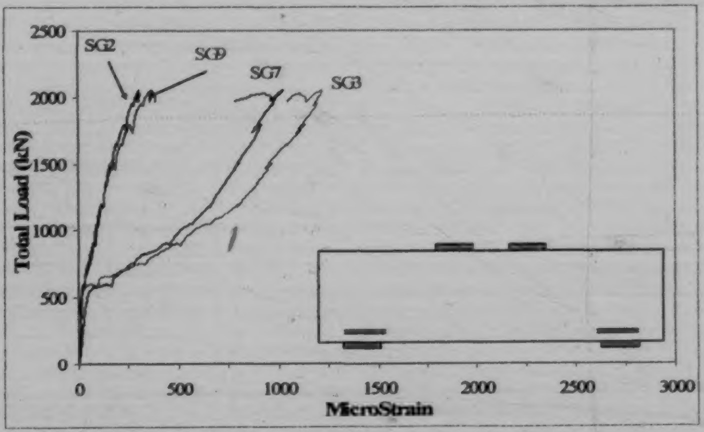

Figure A-54 Strains at the interior and exterior edges of the supports of specimen MS2-3

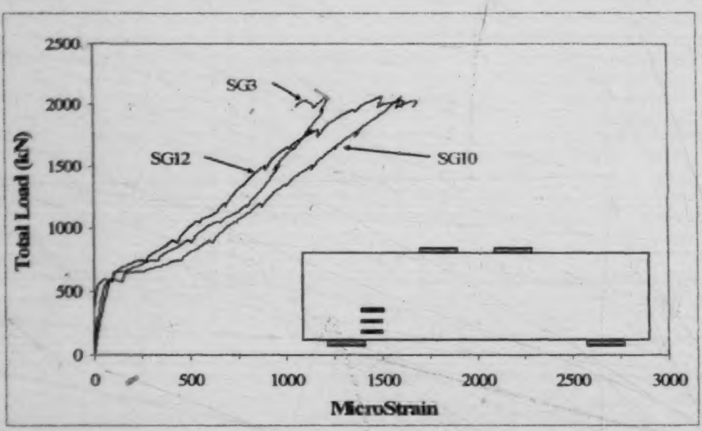

Figure A-55 Strain at the interior edge of one support for the three layers of tension reinforcement of specimen MS2-3

Table A-20 Strains monitored by demec gages rosettes for specimen MS2-3

LOAD (kN)	εy B	εD2 B	εx B	εD1 B	εy A	εD1 A	εx A	εD2 A	Top
	I	II	III	IV	V	VI	VII	VIII	IX
0	0.00000	0.00000	0.00000	0.00000	0.00000	0.00000	0.00000	0.00000	0.00000
150	0.00001	-0.00001	0.00002	0.00004	0.00000	0.00004	0.00000	-0.00003	-0.00017
300	0.00000	-0.00005	0.00003	0.00006	0.00000	0.00009	0.00002	-0.00005	-0.00036
450	0.00000	-0.00005	0.00004	0.00004	-0.00002	0.00020	0.00005	-0.00007	-0.00056
600	0.00016	-0.00011	-0.00003	-0.00003	0.00019	0.00160	0.00095	-0.00013	-0.00071
750	0.00101	-0.00027	-0.00003	0.00048	0.00142	0.00317	0.00166	-0.00021	-0.00090
900	0.00159	-0.00041	0.00012	0.00121	0.00215	0.00452	0.00215	-0.00026	-0.00108
1050	0.00221	-0.00050	0.00057	0.00206	0.00292	0.00587	0.00253	-0.00035	-0.00126
1200	0.00326	-0.00056	0.00123	0.00330	0.00388	0.00701	0.00270	-0.00042	-0.00146
1350	0.00436	-0.00070	0.00178	0.00455	0.00537	0.00853	0.00306	-0.00047	-0.00165
1500	0.00554	-0.00083	0.00231	0.00585	0.00724	0.01027	0.00344	-0.00052	-0.00185
1650	0.00693	-0.00096	0.00285	0.00726	0.00938	0.01224	0.00385	-0.00056	-0.00209
1800	0.00841	-0.00110	0.00333	0.00872	0.01190	0.01455	0.00438	-0.00061	-0.00233
1950	0.01033	-0.00125	0.00386	0.01052	0.01538	0.01770	0.00502	-0.00020	-0.00266

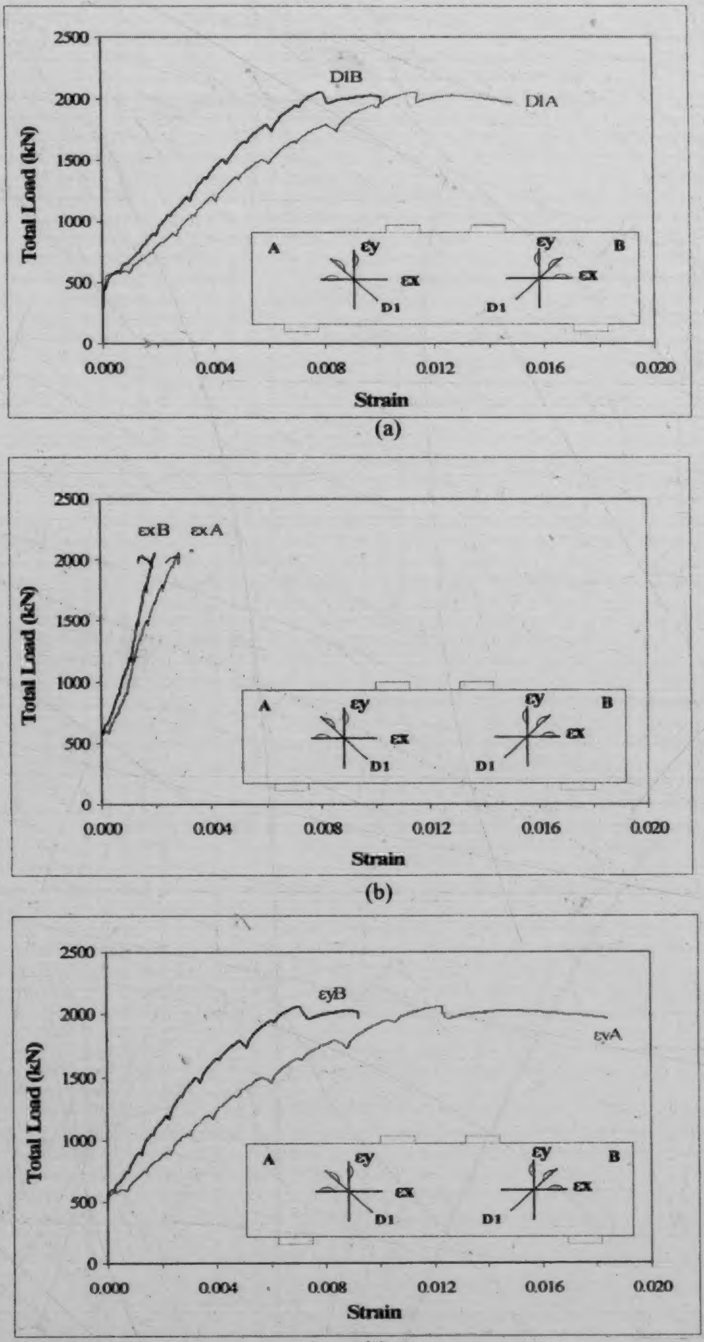

(a)

(b)

(c)

Figure A-56 Average Strains in the (a) diagonal strain D1, (b) horizontal strain and (c) vertical strain of specimen MS2-3

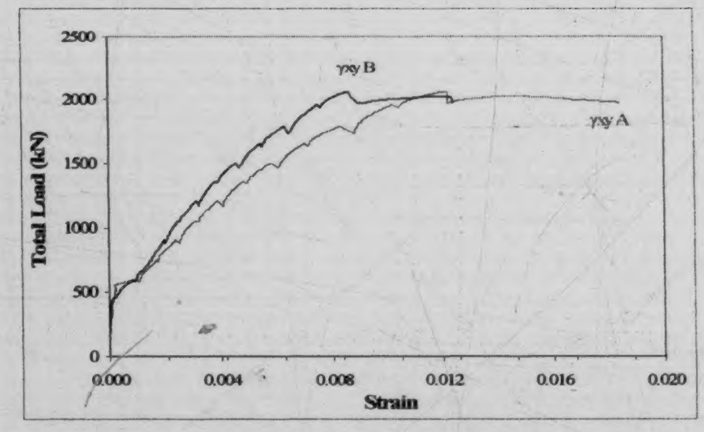

Figure A-57 Maximum shear strain in diagonal struts of specimen MS2-3

A.6 Specimen MS3-2

Table A-21 Loads and deflections at important events during the test of specimen MS3-2

Load (kN)	Deflection (mm)	Event
130	0.62	First flexural crack
258	2.80	First diagonal strut crack side A
298	3.39	First diagonal strut crack side B
976	14.00	Yielding of the first layer of the main tension reinforcement
1087	24.88	Yielding of the third layer of the main tension reinforcement
1154	35.06	Maximum load

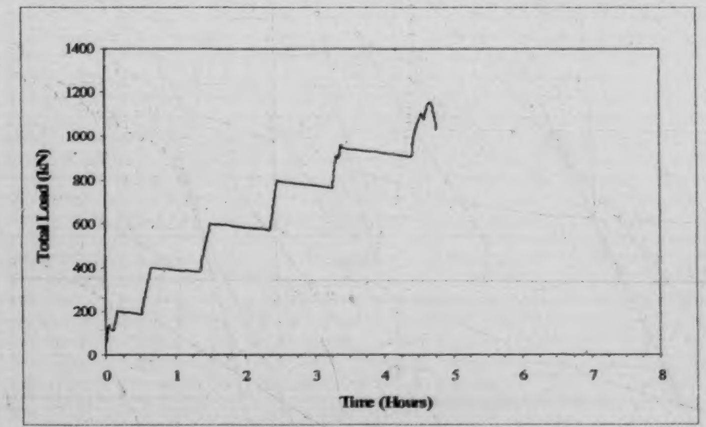

Figure A-58 Load-time response of specimen MS3-2

Table A-22 Flexural and diagonal crack widths at different loading stages of specimen MS3-2

Load (kN)	Maximum flexural crack width (mm)	distance to midspan (mm)	Diagonal crack width at A (mm)	Diagonal crack width at B (mm)
130	First flexural crack			
200	0.1	100	0	0
258	First diagonal strut crack side A			
298	First diagonal strut crack side B			
400	0.25	100	0.15	0.1
600	0.50	100	0.4	0.4
800	0.80	100	0.60	0.60
960	1.25	300	0.80	0.80
1154	Maximum load			

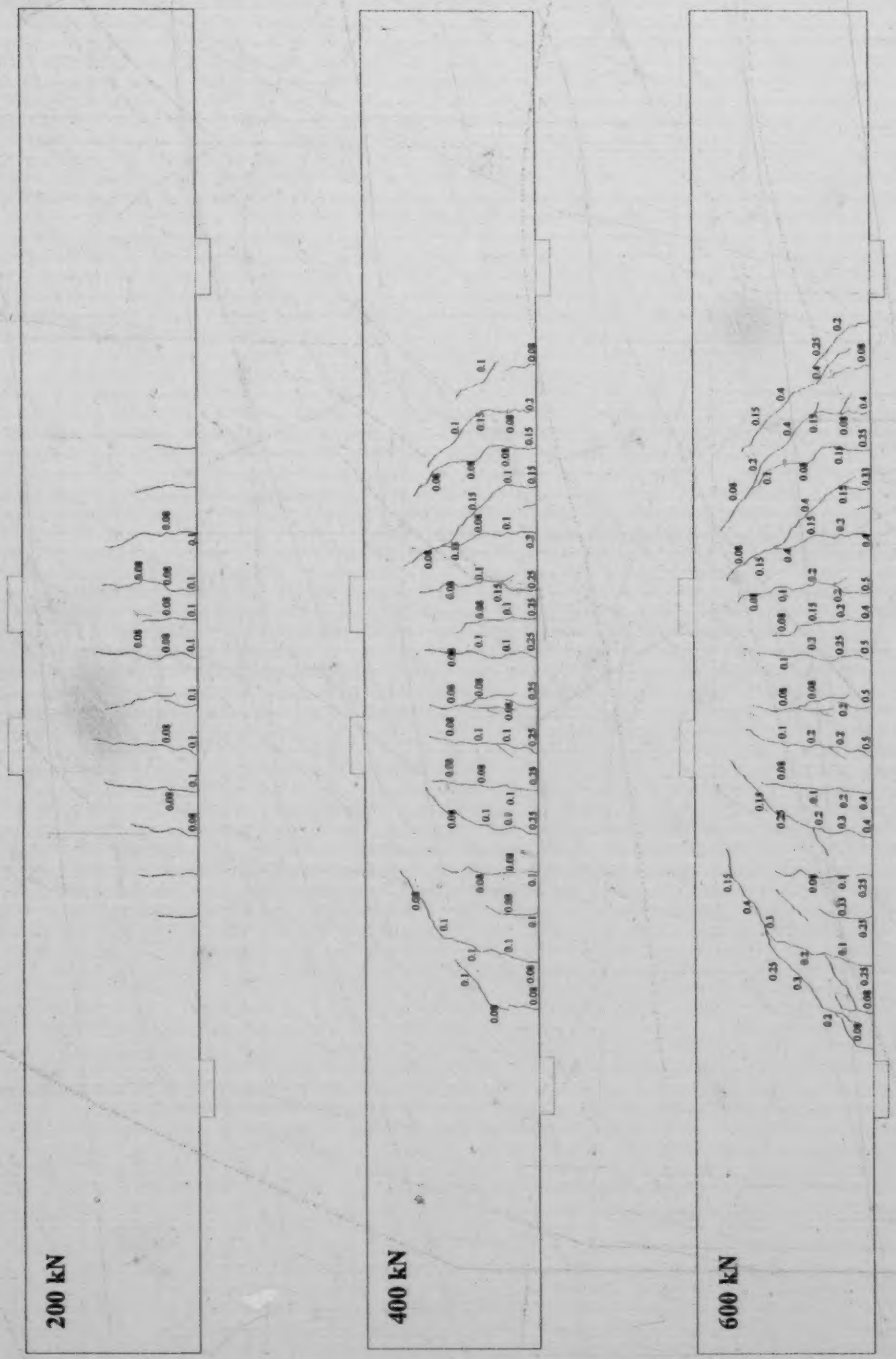

Figure A-59 Crack patterns at 200 kN, 400 kN and 600 kN of loading at test of specimen MS3-2

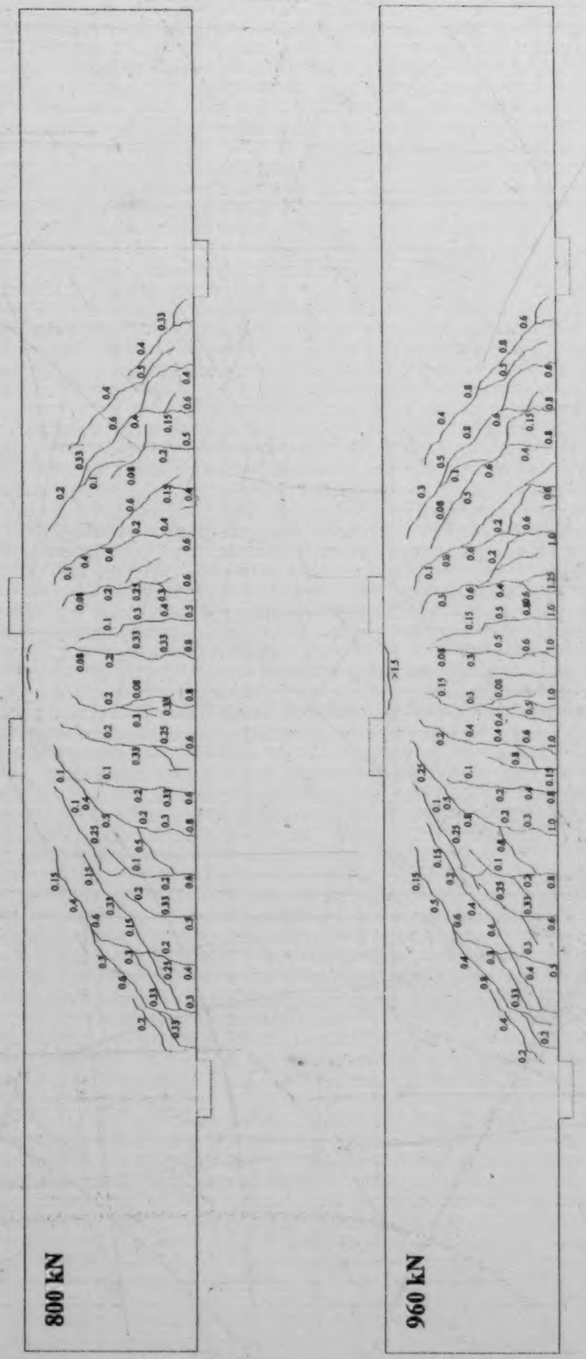

Figure A-60 Crack patterns at 800 kN and 960 kN of loading at test of specimen MS3-2

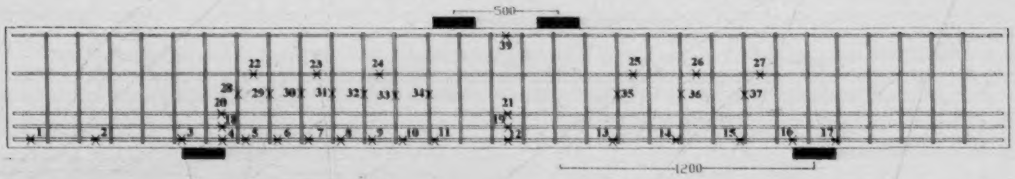

Figure A-61 Strain gages locations of specimen MS3-2

Table A-23 Location of strain gauges for specimen MS3-2

Strain Gauge	Distance from midspan (mm)	side	Strain Gauge	Distance from midspan (mm)	side
1	2250	A	21	0	
2	1950	A	22	1200	A
3	1550	A	23	900	A
4	1350	A	24	600	A
5	1250	A	25	600	B
6	1100	A	26	900	B
7	950	A	27	1200	B
8	800	A	28	stirrup	A
9	650	A	29	stirrup	A
10	500	A	30	stirrup	A
11	350	A	31	stirrup	A
12	0		32	stirrup	A
13	500	B	33	stirrup	A
14	800	B	34	stirrup	A
15	1100	B	35	stirrup	B
16	1350	B	36	stirrup	B
17	1550	B	37	stirrup	B
18	1350	A	38	0	
19	0		39	0	
20	1350	A			

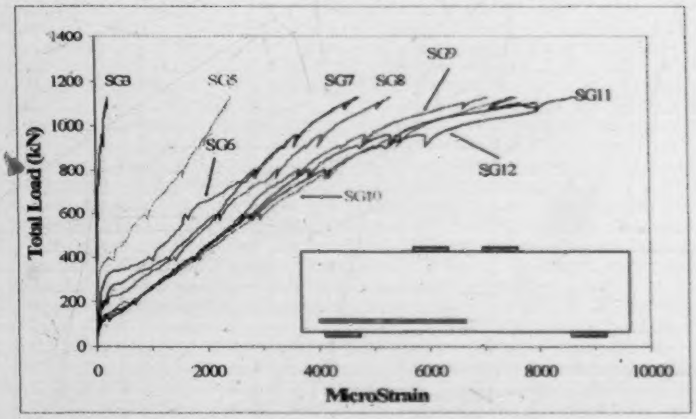

Figure A-62 Strains at a bar located in the lowest layer of main tension reinforcement of specimen MS3-2

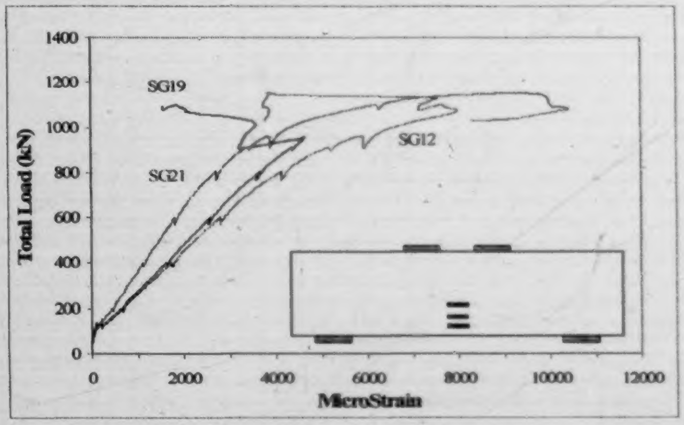

Figure A-63 Strains at midspan of the three layers of main tension reinforcement in specimen MS3-2

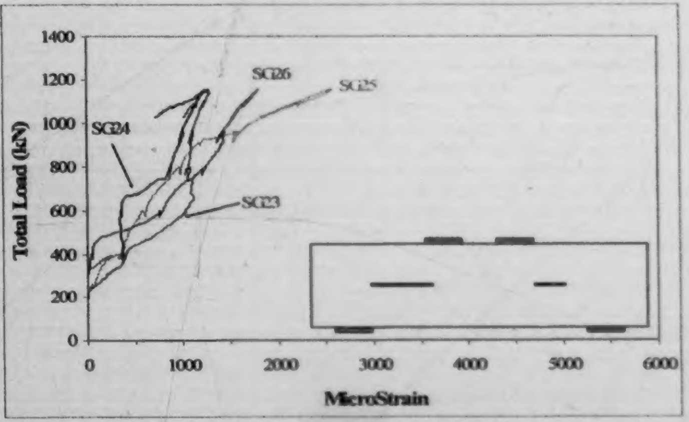

Figure A-64 Strains on the horizontal web reinforcement of specimen MS3-2

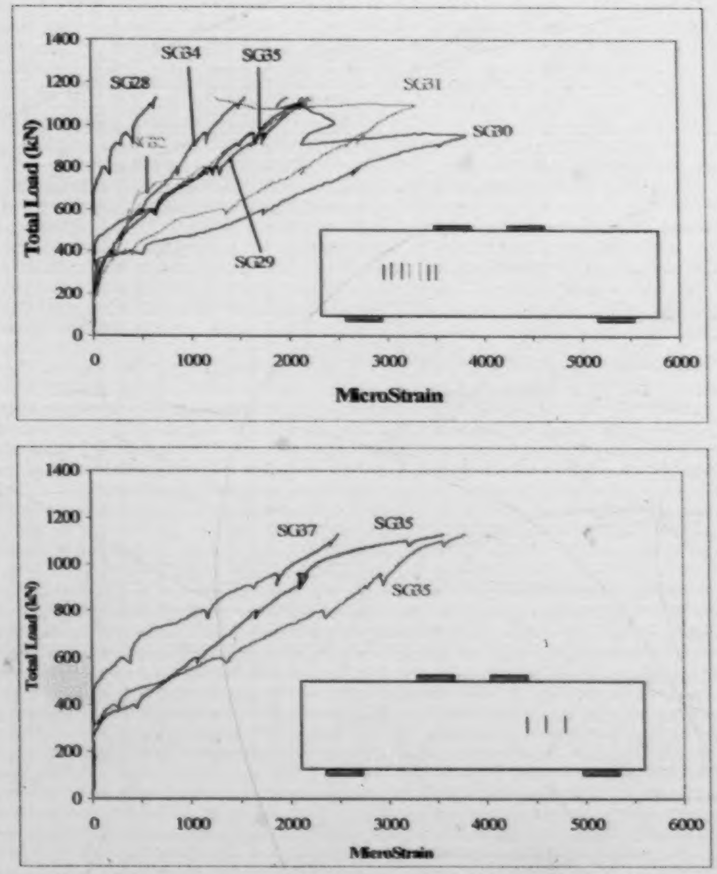

Figure A-65 Strains of stirrups located in the shear spans of specimen MS3-2

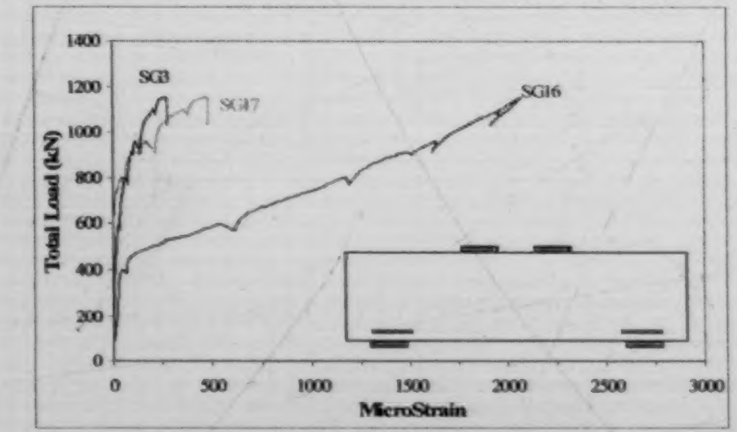

Figure A-66 Strains at the interior and exterior edges of the supports of specimen MS3-2

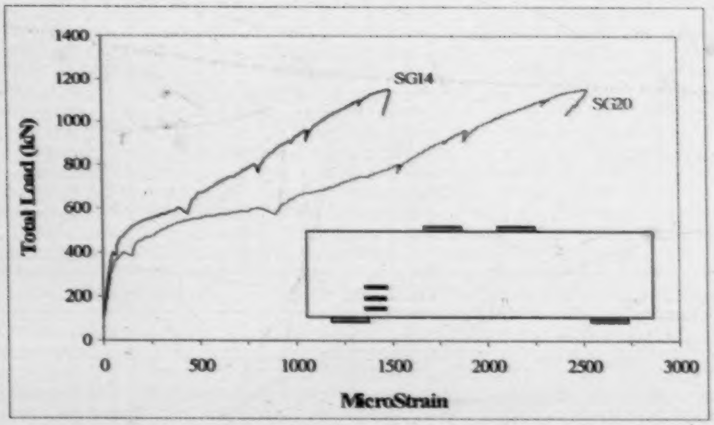

Figure A-67 Strain at the interior edge of one support for the three layers of tension reinforcement of specimen MS3-2

Table A-24 Strains monitored by demec gages rosettes for specimen MS3-2

LOAD (kN)	εy B	εD2 B	εx B	εD1 B	εy A	εD1 A	εx A	εD2 A	Top
	I	II	III	IV	V	VI	VII	VIII	IX
0	0.00000	0.00000	0.00000	0.00000	0.00000	0.00000	0.00000	0.00000	0.00000
200	0.00000	-0.00002	0.00004	0.00007	0.00002	0.00008	0.00009	-0.00003	-0.00038
400	0.00066	-0.00017	0.00090	0.00143	0.00066	0.00087	0.00048	-0.00015	-0.00081
600	0.00255	-0.00023	0.00131	0.00388	0.00268	0.00343	0.00088	-0.00025	-0.00129
800	0.00488	-0.00030	0.00271	0.00672	0.00481	0.00580	0.00137	-0.00041	-0.00195
900	0.00608	-0.00035	0.00272	0.00776	0.00580	0.00674	0.00139	-0.00050	-0.00260
960	0.00672	-0.00035	0.00264	0.00823	0.00623	0.00707	0.00124	-0.00056	-0.00327
1100	0.00937	-0.00039	0.00242	0.01036	0.00881	0.00933	0.00116	-0.00077	-0.00669

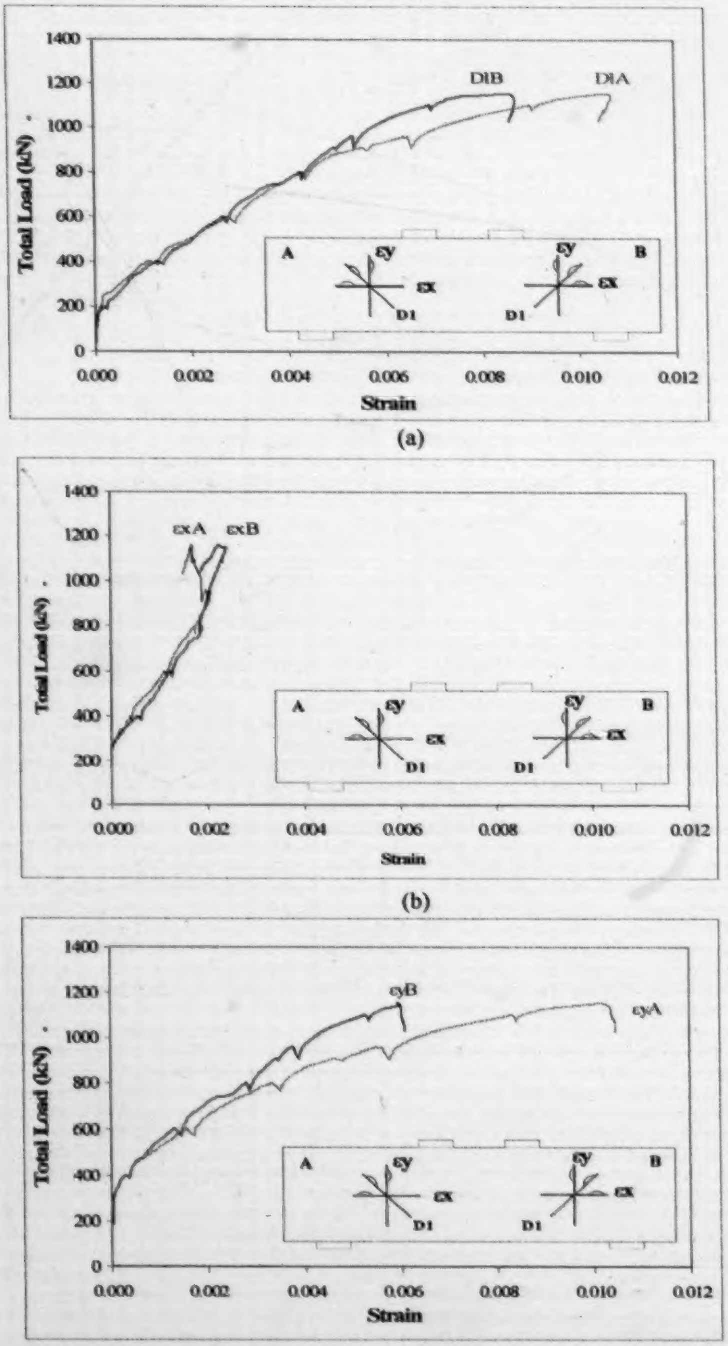

(a)

(b)

(c)

Figure A-68 Average Strains in the (a) diagonal strain D1, (b) diagonal strain D2 and (c) vertical strain of specimen MS3-2

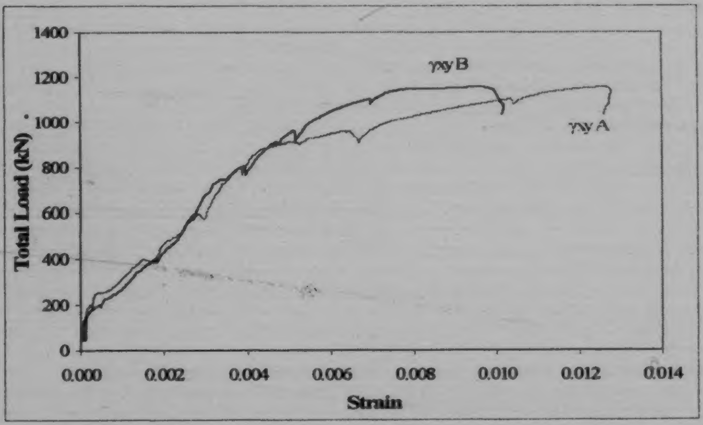

Figure A-69 Maximum shear strain in diagonal struts of specimen MS3-2

A.7 Specimen MW1-2

Table A-25 Loads and deflections at important events during the test of specimen MW1-2

Load (kN)	Deflection (mm)	Event
257	0.40	First flexural crack
393	0.78	First diagonal strut crack side A
450	1.00	First diagonal strut crack side B
1568	7.50	Maximum load

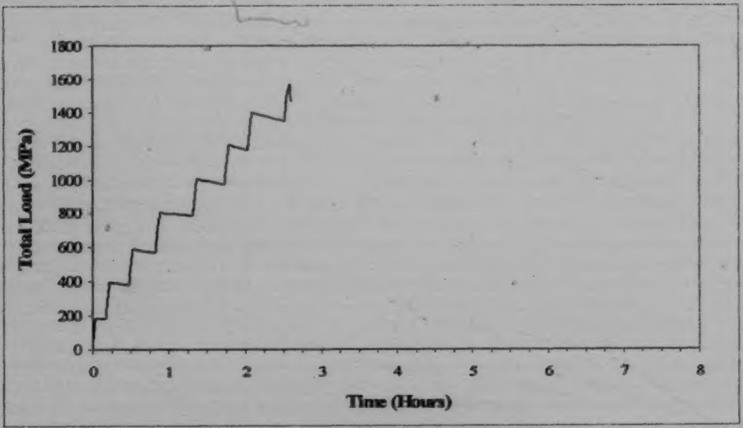

Figure A-70 Load-time response of specimen MS1-1

Table A-26 Flexural and diagonal crack widths at different loading stages of specimen MW1-2

Load (kN)	Maximum flexural crack width (mm)	distance to midspan (mm)	Diagonal crack width at A (mm)	Diagonal crack width at B (mm)
200	0	0	0	0
257	First flexural crack			
393	First diagonal strut crack side A			
400	0.2	0	0.08	0
450	First diagonal strut crack side B			
600	0.4	200	0.4	0.15
800	0.50	0	0.6	0.5
1000	0.60	0	1.00	0.80
1200	0.80	0	1.25	0.80
1400	1.00	200	1.50	1.25
1568	Maximum load			

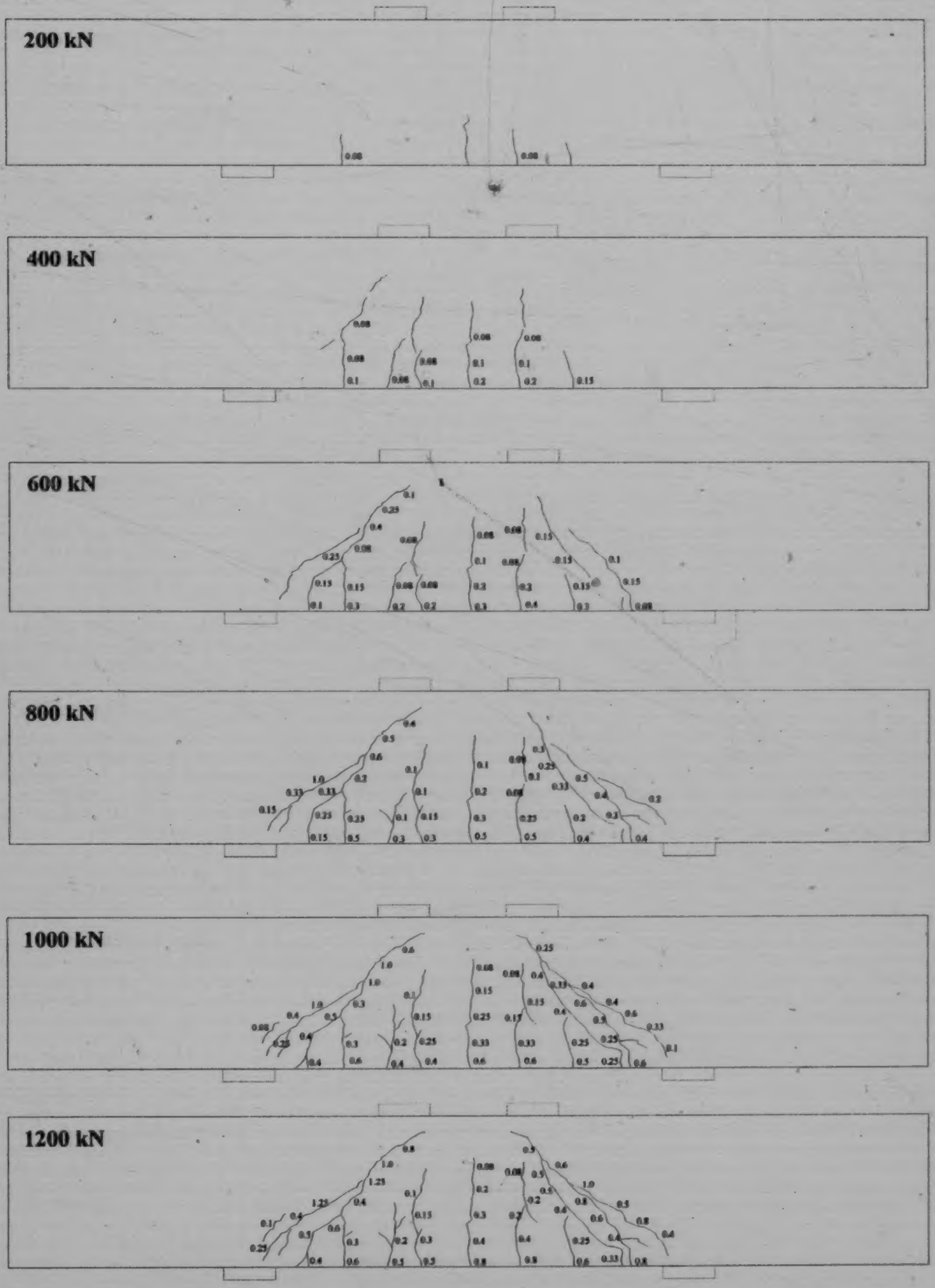

Figure A-71 Crack patterns at different loading stages from 200 kN to 1200 kN of specimen MW1-2

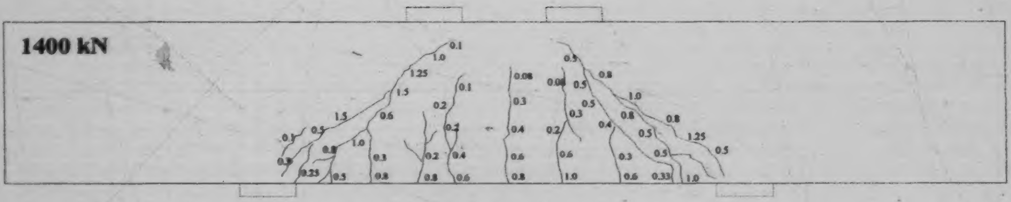

Figure A-72 Crack patterns at 1400 kN of specimen MW1-2

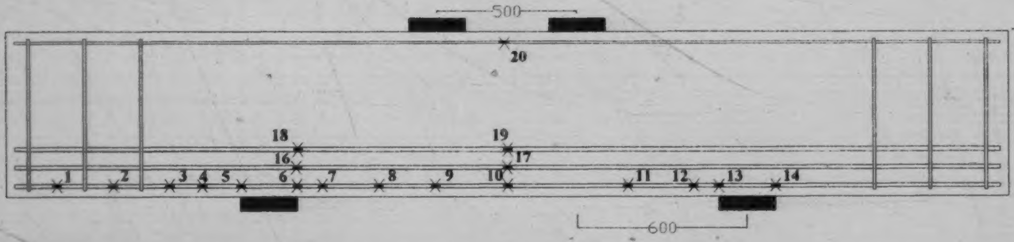

Figure A-73 Strain gages locations of specimen MW1-2

Table A-27 Location of strain gauges for specimen MW1-2

Strain Gauge	Distance from midspan (mm)	side	Strain Gauge	Distance from midspan (mm)	side
1	1600	A	11	460	B
2	1400	A	12	660	B
3	1200	A	13	750	B
4	1070	A	14	950	B
5	950	A	15	0	
6	750	A	16	750	A
7	660	A	17	0	0
8	460	A	18	750	
9	260	A	19	0	
10	0		20	0	

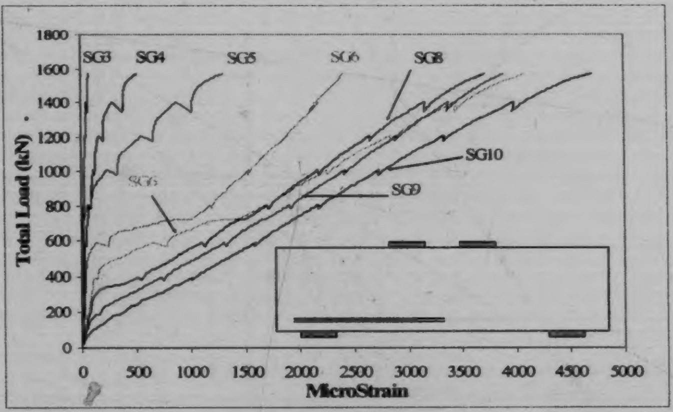

Figure A-74 Strains at a bar located in the lowest layer of main tension reinforcement of specimen MW1-2

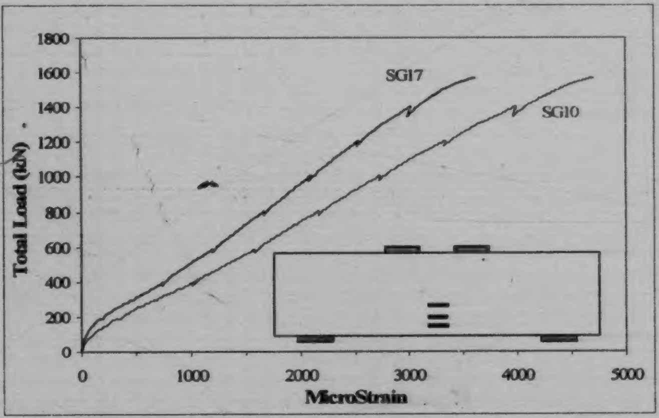

Figure A-75 Strains at midspan of the three layers of main tension reinforcement in specimen MW1-2

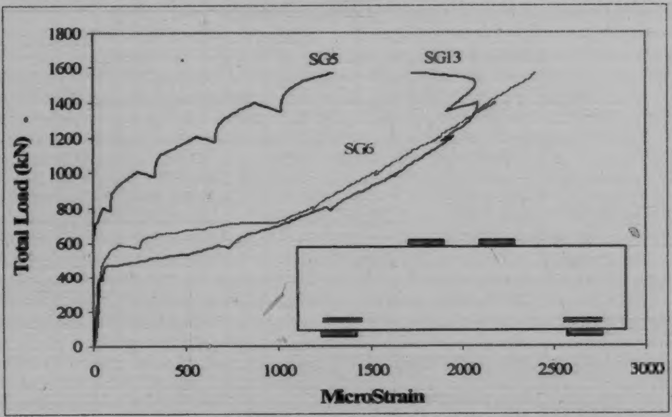

Figure A-76 Strains at the interior and exterior edges of the supports of specimen MW1-2

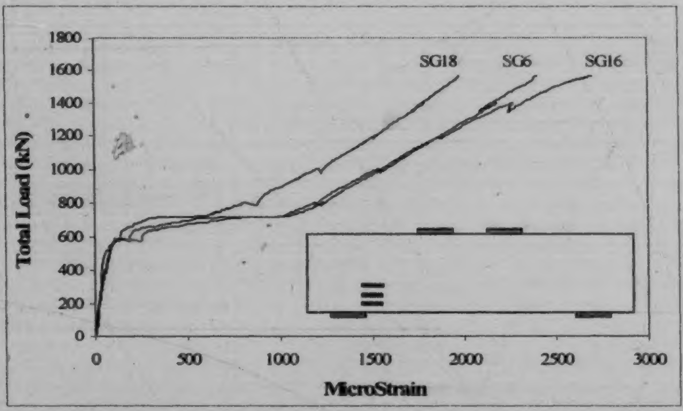

Figure A-77 Strain at the interior edge of one support for the three layers of tension reinforcement of specimen MW1-2

Table A-28 Strains monitored by demec gages rosettes for specim[illegible] MS1-1

LOAD (kN)	εy B	εD2 B	εx B	εD1 B	Top
	I	II	III	IV	IX
0	0.00000	0.00000	0.00000	0.00000	0.00000
200	0.00002	-0.00003	0.00002	0.00005	-0.00012
400	-0.00001	-0.00009	0.00005	0.00012	-0.00032
600	-0.00003	-0.00018	0.00006	0.00012	-0.00049
800	0.00246	-0.00049	0.00172	0.00333	-0.00067
1000	0.00409	-0.00069	0.00280	0.00541	-0.00086
1200	0.00587	-0.00092	0.00388	0.00757	-0.00105
1400	0.00774	-0.00119	0.00499	0.00986	-0.00126

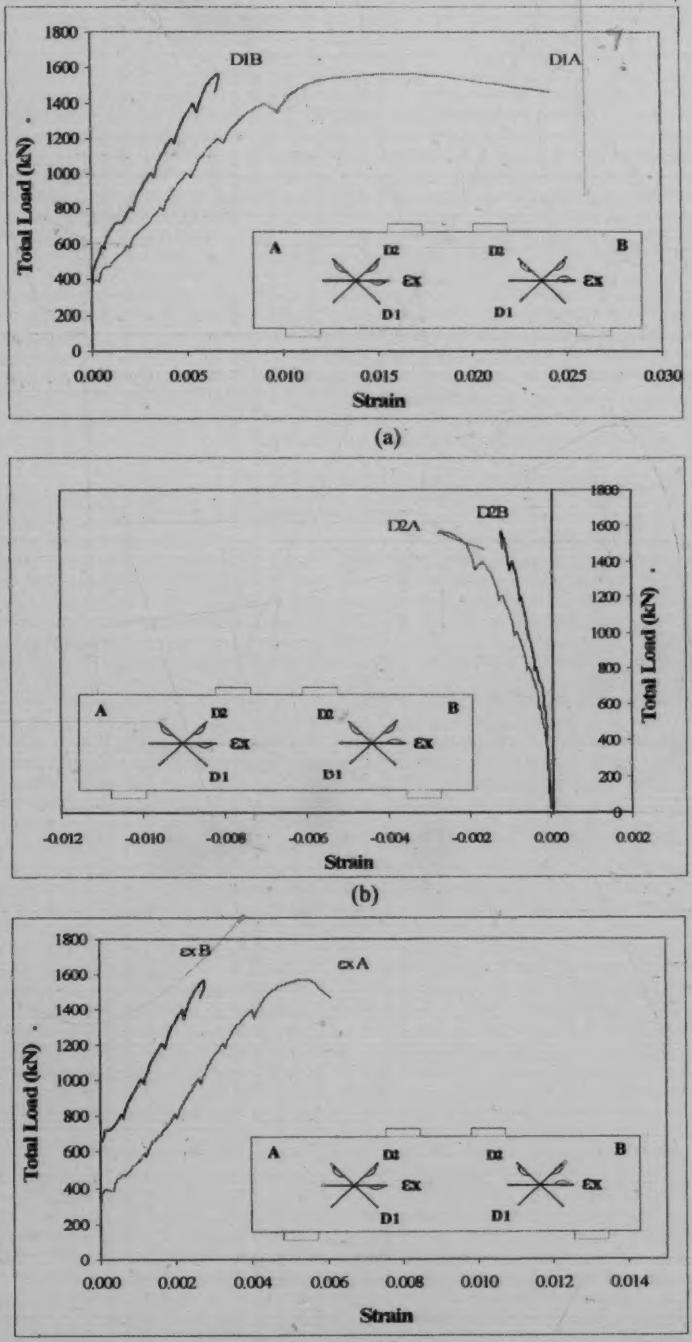

(a)

(b)

(c)

Figure A-78 Average Strains in the (a) diagonal strain D1, (b) diagonal strain D2 and (c) horizontal strain of specimen MW1-2

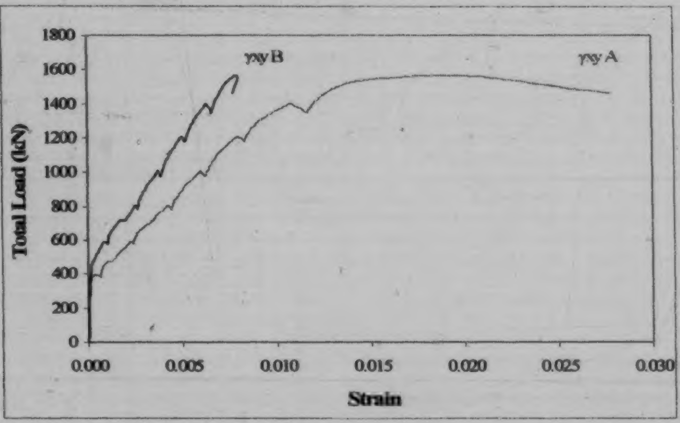

Figure A-79 Maximum shear strain in diagonal struts of specimen MW1-2

A.8 Specimen MW3-2

Table A-29 Deflections and important observations at different load stages for specimen MW3-2

Load (kN)	Deflection (mm)	Event
99	0.47	First flexural crack
247	2.34	First diagonal strut crack side A
283	2.90	First diagonal strut crack side B
350	4.06	Big load drop and strut cracking
411	9.09	Maximum load

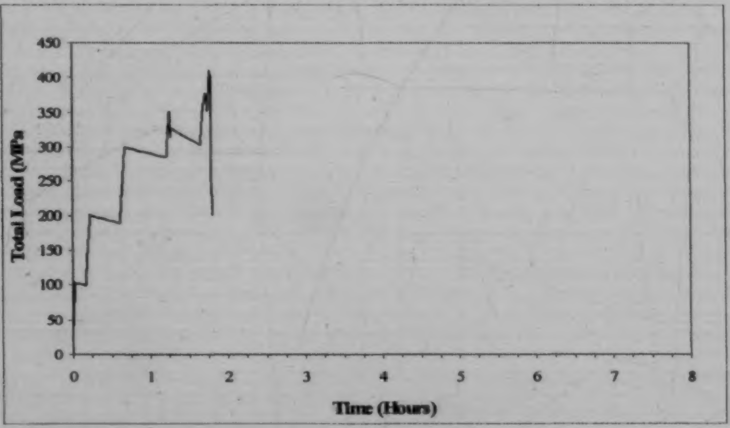

Figure A-80 Load-time response of specimen MW3-2

Table A-30 Flexural and diagonal crack widths at different loading stages of specimen MW3-2

Load (kN)	Maximum flexural crack width (mm)	distance to midspan (mm)	Diagonal crack width at A (mm)	Diagonal crack width at B (mm)
99	First flexural crack			
100	<0.8	0	0	0
200	0.15	0	0	0
247	First diagonal strut crack side A			
283	First diagonal strut crack side B			
300	0.25	0	0.08	0.1
350	Big load drop and increase in strut cracking width rates			
340	0.30	0	0.08	1.50
411	Maximum load			

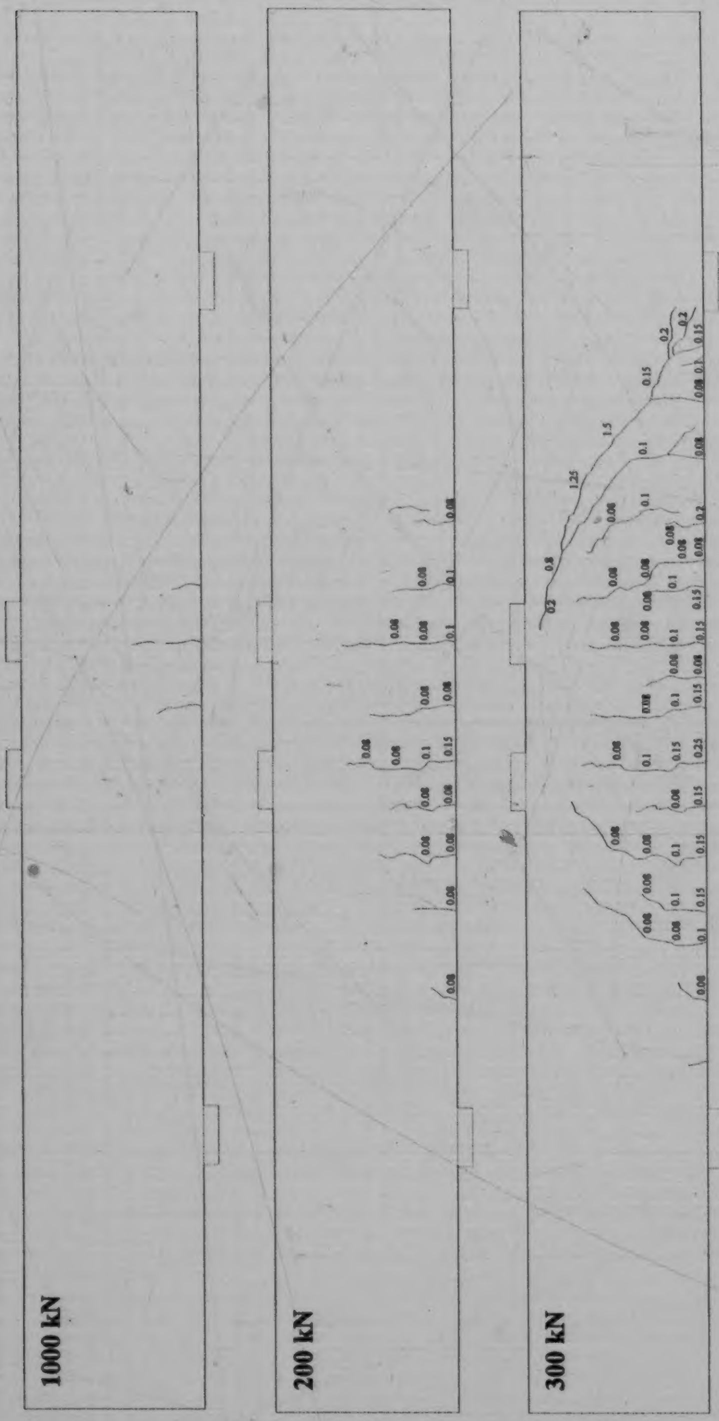

Figure A-81 Crack patterns at different loading stages of specimen MW3-2

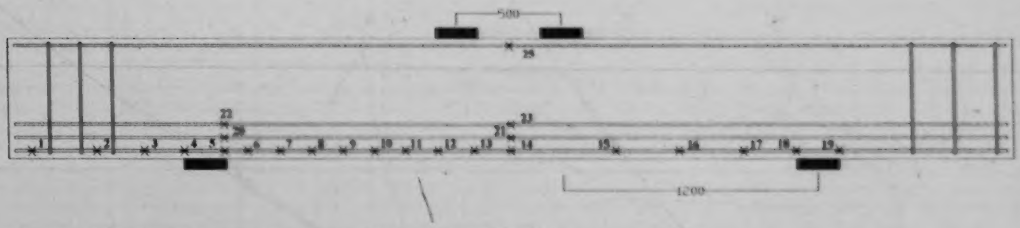

Figure A-82 Strain gages locations of specimen MW3-2

Table A-31 Location of strain gauges for specimen MW3-2

Strain Gauge	Distance from midspan (mm)	side	Strain Gauge	Distance from midspan (mm)	side
1	2250	A	14	0	
2	1950	A	15	500	B
3	1750	A	16	800	B
4	1550	A	17	1100	B
5	1350	A	18	1350	B
6	1250	A	19	1550	B
7	1100	A	20	1350	A
8	950	A	21	0	
9	800	A	22	1350	A
10	650	A	23	0	
11	500	A	24	0	
12	350	A	25	0	
13	200	A			

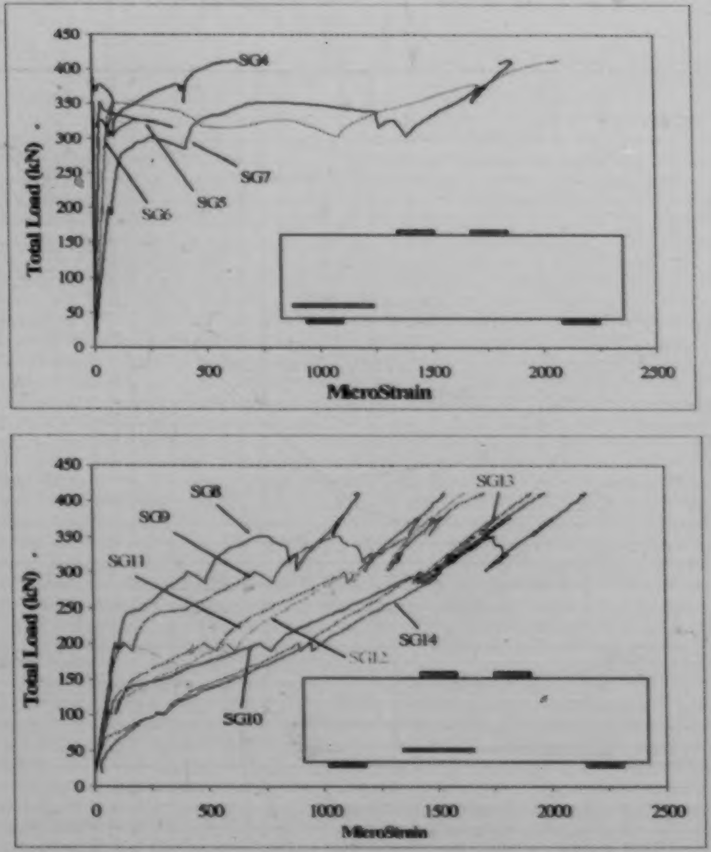

Figure A-83 Strains at a bar located in the lowest layer of main tension reinforcement of specimen MW3-2

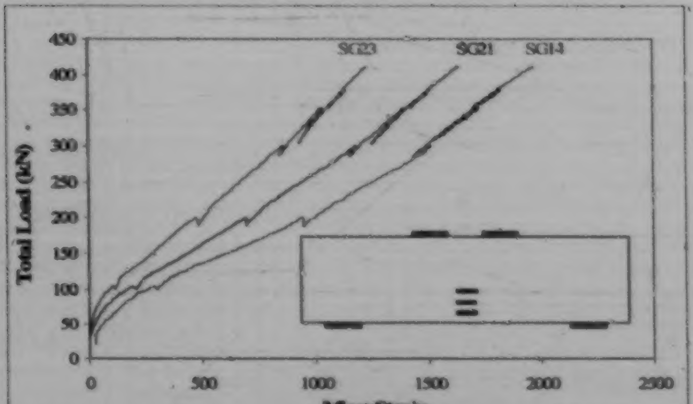

Figure A-84 Strains at midspan of the three layers of main tension reinforcement in specimen MW3-2

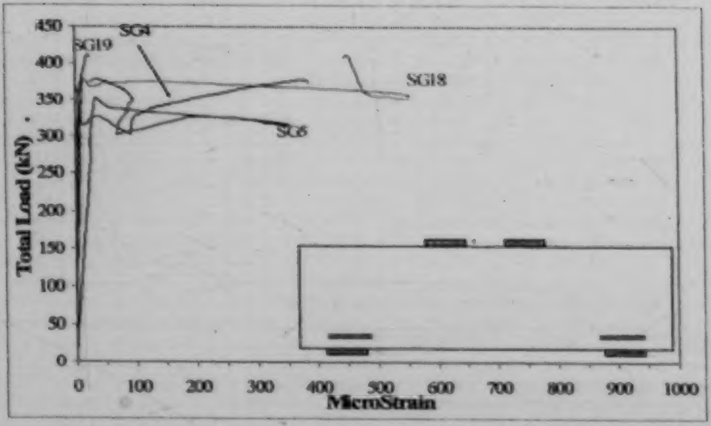

Figure A-85 at the interior and exterior edges of the supports of specimen MW3-2

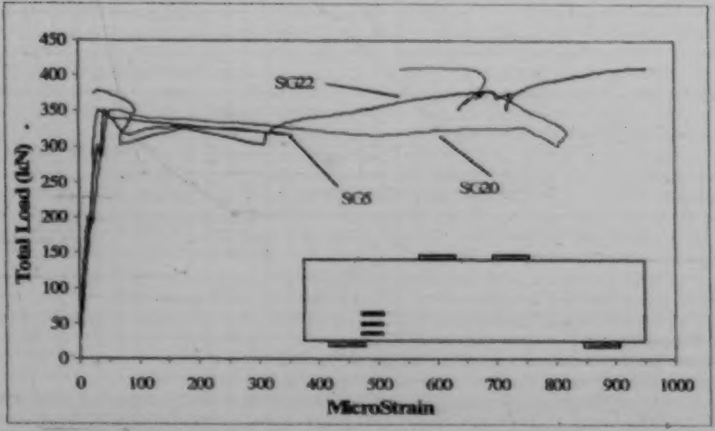

Figure A-86 Strain at the interior edge of one support for the three layers of tension reinforcement of specimen MW3-2

Table A-32 Strains monitored by demec gages rosettes for specimen MW3-2

LOAD (kN)	εy B	εD2 B	εx B	εD1 B	Top
	I	II	III	IV	IX
0	0.00000	0.00000	0.00000	0.00000	0.00000
100	0.00001	-0.00001	0.00001	0.00004	-0.00011
200	-0.00001	-0.00004	0.00003	0.00006	-0.00030
300	-0.00003	-0.00004	0.00005	0.00002	-0.00047

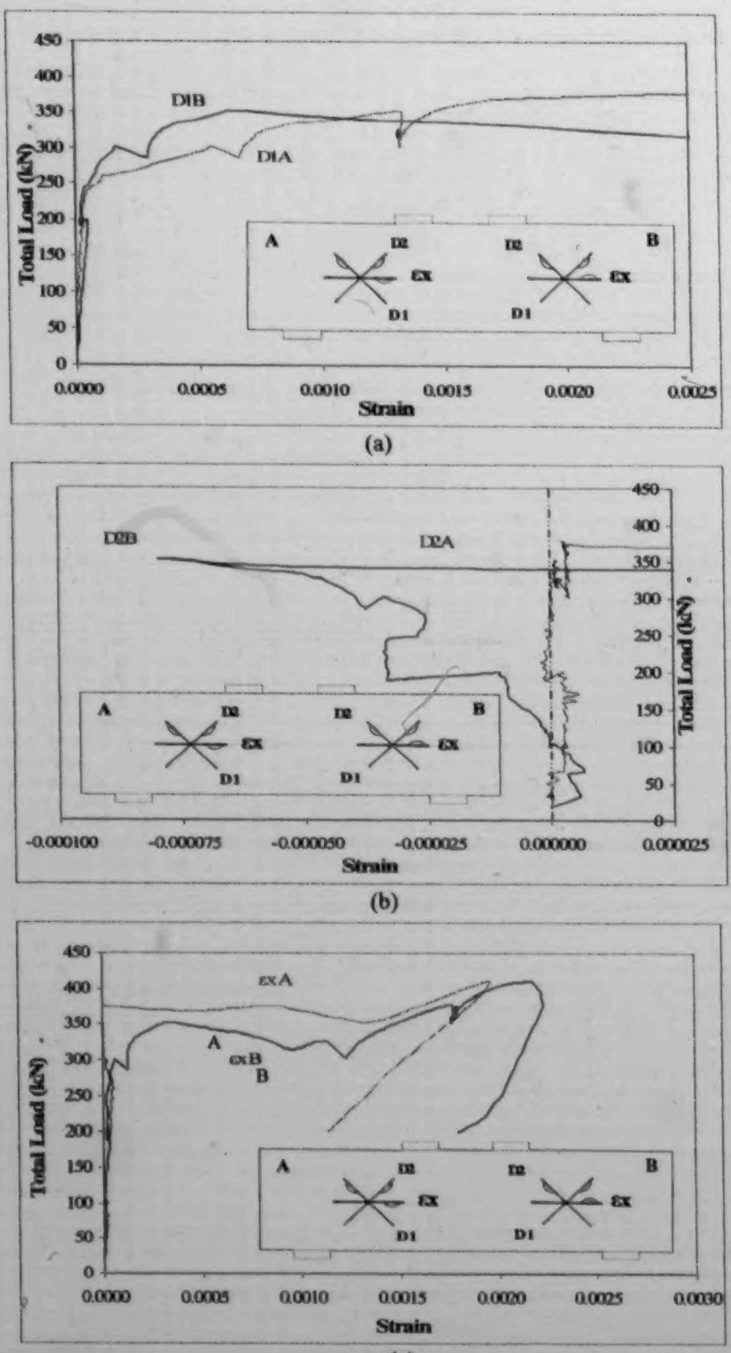

(a)

(b)

(c)

Figure A-87 Average Strains in the (a) diagonal strain D1, (b) diagonal strain D2 and (c) horizontal strain of specimen MW3-2

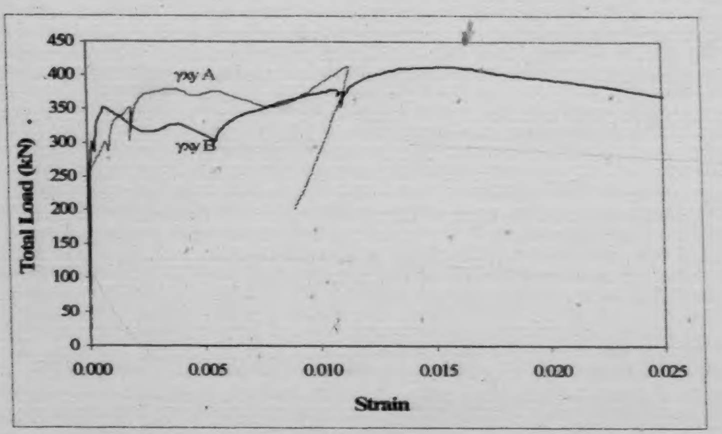

Figure A-88 Maximum shear strain in diagonal struts of specimen MW3-2

A.9 Specimen NS1-4

Table A-33 MS1 Loads and deflections at important events during the test of specimen NS1-4

Load (kN)	Deflection (mm)	Event
102	0.17	First flexural crack
351	0.84	First diagonal strut crack side A
438	0.90	First diagonal strut crack side B
1166	2.95	Yielding of the first layer of the main tension reinforcement
1323	3.65	Yielding of the second layer of the main tension reinforcement
1463	4.82	Yielding of the third layer of the main tension reinforcement
1567	7.53	Maximum load

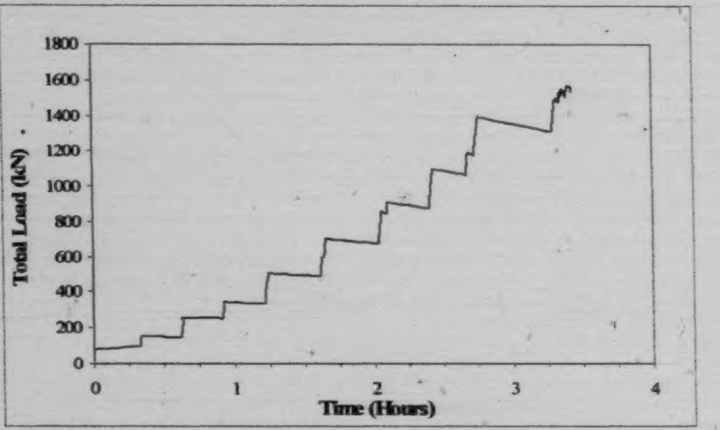

Figure A-89 Load-time response of specimen NS1-4

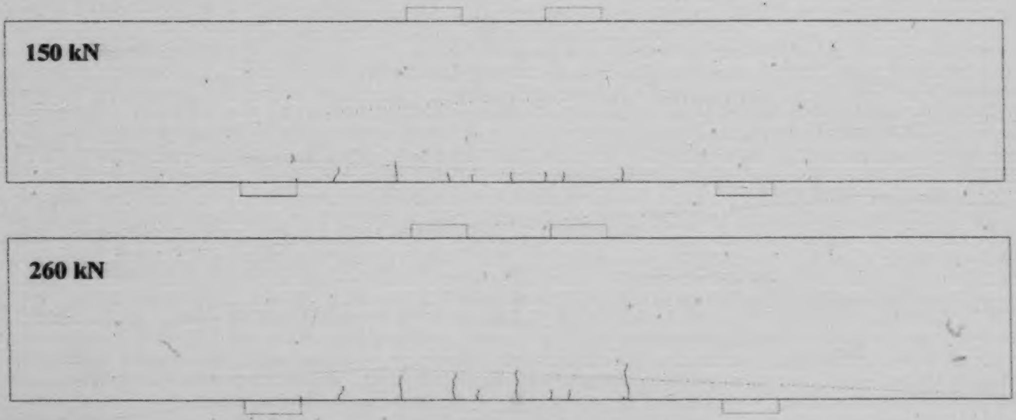

Figure A-90 Crack patterns at 150 kN and 260 kN of specimen NS1-4

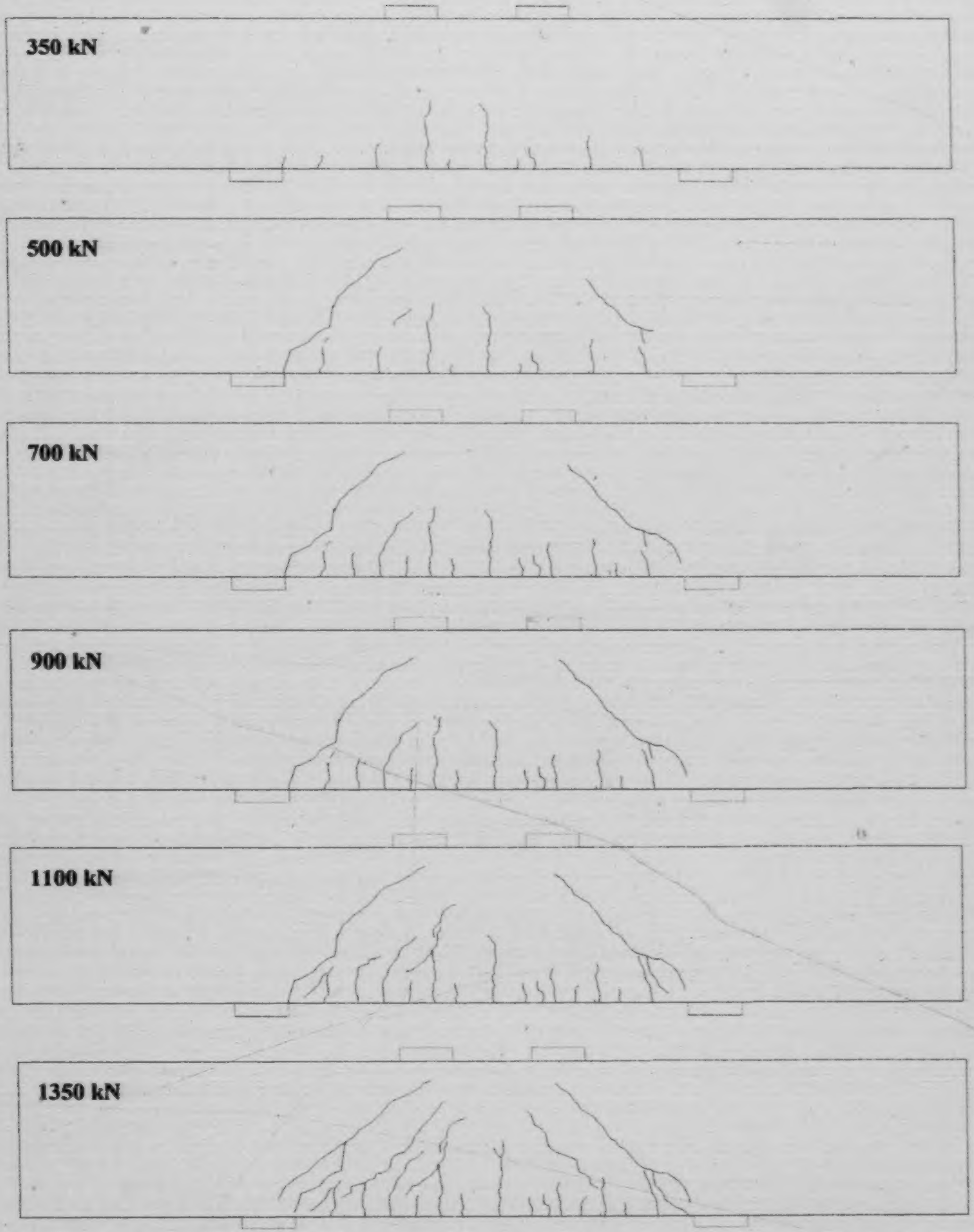

Figure A-91 Crack patterns at different loading stages from 350 kN to 1350 kN of specimen NS1-4

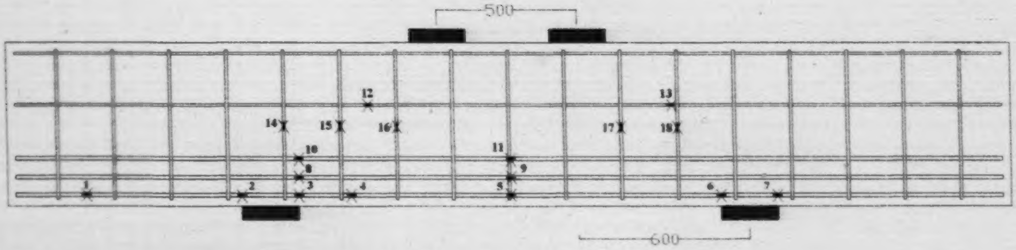

Figure A-92 Strain gages locations of specimen NS1-4

Table A-34 Location of strain gauges for specimen NS1-4

Strain Gauge	Distance from midspan (mm)	side	Strain Gauge	Distance from midspan (mm)	side
1	1285	A	10	750	A
2	950	A	11	0	
3	750	A	12	500	A
4	580	A	13	600	B
5	0		14	stirrup	A
6	750	B	15	stirrup	A
7	950	B	16	stirrup	A
8	750	A	17	stirrup	B
9	0		18	stirrup	B

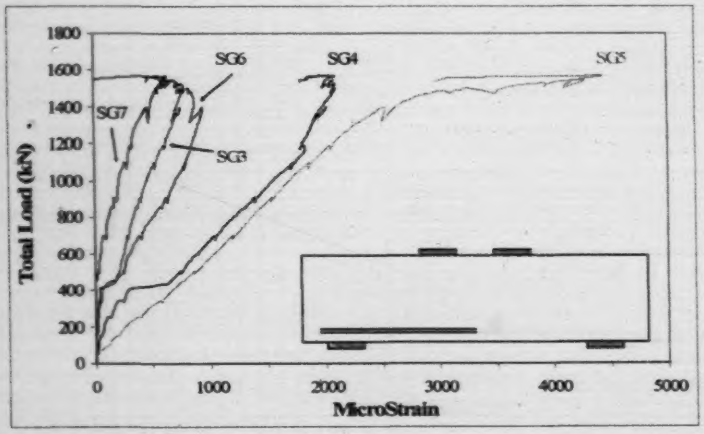

Figure A-93 Strains at a bar located in the lowest layer of main tension reinforcement of specimen NS1-4

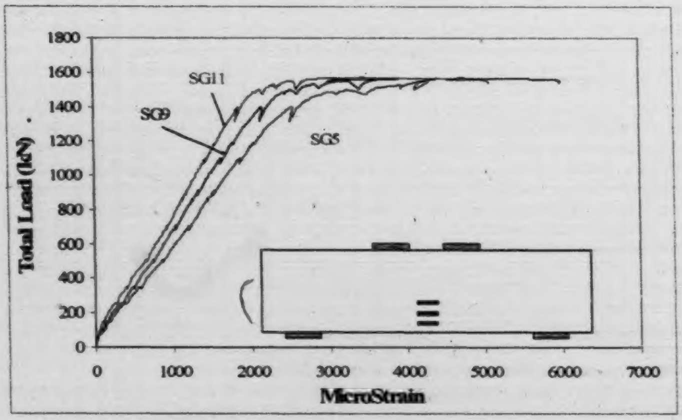

Figure A-94 Strains at midspan of the three layers of main tension reinforcement in specimen NS1-4

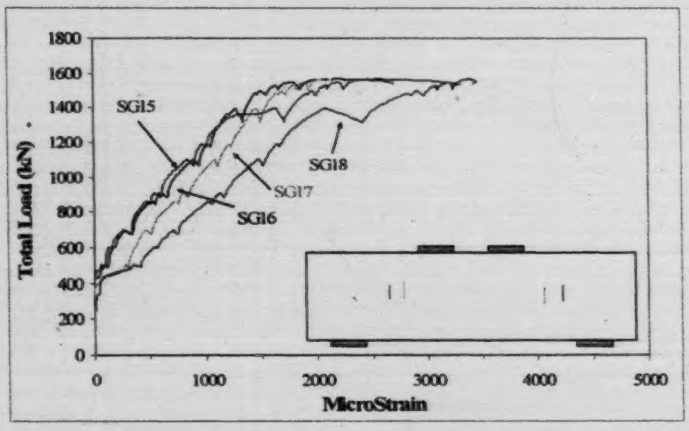

Figure A-95 Strains of stirrups located in the shear spans of specimen NS1-4

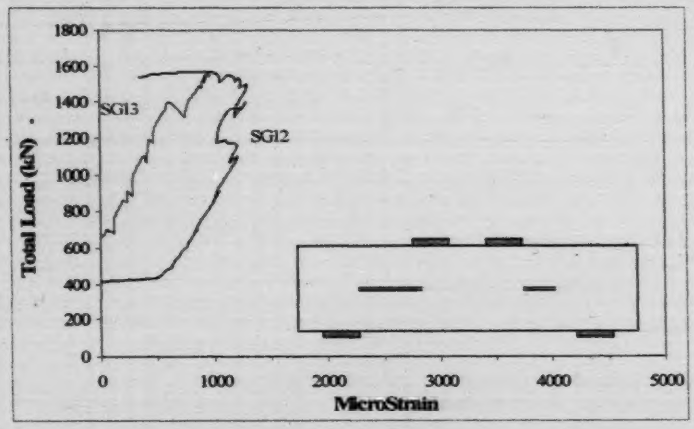

Figure A-96 Strains on the horizontal web reinforcement of specimen NS1-4

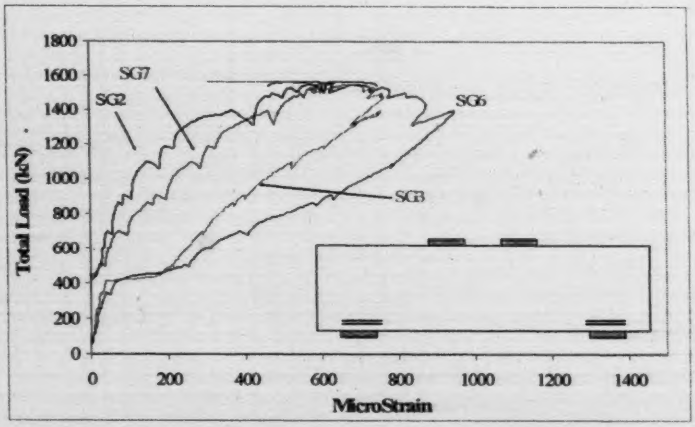

Figure A-97 Strains at the interior and exterior edges of the supports of specimen NS1-4

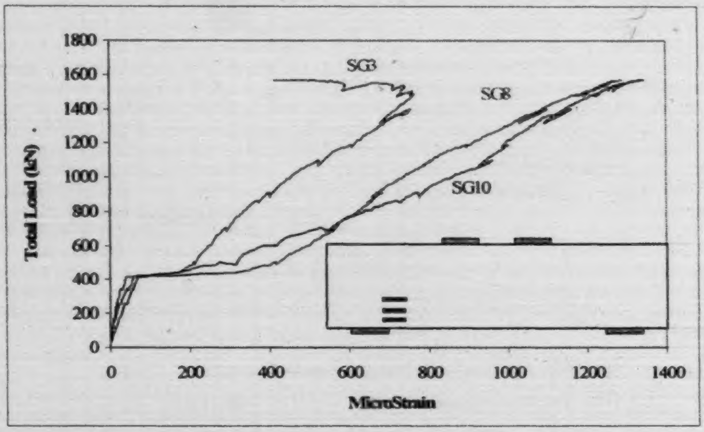

Figure A-98 Strain at the interior edge of one support for the three layers of tension reinforcement of specimen NS1-4

Table A-35 Strains monitored by demec gages rosettes for specimen NS1-4

LOAD (kN)	εy B	εD2 B	εx B	εD1 B	εy A	εD1 A	εx A	εD2 A
	I	II	III	IV	V	VI	VII	VIII
0	0.00000	0.00000	0.00000	0.00000	0.00000	0.00000	0.00000	0.00000
150	0.00001	-0.00004	0.00002	0.00006	0.00001	0.00004	0.00001	0.00002
260	0.00004	-0.00008	0.00004	0.00012	0.00003	0.00006	0.00000	-0.00005
350	0.00011	-0.00012	0.00011	0.00027	0.00000	0.00008	0.00000	-0.00011
500	0.00148		0.00102	0.00202	0.00042	0.00120	0.00014	-0.00020
700	0.00247		0.00142	0.00317	0.00136	0.00250	0.00039	-0.00039
900	0.00369		0.00184	0.00445	0.00228	0.00387		-0.00062
1100	0.00498		0.00223	0.00577		0.00523		-0.00081
1350	0.00773		0.00262	0.00823		0.00760		-0.00125

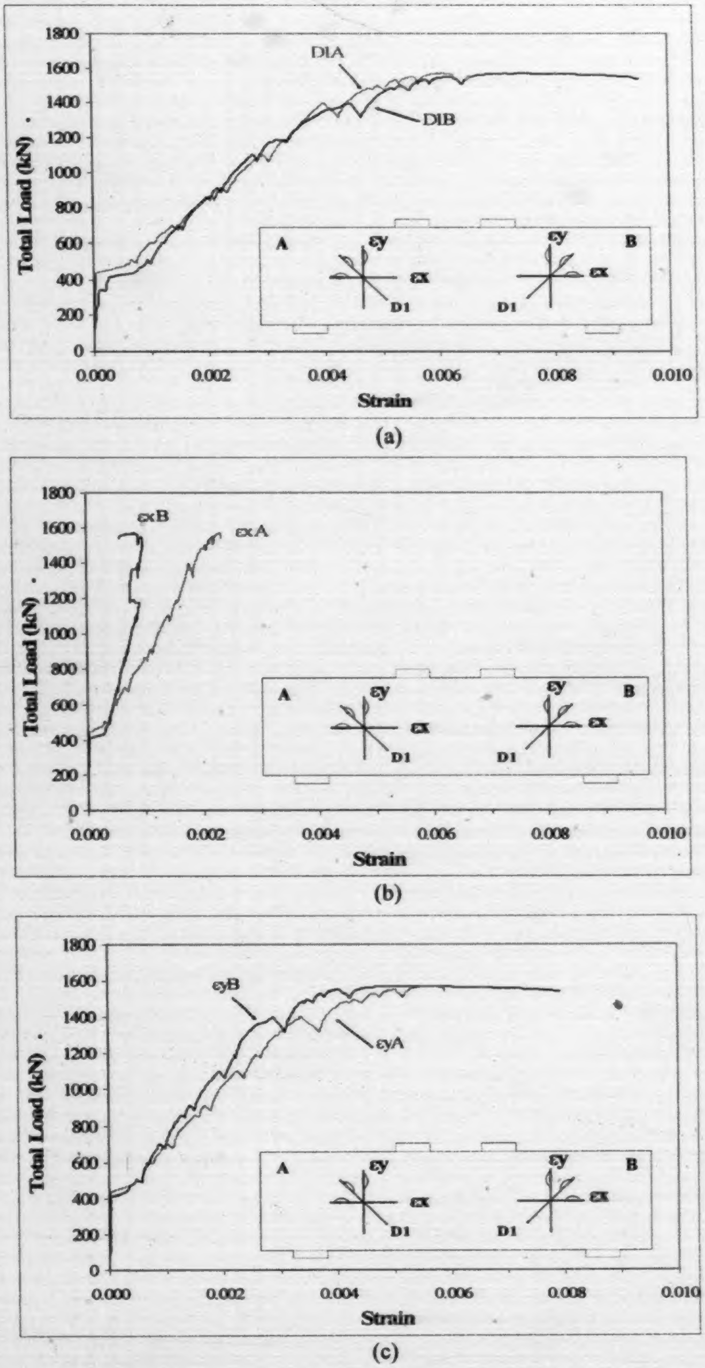

(a)

(b)

(c)

Figure A-99 Average Strains in the (a) diagonal strain D1, (b) diagonal strain D2 and (c) vertical strain of specimen NS1-4

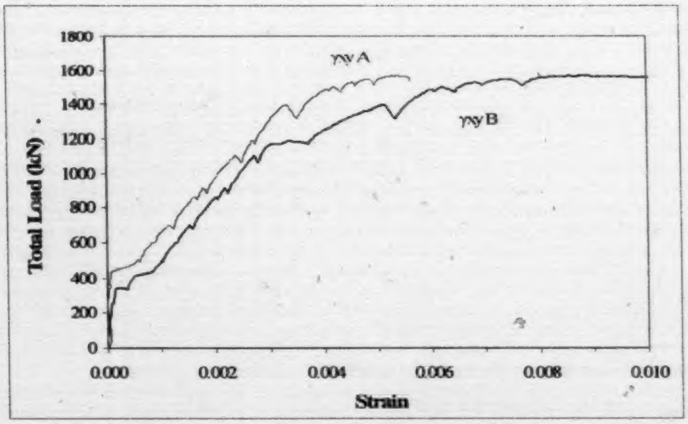

Figure A-100 Maximum shear strain in diagonal struts of specimen NS1-4

A.10 Specimen NS2-4

Table A-36 Loads and deflections at important events during the test of specimen NS2-4

Load (kN)	Deflection (mm)	Event
192	0.80	First flexural crack
314	1.53	First diagonal strut crack side B
342	1.75	First diagonal strut crack side A
774	5.67	Yielding of the first layer of the main tension reinforcement
892	6.88	Yielding of the second layer of the main tension reinforcement
964	7.70	Yielding of the third layer of the main tension reinforcement
1078	13.28	Maximum load

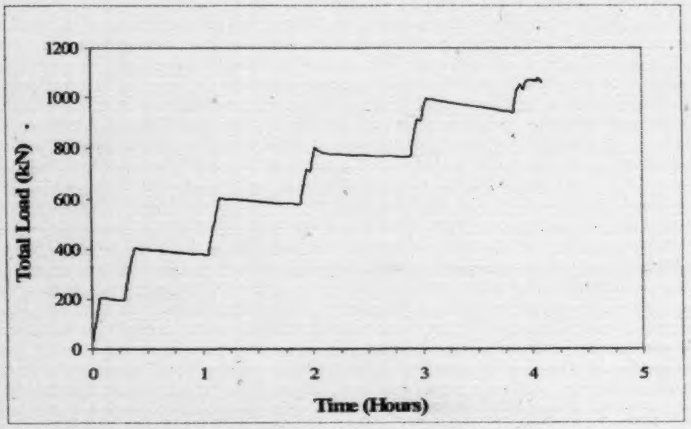

Figure A-101 Load-time response of specimen NS2-4

Table A-37 and diagonal crack widths at different loading stages of specimen NS2-4

Load (kN)	Maximum flexural crack width (mm)	distance to midspan (mm)	Diagonal crack width at A (mm)	Diagonal crack width at B (mm)
192	First flexural crack			
200	<0.08	100	0	0
314	First diagonal strut crack side B			
342	First diagonal strut crack side A			
400	0.15	100	0.15	0.15
600	0.25	100	0.4	0.3
800	0.33	100	0.80	0.60
1078	Maximum load			

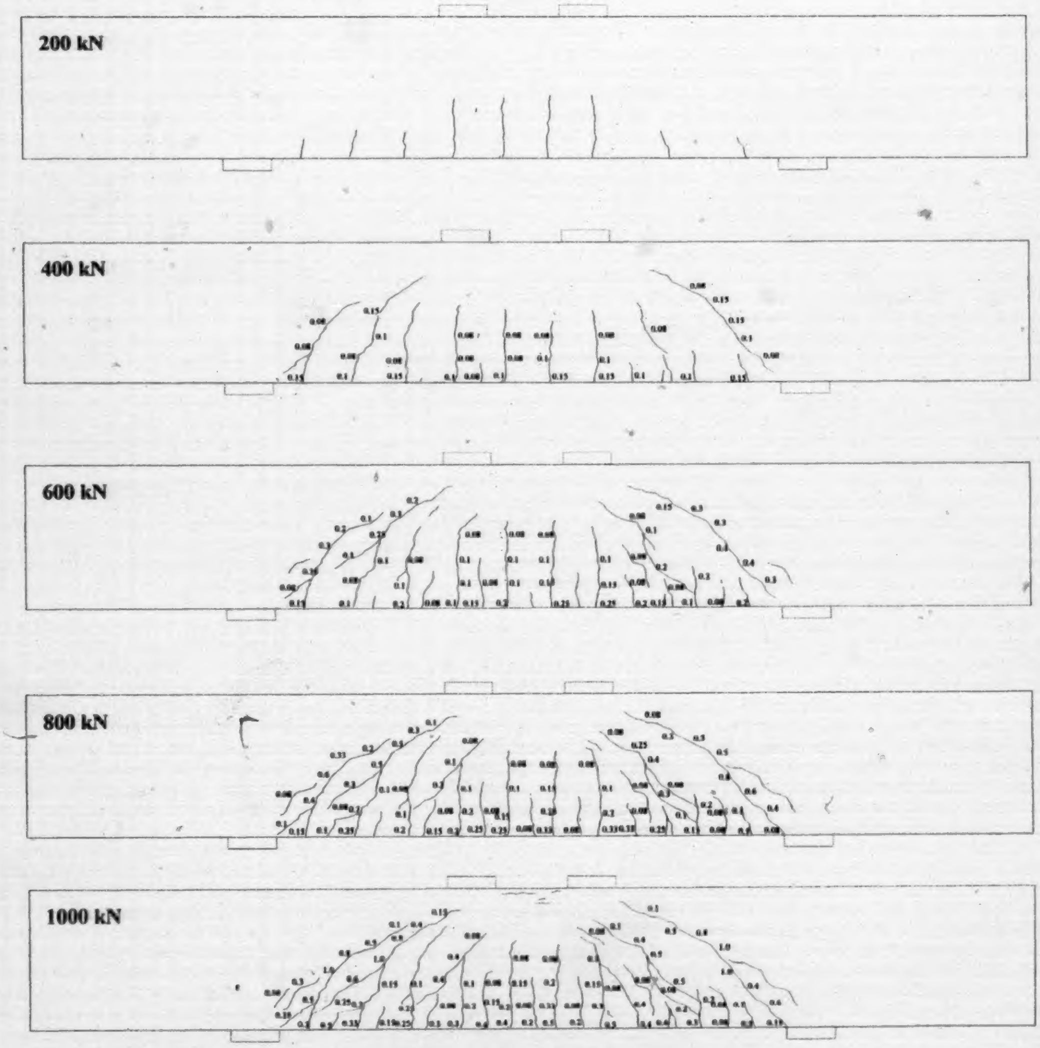

Figure A-102 Crack patterns at different loading stages of specimen NS2-4

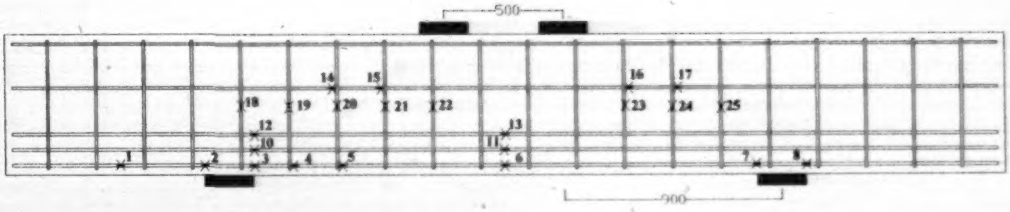

Figure A-103 Strain gages locations of specimen NS2-4

Table A-38 Location of strain gauges for specimen NS2-4

Strain Gauge	Distance from midspan (mm)	side	Strain Gauge	Distance from midspan (mm)	side
1	1600	A	14	500	A
2	1250	A	15	700	A
3	1050	A	16	500	B
4	880	A	17	700	B
5	680	A	18	stirrup	A
6	0		19	stirrup	A
7	1050	B	20	stirrup	A
8	1250	B	21	stirrup	A
9	0		22	stirrup	A
10	1050	A	23	stirrup	B
11	0		24	stirrup	B
12	150	A	25	stirrup	B
13	0				

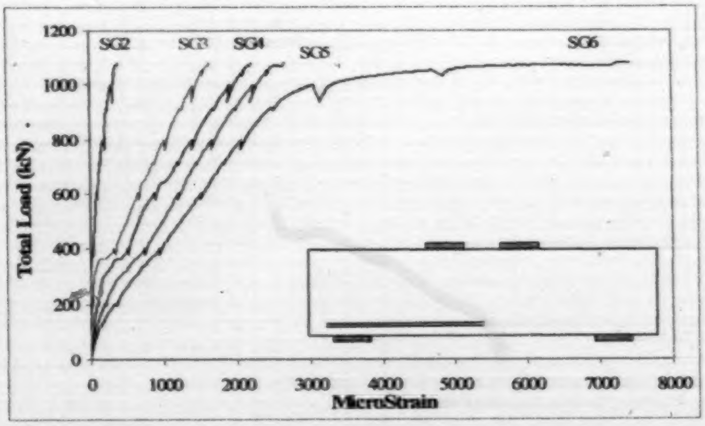

Figure A-104 Strains at a bar located in the lowest layer of main tension reinforcement of specimen NS2-4

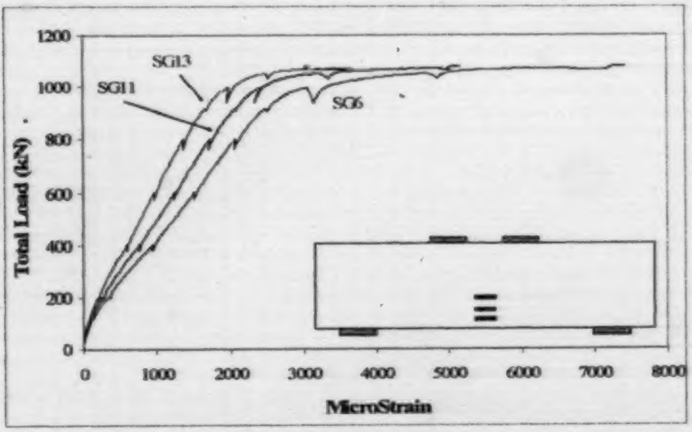

Figure A-105 Strains at midspan of the three layers of main tension reinforcement in specimen NS2-4

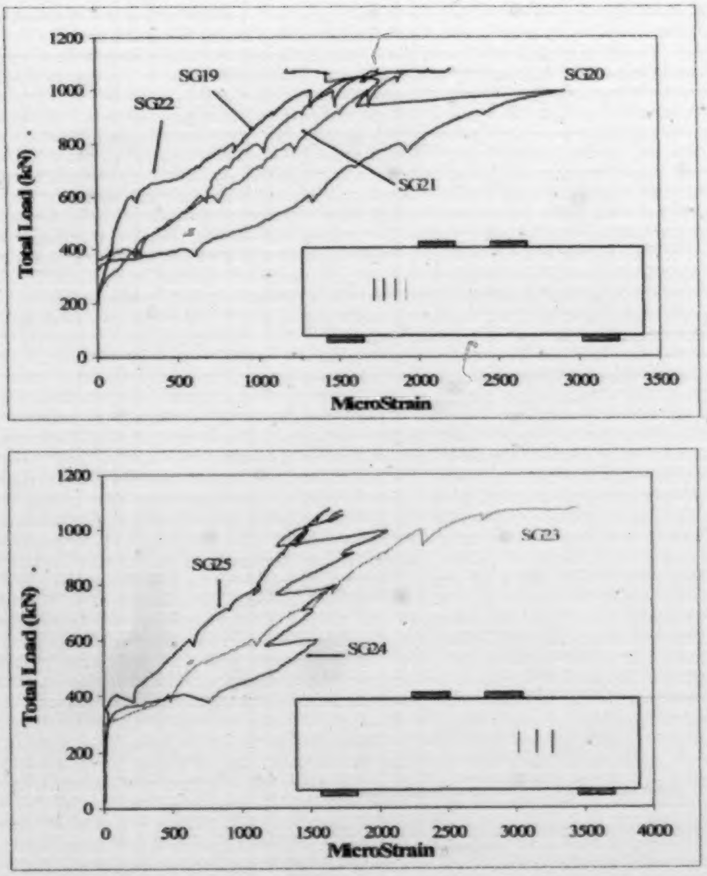

Figure A-106 Strains of stirrups located in the shear spans of specimen NS2-4

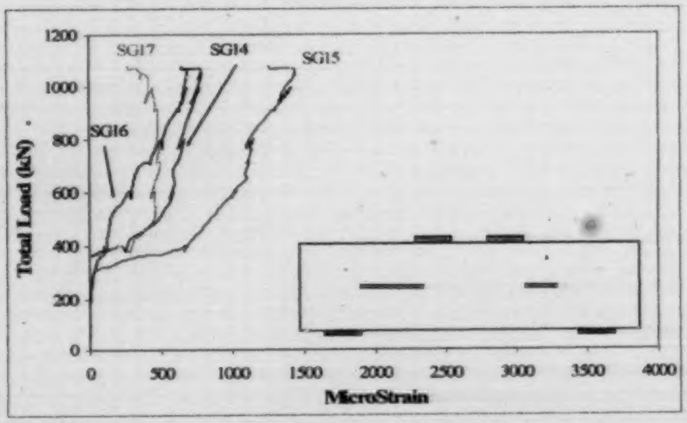

Figure A-107 Strains on the horizontal web reinforcement of specimen NS2-4

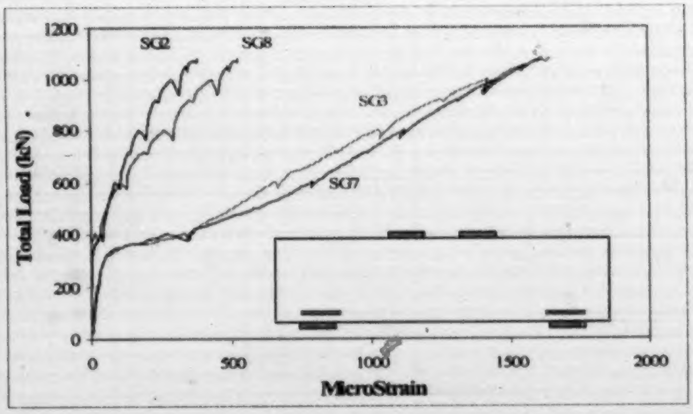

Figure A-108 Strains at the interior and exterior edges of the supports of specimen NS2-4

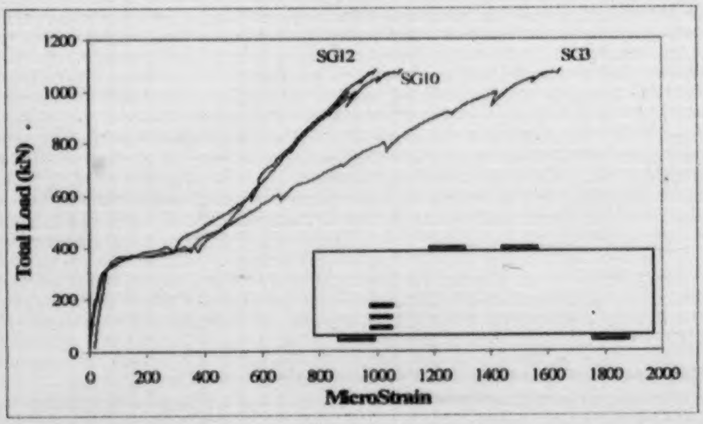

Figure A-109 Strain at the interior edge of one support for the three layers of tension reinforcement of specimen NS2-4

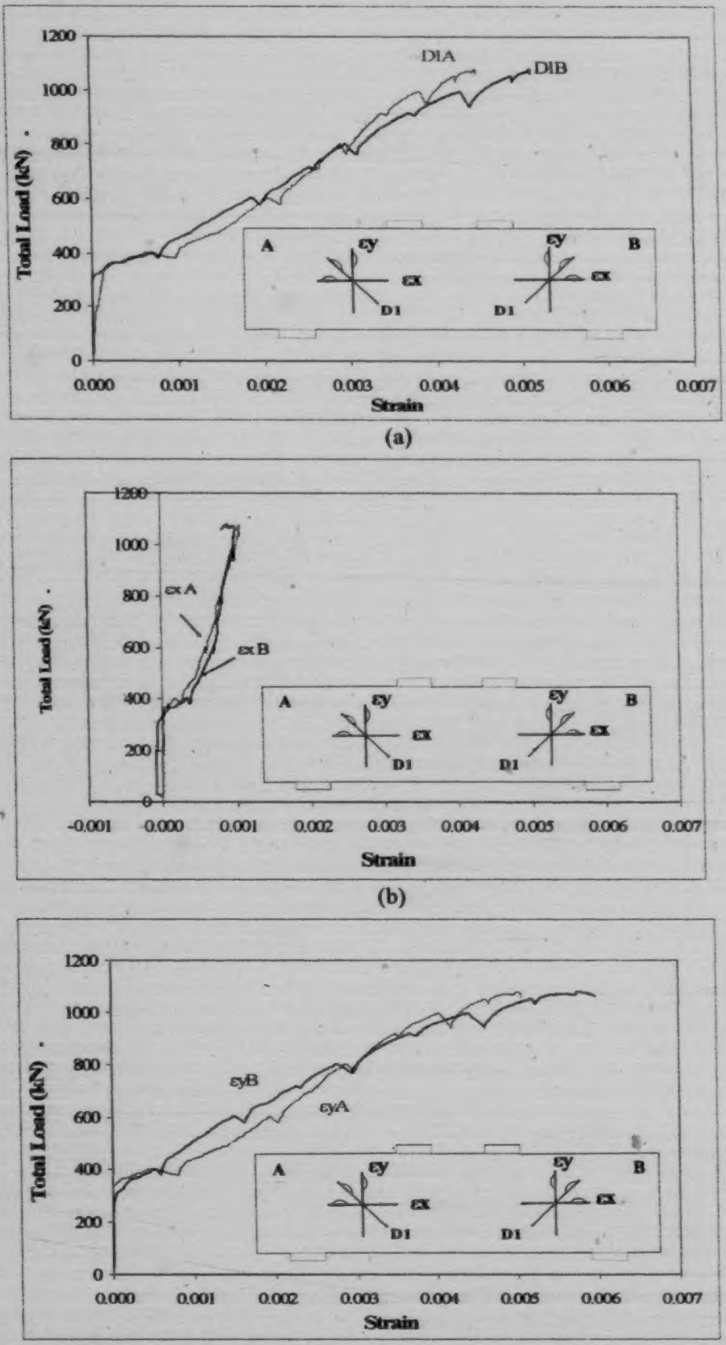

(a)

(b)

(c)

Figure A-110 Average Strains in the (a) diagonal strain D1, (b) horizontal strain and (c) vertical strain of specimen NS2-4

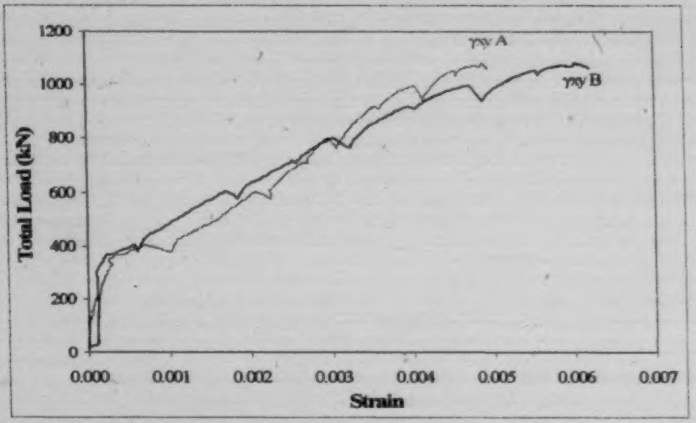

Figure A-111 Maximum shear strain

Table A-39 Strains monitored by demec gages rosettes for specimen NS2-4

LOAD	εy B	εD2 B	εx B	εD1 B	εy A	εD1 A	εx A	εD2 A	Top
	I	II	III	IV	V	VI	VII	VIII	IX
0	0.00000	0.00000	0.00000	0.00000	0.00000	0.00000	0.00000	0.00000	0.00000
200	0.00000	-0.00008	0.00002	0.00008	0.00001	0.00007	0.00001	-0.00006	-0.00034
400	0.00057	-0.00014	0.00093	0.00145	0.00105	0.00137	0.00072	-0.00023	-0.00071
600	0.00276	-0.00003	0.00192	0.00421	0.00296	0.00317	0.00127	-0.00036	-0.00120
700	0.00415	0.00001	0.00219	0.00561	0.00369	0.00382	0.00136	-0.00044	-0.00154
800	0.00517	0.00015	0.00241	0.00663	0.00431	0.00433	0.00140	-0.00047	-0.00180
900	0.00700	0.00038	0.00276	0.00837	0.00538	0.00529	0.00138	-0.00054	-0.00224
1000	0.00840	0.00060	0.00296	0.00965	0.00624	0.00604	0.00126	-0.00060	-0.00289
1050	0.00990	0.00081	0.00310	0.01103	0.00714	0.00674	0.00111	-0.00065	-0.00685

APPENDIX B

B.1 SECTIONAL METHOD

B.1.1 Sectional Flexure Analysis

The assumptions for this analysis are that transversal sections that are plane before bending remain plane after bending.

Simplified equations of the stress block were used to determine the moment capacity of the specimens. The strain of the concrete at the top fiber of the section (ε_c) was defined as 0.0035 for CSA A23.3-04 and 0.003 for ACI 318-05.

As reinforcement in the compression zone was not considered in the analysis, the moment capacity of the specimens was obtained with Equation (B-1).

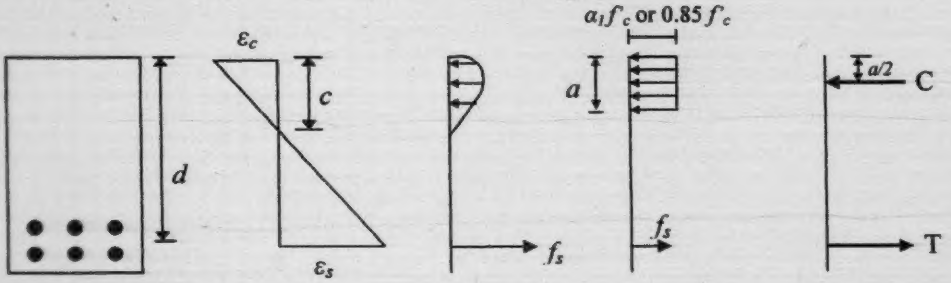

(a) Cross section (b) Strains (c) Stresses (c) Equivalent stresses (d) Forces

Figure B-1 Sectional Flexure Analysis

$$M = f_s A_s \left(d - \frac{a}{2} \right) \tag{B-1}$$

$$\varepsilon_s = \varepsilon_c \frac{d-c}{c} \tag{B-2}$$

$$a = \beta_1 c \tag{B-3}$$

c is the distance from the extreme compression fiber to neutral axis when $C = T$ (see Figure B-1)

For ACI 318-05 code in U.S. customary units (in, psi):

$\varepsilon_c = 0.003$

$$C = 0.85 f'_c a b_w \tag{B-4}$$

$$T = A_s f_s \tag{B-5}$$

$$\beta_1 = 0.85 - 0.05\left(\frac{f'_c - 4000}{1000}\right) \geq 0.65 \tag{B-6}$$

For CSA A23.3-04 code in SI units:

$$\varepsilon_c = 0.0035$$

$$C = \alpha_1 f'_c a b_w \tag{B-7}$$

$$\alpha_1 = 0.85 - 0.0015 f'_c \geq 0.67 \tag{B-8}$$

$$\beta_1 = 0.97 - 0.0025 f'_c \geq 0.67 \tag{B-9}$$

B.1.1.1 Reinforcement properties

The relationship between f_s and ε_s for specimens reinforced with ASTM A1035 is given by equations (B-10), (B-11) and (B-12). The equations are curve fit to tensile coupon test data. The units used are in SI units.

For # 4 in MPa

$$\begin{aligned} f_s &= -1907901700000\varepsilon_s^{\,6} + 376513550000\varepsilon_s^{\,5} - 29325278000\varepsilon_s^{\,4} \\ &+ 1144431800\varepsilon_s^{\,3} - 23498204\varepsilon_s^{\,2} + 244139.22\varepsilon_s \end{aligned} \tag{B-10}$$

For # 6

$$\begin{aligned} f_s &= -2989150700000\varepsilon_s^{\,6} + 554965110000\varepsilon_s^{\,5} - 39762244000\varepsilon_s^{\,4} \\ &+ 1413246500\varepsilon_s^{\,3} - 26509443\varepsilon_s^{\,2} + 256545.2\varepsilon_s \end{aligned} \tag{B-11}$$

For bar #7

$$\begin{aligned} f_s &= 3315187000000\varepsilon_s^{\,6} - 159778900000\varepsilon_s^{\,5} - 9014621500\varepsilon_s^{\,4} \\ &+ 794026990\varepsilon_s^{\,3} - 20834278\varepsilon_s^{\,2} + 239651.15\varepsilon_s \end{aligned} \tag{B-12}$$

B.1.2 Sectional Shear Analysis

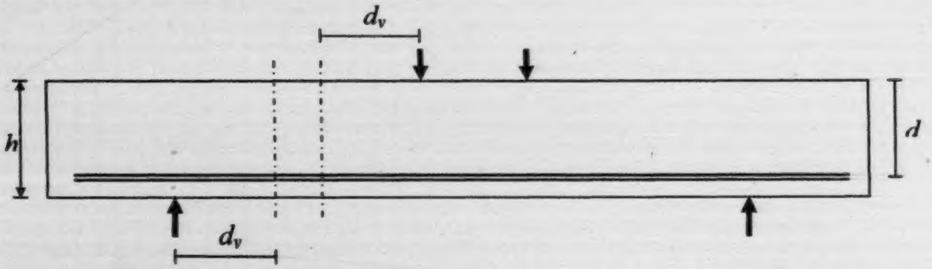

Figure B-2 Location of Sections for shear analysis

The equation used to determine the shear capacity of the beams without web reinforcement was Equation (B-13). For specimens with web reinforcement Equation (B-14) was used. The critical sections for shear evaluated where located at d_v from the centerline of the bearing plates at the supports and d_v from the centerline of the bearing plates at the loading points as shown in Figure B-2. The smaller value of V_C obtained from calculations at these two locations was the value used to calculate the corresponding P_{max}/P_{pv} ratio, where $P_{pv} = 2V_R$.

$$V_R = V_C \tag{B-13}$$

$$V_R = (V_C + V_S) \tag{B-14}$$

For ACI 318-05 code in U.S. customary units (in, psi):

$$V_C = 2\sqrt{f'_c}\, b_w d \tag{B-15}$$

$$V_S = \frac{A_v f_{yt} d}{s} \tag{B-16}$$

For CSA A23.3-04 code in SI units:

$$V_C = \left(\frac{0.40}{1+1500\varepsilon_x}\right)\left(\frac{1300}{1000+s_{ze}}\right)\sqrt{f'_c}\,b_w d_v \tag{B-17}$$

Where

$$\varepsilon_x = \frac{\frac{M_f}{d_v}+V_f}{2E_s A_S} \tag{B-18}$$

$$s_{ze} = \frac{35 s_z}{15+a_g} \geq 0.85 s_z \tag{B-19}$$

$$V_s = \frac{A_v f_y d_v \cot\theta}{s} \tag{B-20}$$

$$\theta = 29 + 7000\varepsilon_x \tag{B-21}$$

d_v is taken as the larger of $0.72h$ or $0.9d$.

s_z should be taken as d_v or as the maximum distance between layers of disturbed longitudinal reinforcement, whichever is less. If minimum transverse reinforcement exists, CSA A23.3-04 establishes that S_{ze} shall be taken as equal to 300 mm. According to Lubell (2006), better predictions are obtained when S_{ze} is taken as the distance, in mm, between stirrups.

Note that for Equation (B-18), E_s was taken as 200000 MPa and linear stress-strain response up to failure was assumed.